Stimulation of angiogenesis and osteogenesis in a dynamic co-culture model of bone tissue engineering

Dissertation

zur Erlangung des Grades

Doktor der Naturwissenschaften

am Fachbereich Biologie

der Johannes Gutenberg-Universität Mainz

Thomas Böse

Mainz, August 2017

Dekan:

1.Berichterstatter:

2.Berichterstatter:

Tag der mündlichen Prüfung:

Danksagung

.

Abbreviations

AA	ascorbic acid
AB	alcian blue
ADM	adipogenic differentiation medium
ALP	alkaline phosphatase
aMEM	alpha minimum essential mediu,
Ang-1	angiopoietin-1
Ang-2	angiopoietin-2
angCC	angiogenic co-cultivation
AR	alizarin red
atMSC	adipose tissue-derived MSC
bFGF	basic fibroblast growth factor
BM	basal medium
bmMSC	bone marrow-derived MSC
BMP-2	bone-morphogenic protein 2
BMP-4	bone-morphogenic protein-4
BMP-6	bone-morphogenic protein-6
BSA	bovine serum albumin
BTE	bone tissue engineering
CC/CCs	co-culture/plural
CD	cluster of differentiation
CD105	endoglin
CD11b	integrin alpha M
CD146	melanoma cell adhesion molecule
CD19	B-lymphocyte antigen
CD29	integrin ß1
CD31	platelet endothelial cell adhesion molecule
CD34	hematopoietic progenitor cell antigen
CD44	hyaluronan receptor
CD45	lymphocyte common antigen
CD73	ecto-5'-nucleotidase
CD90	Thy-1
CDM	chondrogenic differentiation medium
Col-IV	collagen type-IV
Comm.	commercial
CSD	cell seeding density
CSR	cell seeding ratio
d	day
DAPI	4',6-Diamidin-2-phenylindol
DC	differentiation control
Dex	dexamethasone

EC	endothelial cell
ECGM	endothelial cell growth medium
ECO	endochondral ossification
EDTA	ethylenediaminetetraacetic acid
EDX	energy dispersive x-ray spectroscopy
EGM2	Lonza's endothelial cell growth medium 2
ELISA	enzyme linked immunosorbent assay
FACS	fluorescence activated cell sorting
Fcrit	critical F-value
FCS	fetal calf serum
FITC	fluorescein isothiocyanate
FSC	forward scatter
GF/GFs	growth factor/plural
GM	GlutaMAX®
GR	glucocorticoid receptor
h	hour
HDF	human dermal fibroblast
HDMEC	human dermal microvascular endothelial cell
HF	heparin+bFGF (pro-angiogenic supplements)
HLA-DR	human leukocyte antigen class II
HRP	horse reddish peroxidase
HUVEC	human umbilical vein endothelial cell
IF	immunofluorescence
I_{Fl}	intensity of fluorescence/fluorescence intensity
IMO	intramembraneous ossification
ISO-HAS-1	hemangiosarcoma cell line
LMN	laminin
MC/MCs	mono-culture/plural
MSC	mesenchymal stromal/stem cell
N	network
oCC	osteogenic co-cultivation
ODM	osteogenic differentiation medium
OEC	outgrowth endothelial cell
OR-O	oil red-O
OS	osteogenic supplements
PBS	phosphate-buffered saline
PDGF-BB	platelet-derived growth factor B homodimer
PE	polyethylene

pOB	primary osteoblast
prl-oCC	prolonged osteogenic co-cultivation
ROI	region of interest
Saf-O	safranin-O
SEM	standard error of the mean
SSC	sideward scatter
ßGP/bGP	ß-glycerol phosphate
TEER	Transendothelial electrical resistance
TIC	total intracellular collagen content
TL	transmitted light
tNiTi	trabecular nickel-titanium alloy
TRITC	tetramethylrhodamin
TS	test statistic
VEGF	vascular endothelial growth factor
VK	von Kossa
VLS	vessel-like structures
VR	vessel regression
vWF	von Willebrand factor
w/o	without
Wk	week

Index of Content

1 Introduction

The integration of a complex vascular system is an important basis for the development of a successful strategy in the application of *in vitro* generated tissue engineering constructs for bone regeneration. For this purpose, co-cultures of stromal cells with endothelial cells have been developed and evaluated in order to stimulate the formation of vessel-like structures *ex vivo*. When focusing on a therapeutic application an approach involving primary human cells and their *in vitro* processing to achieve tissue formation has to be optimized according to the overall time span and maximum therapeutic outcome. In this context, a minimized processing time will also minimize non-physiological cellular reactions, which could jepoardize the success of a related bone tissue engineering strategy. The most optimal support of the cells and the generated constructs can be maintained by the application of state-of-the-art technologies like perfusion bioreactors. To take into account the cellular complexity of a tissue engineering approach linked to the implementation of a technological aspect into a biological context the present study aimed to develop the basis for a perfusion-based strategy allowing for the generation of prevascularized bone tissue engineering constructs *in vitro*.

To recapitulate the fundamental knowledge as well as the current state of the science, basic knowledge and key findings from the field of bone development, vascularization and angiogenesis as well as bone regeneration are presented in the following chapter. Based on this, the present study will initially highlight the transfer of basic research to the applied science of biomaterial-based tissue engineering using co-culture models. In this context, state-of-the-art-research will be summarized to define a scientific baseline to judge both the novelty and impact of the key findings described by the present study.

1.1 Postnatal bone formation

The adult vertebrate skeleton consists of more then 200 bones of which the majority is formed by endochondral ossification (ECO). Only a minor number of flat bones like the skull and clavicles are formed through intramembraneous ossification (IMO, (Percival and Richtsmeier, 2013). Both types of bone formation begin with a condensation of loose mesenchyme which is avascular and hypoxic (Percival and Richtsmeier, 2013). Avascularity itself was demonstrated or postulated to serve as the basis for condensation growth and the initiation of the ossification during ECO or IMO, respectively (Percival and Richtsmeier, 2013). During ECO, a cartilaginous template forms via differentiation of precursor cells into chondrocytes within the template which is surrounded by the perichondrium. In this context, the chondrogenic differentiation is controlled by the transcription factor Sox9 either directly or indirectly by inhibiting the activity of a second transcription factor Runx2 or by repressing its transcription (Hartmann, 2009, Zhou et al., 2006). In contrast, during IMO cells within the condensed mesenchyme directly differentiate into osteoblastic cells (Hartmann,

2009), although the initiating stimulus remains unidentified in humans (Percival and Richtsmeier, 2013). Only a single study focusing on IMO of chick frontal bone gives more insight by describing the infiltration of condensed mesenchyme layers by bore capillaries in response to hypoxia-induced pro-angiogenic signaling as the basis of an ossification front following vascular invasion of the growing avascular condensation (Thompson et al., 1989). On the other hand, no signaling such as it is involved in ECO is necessary for IMO (Hartmann, 2009, Percival and Richtsmeier, 2013).

While osteoblasts differentiate directly from mesenchymal progenitors during IMO (Percival and Richtsmeier, 2013) the perichondrium that forms around the diaphysis of long bones will be the origin of osteoblast precursors during ECO which is called periosteum upon their appearence (Hartmann, 2009). Within the cartilage template cells mature and become hypertrophic chondrocytes secreting a collagenous matrix. This stage of ECO is linked to the termination of cell proliferation and exit from active cell cycling (Shum and Nuckolls, 2002). After further maturation the secreted matrix will be mineralized, while at the same time the hypertrophic chondrocytes undergo apoptosis (Shum and Nuckolls, 2002). This is linked to the release of high doses of VEGF and vascular invasion into the primary and secondary ossification center (Hartmann, 2009, Long, 2012, Percival and Richtsmeier, 2013). Associated with this, chondrogenic genes like Sox9, 5 and 6 are down regulated while at the same time Runx2 activity is elevated (Hartmann, 2009). The following final chondrogenic maturation and osteoblastic differentiation are coupled via secreted Indian Hedgehog (Ihh) signaling (Long, 2012). The expression of Ihh in turn is controlled by the expression and activity of Runx2 in pre-hypertrophic chondrocytes (Karsenty, 2001). Most importantly, Ihh screted during ECO induces Runx2 expression in the surrounding perichondrium where it is essential for the ostegenic differentiation (Kim et al., 2013, Tu et al., 2012). The same is true for the osteoblastic lineage differentiation within the condensed mesenchyme formed during IMO (Percival and Richtsmeier, 2013). To finally become fully committed osteoblasts the Runx2 expressing osteoblastic precursors require the expression of the transcription factor Osterix/Sp7 (Nakashima et al., 2002). Osteorix regulates the differentiation into adult osteoblasts while supressing chondrocyte differentiation simultaneously (Nakashima et al., 2002). The maturation into matrix-secreting osteoblasts is guaranteed by the downregulation of Runx2, however, the related mechanism remains unknown (Hartmann, 2009). The primary bone developed during hypertrophy and apoptosis of maturating chondrocytes is constantly remodeled by osteoblasts and osteoclasts to form trabecular bone (Hartmann, 2009, Long, 2012, Percival and Richtsmeier, 2013). Osteoclasts develop upon differentiation from hematopoietic precursor cells which invade the forming tissue through the developing vasculature (Engsig et al., 2001). The described processes are common to the development as well as the diaphysial and the epiphysial growth of long bones (Long, 2012, Percival and Richtsmeier,

2013). Similarly, IMO and ECO are involved in the healing of bone fractures (Einhorn and Gerstenfeld, 2015).

1.2 Vascularization and Angiogenesis

All organs and the respective cells of the human body are dependent on a precisely regulated supply of oxygen. Since the physiological diffusion of oxygen into tissues is limited to a maximum distance of around 200 µm (Rouwkema et al., 2008) a highly specialzed network of vessels evolved in the human body that guarantees the supply of each cell within the diffusion limit (Hoeben et al., 2004). The vessel system is constantly remodeled and maintained by angiogenesis, the formation of new blood vessels from pre-existing ones (Carmeliet, 2005). While angiogenesis is the predominant form of vessel formation in the postnatal human body vascularization is the basic process of vessel formation during vascular development in the growing fetus (Risau and Flamme, 1995). The onset of vascular formation is formed by the hemangioblast, a type of precursor cell shown to be the common origin of the vasculogenic/angiogenic system and the hematopoietic system located in the bone marrow (Kennedy et al., 1997). While hemangioblasts develop into endothelial cells they form blood islands that tend to fuse with each other forming a lumen and a subsequent primary capillary plexus (Hoeben et al., 2004). The process of vasculogenesis primarily occurs in the yolk sac during embryogenesis (Chung and Ferrara, 2011). Once the capillary plexus formed, endothelial cells proliferate leading to the formation and growth of new vessels and interconnections thus representing the transition from vasculogenesis to angiogenesis (Bergers and Benjamin, 2003, Chung and Ferrara, 2011). Angiogenesis is finally controlled by a tightly balanced system of pro-angiogenic and anti-angiogenic factors like vascular endothelial growth factor (VEGF) or angiostatin, respectively (Figure 1, Bergers and Benjamin, 2003).

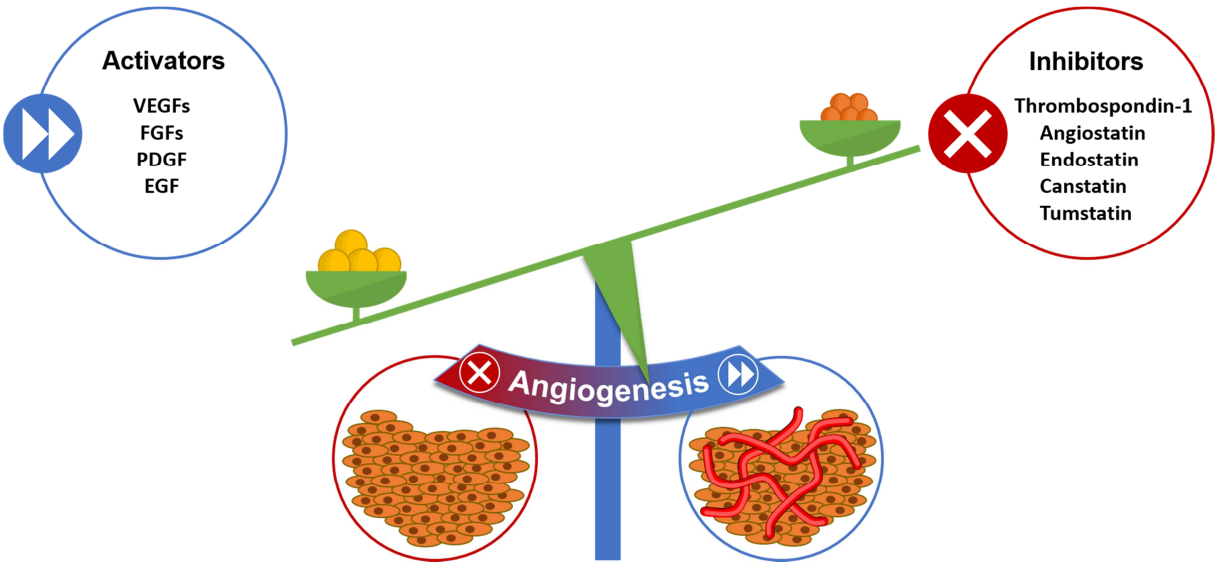

Figure 1: Schematic representation of the tightly regulated angiogenic balance and indication of the most important inhibotors and activators of angiogenesis. Figure adapted from (Bergers and Benjamin, 2003)

Most activators that stimulate the proliferation and migration of endothelial cells are receptor tyrosine kinase ligands (Carmeliet, 2000). Among those VEGF, fibroblast growth factors (FGFs), platelet-derived growth factor (PDGF) and epidermal growth factor (EGF) play major roles in angiogenic induction and stabilization, where EGF in turn enhances the expression of VEGF and FGF (Figure 1, Bergers and Benjamin, 2003). On the side of angiogenic inhibitors thrombospondin-1 was the first described to modulate endothelial-cell proliferation and motility (Volpert et al., 1995). Most interestingly, several inhibitors including the “statins” are derived from proteins that generally do not influence angiogenesis. In principle, whether an endothelial cell will enter an angiogenic or quiescent state, is driven by the levels of activators and inhibitors (Bergers and Benjamin, 2003). In general, angiogenesis is induced by hypoxic conditions (Carmeliet, 2003, Martino et al., 2015). Hypoxia stimulates expression of GF involved in different stages of angiogenesis. As mentioned earlier this includes VEGF, Ang-2 and nitric oxide synthase (NOS). In response to hypoxia vessels dilate and local doses of VEGF (also termed as vasopermeability factors in this context) lead to the disruption of the endothelial cell barrier integrity whereby endothelial cells become migrative (Hoeben et al., 2004). In this context, a specialized subtype of endothelial cells function as tip cells sensing a gradient of pro-angiogenic VEGF generated by hypoxia (Gerhardt et al., 2003). The migrating tip cell upregulates the Notch ligand Delta-like-4 and Notch1 in neighbouring cells thus inducing a stalk-cell phenotype (Hellstrom et al., 2007). Stalk cells are highly proliferative and generate the new blood vessel trunk following the tip cell (Gerhardt et al., 2003). At the same time endothelial cells activated by sensing VEGF release PDGF-BB therefore leading to the recruitment of pericytes to nascent vessels (Bergers and Song, 2005). Pericytic signaling through the Ang-1/Tie2, TGFβ1/TGFβ-receptor-1 and EphringB2/EphB4 pathways activates endothelial cell quiescence and vessel stabilization (Figure 2, Martino et al., 2015). Under normal and healthy conditions angiogenesis occurs during wound healing, organ regeneration or in the female reproductive system during ovulation, menstruation and placenta formation (Bergers and Benjamin, 2003). The induction of an angiogenic phenotype is highly dependent on local changes of the balanced system between angiogenic stimulation and inhibition. The same is true for a disease like cancer where angiogenesis is artificially enhanced by the excessive release of pro-angiogenic VEGF from cancer cells to maintain the oxygen and nutrient supply of the growing cancer (Bergers and Benjamin, 2003, Carmeliet, 2003). Angiogenesis is thus based on signaling pathways that are common to states of disease and health as well as development, regeneration and healing.

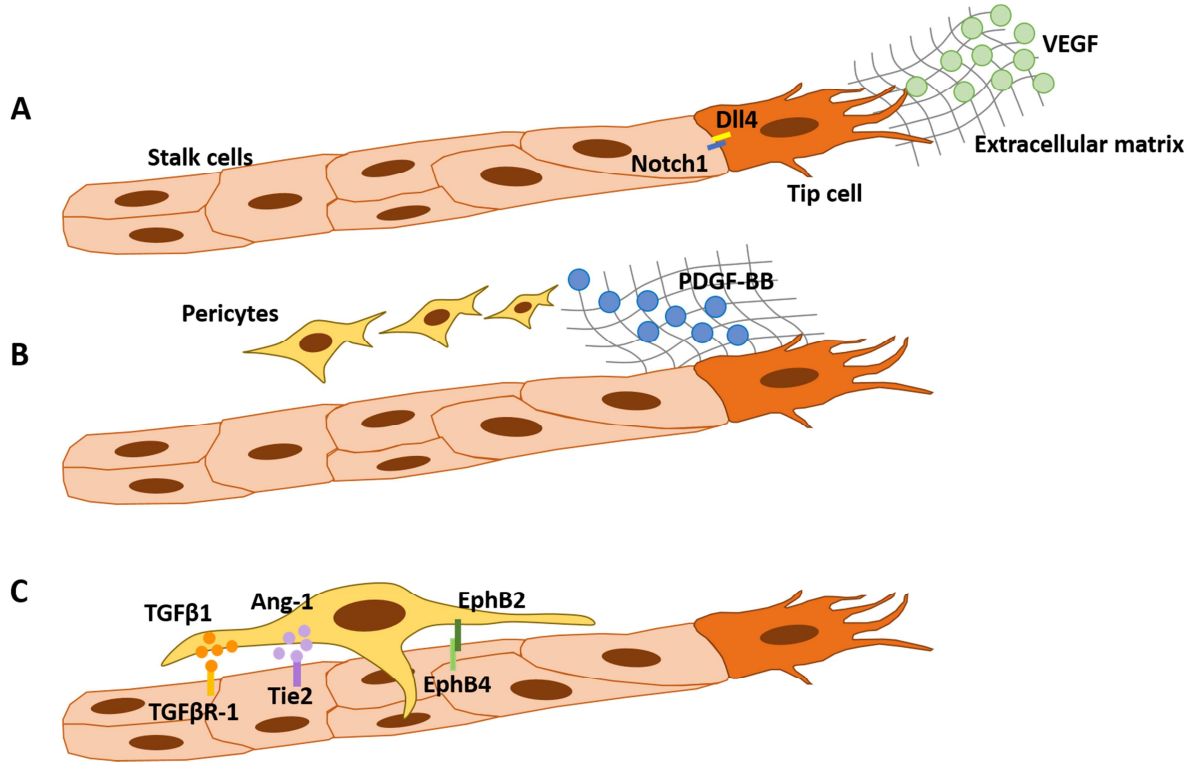

Figure 2: Schematic representation of the main phases of blood vessel growth and the involved signaling pathways: A: Endothelial cells activated by sensing of VEGF gradients in response to hypoxia become migrative tip cells that induce a stalk cell phenotype in adjacent cells through Notch signaling. B: Activated endothelial cells release PDGF-BB leading to the recruitment of pericytes to nascent vessels. C: The crosstalk of pericytes with vessel-associated endothelial cells through Ang-1/Tie2, TGFβ1/TGFβR-1 and EphrinB2/EphB4 signaling induces quiescence and stabilization of newly formed vessels. Figure adapted from (Martino et al., 2015)

1.3 Fracture healing

The healing process of bone fractures is characterized by an initial anabolic phase, which is coupled to the increase of the tissue volume around the fracture. Initially, no *de novo* recruitment of skeletal stem cells that form skeletal and vascular tissue occurs. In close proximity to the fracture a cartilaginous callus forms. Cells that are involved in the callus formation are predominantly recruited from the periosteum. At the border zone to the newly formed cartilage the periosteum swells what initiates the process of new bone formation (Phillips, 2005). Similarly to IMO and ECO this process is linked to blood vessel ingrowth and the increase of blood flow into the fracture area (Figure 3, Einhorn and Gerstenfeld, 2015). As chrondrocyte differentiation within the cartilage progresses towards hypertrophy primary mineralization occurs (Percival and Richtsmeier, 2013). The initial anabolic phase of fracture healing is terminated with chondrocyte apoptosis following chondrocyte hypertrophy (Gerstenfeld et al., 2003a, Lee et al., 1998) and the transition to a following catabolic phase. This phase is primarily characterized by the reduction of the callus volume. The mineralizing cartilage and the primary bone are constantly remodeled by osteoblasts and osteoclasts (Figure 3, Einhorn and Gerstenfeld, 2015,

Gerstenfeld et al., 2003b). The involved osteoclasts and osteoblasts are derived from precursor differentiation due to increased blood inflow or by migration from the fracture proximity, respectively (Mbalaviele et al., 1999, Park et al., 2012). However, increasing angiogenesis will induce secondary bone formation, which is followed by a remodeling by osteoclasts. This phase of bone remodeling is characterized by coupled cycles of osteoblast and osteoclast activity leading to the remodeling of the callus tissue as well as the reconstitution of the original bone structure and marrow cavity, finally resulting in the regeneration of the hematopoietic tissue (Figure 3, Einhorn and Gerstenfeld, 2015). The termination of the catalytic phase is characterized by angiogenic remodeling which includes the regression of the initially increased vascular bed of the callus as well as the reduction of the blood flow to the initial steady-state (Holstein et al., 2013, Melnyk et al., 2008). The different phases of fracture healing are consecutive on the one hand but they are characterized by a significant temporal overlap on the other hand (Figure 3, Einhorn and Gerstenfeld, 2015). In general, the healing of a bone fracture by either ECO or IMO is influenced by the stability of the fixation and immobilization of the involved bones. It was shown by Morgan and colleagues that a decreased fracture stability is linked to a higher degree of cartilage formation and by this ECO (Morgan et al., 2010). In a worst-case scenario excessive instability will impair angiogenesis and thus fracture healing thereby preventing gap-bridging (Claes et al., 2002). In contrast, a high level of fracture stability and immobilization will reduce ECO and support IMO instead (Morgan et al., 2010). However, a slightly decreased stability of fixation was associated with an increased initial angiogenesis and angiogenic remodeling (Claes et al., 2002, Olerud and Stromberg, 1986, Wallace et al., 1994). Independent of the type of ossification involved in fracture healing the infiltration of the injured bone tissue by precursor cells is a critical step that affects the efficiency of the healing process (Wu et al., 2013, Kalfas, 2001, Bastian et al., 2011, Lange et al., 2010). In this context, precursor cells of the stroma termed as mesenchymal stromal cells or mesenchymal stem cells (MSC) are able to reconstitute several different types of tissues involved in bone fracture healing upon multi-lineage differentiation (Park et al., 2012). Together with the fact that this type of precursor cells is further involved in the mesenchymal condensations that form during ECO and IMO (Long, 2012, Percival and Richtsmeier, 2013) MSC have become an attractive cell type to be evaluated and applied to the field of tissue engineering (Kobolak et al., 2015, Richardson et al., 2015).

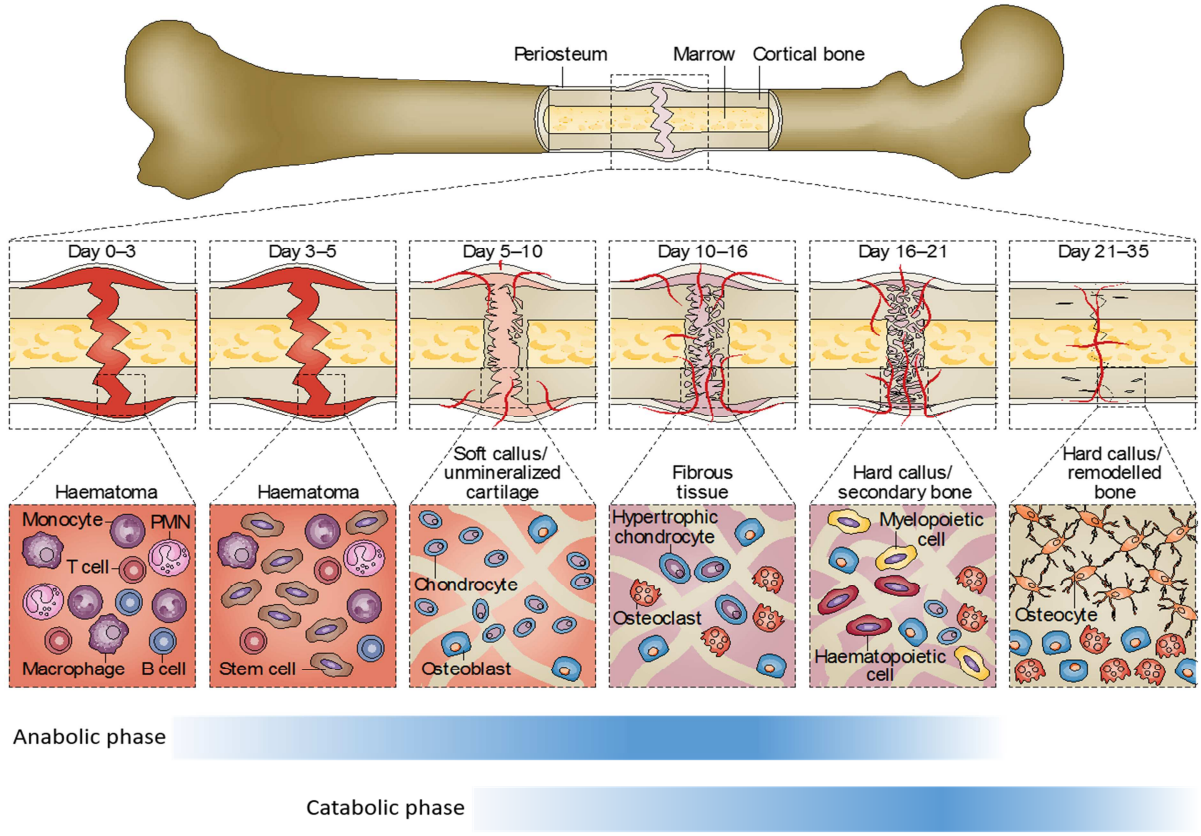

Figure 3: Schematic representation of fracture repair. The two metabolic phases (anabolic and catabolic; indicated by blue bars) of fracture healing overlap with different stages of repair (inflammatory stage, endochondral stage, coupled remodeling; brown bars). The major cell types found at each stage are denoted in the context of the time span of their prevalence. The indicated time scale of healing corresponds to a closed fracture of a mouse femur fixed with an intramedullary rod. Figure taken with permission from (Einhorn and Gerstenfeld, 2015)

1.4 Origins, identification and cultivation of MSC

MSC are a widely used cell type for applications in tissue engineering of the lung, liver, kidney and especially bone (Calle et al., 2014, Zhang et al., 2015, Richardson et al., 2015, Kobolak et al., 2015, Wang et al., 2015). These cells are either isolated from bone marrow aspirates (Medyouf et al., 2014), adipose tissue or lipoaspirates (Francis et al., 2010), peripheral blood (Trivanovic et al., 2013), whartons jelly (Batsali et al., 2013) or trabecular bone fragments (Fuchs et al., 2009a, Unger et al., 2010). Jaiswal and colleagues demonstrated that stromal cells deposit a mineralized matrix when cultivated in the presence of β-glycerol phosphate (Jaiswal et al., 1997). Pittenger et al. were the first to describe the trilineage differentiation potential of MSC giving rise to cells of the osteogenic, adipogenic or chondrogenic lineage during cultivation in cell-respective differentiation media (Pittenger et al., 1999). In the following years MSC were studied extensively and described as the holy grail of autologous stem cells engineering and tissue engineering (Plock et al., 2013).

In 2006 a guideline paper was published by the International Socienty for Stem Cell Therapy (ISCT) which aimed at defining the minimal criteria for the characterization

of human MSC (Dominici et al., 2006). According to this guideline human MSC must be plastic-adherent, positive for the expression of CD105, CD90 and CD73, negative for the expression of CD45, CD34, CD11b, CD19 and HLA-DR and able to differentiate into osteoblasts, chondroblasts and adipocytes *in vitro* (Dominici et al., 2006). Although the ancestry of MSC remained unknown, the framework for the definition of MSC given by the ISCT guideline was widely accepted and applied. Finally, Crisan and colleagues were the first to describe the origin of MSC to physiologically be a subset of $CD146^+$ perivascular cells "wrapped around" blood vessels thereby supplying a stabilization function (Crisan et al., 2008). In an earlier study da Silva Meirelles et al. demonstrated that MSC could be isolated from nearly any tissue of the human body (da Silva Meirelles et al., 2006). Nevertheless, the question remained what MSC truly are (reviewed in (Bianco et al., 2013). In this context, although heavily cited (Dominici et al., 2006) the ISCT guideline is controversely debated since the markers recommended for the flow cytometry-based characterization of MSC are "a set of unspecific markers" (Bianco et al., 2013). Furthermore, only approximately 10% of the clonal strains transplanted *in vivo* are able to form osteogenic tissue, stroma and adipogenic cells and are thus true skeletal stem cells (Bianco et al., 2006). MSC have never been shown to fully differentiate into adipocytes or chondrocytes when transplanted *in vivo* by any representative differentiation assay (Bianco et al., 2013, Bianco et al., 2006). Based on this, the term "mesenchymal stromal cells" is often used instead of "mesenchymal stem cell" to describe the same type of cells, as proposed by Bianco and colleagues (Bianco et al., 2008). Despite the fact of limited identification by flow cytometry MSC can be expanded *in vitro* making them an attractive source for autologous tissue engineering approaches (Consentius et al., 2015, Watson et al., 2014, Casiraghi et al., 2016).

Plastic adherence is used as a major step to isolate MSC via different protocols e.g from bone marrow aspirates (Medyouf et al., 2014), peripheral blood (Trivanovic et al., 2013) or trabecular bone fragments (Kolbe et al., 2011). The isolation of MSC from trabecular bone fragments generates the highest cell yields compared to other sources (Knight and Hankenson, 2013). Noteworthy, MSC from trabecular bone are autologous on the one hand, but limited in their availability due to the highly invasive surgical procedures (Hass et al., 2011). Furthermore, most studies use trabecular bone from the femoral head, which is only available when the affected patients receive a hip transplantation. However, MSC from trabecular bone and the included bone marrow (bmMSC) were shown to exhibit the highest degree of differentiation into cells of the osteogenic lineage and therefore superior to MSC from adipose tissue (atMSC) or Wharton's jelly for bone tissue engineering applications (Fernandez-Moure et al., 2015, Baba et al., 2014). Once attached to cell culture plastic bmMSC are easily expandable to total numbers of up to 100×10^6 cells within 12d under industrial scale conditions (Fekete et al., 2012). In this context, it was shown that the growth rate and differentiation potential of bmMSC were highly dependent of the age and gender of the donating individual (D'Ippolito et al., 1999).

This was also shown to be true for atMSC (Choudhery et al., 2014). Although extensive expansion of bmMSC was shown to be linked to a limited differentiation potential (Banfi et al., 2000, Stenderup et al., 2003) bmMSC can be easily expanded to up to 50 x 10^6 cells in the third passage without losing their osteogenic differentiation potential, as found by the present study. Nevertheless, bmMSC are the most prominent cell type used in bone tissue engineering applications either in a two-dimensional (2D) or three-dimensional (3D) context (Kobolak et al., 2015, Richardson et al., 2015, Yousefi et al., 2016). The trilineage differentiation potential of MSC was first demonstrated in 2D cell cultures (Pittenger et al., 1999). Other studies in 2D focused on the donor age (D'Ippolito et al., 1999) or the plating density (McBeath et al., 2004) and their impact on the degree of differentiation.

1.5 Perfusion bioreactors support the osteogenic differentiation of MSC in 3D

In 3D, bmMSC have been grown on various biomaterials such as hydroxyapatite (Sun et al., 2012, Bjerre et al., 2011), β-tricalcium phosphate (Takahashi et al., 2005), Nitinol (Strauss et al., 2012, Gotman et al., 2013) or collagen scaffolds (Donzelli et al., 2007, Schneider et al., 2010). This was shown to result in the formation of calcified osteogenic tissue constructs. Furthermore, implanted bmMSC-seeded constructs have been shown to successfully enhance bone regeneration after transplantation *in vivo* (Murphy et al., 2011, Jin et al., 2016, Gomide et al., 2012). Several reports found that this effect was supported by medium perfusion through the 3D constructs in perfusion bioreactors (Holtorf et al., 2005c, Glowacki et al., 1998, Thibault et al., 2011, Holtorf et al., 2005a). Using this technology, it was found that not only the degree of differentiation or matrix calcification but also the distribution of bmMSC and secreted matrix was enhanced (Wendt et al., 2003). Most importantly medium perfusion through porous 3D scaffolds guarantees an active transport of nutrients and waste products to and from the center of 3D scaffolds (Brindley et al., 2011) therefore supporting cell metabolism and preventing limited substrate availability, hypoxia and apoptosis (Plunkett and O'Brien, 2011).

In this context, it was shown by others that cells migrate to the peripheral areas of scaffolds cultivated under static conditions while the formation of the resulting “capsule” leads to apoptosis and cell death in the scaffold center (Glowacki et al., 1998, Goldstein et al., 2001). As mentioned earlier, these effects were dramatically reduced when 3D scaffolds were cultivated under dynamic conditions (Glowacki et al., 1998). However, when bmMSC were cultivated in perfusion bioreactors a more precise monitoring of substrate concentrations or gas concentrations had to be applied. It is known that bmMSC respond to shear stress (Sikavitsas et al., 2003, Yourek et al., 2010) or changes in the substrate availability therefore changing metabolic or differentiation rates (Brindley et al., 2011). Similarly, the concentration of O_2 in the cell culture medium drives cellular processes like osteogenic differentiation (Fan et al., 2015), cell proliferation (Holzwarth et al., 2010), apoptosis and glycolysis

(Hughey et al., 2012). Because of the limited instrumentation in small-scale perfusion chambers perfusion bioreactors were preferred which could be stored under controlled conditions in a standard cell culture incubator during the experimental runs. Holtdorf and colleagues used a custom-made perfusion system for the cultivation of bmMSC on 3D calcium phosphate scaffolds (Holtorf et al., 2005c). In another study, Gomes et al. applied a comparable custom-made perfusion bioreactor for the cultivation of MSC on 3D poly-caprolactone scaffolds (Gomes et al., 2006). In the present study a commercial perfusion bioreactor system was used which was shown to result in the reproducible cultivation of tissue engineering constructs under dynamic conditions (Papadimitropoulos et al., 2011, Sadr et al., 2012, Wendt et al., 2003). Most perfusion systems are connected to simple tubing pumps allowing for either a circular or an oscillatory medium perfusion through the 3D scaffolds (Bancroft et al., 2003, Gomes et al., 2006, Holtorf et al., 2005b). Whether unidirectional or bidirectional medium perfusion is superior to one another in the support of bmMSC osteogenesis remains controversial (Case et al., 2011, Jacobs et al., 1998). However, it was shown by several reports that the rate of perfusion and therefore the flow velocity and the resulting shear stress clearly influenced the differentiation of bmMSC (McCoy and O'Brien, 2010). Egger et al. used flow rates of 0.3 – 0.5 mL/min to differentiate MSC seeded on ceramic scaffolds (Egger, 2015). In another report Holtdorf and colleagues demonstrated ALP activity and calcium deposition using a flow rate of 1 mL/min (Holtorf et al., 2005c). In a study investigating the osteogenic differentiation of bmMSC on 3D hydroxyapatite scaffolds using the commercial U-CUP perfusion bioreactor system Sadr at al. found a flow rate of 1000 um/s to be most optimal for the seeding of bmMSC on 3D scaffold and a rate of 100 um/s to be most optimal for their cultivation and osteogenic differentiation (Sadr et al., 2012). Taken together, these studies underline the ability of MSC to respond to mechanical stimuli based on shear stress.

1.6 Biomaterials as the basis for the osteogenic differentiation of MSC in 3D

This property of MSC was also investigated in another category of mechanical stimuli – namely the stiffness of the growth substrate. It was found that MSC sense the rigidity of the growth substrate based on chromatin condensation (Heo et al., 2015). The same report demonstrated that MSC possess a mechanical memory making them sensitive to biomaterial-based priming into a certain lineage of differentiation (Heo et al., 2015). In this context it was found that a high elasticity modulus (= high stiffness) increases the degree of osteogenic differentiation while a low elasticity modulus supports adipogenic differentiation (Gobaa et al., 2011, Swift et al., 2013). For these reasons it is accepted that 3D scaffolds supplying a high strength, stability and stiffness are favorable for applicaions in bone tissue engineering (Bose et al., 2012).

An impressive number of studies focused on the investigation and evaluation of different biomaterials for their feasibility in bone tissue engineering with the most prominent types of 3D biomaterials being various forms of ceramics like hydroxyapatite or tricalcium phosphate (extensively reviewed in (Bose et al., 2012, Karageorgiou and Kaplan, 2005, Stevens, 2008)). One feature of these materials is their resorbability by e.g. osteoclasts (Matesanz et al., 2014, Nakamura et al., 2016). Nevertheless, to increase the life time of bone tissue engineering biomaterials or to mimic the complex properties of natural bone new materials are developed, including blends of metal ions like Nitinol (Gotman, 2010, Gotman and Reiner, 2010). Although these materials are non-resorbable they can be engineered to closely mimic the load-bearing properties (e.g. stiffness and elasticity) of natural bone. In this context, Gotman and colleagues developed an approach to generate trabecular Nitinol (tNiTi) scaffolds of varying size (Gotman, 2010). With an average pore size of 150 – 350 µm and a porosity of 87% these scaffolds exhibit a structure that is comparable to the trabecular structure of spongious bone which is characterized by pore sizes of up to 1 mm and a porosity of 50 - 90% (Keaveny et al., 2001, Karageorgiou and Kaplan, 2005). Similarly, tNiTi scaffolds could be successfully engineered to provide an elasticity modulus in range comparable to natural bone (Gotman, 2010). In *in vitro* experiments using human MSC tNiTi scaffolds were shown to allow for cell adherence and cytocompatibility (Gotman, 2010). The same report demonstrated that tNiTi supported the osteogenic differentiation of MSC under static conditions (Gotman, 2010). Although the release of Nickel (Ni) ions was shown by other reports to induce cytotoxicity and oxidative stress in human cells (Chen et al., 2003, Kanaji et al., 2014) no inhibitory effects of Ni ion release from tNiTi scaffolds were detectable, neither in terms of MSC proliferation nor in connection to MSC osteogenesis (Gotman, 2010). Based on these facts tNiTi is a promising candidate for applications in bone tissue engineering using human MSC. Since to date the supportive function of tNiTi (as processed by Gotman and colleagues) on the osteogenic differentiation was only evaluated under static conditions (Gotman, 2010) one important aim of the present study was to investigate the osteogenesis of MSC on tNiTi scaffolds under dynamic conditions using a perfusion bioreactor system.

1.7 Cocultures in bone tissue engineering

With respect to the complex interplay of various cell types in a growing or healing tissue the communication of these cell types either in an autocrine or in a paracrine fashion becomes a major focus point. Due to the multicellular environment in the regenerative niche it is known that paracrine signaling generates the release of e.g. growth factors (GFs), which can be recognized and bound by specific receptors that are expressed on the membrane of another cell type, thus inducing receptor phosphorylation, intracellular signaling and the induction of a biological response (Einhorn and Gerstenfeld, 2015, Forbes and Rosenthal, 2014, Gurtner et al., 2008). Because of the variety of different cell types in a growing or healing tissue it is technically highly complex, if not impossible, to examine the exact gene expression

and protein release profile of a single cell type *in vivo* (Kirkpatrick et al., 2011). Furthermore, the physiological situation represents a non-steady and constantly changing environment of GFs, cytokines and chemokines further complicating the identification of factors that induce a certain phenotype (Kirkpatrick et al., 2011). For these reasons the investigation of all cell types of a tissue of interest under highly controlled conditions *in vitro* is an attractive tool to overcome the limitations present *in vivo*. However, the importance of direct cell-cell contacts as well as the release of gene products in a paracrine manner is underestimated in such cell culture models (Kirkpatrick et al., 2011). Therefore, co-culture models were developed to circumvent the obstacles mentioned above.

By studying at least two different cell types in direct contact or non-direct contact models various biological functions and signaling pathways could be investigated in more detail (Kirkpatrick et al., 2011, Chen et al., 2015, Freese et al., 2014, Sterneckert et al., 2014, Seton-Rogers, 2013). In bone tissue engineering co-culture models are used to study for instance the function and communications of osteoblasts with osteoclasts (Heinemann et al., 2011, Marino et al., 2014) or the formation and maturation of vascular structures in a bone tissue engineering context (Dohle et al., 2014, Dohle et al., 2010, Fuchs et al., 2007, Fuchs et al., 2009b, Unger et al., 2010, Unger et al., 2005, Unger et al., 2007). The vascular network formation is well understood and details in cellular communication were described by many reports using co-culture models (extensively reviewed in (Unger et al., 2015)). However, when following a tissue engineering approach the technical requirements of such a co-culture system have to be considered (Kirkpatrick et al., 2011). In this context, it is well known that the cell seeding ratios (CSR) and thus the corresponding cell seeding densities (CSD) of each cell type (McBeath et al., 2004), the medium composition (Govindasamy et al., 2010) and the experimental duration (Medyouf et al., 2014) clearly affect gene expression, protein expression and by this autocrine and paracrine signaling thus driving general biological processes like angiogenesis (Kirkpatrick et al., 2011).

Unger and colleagues investigated the formation of vessel-like structures *in vitro* using co-culture models of primary human osteoblasts (pOB) with human dermal microvascular EC (HDMEC) using a CSR (pOB:HDMEC) of 1:6 or 1:4 with varying absolute cell numbers (Unger et al., 2010, Unger et al., 2005, Unger et al., 2004, Unger et al., 2007). In co-cultures of pOB with outgrowth endothelial cells (OEC) derived from peripheral blood Fuchs and colleagues co-cultivated 0.3 x 10^6 pOB with 0.2 x 10^6 OEC (Fuchs et al., 2009a, Fuchs et al., 2007, Fuchs et al., 2009b). Similar CSD and a constant CSR of 3:2 were applied in studies conducted by Dohle et al. and Kolbe et al. using CC models of pOB with OEC and MSC with OEC, respectively (Dohle et al., 2014, Dohle et al., 2010, Dohle et al., 2011, Kolbe et al., 2011). Other studies used CSR (MSC:EC) of 1:1, 1:4 or 4:1 as well as 1:5 in CC models of HUVEC with MSC (Leszczynska et al., 2013) or microvascular EC with MSC (Freiman et al., 2016), respectively. Similar to the above-mentioned studies the

applied absolute cell numbers of each cell type were varied in the same manner. Most importantly, the CSR are of major influence on the paracrine signaling since it was demonstrated that cells, for example, respond in a dose-dependent manner to the local release of GFs like VEGF (Ozawa et al., 2004a). This suggests that the released level of different GF and cytokines create a certain therapeutic window allowing for an optimal stimulation of a specific biological process. Thus, it was shown by Lobov and colleagues that the release of angiopoietin-2 (Ang-2) next to VEGF is essential for the induction of angiogenesis *in vivo* but that vessel regression is obtained once VEGF secretion is decreased or diminished (Lobov et al., 2002). Similarly, it is known that angiopoietin-1 (Ang-1) and Ang-2 compete for binding to the Tie2 receptor, thus enabling either vessel stabilization or a proangiogenic stimulus (Asahara et al., 1998, Bogdanovic et al., 2006). Finally, different level of GF or cytokines released to the CC will be detected by a certain amount of binding sites defined by the number of specific receptors expressed by a certain cell type incorporated at a certain CSD (Rizzino et al., 1988) in the CC model. A dose-optimal relation of CSD of MSC and EC as well as their support of vessel formation was also investigated in the present study.

Nevertheless, when CC systems are established, the choice of the correct cell culture medium is an important parameter that has to address the different cell types in terms of metabolism, cell signaling and protein secretion (Kirkpatrick et al., 2011, Kolbe et al., 2011). Often, the cell culture medium is optimized towards the support of the more sensitive cell type (Kirkpatrick et al., 2011) e.g. EC in CC of EC with MSC or pOB (Dohle et al., 2010, Fuchs et al., 2007, Kolbe et al., 2010, Unger et al., 2007). Moreover, cell culture media often have to be supplemented with external GFs to allow for the stimulation of diverse cellular processes. By using *in vitro* CC systems of HUVEC or HDMEC with pOB it was shown by Santos and colleagues that a basal EC medium without external supplementation of GF like VEGF or bFGF is sufficient to support vascular network formation (Santos et al., 2007, Santos et al., 2009). However, osteogenic differentiation as an important element of vascularized osteogenic tissue constructs was not investigated in these studies. To induce osteogenic differentiation of MSC the corresponding media are supplemented with dexamethasone (Dex), βGP and ascorbic acid (AA) (Pittenger et al., 1999). Thus, the impact of these factors on EC has to be considered in the corresponding CC models, especially on the level of GF secretion. By simple combination of the EC media EGM2 with the pro-osteogenic factors Dex and βGP, Pedersen and colleagues demonstrated the formation of tube-like structures and the deposition of a calcified matrix in a CC model of HUVEC with MSC cultivated for 2 Wk (Pedersen et al., 2012). Similarly, Correia et al. described the formation of tube-like structures and the expression of osteogenesis-related proteins like bone-sialoprotein (BSP) in a CC model of HUVEC with MSC (Correia et al., 2011). However, both studies do not provide insights into the dynamics of extracellular matrix calcification or changes in GF signaling following induction of osteogenesis in MSC. Most importantly, the

supplemented osteogenic factors as well as their applied concentrations were demonstrated to exhibit negative effects on the formation of vascular structures.

In this context, DiMarco and colleagues demonstrated a negative influence of inorganic phosphate (P_i) concentrations above 2.5 mM on the angiogenic potential of EC (Di Marco et al., 2008, Di Marco et al., 2013). In human peripheral blood level of P_i above 1.5 - 2 mM were linked to artherosclerosis (Lanzer et al., 2014, Lau et al., 2010, Nishizawa et al., 2005). Although βGP is an organic source of phosphate its conversion to P_i is driven by the ALP (Ahlers, 1975, Bellows et al., 1991, Bellows et al., 1992), which is increasingly expressed and active during the osteogenic differentiation of MSC (Vanstraalen et al., 1991). Therefore, it is very likely that a high level of organic phosphate supplementation generates elevated level of P_i. Additionally, increased level of P_i were demonstrated to be pro-apoptotic in EC (Di Marco et al., 2008) and discussed to induce non-specific cellular calcification following apoptosis (Langenbach and Handschel, 2013) as well as spontaneous precipitation of calcium phosphates (Schack et al., 2013, Tenenbaum and Heersche, 1982). However, the apoptotic effect of phosphate supplementation can be “buffered” by the supplementation of Dex on the one hand, which will restrict vascularization and angiogenesis on the other hand. It is known that Dex exhibits an anti-apoptotic and anti-inflammatory stimulus on various cell types *in vitro* and *in vivo* (Bailly-Maitre et al., 2001, Makrydima et al., 2014, Messmer et al., 2000, Newton et al., 2002). Nevertheless, Logie at al. showed that Dex supplementation inhibits angiogenic changes in EC by binding to the glucocorticoid receptor (GR) and thus decreasing the responsiveness of EC to VEGF (Logie et al., 2010). Moreover, Dex supplementation was demonstrated to reduce the expression of VEGF by bone marrow stromal cells in a time-dependent fashion (Guzman-Morales et al., 2009) therefore potentially decreasing their pro-angiogenic capacity. These facts have to be taken carefully into account in CC models of EC with MSC that address the stimulation of angiogenesis and osteogenesis in the same system.

Moreover, it is noteworthy that extensively supplemented EC media like EGM2 (Lonza) often include VEGF, basic fibroblast growth factor (bFGF), epidermal growth factor (EGF), insulin-like growth factor (IGF) and heparin, which will externally stimulate angiogenesis on the one hand, but very likely “mask” autocrine and paracrine signaling between the incorporated cell types and potentiate a certain biological response on the other hand. This has to be considered, depending on whether a therapeutic approach or a certain cellular signaling function is in the main focus of research. Furthermore, extrinsic stress factors like excessive GF supplementation are known to induce unwanted cellular responses like cellular senescence (Tominaga, 2015, Campisi and d'Adda di Fagagna, 2007). Therefore, a cell culture media that enables and supports the basic cellular crosstalk within the CC model might be favorable. As mentioned earlier, Santos and colleagues demonstrated the formation of vascular structures in CC models of HDMEC with osteoblastic cells in the complete absence of external GF like VEGF or bFGF

(Santos et al., 2007, Santos et al., 2009). This study highlights the angiogenic capacity of paracellular crosstalk in these models. Due to unspecific side effects in a physiological environment (Sullivan et al., 1998, Collantes and Younossi, 2005, Bommer et al., 1987), external GF supplementation is critical in a therapy-relevant context. Therefore, the present study focused on the development of a sequential medium strategy, based on minimal GF supplementation to address angiogenesis and osteogenesis in a common CC system.

1.8 Aim of the study

The development of new candidate materials and strategies for the enhancement of prevascularization, osteogenic differentiation and osteo-integration are key points for the establishment of successful bone tissue engineering (BTE) strategies. It is well known that 3D biomaterials exhibit an increased ingrowth and bone regeneration capacity upon implantation *in vivo* when pre-seeded with stromal precursor cells. The same is true for 3D scaffolds that carried an *in vitro* pre-formed vascular bed. It is thus likely that a therapeutic approach which would combine the osteogenic potential of pre-seeded osteogenic precursor cells with a pre-formed vascular bed might be a promising strategy to enhance the osteo-regenerative capacity of 3D biomaterials. Therefore, the aim of the present study was to develop the basis for a perfusion-based 3D CC model that allows for the generation of prevascularized and osteogenically primed tissue engineering constructs. Based on previously published results (Gotman et al., 2013) the osteogenic differentiation of MSC was evaluated under dynamic conditions on 3D tNiTi scaffolds using a state-of-the-art technology. 3D tNiTi scaffolds permit osteogenic differentiation of MSC under static conditions and represent a promising candidate material for BTE applications, based on their bone-mimicking properties. The present study aimed to transfer the obtained results to a CC of MSC with EC with a view to investigate the possibility of simultaneously stimulating osteogenesis and angiogenesis. CC systems exhibit complex autocrine and paracrine signaling and represent a multiparametric complex in which different parameters are affected in a multi-dimensional way. To identify key parameters and characterize their functional ranges a scaling-down from 3D to 2D was performed. This should allow a screening of medium in order to identify single factor interactions in a simultaneous stimulation approach, while excluding gradients and mechanical stimuli occuring in a dynamic 3D microenvironment. In addition, further studies were aimed at investigating a sequential approach, in which the osteogenic differentiation of MSC and the induction of vascular network formation were sequentially stimulated in a manner similar to the sequential phases of the fracture healing process *in vivo*. These studies have demonstrated that the paracellular crosstalk of MSC with EC can be manipulated using a sequential tissue engineering approach, in order to generate prevascularized osteogenic tissue constructs *in vitro* in short time periods of cell culture.

2 Materials & Methods

2.1 Materials

2.1.1 Devices

Table 1: Devices

Devices	Model	Company
Analytical balance	AI205	Sartorius
Balance	LC420	Sartorius
Cell counter	CASY – TTC	Roche
Cell culture incubator	C200	Labotect
Centrifuge	Megafuge 1.0	Heraeus
Flow cytometer	FACSCalibur	BD Biosciences
Microplate reader	GENios Plus	Tecan
Freezing container	Mr. Frosty	Nalgene
Handoperator	Vacuboy	ibs|tecnomara
Hand pipettes	0.2 µL – 1000 µL	Gilson
Heating cabinet		Thermo Scientific
Liquid nitrogen tank	MVE Cryosystem 3000	German-Cryo
Magnet	Dynal MPC-1	Dynal Biotech
Microcentrifuge	120	Hettich Zentrifugen
Microcentrifuge	Galaxy Mini	VWR
Microplate washer	Hydro Control	Tecan
Multipipette	Plus	Eppendorf
Neubauer chamber	Neubauer improved	Marienfeld
pH-meter	Inolab pH 730	WTW
Pipette aid	Pipetboy	Integra Biosciences
Power supply	Power pac 3000	Bio-Rad
Rolling mixer	RM5	Karl Hecht GmbH
Shaker	UNIMAX1010	Heidolph
Steam sterilizer	Varioklav Typ 500	HP Labortechnik
Sterile hood	LaminAir® HB2448	Heraeus
Sterilizer	Type 18115300002020	WTC Binder
Perfusion bioreactor	U-CUP	Cellec Biotek
Vacuum system	Vacusafe	ibs|tecnomara
Vortexer	Vortex Genie-2	Scientific Industries
Waterbath		Medingen

2.1.2 Microscopes

Table 2: Microscopes

Model	Company
BZ-9000 Widefield Microscope	Keyence
CTR6000 Widefield Microscope	Leica
TCS SP2 Confocal microscope	Leica
M205 FA Stereo Microscope	Leica
Eclipse TS100	Nikon
ESEM Quanta 200 FEG	FEI
EDX INCA 350 Energy	Oxford Intruments

2.1.3 Consumables

Table 3: Consumables

Consumable	Company
1.5 ml, 2 ml safelock tubes	Eppendorf, Hamburg
24-well Transwell® systems	Corning, Chelmsford St. Lowell
25 cm^2, 75 cm^2 cell culture flasks	Greiner bio-one, Frickenhausen
15 ml, 50 ml tubes	Greiner bio-one, Frickenhausen
5 ml Polystyrene Round-Bottom Tube (FACS Tubes)	Corning
12-, 24-, 96-well cell culture plates	TPP, Trasadingen
12-, 24-, 96-well cell culture plates	Greiner bio-one, Frickenhausen
Bare Cannula	BD
Cell Strainer	BD Falcon
Combitips Plus® 2.5 mL, 5 mL, 10 mL	Eppendorf
Cover slips, 24x50mm	Menzel, Braunschweig
Cryovials	Nalgene, Rochester
Cryo Babies®	Diversified Biotec
Glass pasteur pipettes	VWR
Interlink system injection site	Baxter Healthcare
Lab Gloves	Semper Care
Nunc MaxiSorp® flat-bottom 96-well plates	Thermo Scientific, Bonn
Nunc Thermanox™ coverslips	Thermo Scientific, Bonn
Parafilm	Bemis Felxible Packaging
Pipet tips	Greiner bio-one, Frickenhausen
Scalpels	Braun, Tuttlingen
Serological pipettes 2.5 mL, 5 mL, 10 mL, 25 mL	Greiner bio-one, Frickenhausen
Syringes Omnifix 3 mL, 10 mL	Braun
Syringe filters 0.2 µm	Nalgene, Rochester
U-CUP Disposable bioreactor	Cellec Biotek AG
U-CUP scaffold adaptors 8 mm	Cellec Biotek AG
Waste bags	Roth GmbH

2.1.4 Chemicals

Table 4: Chemicals

Chemical	Company
Aqua dest	Braun
Acetone	Riedel deHäen
Acetic acid	Riedel deHäen
Alcian blue	Chroma
Ascorbic acid 2-phosphate	Sigma-Aldrich
β-glycerol phosphate	Sigma-Aldrich
BSA fraction V	GE Helathcare
Dexamethasone	Sigma-Aldrich
Diethanolamine	Sigma-Aldrich
EDTA	Sigma-Aldrich
Ethanol 100 %	Roth GmbH
FACS Clean Solution	BD Biosciences, Franklin Lakes
FACS Rinse Solution	BD Biosciences, Franklin Lakes
FACSFlow™	BD Biosciences, Franklin Lakes
Fluoromount-G™	Southern Biotech, Birmingham
HEPES	Sigma-Aldrich, St. Louis
Hoechst 33342	Sigma-Aldrich, St. Louis
Methanol	Fisher Scientific
NaCl	Merck, Darmstadt
NaOH	Sigma-Aldrich
Oil Red O	Sigma-Aldrich
PFA	Merck, Darmstadt
Phalloidin-TRITC	Sigma-Aldrich
p-nytrophenol	Sigma-Aldrich
p-nytrophenyl phosphate	Sigma-Aldrich
Sodium thiosulfate	Merck-Millipore
Silver nitrate	Merck-Millipore
Triton X-100	Sigma-Aldrich, St. Louis
Tween20	Serva, Heidelberg

2.1.5 Kits

Table 5: Kits

Kit	Application	Company
BCA Protein Assay Kit	Protein Quantification	Pierce
Osteogenesis Quantitation Kit	Alizarin Red staining + Quantification	Millipore
Leucocyte Alkaline Phosphatase Kit	Alkaline phosphatase activity staining	Sigma-Aldrich
VEGF DuoSet Kit	ELISA	R&D Systems
Angiopoietin-1 DuoSet Kit	ELISA	R&D Systems
Angiopoietin-2 DuoSet Kit	ELISA	R&D Systems
BMP-4 DuoSet Kit	ELISA	R&D Systems
Sircol Collagen Assay	Quantification of total collagen	Biocolor
Calcium OCP 1+1 Kit	Quantification of calcium	Axiom Diagnostic
AnnexinV Apopotosis Detection Kit	Detection of apoptotic cells	BD Pharmigen

2.1.6 Histochemical solutions

Von Kossa staining solution
5 % silver nitrate in dH_2O, sterile filtered, protected from light

Thiosulfate solution
5 % thiosulfate in dH_2O, sterile filtered, protected from light

ALP fixing solution (ALP activity staining)
2.5 mL citrate solution (Leucocyte Alkaline Phosphatase Kit, Sigma-Aldrich), 6.5 mL acetone, 0.8 mL 37 % formaldehyde

ALP activity staining solution
0.1 mL alkaline Fast-Red-Violet solution (Leucocyte Alkaline Phosphatase Kit, Sigma-Aldrich), 0.1 mL sodium nitrite solution (Leucocyte Alkaline Phosphatase Kit, Sigma-Aldrich), 2 min incubation, 4.5 mL dH_2O; 0.1 mL alkaline naphtol AS-BI solution (Leucocyte Alkaline Phosphatase Kit, Sigma-Aldrich)

Alcian blue solution
1% alcian blue in 3% acetic acid, sterile filtered, protected from light

2.1.7 Buffers

Table 6: Buffers and working solution

Buffer/Working solution	Composition	Application
CS buffer	0.1 M PIPES 1 mM EGTA 4 % PEG 0.4 % NaOH pH 6.9	3.7% PFA
PBS 20x	160 g NaCl 4 g KCl 4 g KH_2PO_4 ad 1 l H_2O working solution pH 7.2 wash buffer: + 0.05% Tween20	ELISA
Reagent Diluent	1 x PBS 1 % BSA pH 7.2 – 7.4	ELISA
RIPA Buffer	150 mM NaCl 1 mM EDTA 1 % sodium deoxycholate 0.1 % SDS 1 % TRITON X-100 1 mM PMSF 1:1000 protease inhibitor	Isolation of protein
Buffy Coat Buffer	2.5 ml FCS 2ml EDTA (2mM) adjust to 1 L PBS	Isolation of OEC
ALP substrate buffer	1M diethanolamine pH 9.8 (HCl) protected from light	ALP activity assay
ALP substrate solution	0.2 % p-nytrophenyl phosphate In ALP substrate buffer	ALP activity assay
ALP stop solution	2 M NaOH 0.2 mM EDTA	ALP activity assay

2.1.8 General cell culture media

Table 7: General cell culture media

Medium	Company	Supplements
Endothelial Cell Basal Medium MV (ECBM)	PromoCell	15% FCS 100 U/ml / 1+00 µg/ml P/S 28 mM HEPES
Endothelial Cell Growth Medium MV (ECGM)	PromoCell	15% FCS 100 U/ml / 1+00 µg/ml P/S 28 mM HEPES 10 mg/ml sodium heparin 2.5 ng/ml bFGF
Endothelial Cell Basal Medium-2 + BulletKit (= Endothelial Cell Growth Medium EGM2)	Lonza	10 ml FBS, 0.2 ml Hydrocortisone, 2 ml hFGF, 0.5 ml VEGF, 0.5 ml IFG-1, 0.5 ml ascorbic acid, 0.5 ml hEGF, 0.5 ml Heparin (supplements from the kit) + 25 ml FCS, 5 ml P/S
Medium 199	Sigma-Aldrich	100 U/ml / 100 µg/ml P/S
DMEM/F12, GlutaMAX	Gibco	10 % FCS 1 % P/S
αMEM, GlutaMAX	Gibco	αMEM, GlutaMAX 10 % FCS 1 % P/S
StemPro osteogenic differentiation medium	Gibco	Osteogenic supplements
StemPro adipogenic differentiation medium	Gibco	Adipogenic supplements
StemPro chondrogenic differentiation medium	Gibco	Chondrogenic supplements

2.1.9 Special cell culture media

Table 8: Special cell culture media

Special Medium	Supplements
MSC expansion medium	DMEM/F12, GlutaMAX 10 % FCS 1 % P/S
Basal medium (Basal)	αMEM, GlutaMAX 10 % FCS 1 % P/S
Osteogenic differentiation medium (ODM)	αMEM, GlutaMAX 10 % FCS 1 % P/S 100 nM dexamethasone 10 mM β-glycerol phosphate 50 µM ascorbic acid 2-phosphate
ODM-Dex	αMEM, GlutaMAX 10 % FCS 1 % P/S 10 mM β-glycerol phosphate 50 µM ascorbic acid 2-phosphate
ODM-βGP	αMEM, GlutaMAX 10 % FCS 1 % P/S 100 nM dexamethasone 50 µM ascorbic acid 2-phosphate

2.1.10 Cell culture solutions

Table 9: Cell culture solutions

Solution	Company
Albumin solution, 35% in DPBS	Sigma-Aldrich
bFGF	Sigma-Aldrich
Collagen type I, rat tail	BD Biosciences,
DMSO	Sigma-Aldrich
Dulbecco´s phosphate buffered saline	Sigma-Aldrich
Dynabeads®CD31	Invitrogen
Fetal calf serum	Sigma-Aldrich
Fibronectin	Roche
Gelatin	Sigma-Aldrich
GlutaMAX-I	Gibco
Penicillin/Streptomycin mix	PromoCell
Sodium heparin	Sigma-Aldrich
Versene	Gibco

2.1.11 Primary human cells

Table 10: Primary human cells

Abbreviation	Type	Origin / Source
MSC	Mesenchymal stromal/stem cells	Trabecular bone/ Femoral head
OEC	Outgrowth endothelial cells	Peripheral blood
HDMEC	Human dermal microvascular endothelial cells	Human foreskin
HUVEC	Human umbilical vein endothelial cells	Umbilical vein

2.1.12 Cell lines

Table 11: Cell lines

Abbreviation	Type	Origin / Source
ISO-HAS-1	Human endothelial cell line	Human hemangiosarcoma / Unger et al. 2002

2.1.13 Enzymes

Table 12: Enzymes

Enzyme	Company
Accutase	PromoCell
Versene	Gibco
Dispase	Gibco
Streptavidin-HRP	Amersham Pharmacia Biotech
Trypsin 2.5%	Gibco
Trypsin-EDTA 0.25%	Gibco
Collagenase (fr. *clostridium histolyticum*)	Sigma-Aldrich

2.1.14 Primary antibodies

Table 13: Primary antibodies

Antibody	Company	Dilution	Application	Cat.No.
Mouse anti-human Collagen type IV	Sigma-Aldrich	1:50	IF	C1926
Mouse anti-human Laminin	Sigma-Aldrich	1:50	IF	L8271
Mouse anti-human CD31	Dako	1:50	IF	M0823
Rabbit anti-human vWF	Dako	1:500	IF	A008202
Rabbit anti-human Collagen type I	Meridian Life Science	1:50	IF	T40103R
Rabbit anti-human Collagen type I	GeneTex	1:50	IF	GTX41286

2.1.15 Secondary antibodies

Table 14: Secondary antibodies

Antibody	Company	Dilution
Alexa Fluor®488 donkey anti-goat	Invitrogen, Carlsbad	1:1000
Alexa Fluor®488 donkey anti-rabbit	Invitrogen, Carlsbad	1:1000
Alexa Fluor®488 goat anti-mouse	Invitrogen, Carlsbad	1:1000
Alexa Fluor®546 goat anti-rabbit	Invitrogen, Carlsbad	1:1000

2.1.16 Antibodies for flow cytometry

Table 15: Antibodies for flow cytometry

Antigen	Fluorophore	Company
CD105	FITC	Miltenyi Biotec
CD34	FITC	Miltenyi Biotec
CD11b	FITC	eBioscience
HLA-DR	APC	Miltenyi Biotec
CD45	FITC	Miltenyi Biotec
CD73	APC	Miltenyi Biotec
CD90	FITC	Miltenyi Biotec
CD31	APC	Miltenyi Biotec
CD146	FITC	Miltenyi Biotec
CD146	PE	Becton/Dickinson
CD44	FITC	Miltenyi Biotec
CD29	APC	Miltenyi Biotec
CD29	PE	Becton/Dickinson
CD19	APC	Miltenyi Biotec

2.1.17 Isotype controls for flow cytometry

Table 16: Isotype controls for flow cytometry

Isotype	Fluorophore	Company
IgG1	FITC	Miltenyi Biotec
IgG1	APC	Miltenyi Biotec
IgG1	PE	Becton/Dickinson
IgG1	FITC	eBioscience
IgG2a	FITC	Miltenyi Biotec
IgG2a	APC	Miltenyi Biotec

2.1.18 Software

Table 17: Software

Software	Company
ImageJ 1.47n	National Institute of Health, Bethesda, MD, USA
FIJI	Open Source
GraphPad Prism 5.01	GraphPad Software Inc., La Jolla, CA, USA
Photoshop CS5 12.0 x64	Adobe Systems GmbH, München, Germany
CellQuestPro	BD Biosciences, Heidelberg, Germany
Microsoft Excel	Microsoft, Redmond, WA, USA

2.2 Methods

2.2.1 General cell culture

2.2.1.1 Cultivation of cells

For all experiments in the present thesis MSC, OEC, HUVEC and HDMEC were isolated from human bone marrow, peripheral blood, umbilical cord and foreskin, respectively, following established protocols (Fuchs et al., 2006, Jaffe et al., 1973, Kolbe et al., 2011, Peters et al., 2002). All cells were isolated according to the guidelines of the local ethics commission for informed consent. The entire cell culture-related workflow as well as all cell culture-related experiments were performed under sterile conditions in laminar flow work benches. All solutions and cell culture-related objects were either sterilized at 121℃ and 2 bar for 20 minutes in an autoclave, at 180 ℃ for 30 minutes in a hot air oven or filtered through 0.2 µm sterile filters prior to its use, if not delivered sterile from the manufacturer. All cell culture experiments were performed under standard conditions at 37℃, 5 % CO_2 saturation and 95 % humidity in a CO_2 incubator. The cell cultures were continuously monitored microscopically and only used if free of visual contamination and following phenotypic characterization (see below).

2.2.1.2 Passaging of cells

For further studies, the various endothelial cells were harvested at a confluence of 90 to 100 % and MSC when cells had reached a confluence of approximately 80 %. For this, cells were trypsinized by incubation in 1 mL trypsin/EDTA mixed with 1 mL of PBS for 5 minutes at 37℃. The process was controll ed by microscopic observation. After complete cell detachment, trypsin was inactivated by adding PBS containing 10 % FCS. The cell suspension was transferred into 15 mL Falcon tubes and centrifuged at 400 x g for 5 minutes. The cells were resuspended in cell-type specific cell culture medium (Table 18) and were then seeded into uncoated (MSC) or coated (HDMEC: gelatin; OEC: fibronectin; HUVEC: gelatin; ISO-HAS-1: uncoated) T75 flasks. Passaging was performed using cell type-specific splitting ratios (Table 18).

Table 18: Summary of cell type specific culture conditions

Cell Type	Coating	Medium	Splitting Ratio	Range of Passages
bmMSC	uc	ExpM	1:4	3-6
HDMEC	Gelatin	ECGM	1:3	Max. P3
OEC	FN	EGM-2	1:3	5-20
HUVEC	Gelatin	M199	1:3	Max. P3
ISO-HAS-1	uc	ECGM	1:3	20-50

2.2.1.3 Freezing, long-term storage and thawing of cells

First, cells were harvested by trypsinization, washed in PBS containing 10 % FCS and centrifuged at 400 x g for 5 minutes. To avoid cell damage due to ice crystal formation the cell pellet was resuspended in freezing medium consisting of 10 % DMSO and 90 % FCS and transferred into cryogenic vials. For a controlled cooling-down the cryogenic vials were stored in a Mr. Frosty Freezing Container, guaranteeing a constant freezing rate of -1°C/minut e. After keeping the container at -80°C for additional 24 h the vials were transferred into liquid nitrogen for long-term storage at -196°C. Frozen cells were thawed by rapi dly placing the cryogenic vials after removal from liquid nitrogen into a 37°C water bath for two minutes and transferring the thawed cell suspension into 15 mL Falcon tubes containing preheated medium. The suspension was subsequently centrifuged at 400 x g for 5 minutes. The supernatant was discarded and the cell pellet was resuspended in fresh expansion medium (cell-type specific; see Table 18). Following this, the cell number was determined using a hemocytometer. Dead cells were excluded using the dye exclusion method. Generally, 100 µL of the cell suspension were mixed with 150 µL PBS and 250 µL of a 0.4 % trypan blue staining solution to give a final 1:5-dilution of the suspension. Cells were incubated in this suspension for 5 minutes at room temperature in order to allow for penetration of the trypan blue into dead cells. The total number of viable cells was calculated using Equation 1. The cells were seeded at a density of 10.000 cells/cm^2 in uncoated T75 flasks. Medium was replaced every second to third day.

Equation 1:

$$\text{Total number of viable cells per mL} = \frac{\text{cells of four large squares}}{4} \times \text{dilution} \times 10^4$$

2.2.2 Isolation of primary human cells and cell lines

2.2.2.1 Mesenchymal stem cells (MSC)

Primary human mesenchymal stem cells were isolated from cancellous bone fragments of the femoral head of patients that underwent hip transplantation at the Zentrum für Orthopädie und Unfallchirurgie at the University Medical Center, Mainz, Germany. All cells were isolated from healthy male or female donors between the ages of 20 to 90 years according to the ethical guidelines of the University Medical Center Mainz. First, the femoral head was washed three times in PBS, supplemented with 1 % P/S and transferred into a 15 cm petri dish containing fresh DMEM/F-12-GlutaMAX® medium, supplemented with 20 % FCS and 1 % P/S. From the center region of the femoral head small bone fragments were pinched off using a bone rongeur. The bone fragments were transferred into a 50 mL falcon tube using a sterile forceps and washed three times with PBS containing 1 % P/S to wash out

bone marrow associated cells. All PBS used was collected in 50 mL Falcon tubes and subsequently filtered through a cell strainer with a pore size of 40 µm. The filtered PBS containing small matrix fragments and sheared off cells was centrifuged at 400 x g for 5 minutes. Afterwards the supernatant was discarded and the remaining cell pellet was resuspended in DMEM/F-12-GlutaMAX® (20 % FCS, 1 % P/S). The total cell number was determined using a hemocytometer. The cells were subsequently seeded into uncoated T75 flasks at a density of 10,000 cells/cm^2. Medium exchange was performed every day until the first passage using DMEM/F-12-GlutaMAX® supplemented with 20 % FCS, 1 % P/S and 5 ng/mL bFGF in passage 0. When reaching passage 1 the concentration of FCS was reduced to 10 % while keeping the other supplements constant. After this, medium was changed every second or third day.

2.2.2.2 Dermal microvascular endothelial cells (HDMEC)

Primary HDMECs were isolated according to the ethical guidelines of the University Medical Center Mainz from explanted foreskin. The biopsy specimen was first washed two times with sterile PBS, whereby large blood vessels and connective tissue were removed with scissors and forceps, until finally the skin sample was flattened. Following this preliminary purification, the skin was cut into small pieces of approximately 2 x 2 mm size and transferred into a 15 mL Falcon tube. Five milliliter of a 2,36 U/mL dispase solution were added to the Falcon tube. The segments were incubated overnight at 4℃. The next day the dispas e solution was discarded and the foreskin pieces were transferred into a sterile dish and the epidermis was removed using a sterile forceps. The remaining dermis pieces were transferred into a new 50 mL Falcon tube and covered with 5 mL of a 0,48 mM Versene solution containing 80 µL of a 2,5 % trypsin solution. The cap of the Falcon tube was tightly sealed with parafilm, after which the tube was incubated for 2 h at 37℃ in a water bath to further digest the tissue samples. The digestion was stopped by adding 2 mL FCS to the tube and adding sterile PBS to a total volume of 40 mL. The resulting suspension containing separated cells and tissue fragments was transferred to a sterile dish, where the fragments were squeezed with the back end of a sterile syringe to remove additional cell material. The suspension was filtered through a 100 µm cell strainer to remove remaining tissue fragments. The filtered cell suspension was centrifuged for 5 minutes at 1200 rpm at room temperature. The resulting cell pellet was resuspended in 10 mL endothelial cell growth medium (ECGM, Endothelial Cell Basal Medium + 15 % FCS, + 1 % Penecillin/Streptomycin, + 10 µg/mL sodium heparin, + 2,5 ng/mL bFGF) and plated onto a gelatin coated T75 cell culture flask. This stage was referred to as passage 0 (P0). To allow for cell attachment the flask was incubated at standard cell culture conditions (5 % CO2, 37℃, 95 % humidity) for 24 h. Following this phase, the medium was changed. The cells were cultivated until a confluent monolayer of endothelial cells grew out and exhibited a typical cobblestone-like morphology. In parallel, the medium was changed every 4 to 5 days.

2.2.2.3 Outgrowth endothelial cells (OEC)

OEC were isolated from peripheral blood buffy coats collected from healthy male or female donors of varying age donated by the Transfusionszentrale der Universitätsmedizin Mainz, Germany. The mononuclear cell fraction was first separated by density gradient centrifugation from the peripheral blood. For this, 15 mL of Ficoll® solution with a specific density of 1.077 g/mL were transferred into a 50 mL Falcon tube and carefully overlayed with 35 mL of the buffy coat mix. The buffy coat mix was prepared by diluting blood from the buffy coat in buffy coat buffer (PBS + 0.5 % FCS + 2 mM EDTA) in a proportion of 1:2. Subsequently the overlay was centrifuged at 400 x g for 35 minutes at room temperature with the brake kept off. The process resulted in an orientation of the cell fractions along the density gradient, in which the erythrocytes and granulocytes are found on the bottom of the Falcon tubes, followed by the Ficoll® phase, the whitish interphase and the phase of remaining plasma mixed with buffer on top. The plasma-buffer phase containing thrombocytes was discarded, whereas the interphase containing the mononuclear cell fraction (the whitish interphase) was carefully removed and transferred to a new Falcon tube. The cells were washed in 50 mL PBS and centrifuged at 400 x g for 10 minutes. The washing step was repeated two times. The remaining cell pellet was finally resuspended in endothelial cell growth medium (EGM2) containing the supplements from the kit, 5 % FCS and 1 P/S. From the cell suspension the cell number was determined using a hemocytometer. Following this, 5 x 10^6 cells per well were seeded on collagen I-coated (10 µg/mL) 24-well cell culture plates and cultivated under cell culture conditions. Medium exchange was performed every second day. After one week of cultivation the cells were detached by trypsinization, washed and seeded at a density of 0.5 x 10^6 cells per well on fresh fibronectin-coated (10 µg/mL) 24-well cell culture plates and cultivated further for 2 to 3 weeks. During this cultivation phase colonies of late outgrowth endothelial cells with a typical cobblestone-like morphology developed. These colonies were finally detached, pooled and re-seeded onto fibronectin-coated 24-well cell culture plates for expansion. The passaging of OEC was continued at a splitting ratio of 1:2 until the desired cell number was reached. Outgrowth endothelial cells of passage 5 to 20 were used in the studies.

2.2.2.4 Umbilical vein endothelial cells (HUVEC)

HUVECs were isolated from the veins of umbilical cords (UC) by enzymatic digestion. The UC were obtained after delivery and placed in transport buffer consisting of HEPES buffer supplemented with 1% (Pen/Strep), 1 % Ciprofloxacin Kabi and 1% Fungizone. The isolation of HUVEC from UC was done within 4d. Initially, the transport buffer was discarded and residues of blood were removed from the UC. Small slices were removed from both ends of the UC using a sterile scalpel and subsequently a blunt cannula was inserted into the center of the UC. Following this, the UC was flushed three times with HEPES buffer using a sterile syringe and

afterwards filled with enzymatic solution (0.05 % collagenase type I in HEPES buffer) using a fresh syringe. The cannulas were sealed and the UC was incubated for 15 minutes in a 37℃ incubator. Following the incubati on period, the enzymatic solution was transferred into a sterile 50 mL Falcon tube. The UC was flushed 3 additional times with HUVEC medium and carefully kneaded between the flushing steps. All medium used for the flushing was collected in the 50 mL Falcon tube. The resulting cell suspension was centrifuged at 390 x g for five minutes and the resulting cell pellet was resuspended in M199 medium supplemented with 20% FCS, 1% Pen/Strep, 0.34 % GlutaMAX®-I, 25 µg/ml endothelial cell growth supplement (ECGS) and 25 µg/ml sodium heparin. The cells were seeded on T25 flasks pre-coated with 0.2 % gelatin and cultivated under cell culture conditions referred to as P0. Medium was replaced every 2 to 3 days.

2.2.2.5 Endothelial cell line ISO-HAS-1

The endothelial cell line ISO-HAS-1 was derived from a single-cell clone expansion from the original ISO-HAS cell line isolated from a human hemangiosarcoma (Masuzawa et al., 1999, Unger et al., 2002). The ISO-HAS-1 cell line was used to evaluate experimental observations obtained from experiments with primary EC. For studies, ISO-HAS-1 cells were cultivated in ECGM.

2.2.3 Cell culture procedures

2.2.3.1 Characterization of human mesenchymal stem cells

Human MSC were characterized by flow cytometry and determination of the extent of their trilineage differentiation potential. Flow cytometry was used to determine the expression pattern of several surface markers according to a guideline of the ISCT for the isolation and characterization of mesenchymal stem cells (Dominici et al., 2006). For this, each MSC donor was analyzed for the expression of CD11b, CD19, CD29, CD31, CD34, CD44, CD45, CD73, CD90, CD105, CD146 and HLA-DR after thawing and expansion, prior to its use in any experiments. Additionally, each donor cell fraction was analyzed in a differentiation assay for its ability to differentiate into adipocytes, chondrocytes and osteoblasts. The differentiation assays were performed in 24-well cell culture plates or as pellet cultures (chondrogenic differentiation) using the commercially available StemPro® adipocyte or chondrocyte/osteocyte differentiation medium supplemented with adipogenic, condrogenic or osteogenic supplements from the kit, respectively.

2.2.3.2 Induction of osteogenic differentiation using customized medium

The osteogenic differentiation was induced by adding 100 nM dexamethasone, 10 mM β-glycerol phosphate and 50 µm ascorbic acid-2-phosphate to the cell culture medium, yielding an osteogenic differentiation medium (ODM). In experiments comparing the influence of the basal medium on the degree of osteogenesis

DMEM/F-12-GlutaMAX, αMEM-GlutaMAX$_2$ containing 2 mM GlutaMAX and αMEM-GlutaMAX$_{10}$ containing 10 mM GlutaMAX were used as basal medium for ODM. In experiments evaluating the impact of storage of the osteogenic supplements on the osteogenic differentiation DMEM/F-12-GlutaMAX and αMEM-GlutaMAX$_2$ were used as basal medium for ODM. In all following experiments αMEM-GlutaMAX$_2$ was used as basal medium in ODM. In addition to adding osteogenic supplements, ODM was further supplemented with 10 % FCS and 1 % P/S in all experiments. For the induction of osteogenesis in cell seeding density (CSD)-dependent experiments cell seeding densities of 3,000, 10,000, 20,000, 50,000, 100,000 and 200,000 MSC/cm^2 were investigated. For all other studies a CSD of 20,000 MSC/cm^2 was applied.

2.2.3.3 Osteogenic differentiation on two dimensional cell culture plastics

All 2D experiments were performed in 24-well cell culture plates. Basically, 20.000 MSC/cm^2 were seeded on uncoated wells and cultivated for 24 hours in expansion medium to allow for adherence, after which the medium was changed to ODM. The medium was exchanged every second to third day during a cultivation period of 28 days. The degree of osteogenesis in 2D experiments was assessed by quantification of calcium deposition using Alizarin Red (AR) staining and the deposition of phosphate using von Kossa (VK) staining. Additionally, all samples were stained for the expression of the alkaline phosphatase (ALP).

2.2.3.4 Osteogenic differentiation on three dimensional scaffolds

The osteogenic differentiation of MSC in 3D was investigated on trabecular Nitinol (tNiTi) scaffolds produced by the Department of Materials Science and Engineering, Technion Israel Institute of Technology, Haifa, Israel according to the method published by Gotman and colleagues (Gotman, 2010). All scaffolds were seeded dynamically in MSC expansion medium using a flow velocity of 1000 µm/s according to the protocol previously reported for expanded MSC using a U-CUP perfusion bioreactor (Sadr et al., 2012). The scaffolds were seeded with 20.000 MSC/cm^2 over a period of 24 h to allow for adherence. After this, the medium was changed to ODM. Scaffolds that served as static controls were transferred into an upright T25 flask. Scaffolds that served as basal controls were cultivated in basal medium without the addition of osteogenic supplements. All dynamic differentiation experiments were performed over a period of 28 days in a total volume of 7 mL. The medium was exchanged once a week. The degree of osteogenesis on three dimensional scaffolds was assessed by i: the quantification of calcium deposition using calcium OCP 1:1 assay, ii: the quantification of the alkaline phosphatase activity, iii: the immunofluorescent staining of the osteogenesis-specific protein collagen I, and iv: the quantification of the total intracellular collagen content (TIC).

2.2.3.5 Co-cultivation of MSC with EC to induce vascularization

Co-cultures (CC) of MSC with EC were performed using a constant MSC CSD of 20,000 MSC/cm^2 seeded onto gelatin-coated cell culture plastics in MSC expansion medium. Following 24h to allow for cell attachment, EC were added in endothelial cell growth medium. This event represented the time point t = 0d. The co-cultures were performed for 7 to 14d in ECGM. For experiments investigating different CSR in CC of MSC with HDMEC, the CSD of HDMEC was lowered from 80,000 to 40,000, 13,333 and 5,000 EC/cm^2 representing a CSR of 1:4 (Unger et al., 2010, Unger et al., 2007), 1:2, 1:0.66 (Dohle et al., 2010, Dohle et al., 2011, Fuchs et al., 2009b, Kolbe et al., 2011, Li et al., 2014) and 1:0.25.

2.2.3.6 Osteogenic co-cultivation of prevascularized MSC/EC co-cultures

The osteogenic co-cultivation (oCC) was used to induce osteogenic differentiation of MSC in prevascularized MSC/EC CC. The oCC represents a switch of the cell culture medium from ECGM to ODM following a prevascularization phase of 7d or 14d.

2.2.4 Calcium assays and immunohistochemical methods

2.2.4.1 Quantification of matrix mineralization using Alizarin Red (AR) staining

On account of its binding affinity to calcium ions, Alizarin Red staining was used to visualize and quantify the calcium deposition in 2D osteogenic differentiation cultures. For this, the corresponding samples were fixed with 3.7 % PFA for 10 minutes and washed two times with fresh PBS. Subsequently, 500 µL of the AR solution were added to each well and incubated for 20 minutes at room temperature. After this, the supernatant was discarded and the samples were washed three times with de-ionized water. Mild shaking was applied during the 5 minutes washing steps. After unbound AR was washed away, 500 µL of fresh PBS was added. The resulting red-colored calcium deposition of each sample was monitored using a transmitted light microscope. Samples prepared in 24-well cell culture plates were monitored as merged images, consisting of 48 single images recorded as 8 bit gray scale value images. For all merge processes the same coordinates for the microscopic stage were used. Following this, 300 µL of 10 % acetic acid were added to the wells and incubated for 10 minutes. Afterwards the samples were shaken intensely and the supernatant was transferred into eppendorf cups and heated up to 95℃ for 5 minutes. Subsequently, the absorption of each sample was measured at a wavelength of 405 nm. The final concentration of AR was determined from a standard dilution from the AR stock solution supplied with the kit.

2.2.4.2 Quantification of calcium deposition using OCP 1:1 assay

The Calcium OCP 1:1 assay was used for the quantification of calcium in the mineralized matrix of 3D osteogenic scaffolds. For this, the calcium fraction was dissolved by incubation of the samples in 1 M HCl for 10 minutes. Three dimensional

samples were prepared by adding 300 µL of 1 M HCl to a scaffold fragment. From the acidic solution 20 µL were transferred into a well of a flat-bottomed 96-well cell culture plate and incubated with 100 µL of a working solution consisting of a 1:1 mixture of the buffers R1 and R2 supplied with the kit. After 5 minutes of incubation at room temperature the absorbance of each well was measured at a wavelength of 560 nm using a TECAN Genios plus microplate reader. The concentration of each sample was determined by correlation of the mean value of triplicate measurements with a standard curve.

2.2.4.3 Staining of phosphate deposition using Von Kossa (VK) staining

During VK staining phosphate is exchanged against silver ions resulting in a brownish/black staining when samples are exposed to light. Initially, the samples were fixed with 3.7 % PFA for ten minutes. Following this, the corresponding specimens were washed three times with deionized water and subsequently incubated for one hour in 500 µL of a 5 % silver nitrate solution under exposure to light. Following this, the samples were washed again three times with deionized water and incubated for two minutes in 500 µL of 5 % thiosulfate solution. Afterwards, the specimens were washed again and finally covered with 500 µL of deionized water. Microscopic images were obtained immediately after the sample preparation. Samples prepared in 24-well cell culture plates were monitored as merged images consisting of 48 single images recorded as 8 bit gray-scale value images. For all merging processes the same coordinates for the microscopic stage were used.

2.2.4.4 Alcian Blue (AB) staining

The Alcian Blue (AB) staining was performed to visualize the deposition of glycosaminoglycans (GAG) during the chondrogenic differentiation of MSC or in co-cultures of MSC with HDMEC in 24-well plates. For this, the corresponding samples were fixed in 3.7 % PFA for 10 minutes and subsequently washed 3X using deionized water. Each well was covered with 500 µL of a 1 % AB solution (1 g of AB dissolved in 3 % acetic acid solution) and incubated for 20 minutes. Following this, the supernatant was discarded and the samples were washed 5 times with deionized water. Finally, the wells were air-dried and monitored using a stereomicroscope in transmitted light mode.

2.2.4.5 Non-fluorescent staining of the alkaline phosphatase

This staining was performed using the Leucocyte Alkaline Phosphatase Kit. The samples were first fixed with 300 µL of ALP-fixation solution for 30 seconds. Subsequently, the wells were washed 3X with PBS and then incubated with the ALP-staining solution for 15 minutes protected from light. Afterwards, the wells were washed 3X with fresh PBS and finally covered with 500 µL of PBS after which microscopic images were obtained.

2.2.4.6 Oil Red O staining

This staining was performed to demonstrate the existence of fatty droplets in differentiation cultures cultivated in StemPro adipogenesis differentiation medium (AP ADM). The first step was to dissolve 0.35 g of Oil Red O (OR-O) in 100 mL isopropanol to serve as a stock solution. From this stock solution 6 mL was mixed with 4 mL of deionized water resulting in a working solution that was stable for two hours. This working solution was always prepared fresh prior to use. Samples to be stained were fixed by adding 300 µL of 3.7 % PFA to each corresponding well for 10 minutes. Afterwards, the wells were washed three times with PBS and incubated with 500 µL of 60 % isopropanol for five minutes. Subsequently, the isopropanol was discarded and 500 µL of the working solution were added to each sample and incubated for 20 minutes. Following this, the supernatant was removed and discarded and the wells were washed 3X times with deionized water. Finally, all wells were examined microscopically and images were obtained using the Keyence BZ-9000 fluorescence microscope.

2.2.5 Protein Analyses

2.2.5.1 Isolation of protein

The total protein from multi-well cell culture plate samples as well as from scaffold samples was isolated by incubation of the sample in 500 µL of RIPA buffer for 10 minutes. Prior to this a protease inhibitor cocktail was added fresh to the RIPA buffer. Subsequently, the protein lysates were transferred into fresh 1.5 mL eppendorf cups and stored at -20℃. The protein concentration was determined using the BCA kit.

2.2.5.2 Determination of protein concentrations

The colorimetric quantification of protein was performed using the BCA-Protein_Assay_reagent-Kit in flat-bottomed 96-well cell culture plates. The protein concentration was assessed as the mean value of triplicate measurements. Substantially, all samples were pre-diluted 1:10 with PBS and 25 µL of the dilution were transferred to a well of a 96-well cell culture plate. To establish a calibration curve, a BSA standard was serially diluted and 25 µL of each dilution was transferred to the plate. Following this, 200 µL of a working solution containing 50 parts of reagent A and 1 part of reagent B from the kit were added to each of the wells. Furthermore, a blank sample containing 225 µL of PBS was prepared. The plate was sealed with parafilm and gently mixed on a shaker for 30 seconds. Afterwards, the sealed plate was incubated at 37℃ for 30 minutes protected from light. Following a cooling phase to reach room temperature the absorption at wavelength of 550 nm was measured using a TECAN GENios plus microplate reader.

2.2.5.3 Flow cytometry

In preparation for flow cytometry, the cells were detached by trypsinization, washed with PBS and centrifuged at 400 x g for 5 minutes. The supernatant was discarded and the cell pellet resuspended in warm cell culture medium, before the total cell number was determined using a hemocytometer. The total amount of cells needed, including 0.2 x 10^6 cells per staining, was transferred into a new 15 mL Falcon tube and centrifuged again at 400 x g for 5 minutes. The resulting cell pellet was resuspended in PBS containing 1 % BSA to allow for appropriate blocking of non-specific antibody binding sites. The required volume of blocking solution was dependent on the number of single stains planned. Generally, each specific antibody staining was performed in a total volume of 90 µL in a 5 mL Falcon round-bottom tube (FACS tube). A total volume of 5 µL of each specific antibody or isotype control was added to the sample volume and incubated at 4˚C for 15 minutes. After this, 3 mL of PBS were added and the suspension was centrifuged at 400 x g for 5 minutes. After discarding the supernatant, the resulting cell pellet was resuspended in 500 µL fresh PBS. The stained samples were immediately analyzed with the FACSCalibur flow cytometer using the CellQuest Pro Software. All samples to be analyzed were kept at 4 ℃ in the refrigerator. First, the voltages of the forward scatter (FSC) and the sideward scatter (SSC) were adjusted, depending on the size of the cells. The photomultiplier tubes FL-1, FL-2, FL-3 and FL-4 were adjusted according to the fluorescence levels of the isotype controls. An intensity value of 10^1 was set as the intensity limit. Cells with fluorescence intensity above 10^1 were regarded as positive for the expression of a certain marker. In addition, a negative control represented by unstained cells of each donor and cell type was analyzed to determine the level of autofluorescence. Since all analyses were performed as single stains or double stains using a combination of FITC and APC-labeled antibodies no compensation of the PMT was necessary. All quantifications were performed from measurement duplicates in density plots based each on 50.000 events counted.

2.2.5.4 Enzyme Linked Immunosorbent Assay ELISA

ELISA was performed using R&D DuoSet® ELISA systems to detect and quantify GFs released into the supernatant of 2D and 3D cell culture systems. Initially, 100 µL of the capture antibody diluted in PBS were transferred into each well of a 96-well flat-bottom high protein-binding capacity plate. The plate was incubated overnight at room temperature. Afterwards the plate was washed 3X with wash buffer (PBS + 0.05 % Tween20, pH 7.2 – 7.4) using an automated washer, and the supernatant removed. This was followed by the addition of 300 µL of reagent diluent (PBS + 1 % BSA, pH 7.2 – 7.4, 0.2 µm sterile filtered) to each well and incubation for 1 h to allow for appropriate blocking. Next, the plate was repeatedly washed with wash buffer (3x) and covered with 100 µL of standard solutions (standard diluted in reagent diluent), blank (reagent diluent) or sample solution (if stated dilution was performed in reagent diluent) to be incubated for 2 h at room temperature. The plate was repeatedly

washed with wash buffer after the incubation period. Afterwards, 100 µL of detection antibody (diluted in reagent diluent) were added to each well of the 96-well plate and incubated for 2 h at room temperature, after which three washing steps were performed. Then, 100 µL of streptavidin-HRP working solution were added to each well and incubated for 20 minutes in the dark. The plate was washed three times using wash buffer, and after the final wash 100 µL of substrate solution were added to each well and incubated for 20 minutes in the dark. The substrate conversion was stopped by adding 50 µL of stop solution (2 N H_2SO_4) to each well. Finally, the plate was measured at a wavelength of 450 nm using a microplate reader. The concentration of each GF was determined by correlation with the standard curve. The results are given as absolute mean concentrations (ng/mL) from three biological replicates.

2.2.5.5 Alkaline phosphatase activity assay

The activity of the alkaline phosphatase was measured from protein lysates. To carry out the assay, 20 µL of each sample were transferred into the well of a 96-well cell culture plate. All measurements were performed as triplicates. To each well 60 µL of the substrate solution were added. This solution was prepared fresh prior to its use by dissolving 0.2 % of p-nitrophenyl phosphate (p-NPP) in substrate buffer. The substrate buffer consisted of a 1 M diethanolamine HCl solution adjusted to a pH of 9.8. After adding the substrate solution, the plate was sealed and incubated for 45 minutes at 37℃ protected from light. Subsequently, 80 µL of the stop solution were added to each well. The stop solution was prepared by mixing a 2 M NaOH solution with a 0.2 mM EDTA solution. Following this, a calibration curve was generated by serial dilution of a p-nitrophenol (p-NP) standard solution in stop solution. From each standard 160µL were transferred to the plate. Afterwards the absorbance of each well was measured at a wavelength of 405 nm using a TECAN GENios plus multiplate reader. The final ALP activity was determined by correlation of the sample values with the standard curve after subtraction of the blank value.

2.2.5.6 Immunofluorescence staining

For immunofluorescence (IF) staining all samples were fixed with 3.7 % paraformaldehyde (PFA) at room temperature for ten minutes, after which samples were washed 3X with fresh PBS. After this, the samples were covered with 500 µL PBS and incubated at 60℃ for 1 hour for antigen re trieval. After a cooling period of 20 minutes to reach room temperature the samples were washed again with PBS. To allow for appropriate blocking 500 µL of a blocking buffer consisting of PBS supplemented with 0.5 % triton X-100, 6 % FCS and 1 % BSA were added for 30 minutes. Afterwards, the supernatant was discarded and 300 µL of the primary antibody diluted in antibody buffer consisting of PBS supplemented with 0.1 % trition X-100, 6 % FCS and 0.1 % BSA were added and incubated overnight at 4℃. Samples were then allowed to reach room temperature and were then washed 3X

with PBS, for five minutes each. Next, 300 µL of the secondary antibody diluted in antibody buffer were added to the samples and incubated for two hours at room temperature. Subsequently the samples were washed 3X with PBS and counter-stained with DAPI diluted 1:5.000 in PBS for five minutes. The specimens were then washed 3X and finally covered with 500 µL of PBS. Images were captured using a Keyence BZ-9000 fluorescence microscope.

2.2.5.7 F-actin staining using phalloidin-TRITC

To stain F-actin on the cells, samples were fixed using 3.7 % PFA for 10 minutes and subsequently washed 3X using PBS. A blocking buffer consisting of PBS supplemented with 0.5 % triton X-100, 6 % FCS and 1 % BSA was then added to each sample for 30 minutes. Afterwards, the supernatant was removed and the samples were covered with 500 µL of phalloidin-TRITC staining solution (0.5 µg/mL phalloidin-TRITC in PBS + 1 % BSA) and incubated for 20 minutes at room temperature protected from light. Following this, the supernatant was removed and the samples were washed several times using PBS.

2.2.5.8 Determination and quantification of apoptosis using AnnexinV

For the determination of apoptotic cells in MC of HDMEC cultivated in ODM the AnnexinV kit was used according to the manufacturer's protocol. First the cells were detached using trypsin and washed several times with cold PBS. After centrifugation of the suspension the resulting cell pellet was resuspended in binding buffer to give a final cell density of 1×10^6 cells/mL. A subvolume of 100 µL was transferred into a new FACS tube to which 5 µL of anti-AnnexinV-PE antibody and 5 µL of 7-Amino-Actinomycin (7-AAD) were added to the tube and incubated for 15 minutes at room temperature protected from light. Following this, 1 mL of binding buffer was added to each tube and this was then centrifuged at 400 x g for 5 minutes. The resulting cell pellet was resupended in 400 µL binding buffer and immediately analyzed using a FACSCalibur flow cytometer and the CellQuestPro software. The PE signal was detected in FL2 while the 7-AAD signal was detected in FL3.

2.2.6 Image Analyses

2.2.6.1 Quantification of AR, VK and AB staining intensities

Images of the stains were obtained as 8-bit gray scale value images using a Keyence BZ-9000 fluorescence microscope in the transmitted light mode. The quantification of gray scale value images of AR and VK stains was performed using the open source software FIJI based on ImageJ 1.47n. Basically, each merged image was analyzed at the single image level for the mean gray value using the batch analysis method. Since fixed coordinates were used during the image acquisition each single image represented a constant position in the resulting merged image. For the AB staining analysis, the stereomicroscopic images were analyzed on a whole. From each single

image (AR, VK or AB staining) the mean gray value (MGV) was quantified and subtracted from 2^8, the maximum number of gray values in an 8-bit gray scale value image, resulting in a value referred to as the gray value difference (GVD) in the present study. The same procedure was applied to the images of the corresponding basal controls using the same coordinates during image acquisition, whereby the control values were subtracted from the values of the differentiation cultures. The GVD was used to evaluate the degree of calcium, phosphate and GAG deposition in osteogenic differentiation cultures.

2.2.6.2 Quantification of vessel-like structure formation

The quantification of vessel formation by image analysis was based on immunofluorescence staining (IF) for CD31. Vascular structures were highly positive for the expression of CD31. Each stain was captured as 8-bit grey scale value images using a Keyence BZ-9000 fluorescence microscope. All images were processed using the open source software FIJI based on ImageJ 1.47n. First, background correction was applied using the rolling ball method according to Sternberg's algorithm (Sternberg, 1983). This was followed by automated thresholding (Image → Adjust → Threshold) and transformation of the images into binary images. Using the Analyze Particles function (Analyze → Analyze Particles) objects with an area below 500 px^2 and a circularity > 0.5 were excluded from the resulting mask image. The edges of the binary structures were smoothened using the Median function with a radius of 2 pixels (Process → Filters → Median). By repeating the Analyze Particles function for objects with an area above 500 px^2 (to infinity) and a circularity < 0.3 the area of the analyzed particles is taken as a representation of the Vascular Area. Afterwards the mask image was transformed into a skeleton using a thinning algorithm by applying the Skeletonize function (Plugins → Skeleton → Skeletonize (2D/3D)). By applying the Analyze Skeleton (2D/3D) function the generated skeleton of the mask image was characterized for the number of networks, the mean network length, the total number of branches, the number of branches per network and the number of branch points per network. From each sample eight images were obtained in a clockwise direction containing one image from the center region.

2.2.6.3 Quantification of F-actin using phalloidin-TRITC

The quantification of F-actin by image analysis was based on immunofluorescence staining (IF) for F-actin using phalloidin-TRITC. The F-actin stained samples were captured as 8-bit RGB images using a Keyence BZ-9000 fluorescence microscope. All images were processed using the open source software FIJI based on ImageJ 1.47n. First, background correction was applied using the rolling ball method according to Sternberg's algorithm (Sternberg, 1983). The overall intensity of TRITC (mean grey value) was then measured by applying the Measure function (Analyze → Measure) to the red channel image of the RGB achieved by the Channel splitting

function (Image → Color → Split Channels). For each sample six random images were obtained in a clockwise direction including one image from the center region. For structural analysis of peripheral F-actin rings the line tool was used to allow for the analysis of the intensity profile (Analyze → Plot Profile).

2.2.7 Statistics

If not otherwise indicated all experiments were performed with three biological replicates. If not otherwise stated all quantitative measurements were performed with three technical replicates. Data are shown as means ± standard error of mean (SEM) calculated in Microsoft EXCEL. The analysis for statistical significance was performed in EXCEL or GraphPad Prims 5 using paired student's t-test for the comparison of couples of experimental groups with a significance level set at $\alpha = 0.05$. Statistical significance was indicated as follows:
*: $p < 0.05$
**: $p < 0.01$
***: $p < 0.001$
All experiments investigating the influence of medium perfusion through tNiTi scaffolds on the osteogenic differentiation of MSC were repeated with three biological replicates including two scaffolds per group. The results are presented as means ± standard error (SEM). The analysis of matrix mineralization using SEM and EDX was performed on one representative donor. Statistical analysis was performed in Microsoft Excel using the paired student's t-test for the comparison of couples of experimental groups. No global statistical analysis was performed. The normal distribution of the data was investigated using the Analyse-it® tool for Microsoft EXCEL. No statistical evaluation was performed on data shown on the single donor level or on data obtained by EDX.
Data obtained by flow cytometry (characterization of MSC/HDMEC/OEC/HUVEC, phalloidin-TRITC measurements, detection of apoptotic cells) are shown for one individual representative donor, if not otherwise indicated.
The statistical impact of single medium supplements on the formation of vascular structures was evaluated by single factor analysis of variance (ANOVA) in Microsoft EXCEL analyzing the probability of two data sets being derived from the same basic set. For this, obtained data were sorted according to the addition or exclusion of a single factor (Supplementary Table 2). The analyzed data sets were derived from a common basic set and therefore not significantly different when the ANOVA-generated test statistic (TS) was smaller than the ANOVA-generated critical F-value ($TS < Fcrit$) and when the p-value was above the level of significance ($p > 0.05$) (Supplementary Table 3).

3 Results

3.1 Characterization of human mesenchymal stromal cells

To characterize the cells used in this study the guidelines of the International Society for Cell Therapy (ISCT) for characterization of MSC were followed (Dominici et al., 2006). The cells isolated by the protocol as described in the methods section exhibited multi-lineage differentiation potential as well as a profile of surface markers as recommended by the guideline paper. Thus, following the inductive cultivation in adipogenic, osteogenic and chondrogenic medium the cells showed clear evidence of adipogenic, osteogenic and chondrogenic differentiation (Figure 4). The formation of oily droplets indicating the differentiation of MSC into adipocytes was shown by positive oil-red-O staining (Figure 4A). The fast-red-violet stain, the alizarin-red stain and the von Kossa stain demonstrated the increased expression of alkaline phosphatase as well as the deposition of calcium and phosphate in the cultures of MSC cultured in osteogenic differentiation media (Figure 4B, C and D). Chondrogenic differentiation in pellet cultures was shown by a strong alcian blue (AB) staining reaction as well as by a positive localization of aggrecan (Figure 4E and F). Additional FACS analyses revealed that the cells were highly positive for the expression of CD73, CD90, CD105, CD29 and CD44 (Figure 4G, H, I, O and P). In contrast, the same cells were found to be negative for the expression of the cell surface markers HLA-DR, CD11b, CD34, CD45, CD19 and CD31 (Figure 4J-N and Q, respectively). Our findings are in accordance with the suggested minimal criteria for the characterization of mesenchymal stem cells as defined in the ISCT guidelines. Therefore, the cells isolated by our protocol were considered to be human mesenchymal stem cells (hMSC).

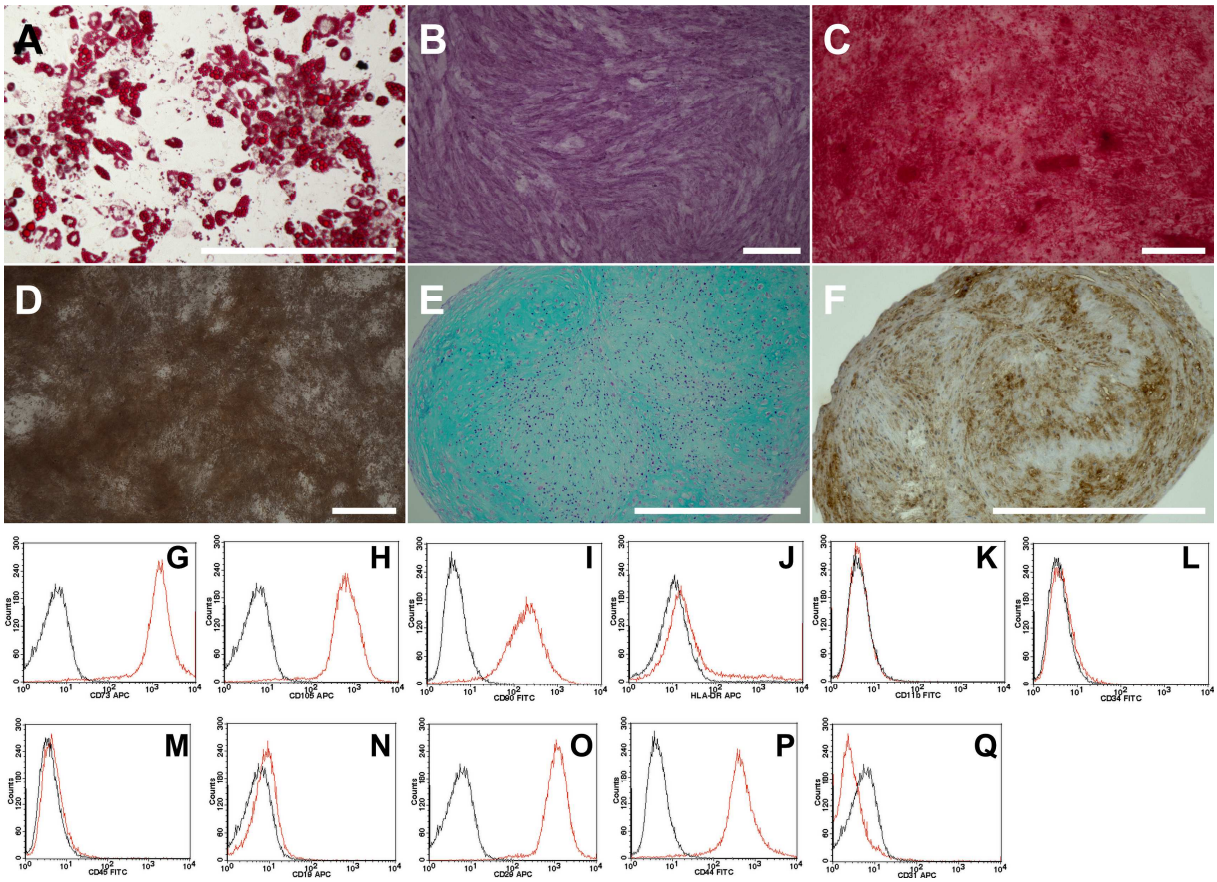

Figure 4: Characterization of human MSC isolated from trabecular bone of the femur head. A-F: Proof of tri-lineage differentiation potential using OR-O staining for adipogenic differentiation (A), ALP activity staining + AR staining + VK staining for osteogenic differentiation (B, C, D, respectively) and immunohistchemical stains with AB and aggrecan for chondrogenic differentiation (E and F). G-Q: Evaluation of the expression of surface molecules using flow cytometry.

3.2 Influence of dynamic cultivation on the osteogenic differentiation of hMSC

Based on the initial characterization MSCs were transferred into a biologically-relevant environment and the osteogenic differentiation was investigated under comparative static and dynamic conditions on 3D scaffolds in a perfusion bioreactor. 3D trabecular Nitinol (tNiTi) scaffolds were used as biomaterial. It was previously shown by our cooperation partners that MSC seeded onto tNiTi scaffolds exhibit an osteogenic phenotype when cultured under static conditions (Gotman et al., 2013). To proceed one step further, MSC-seeded tNiTi scaffolds were cultivated under comparative static and dynamic conditions in either basal medium (Basal) or osteogenic differentiation medium (ODM) for 4 wk. MSC were seeded at a cell seeding density (CSD) of 20,000 MSC/cm^2 (found to result in the highest formation of osteogenic matrix, Supplementary Figure 1). The cell-seeded scaffolds were cultivated either in αMEM-GlutaMAX® basal medium (Basal) or αMEM-GlutaMAX® supplemented with osteogenic factors (ODM) to stimulate osteogenic differentiation. A comparison of different media showed that MSC growing in αMEM-GlutaMAX®

supplemented with osteogenic inducing compounds exhibited the most osteogenic differentiation compared to other media formulations (Supplementary Figure 2).

Following 4 wk of static or dynamic cultivation the samples were analyzed for the expression of the osteogenic proteins ALP and collagen type 1 as well as for the presence of a mineralizated osteogenic matrix. The cultivation of MSC in ODM medium led to a 3- to 20-fold increase in ALP activity compared to MSC cultured in Basal alone. A further 1.3- to 4-fold enhancement was observed in MSC cultured in ODM under dynamic conditions compared to cells cultured in ODM under static differentiation conditions. No differences were observed in cells grown in Basal under static or dynamic conditions (Figure 5A). The effect was not statistically significant, although a similar pattern was observed for all of the investigated donors (Figure 5B). The same pattern was found in the amount of calcium deposition in the newly formed and mineralized matrix. Calcium levels varied only slightly in MSC grown in Basal under static conditions (e.g. donor 2: $1.93x10^{-4}$ mg/cm^2 (Basal)) compared to cells grown in ODM ($2.05x10^{-4}$ mg/cm^2). In contrast, a statistically significant 2- to 5-fold increase in calcium deposition was observed in cells grown in ODM under dynamic conditions compared to cells grown under static conditions (Figure 5C). The formation of minerals in the extracellular matrix could be visualized by scanning electron microscopy. It appeared that mineralization occurred under dynamic conditions in ODM (Figure 5F and G), whereas no mineralization was detectable in the extracellular matrix of static or dynamic cultures in BM (Figure 5D and E).

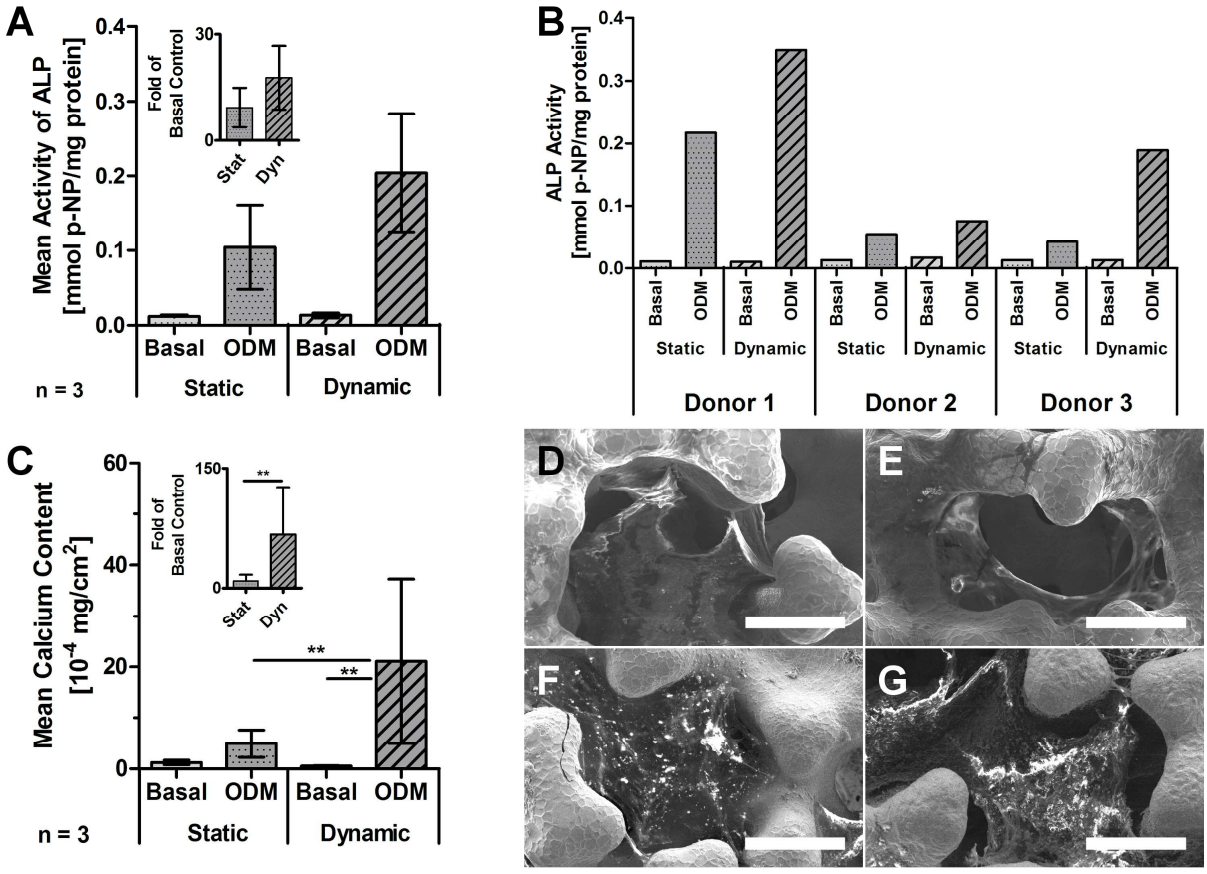

Figure 5: Determination of ALP activity and calcium deposition in static and dynamic cultures under ODM and Basal culture conditions. A: ALP activity shown as mean values of three different donors. The small insert graph compares ALP activity of static and dynamic cultures normalized to activity observed by cells cultured in Basal. B: Although a statistical significance could not be demonstrated, a common pattern demonstrates an enhanced ALP activity due to flow was observed with each single donor. C: Determination of the calcium content in the secreted matrix as mean values from three donors (n = 3). Asterisks indicate statistically significant changes (** = $p < 0,01$). D: SEM of cultures grown under static conditions in Basal. E: SEM of cells grown under dynamic conditions in Basal. F: SEM of static samples in ODM and G: SEM of dynamically grown samples in ODM; Scale bars = 200 µm

Energy-dispersive X-ray analysis (EDX) was used to obtain a qualitative evaluation of matrix mineralization (Bonewald et al., 2003). Images obtained by SEM indicated the presence of minerals in the extracellular matrix (Figure 5D and E, Figure 6A and B). For the EDX analyses the regions of interest (ROI) were defined as rectangles for the determination of the deposition of calcium phosphate in a specified area or as single points to evaluate a possible co-localization of calcium and phosphorus (Figure 6A and B). As seen from Table 19 phosphorus was detectable in all samples cultivated in ODM. Importantly, the atomic contents of calcium and phosphorus were elevated approximately 2 to 3-fold in the samples grown in ODM under dynamic conditions compared to ODM cultures grown under static conditions (Table 19). In addition, single point EDX analyses revealed the co-localization of calcium and phosphorus on tNiTi in ODM under both culture conditions. On the other hand, no calcium phosphate deposits were detectable in samples from the static or dynamic cultures growing in BM (Table 19).

Table 19: Determination of the atomic content of calcium and phosphorus in areas and at single points represented in Figure 6. Related spectra of the samples “Static ODM” and “Dynamic ODM” are shown in Figure 7 and Figure 8, respectively.

Differentiation Condition	Region of Interest	Calcium [Atomic%]	Phosphorus [Atomic%]
Static Basal Control	Not Shown	0.00	0.00
Dynamic Basal Control	Not Shown	0.00	0.00
Static ODM	1 (Area, Material)	0.00	0.00
	2 (Area)	1.17	1.01
	3 (Area)	1.83	1.36
	4 (Single Point)	1.74	1.54
	5 (Single Point)	1.42	0.94
	6 (Single Point)	0.53	0.58
	7 (Single Point)	1.37	0.99
Dynamic ODM	1 (Area, Material)	0.00	0.00
	2 (Area)	2.96	2.63
	3 (Area)	2.66	2.53
	4 (Single Point)	2.50	2.27
	5 (Single Point)	4.53	4.20

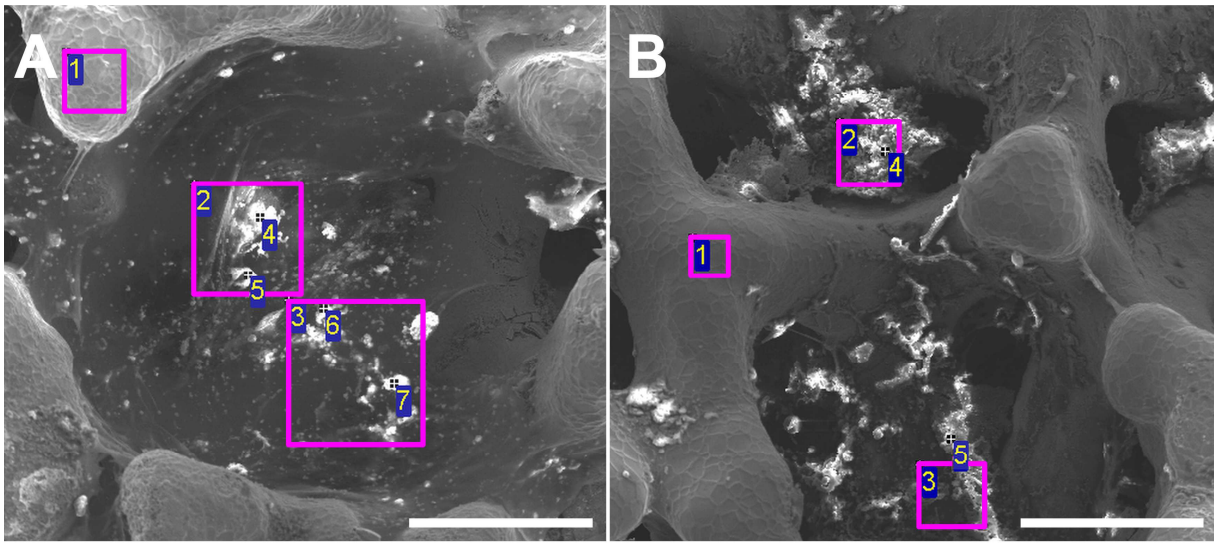

Figure 6: Formation of calcium phosphate minerals in the calcified matrix of MSC grown on tNiTi under static and dynamic culture conditions. A: Static and ODM; B: Dynamic and ODM; Numbers indicate the region of interest (ROI) analyzed by EDX – magenta rectangles indicate area-based EDX analyses. ROI 4-7 in A and 4 and 5 in B represent single point EDX analyses for the co-localization of calcium and phosphorus. Scale bars = 200 µm

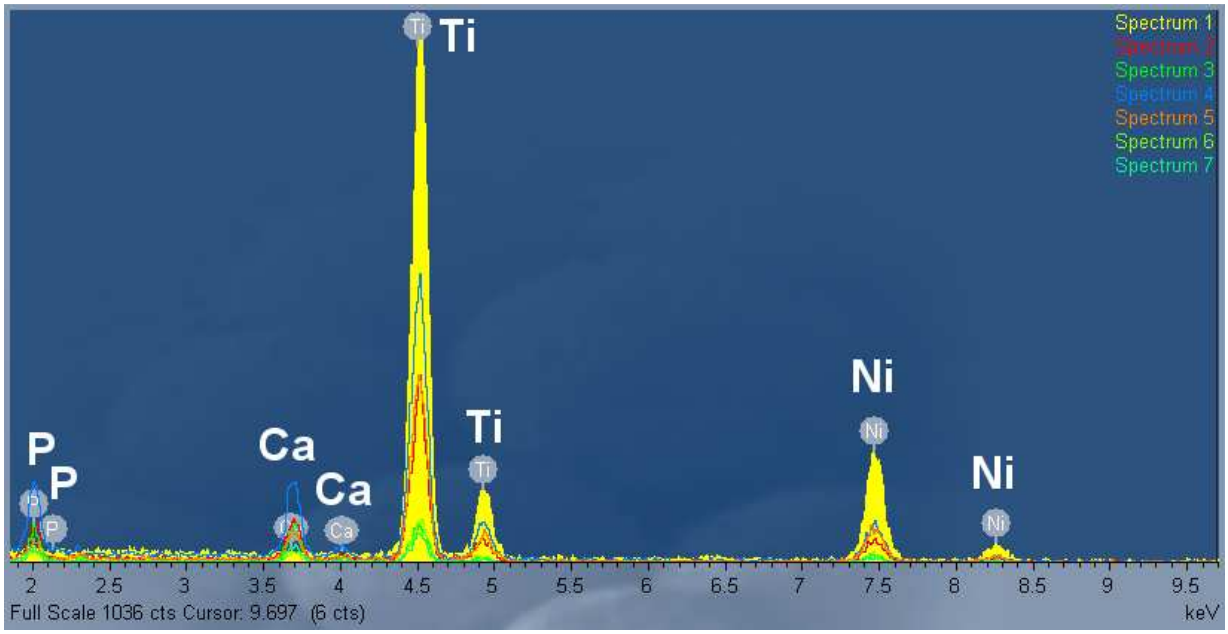

Figure 7: EDX spectra of ROI shown in Figure 6A. Spectrum 1 represents the material reference position. The spectra 4, 5, 6 and 7 represent single spot spectra for the co-localization of calcium and phosphorus. Elements indicated by grey filled circles. Abbreviation of elements: Ca: Calcium; P: Phosphorus; Ti: Titanium; Ni: Nickel

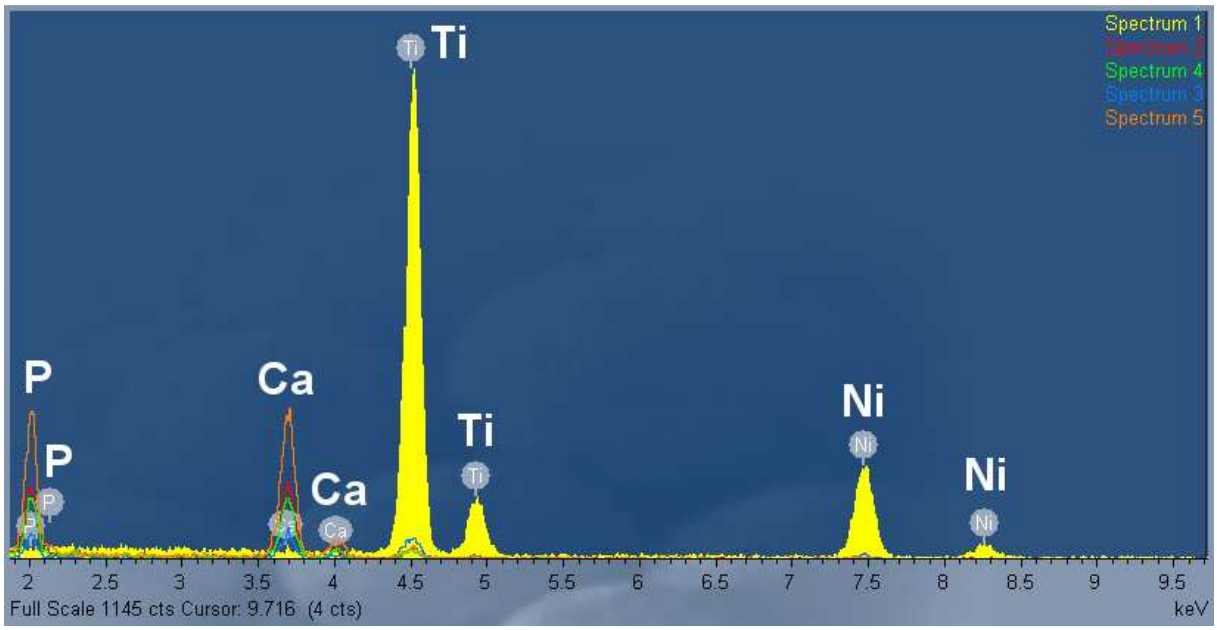

Figure 8: EDX spectra of ROI shown in Figure 6B. Spectrum 1 represents the material reference position. The spectra 4 and 5 represent single spot spectra for the co-localization of calcium and phosphorus. Elements indicated by grey filled circles. Abbreviation of elements: Ca: Calcium; P: Phosphorus; Ti: Titanium; Ni: Nickel

Following the quantitative and qualitative analysis of matrix mineralization a study of the distribution and composition of matrix formed by MSC throughout the tNiTi scaffold body in response to dynamic conditions was performed. It is known that dynamic cultivation results in an enhanced distribution and uniformity of cellular matrix on 3D scaffolds (Wendt et al., 2003). The distribution of cells visualized by a DAPI cell nuclear stain is shown in Figure 9 (A-D). In scaffolds cultivated under dynamic conditions an improved distribution of cells was found (Figure 9B and D), with high numbers of cells observed in the inner portions of the scaffold. In statically cultivated cells, cell growth was predominantly limited to the surface regions (Figure 9A and C). Immunofluorescence staining for collagen type I, one of the principal proteins in natural bone, showed a similar distribution. Figure 9 (E-H) demonstrates that cells grown in ODM exhibited an increased fluorescence signal for collagen type I compared to cells grown in BM. It is important to note that this collagenous matrix was mostly found on the scaffold surface in the static samples (Figure 9E and G), whereas under dynamic conditions, an increased fluorescence signal was also observed in the scaffold center (Figure 9F and H). Microscopic evaluation demonstrated that the degree of matrix calcification was dependent on medium and culture conditions. Calcified matrix was found to be distributed in all areas of the 3D scaffold in samples cultured in ODM under dynamic conditions as detected by stereomicroscopic analyses of scaffold cross sections (Figure 9I-L). Strongly calcified matrix was found in the scaffold center, as well as on the surface of tNiTi scaffolds cultivated under dynamic and ODM conditions (Figure 9L and P). On the other hand, calcified matrix was found to be limited to the scaffold surface of statically grown cells under ODM conditions (Figure 9K and O). The same surface-limited matrix

deposition was found on tNiTi scaffolds and cells grown in Basal (Figure 9I and M). In the dynamically, Basal cultivated cultures the deposition of matrix occurred in close proximity to the trabeculae of the tNiTi scaffolds and was therefore very difficult to detect by stereomicroscopy (Figure 9J and N).

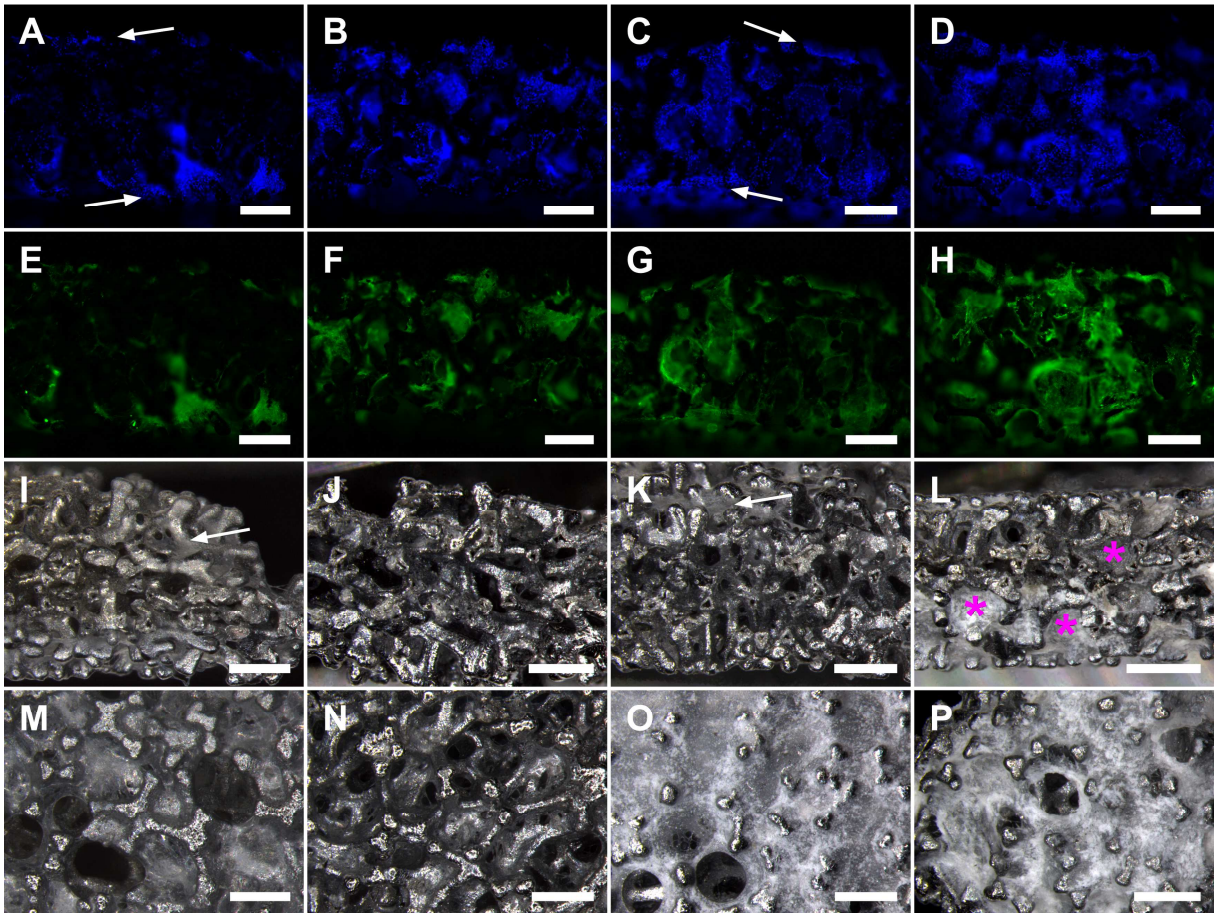

Figure 9: Analysis of MSC growth and distribution of osteogenic matrix on tNiTi scaffolds cultivated under comparative static and dynamic culture conditions for 4 wk. A, E, I, M: Basal/static. B, F, J, N: Basal/dynamic, C, G, K, O: ODM/static. and D, H, L, P: ODM/dynamic. A-D: Analysis of cell distribution using DAPI cell nuclei stain. E-H: Distribution of collagen type I. I-L: Stereomicroscopic evaluation of distribution of calcified matrix in cross sections. M-P: Stereomicroscopic overview of the scaffold surface. Arrows indicate predominant growth areas in static samples (A, C, I, K). Asterisks indicate highly calcified areas in the scaffold center (L). Scale bars = 500 µm

Having shown stronger differentiation potential of hMSC under dynamic conditions, studies were performed to determine whether medium perfusion alone through tNiTi scaffolds could serve as a mechanical inducer of osteogenesis in the MSC cultures. To determine this, the above described perfusion experiments were repeated using ODM medium but omitting dexamethasone (ODM-Dex). Dexamethasone is a synthetic glucocorticoid able to induce osteogenic differentiation in MSC cultures (Grigoriadis et al., 1988). After 4 weeks of cultivation in ODM-Dex, the activity of ALP as well as the deposition of calcium was found to be clearly decreased compared to

cells cultured in the standard differentiation medium ODM (Figure 10A/B and C/D). The levels for ALP activity and calcium in ODM-Dex cultures were comparable to the cultures in Basal with each respective donor (Figure 10A and B). Furthermore, SEM analyses of the extracellular matrix showed an absence of the formation of minerals in ODM-Dex grown cultures under static conditions as well as in ODM-Dex grown cultures under dynamic conditions (Figure 11C and D, respectively). Therefore, medium perfusion alone through tNiTi scaffolds did not induce mineralization of extracellular matrix produced by hMSC. In contrast, the evaluation of collagen type I matrix deposition revealed an increased deposition in ODM-Dex cultures compared to scaffolds cultivated in Basal (Figure 11E versus G, Figure 11H versus J). This increase of collagen type I matrix deposition in cells cultured in ODM-Dex was observed under both static and dynamic conditions. However, the deposition of collagen type I in ODM-Dex samples was slightly enhanced in cells on scaffolds under dynamic conditions (Figure 11G versus J). This indicated a possible effect by medium perfusion on the expression of collagen type I by hMSC on tNiTi. This trend was also observed by the quantification of the total intracellular collagen content (TIC) in cells grown in Basal, ODM and ODM-Dex cultures under static conditions (Figure 11A). An increased TIC was detected in ODM-Dex cultures grown under dynamic conditions compared to the corresponding Basal grown cells under dynamic conditions or the ODM-Dex cultures under static conditions (Figure 11A). These results are consistent among the respective donors (Figure 11B) and indicate that medium perfusion alone affects the expression of collagens. Furthermore, enhanced levels of TIC were observed in cells cultured in ODM under dynamic conditions compared to cells grown under static conditions. This appeared to indicate that medium perfusion was responsible for the increase of the TIC (Figure 11A). Although no statistical significance was detected, this pattern was observed for each of the different MSC donors (Figure 11B).

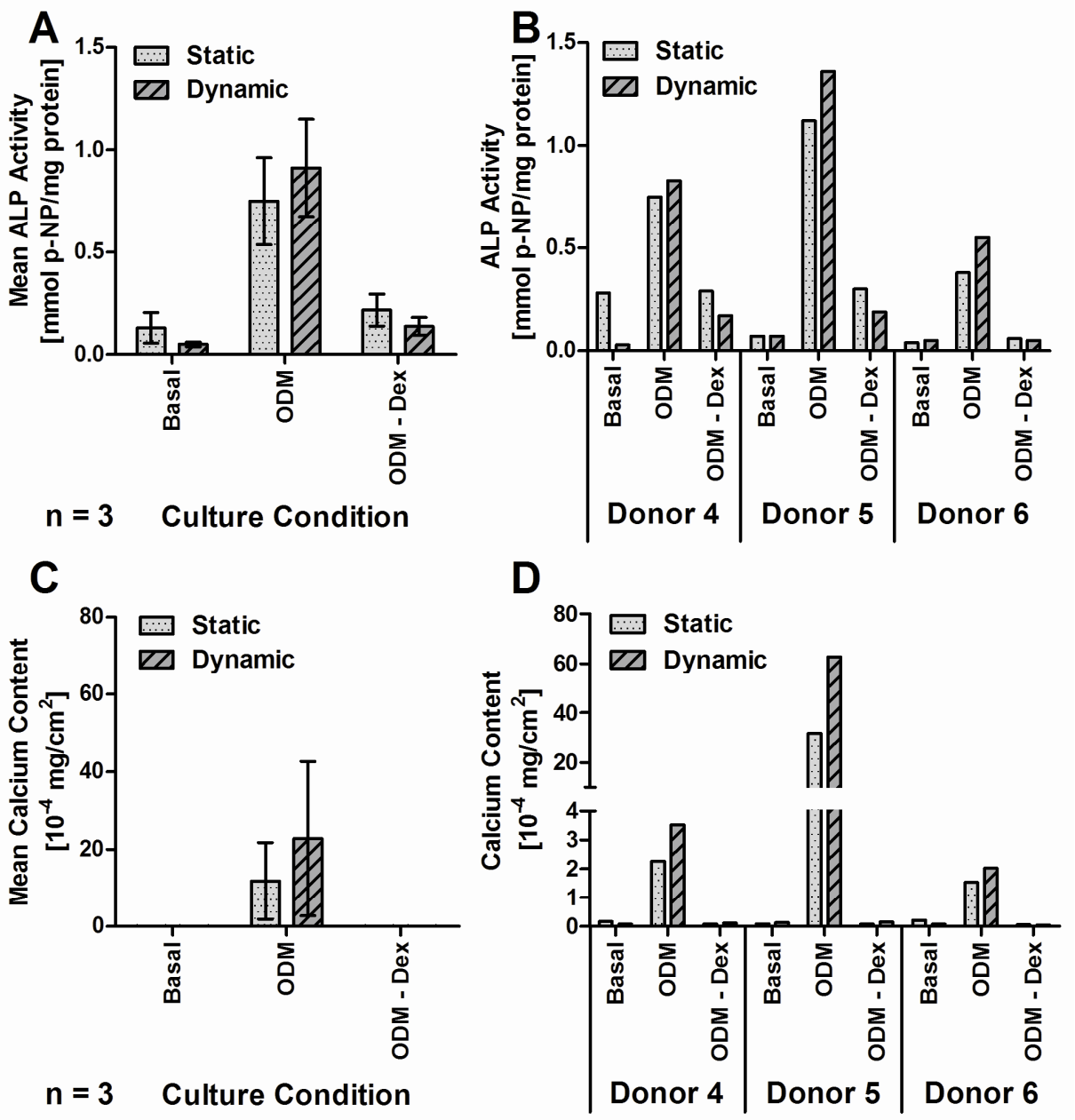

Figure 10: Evaluation of the influence of medium perfusion on osteogenic inductivity of cells grown in medium in the presence and in the absence of Dex. A: Determination of the mean ALP activity from three biological replicates (± SEM). The small insert graph compares ALP activity in static and dynamic ODM and ODM-Dex cultures normalized to the respective cultures grown in Basal. B: ALP activity shown at the single donor level. C: Determination of the mean calcium content in the extracellular matrix from three biological replicates (± SEM). The small insert graph compares the mean calcium content in static and dynamic ODM and ODM-Dex cultures normalized to the respective cultures grown in Basal. D: Levels of calcium content shown for each single donor.

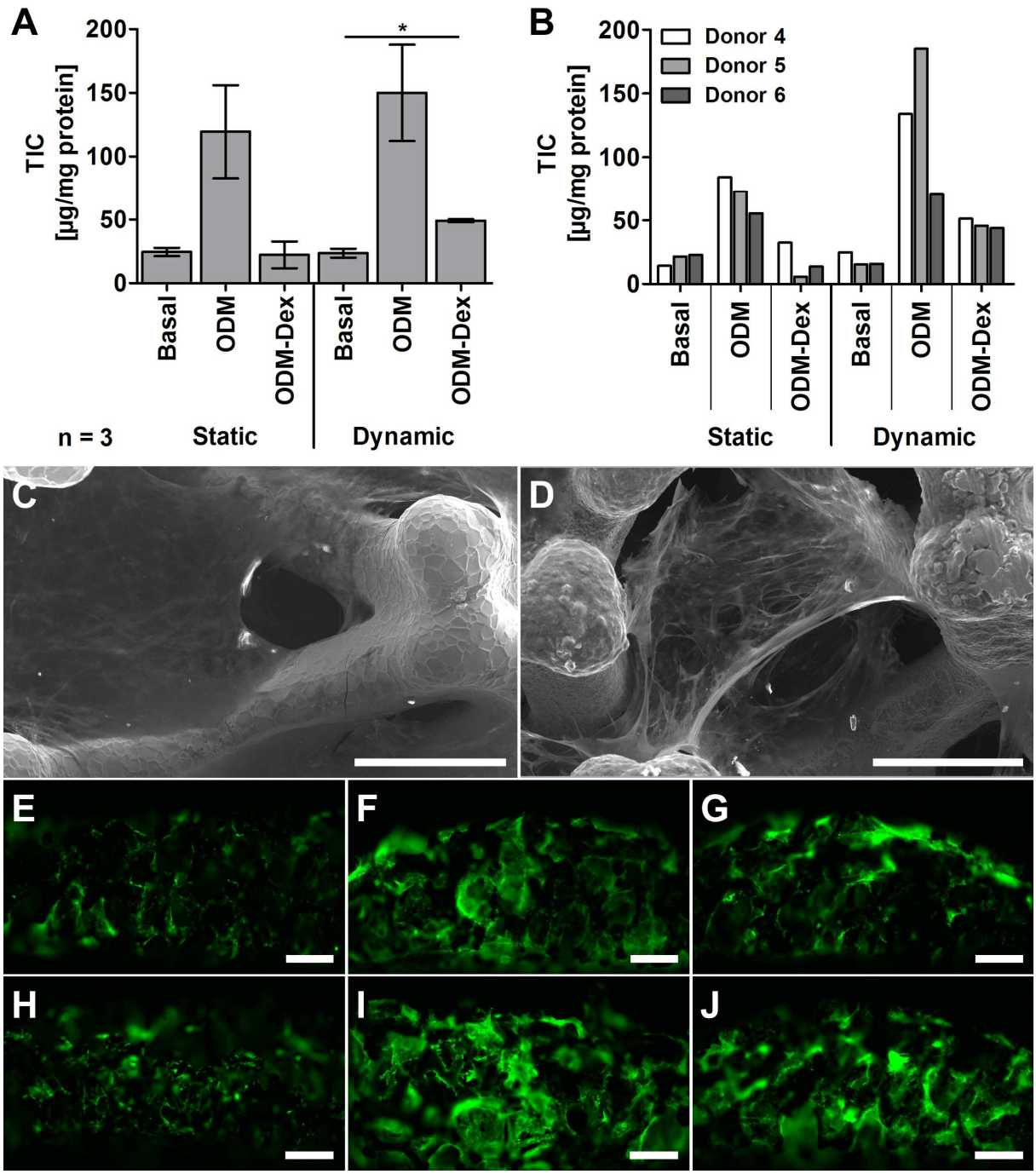

Figure 11: Evaluation of the osteogenic inductivity of cells under medium perfusion in the absence of Dex. A: Determination of total intracellular collagen content (TIC) from three biological replicates (± SEM). B: Determination of TIC levels for single donors. Statistically significant differences are indicated by asterisks: "*": $p < 0.05$, "**": $p< 0.01$; No evidence of mineral formation on the extracellular matrix in cells grown under static (C) and dynamic (D) conditions in ODM–Dex was observed. Scale bars = 200 µm. E-G: IF-based evaluation of collagen type I deposition in cross sections of MSC-seeded tNiTi scaffolds cultivated under static conditions. Scale bars = 500 µm. E: Basal/static, F: ODM/static, G: ODM-Dex/static. H-J: IF-based evaluation of collagen type I deposition in cross sections of MSC-seeded tNiTi scaffolds cultivated under dynamic conditions, H: Basal/dynamic, I: ODM/dynamic, J: ODM-Dex/dynamic. Scale bars: 500 µm

3.3 Prevascularization in MSC-EC co-cultures is influenced by the cell seeding density and the cell seeding ratio

A more biologically-relevant TE model for clinical application would include endothelial cells with the MSCs, as vascularization is essential for bone regeneration. To evaluate the above described cell culture model, studies were carried out including endothelial cells. The co-cultivation of MSC with endothelial cells (EC) or osteoprogenitor cells with EC has been shown to result in vascularization and the formation of tube-like structures *in vitro* (Unger et al., 2005, Kolbe et al., 2011, Dohle et al., 2010, Dohle et al., 2011). Thus, the CSD shown to be the most optimal for the osteogenic differentiation of MSC was used as a starting point for the evaluation of the formation of tube-like structures in MSC/EC co-cultures on tNiTi.

3.3.1 Characterization of HDMEC, HUVEC and OEC

Prior to the evaluation of co-culture systems, the different types of EC were characterized by immunofluorescence staining for cell type-specific proteins and flow cytometry. Primary HDMEC were found to be positive for the expression of CD31 (Figure 12A and H), vWF (Figure 12B) Col-IV (Figure 12C), LMN (Figure 12D), CD34 (Figure 12I), CD146 (Figure 12J) and CD105 (Figure 12K).

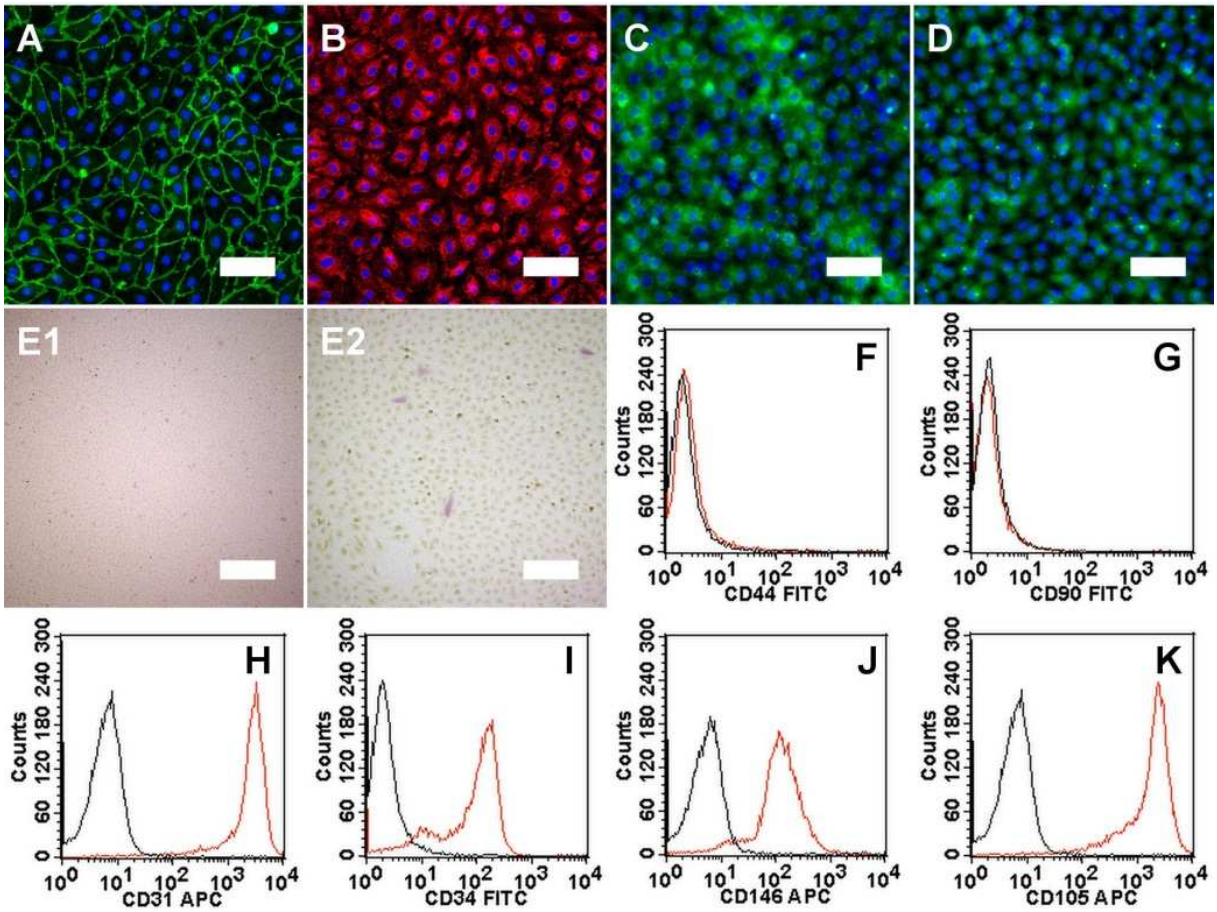

Figure 12: Characterization of HDMEC by IF staining for cell nuclei (blue), CD31 (A), vWF (B), Col-IV (C), LMN (D), staining for ALP activity (E1/E2) and flow cytometry analyses for the expression of CD44 (F), CD90 (G), CD31 (H), CD34 (I), CD146 (J) and CD105 (K); Scale bars in IF images: 200 µm; Scale bars in ALP activity stains: Overview (E1) = 500 µm, Zoom (E2) = 200 µm

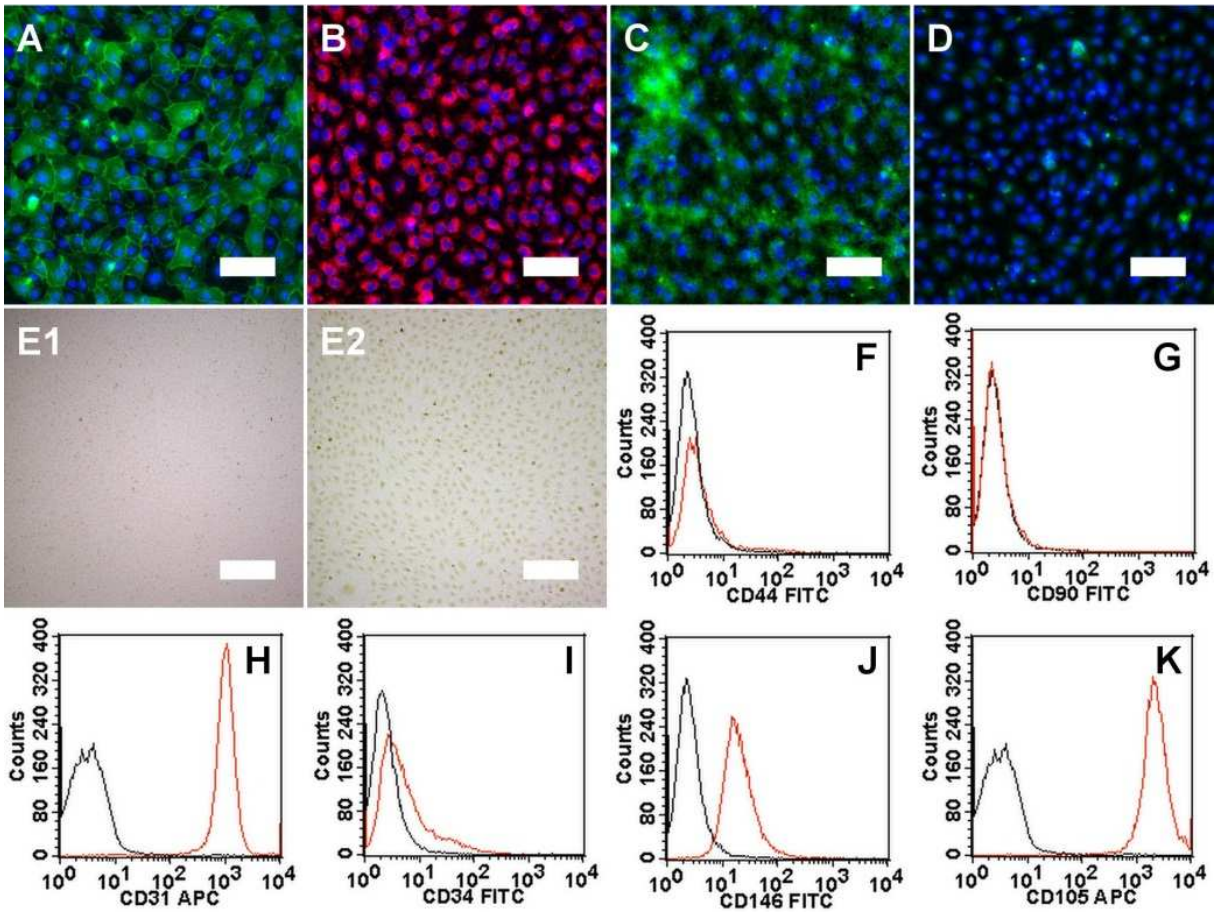

Figure 13: Characterization of HUVEC by IF for cell nuclei (blue), CD31 (A), vWF (B), Col-IV (C), LMN (D), staining for ALP activity (E1/E2) and flow cytometry analyses for the expression of CD44 (F), CD90 (G), CD31 (H), CD34 (I), CD146 (J) and CD105 (K); Scale bars in IF images: 200 µm; Scale bars in ALP activity stains: Overview (E1) = 500 µm, Zoom (E2) = 200 µm

In contrast, HDMEC were found to be negative for the expression of CD44 (Figure 12F), CD90 (Figure 12G) and ALP (Figure 12 E1 and E2). Primary HUVEC gave positive findings for the expression of CD31 (Figure 13A and H), vWF (Figure 13B), Col-IV (Figure 13C), CD146 (Figure 13J) and CD105 (Figure 13K). Laminin and CD34 were both found weakly expressed on HUVEC (Figure 13D and I). Furthermore, HUVEC reacted negatively for the expression of CD44 (Figure 13F), CD90 (Figure 13G) and ALP (Figure 13 E1 and E2). Primary OEC were found to be positive for the expression of CD31 (Figure 14A and H), vWF (Figure 14B), Col-IV (Figure 14C), CD34 (Figure 14I) and CD105 (Figure 14K). Laminin and CD146 were both found slightly expressed on OEC (Figure 14D and J). Additionally, OEC demonstrated no expression of CD44 (Figure 14F), CD90 (Figure 14G) and ALP (Figure 14 E1 and E2).

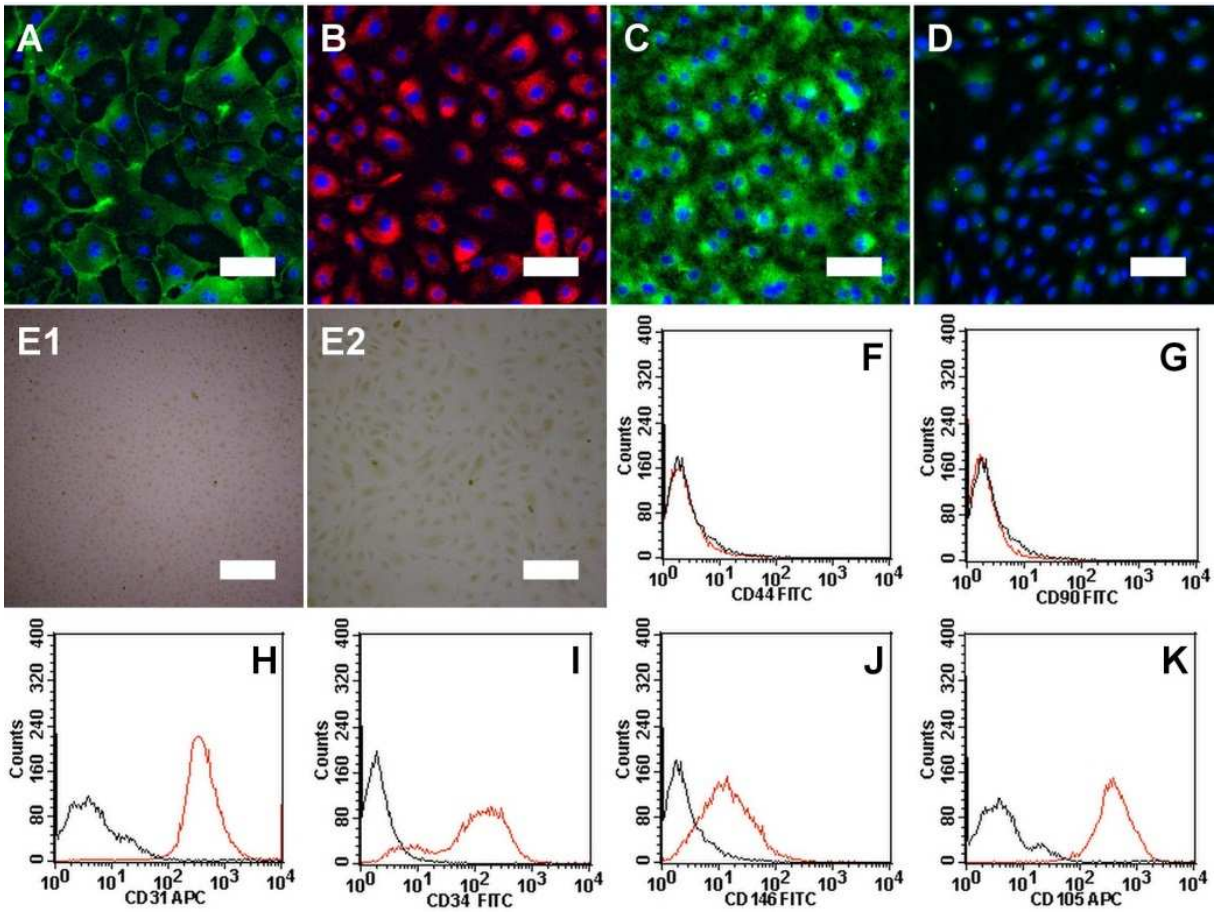

Figure 14: Characterization of OEC by IF staining for cell nuclei (blue), CD31 (A), vWF (B), Col-IV (C), LMN (D), staining for ALP activity (E1/E2) and flow cytometry analyses for the expression of CD44 (F), CD90 (G), CD31 (H), CD34 (I), CD146 (J) and CD105 (K); Scale bars in IF images: 200 µm; Scale bars in ALP activity stains: Overview (E1) = 500 µm, Zoom (E2) = 200 µm

Table 20: Phentotypic comparison of HDMEC, HUVEC and OEC summarizing the detection of proteins by IF or FACS as demonstrated in Figure 12, Figure 13 and Figure 14

Marker	HDMEC	HUVEC	OEC
CD31	+	+	+
vWF	+	+	+
Col-IV	+	+	+
LMN	+	very low	low
CD34	+	low	+
CD146	+	+	low
CD105	+	+	+
CD44	-	-	-
CD90	-	-	-
ALP	-	-	-

3.3.2 Optimized prevascularization in MSC/HDMEC co-cultures

HDMEC were co-cultivated with MSC to investigate the influence of the CSD and the corresponding cell-seeding ratio (CSR) on the formation of vessel-like structures. For this, MSC/HDMEC CCs with varying MSC:HDMEC CSR of 1:4 (Unger et al., 2010, Unger et al., 2004), 1:2, 1:0.66 (Dohle et al., 2010, Fuchs et al., 2007, Kolbe et al., 2011) and 1:0.25 were cultivated for 2 wk in ECGM. Subsequently, the formation of tube-like structures was quantified using image analysis based on IF staining for EC-specific CD31. Additionally, the CCs were evaluated for the expression of vWF and Col-IV using IF staining and for the expression of Ang-1, Ang-2 and VEGF in cell culture supernatants using ELISA.

It can be seen from Figure 15A that a decreasing proportion of HDMEC led to an increased formation of vessel-like structures (Figure 15A – CD31/DAPI). Additionally, the microscopic observations revealed an increased size and density of the microcapillary-like networks formed (Figure 15A – CD31/DAPI). The immunofluorescence staining for vWF and Col-IV show a strong expression of vWF in vascular structures at a CSR of 1:0.66 and 1:0.25 which overlapped with a strong deposition of Col-IV in the basal lamina of the vascular structures (Figure 15A – Col-IV/vWF/DAPI). Lower intensities in vWF expression and Col-IV deposition were found at CSR of 1:2 and 1:4 (Figure 15A – Col-IV/vWF/DAPI). Image analysis was used to quantify the initial visual differences observed in network size and network densities (Figure 15B). Although the total number of networks (N/cm2) was highest at at CSR of 1:2 (Figure 15B - Networks) an increased network density was detected at CSR of 1:0.66 and 1:0.25 compared to 1:4 (Figure 15B - Networks). All other parameters characterizing vasculogenesis and angiogenesis showed a consistent highest value for a CSR of 1:0.66. No additional changes were detected for a CSR of 1:0.25 (Figure 15B). Due to donor-dependent variation of the absolute values no statistical significance was detected. Despite this, all individual donors exhibited a similar pattern (Supplementary Figure 4).

To evaluate the level of GF release in CCs, cell culture supernatants were analyzed for the expression of VEGF, Ang-1 and Ang-2. These GFs are known to play key-regulatory roles in the processes of vascularization and angiogenesis (Lobov et al., 2002). The expression of VEGF was found to be inversely proportional to a decreasing proportion of HDMEC after 7d (Figure 15C - VEGF/7d). After 14d VEGF was constantly expressed at approximately 4 ng/mL independent on the CSR (Figure 15C - VEGF/14d). Ang-1 was expressed at constant levels in CC after 7d and slightly increased after 14d at a CSR of 1:0.66 or 1:0.25 compared to 1:4 and 1:2 (Figure 15C - Ang-1/14d). Expression of Ang-2 decreased after 7d with decreasing levels when endothelial ratios were lowered from 4 to 0.25 (Figure 15C Ang-2– CC/7d). After 14d Ang-2 was found to be expressed at similar concentrations independent of the CSR in the CCs (Figure 15C - Ang-2/14d). Monoculture controls of MSC MCs and HDMEC MCs demonstrated that MSC represent the main source of VEGF and

Ang-1, while Ang-2 was predominantly expressed by HDMEC (Supplementary Figure 3). Taken together these results indicate that the formation of vascular structures *in vitro* is influenced by the CSR. In this context, a CSR of 1:0.66 was identified as the most optimal for the formation of microcapillary-like structures in the CC model.

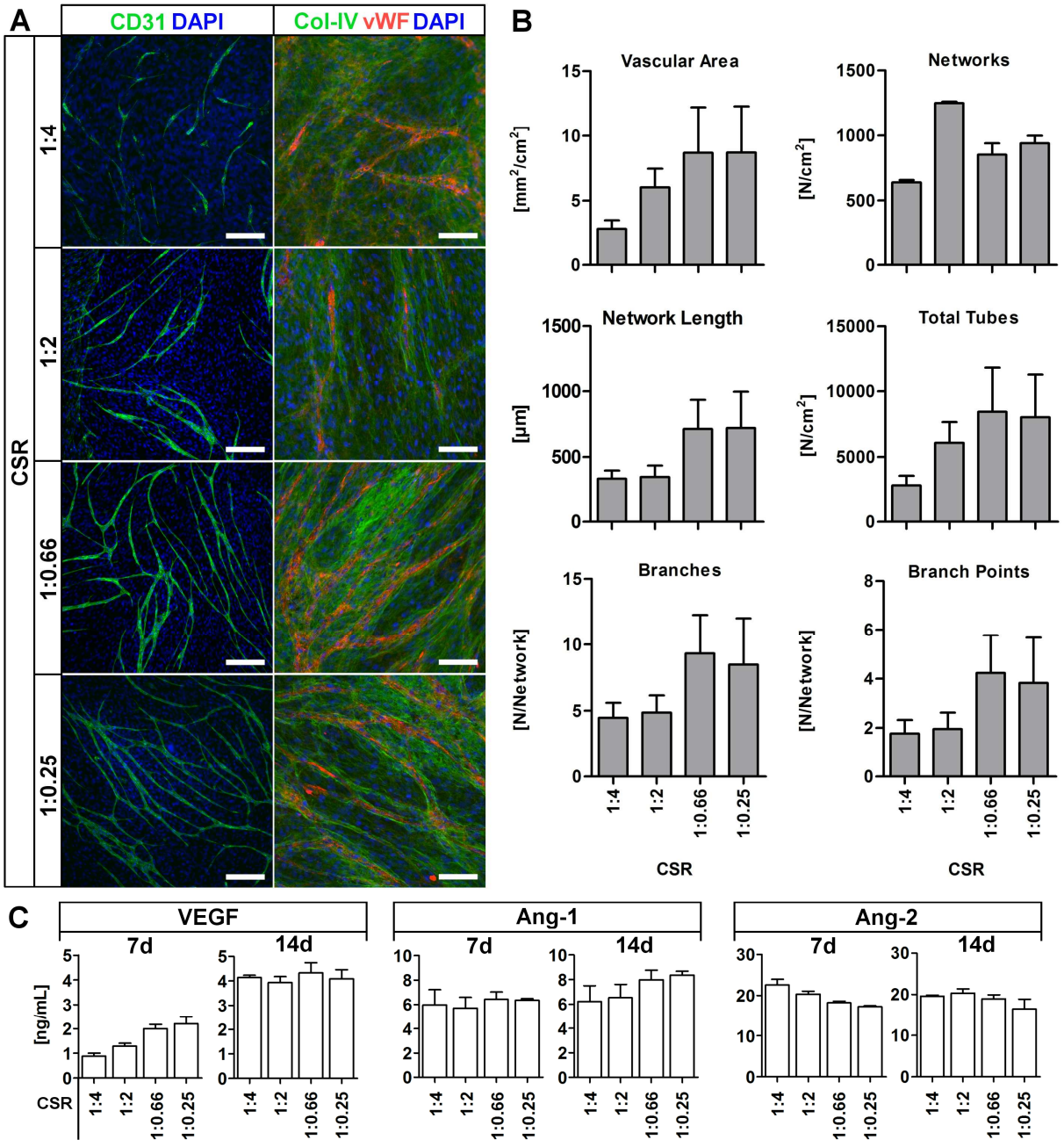

Figure 15: Influence of the CSR on the formation of VLS in CCs of MSC with HDMEC. A: IF staining for CD31, Col-IV, vWF and cell nuclei (DAPI) for CSR-dependent formation of vessel-like structures and the existence of a basal lamina, Scale bars: 500 µm; B: Image-based quantification of parameters characterizing vasculogenesis and angiogenesis in CSR-dependent CCs based on IF staining for CD31; C: CSR-dependent quantification of released level of VEGF, Ang-1 and Ang-2 after 7d and 14d in supernatants of MSC/HDMEC CCs, MSC MCs and HDMEC MCs

3.3.3 Optimized prevascularization in MSC/OEC co-cultures

The CSD of 20,000 MSC/cm^2 and a CSR of 1:0.66 were utilized in a CC system that combines MSC with OEC. It has previously been shown that CCs of primary human osteoblasts (pOB) with OEC or CCs of MSC with OEC form microcapillary-like structures when absolute cell numbers of 300,000 pOB/MSC and 200,000 OEC were used per well in a 24 well cell culture system (Dohle et al., 2010, Dohle et al., 2011, Fuchs et al., 2007, Kolbe et al., 2011). The value given in the literature represents a CSD of 1.61x10^5 MSC/cm^2. At a similar CSD (1x10^5 MSC/cm^2) MSC were shown in a previous section to exhibit a reduced degree of osteogenic differentiation compared to a CSD of 20,000 MSC/cm^2. Therefore, studies were performed to determine if microcapillary-like structures were formed in MSC/OEC CCs when the CSD for MSC was reduced to 20,000/cm^2 or more while the CSR was kept constant at 1:0.66. For this, comparative MSC/OEC CCs were evaluated using CSD of 3,000/2,000; 10,000/6666; 20,000/13,333; 50,000/33,333 and 100,000/66,666 (MSC/OEC) per cm^2. In addition, a CC control combining 300,000 MSC and 200,000 OEC per well was included (according to (Dohle et al., 2010, Dohle et al., 2011, Fuchs et al., 2007, Kolbe et al., 2011)). After 2 wk of co-cultivation in EGM2 the CCs were analyzed for the formation of microcapillary-like structures which were identified by IF staining for CD31. The microscopic evaluation showed the formation of vessel-like structures in MSC/OEC CCs using CSD of 3,000/2,000; 10,000/6666; 20,000/13,333 and 50,000/33,333 cells/cm^2 (Figure 16A, B, C, D, respectively).

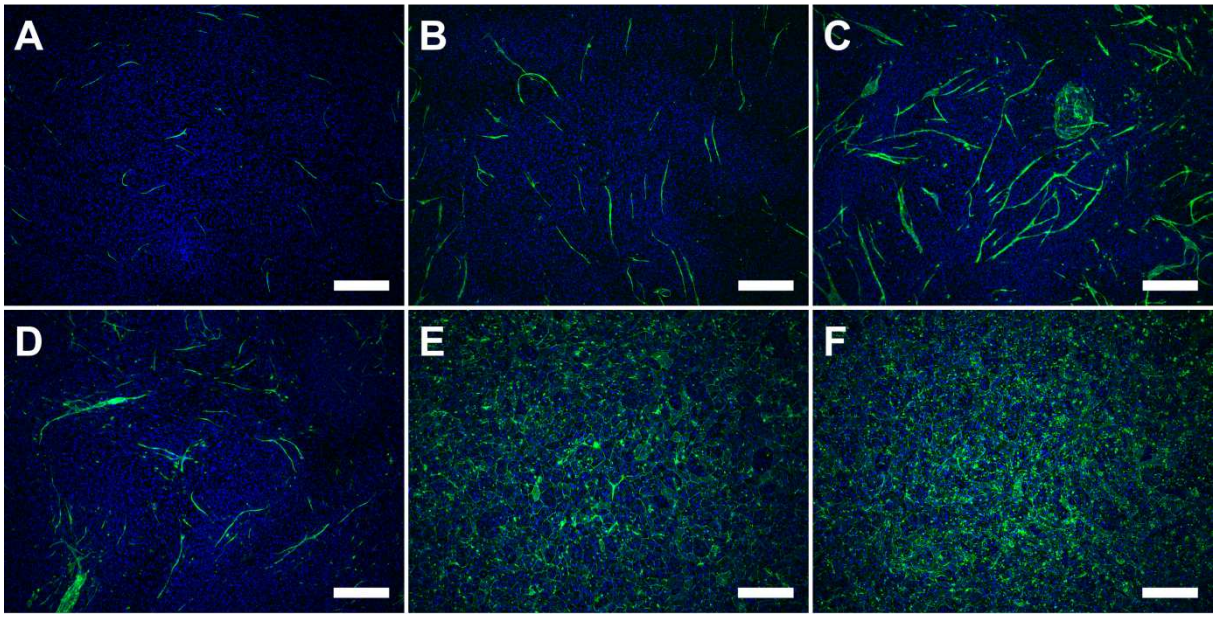

Figure 16: Influence of varying total cell numbers at constant CSR on the formation of VLS in MSC/OEC CCs. A: 3,000/2,000 per cm^2; B: 10,000/6,666 per cm^2; C: 20,000/13,333 per cm^2; D: 50,000/33,333 per cm^2; E: 100,000/66,666 per cm^2; F: 300,000/200,000 per well; Scale bars: 500 µm

Optically a maximum density of vessel-like structures was achieved when 20,000 MSC and 13,333 OEC were combined (Figure 16C). In contrast, a distinctive

reduction in the formation of microvessel-like structures was observed in MSC/OEC CCs when 100,000/66,666 (MSC/OEC)/cm2 and 300,000/200,000 (MSC/OEC)/well cells were used (Figure 16E and F, respectively). The image-based quantification of the microcapillary-like structures formed in the MSC/OEC CCs showed a similar result for the various characteristic parameters related to vascularization and angiogenesis (Figure 17).

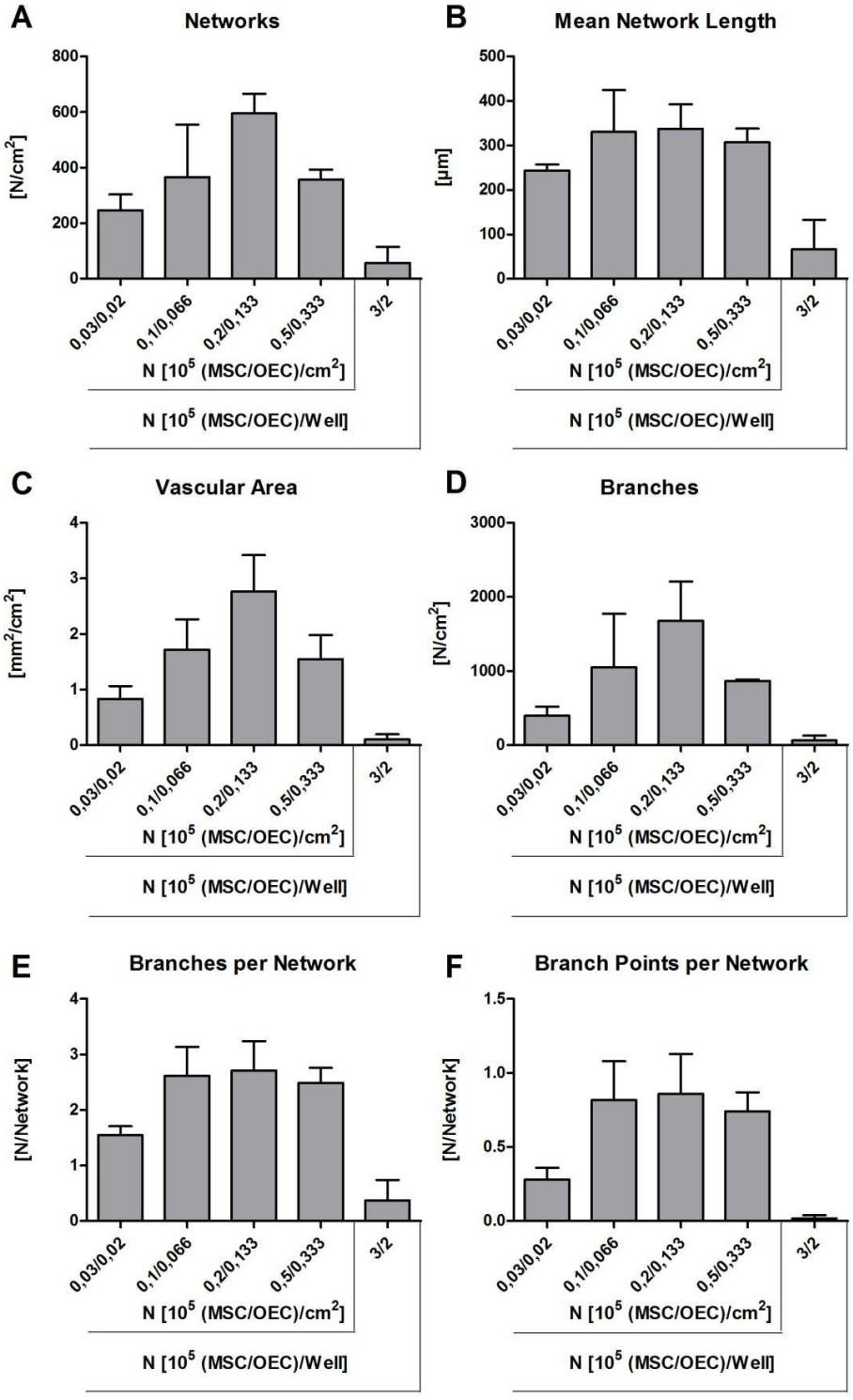

Figure 17: Image-based quantification of CSD-dependent VLS in MSC/OEC CCs and comparison of characteristic angiogenesis-related parameters; A: Total number of networks per area; B: Mean network length; C: “Vascular area” – representative area covered by angiogenic structures; D: Number of branches per area; E: Number of branches per network; F: Number of branch points per network; G: Number of triple points per network; H: Number of quadruple points per network

The highest mean values for the number of networks (Figure 17A), the mean network length (Figure 17B), the covered vascular area (Figure 17C), the number of branches per area (Figure 17D), the number of branches per network (Figure 17E) and the number of branch points per network (Figure 17F) were obtained when MSC/OEC CCs were performed with 20,000/13,333 (MSC/OEC)/cm2. In contrast, using the absolute cell numbers previously published for CCs resulted in the lowest values for all of the typical characteristic vasculogenic/ angiogenic structures evaluated (Figure 17– 3/2).

3.4 Evaluation of the co-stimulation of angiogenesis and osteogenesis in MSC/EC co-cultures

As found by the CSD-dependent evaluation of osteogenesis in MSC MCs and CSD/CSR-dependent formation of vessel-like structures in MSC/EC CCs, an MSC CSD of 20,000/cm^2 induced the highest response in both osteogenic differentiation and vessel-like structure formation.

Based on this a screening approach was conducted in order to identify a cell culture medium that would result in the simultaneous induction of osteogenesis by the MSC and the formation of microcapillary-like structures by the endothelial cells. Generally, for osteogenic differentiation of MSC, Dex, AA and βGP are added to the cell culture medium (Pittenger et al., 1999). For the growth of HDMEC, ECGM is generally used as cell culture medium (Peters et al., 2002, Peters et al., 2008, Unger et al., 2010, Unger et al., 2005, Unger et al., 2007). Furthermore, it is necessary to add GFs like bFGF and heparin for optimal EC proliferation and migration (Araki et al., 1990, Shing et al., 1984). Based on the above, an initial CC medium was mixed to stimulate the growth and proliferation of both cell types as well as endothelial microcapillary formation and MSC differentiation to osteoblasts. ECGM including bFGF and heparin was used as the basic medium to which the osteogenic differentiation supplements (OS), Dex, AA and βGP were added. Since FCS was added at a concentration of 15 % to ECGM in previous studies (Peters et al., 2002, Peters et al., 2008, Unger et al., 2010, Unger et al., 2005, Unger et al., 2007) and osteogenesis was evaluated using 10 % FCS in the above described studies, both concentrations were included in the evaluation process. The resulting variations of medium to be screened for the induction of osteogenesis and formation of vessel-like structures are given in Table 21. Additionally, controls were performed in MSC basal medium (αMEM + 10% FCS) or MSC basal medium supplemented with OS. After 2 wk the CCs were analyzed for the formation of microcapillary-like structures and the calcification of the extracellular

matrix using IF staining for CD31 as well as AR and VK staining, respectively. The formation of vessel-like structures was quantified using image analysis.

Table 21: Overview of ECGM-based media with different combinations of FCS, HF (heparin+bFGF) and osteogenic supplements (OS) used for evaluating the growth and differentiation of CCs of HDMEC with MSC. +/- indicates addition of or cultivation without HF/OS

Medium Abbreviation	FCS [%]	HF	OS
10/-/-	10	-	-
10/-/+	10	-	+
10/+/-	10	+	-
10/+/+	10	+	+
15/-/-	15	-	-
15/-/+	15	-	+
15/+/-	15	+	-
15/+/+	15	+	+

The microscopic evaluation showed no vessel formation in CCs cultivated in MSC basal medium without or with OS (Figure 18 AI/AII and BI/BII, respectively). Vessel formation could be observed in CCs cultivated in ECGM independent of the concentration of FCS when cultivated with the supplements HF alone (ECGM10/+/-; ECGM15/+/-; Figure 18 CI/CII and GI/GII, respectively). The quantification of the microcapillary-like structures formed and all related parameters including the vascular area (Figure 19A), network density (Figure 19B), the mean network length (Figure 19C), the number of branches per area (Figure 19D), the number of branches per network (Figure 19E) and the number of branch points per network (Figure 19F) resulted in the maximum values for the respective media. Addition of OS completely inhibited vessel-like structure formation (Figure 18 DI/DII and HI/HII, Figure 19), whereas CCs in ECGM without any supplementation demonstrated some formation of vessel-like structures (Figure 18 EI/EII and Figure 18 I-I/I-II). Nevertheless, the characteristic vessel-like structures were found to be decreased compared to the quantification of vessel-like structures in CCs cultivated in ECGM supplemented with HF (ECGM10/+/- or ECGM15/+/-) (Figure 19). Additionally, the resulting vessel-like structures exhibited a fragile and perforated phenotype as indicated by IF staining for CD31 (Figure 18 EII and I-II). A similar effect was observed when MSC/HDMEC CCs were cultivated in ECGM supplemented with OS alone (Figure 18 FI/FII and JI/JII). The quantification of vessel-like structures resulted in the lowest values under these cultivation conditions (Figure 19).

Independent on the vessel formation all CCs cultivated in ECGM-based medium exhibited a negative AR and VK staining (Figure 18CIII-JIII and CIV-JIV). The same

was true for CCs cultivated in MSC basal medium (Figure 18 AIII and AIV). In contrast, the cultivation of CCs in MSC basal medium supplemented with OS gave both a positive AR and VK staining (Figure 18 BIII and BIV). A similar result was obtained for MSC MCs that were cultivated in the same media to serve as a differentiation control (Figure 20). When MSC MCs cultivated in ECGM-based media were stained for the expression and activity of ALP it was found that ALP was highly expressed when HF or OS or a combination thereof was added to ECGM (Figure 20 – CI, DI, FI, GI, HI and JI). In contrast, when MSC were cultivated in ECGM without supplementation with HF or OS a low staining intensity was observed (Figure 20 EI and I-I). This intensity was comparable to MSC cultivated in MSC basal medium (Figure 20 AI). To evaluate which single supplements (FCS, HF or OS) exhibit a significant effect on the formation of vascular structures in the CCs a single factor analysis of variance (ANOVA) was performed. It was found that the variation of FCS had no significant impact on vessel-like structure characteristics. This was confirmed by the test statistic (TS) which was smaller than the critical F-value (TS < Fcrit) and by the p-value being higher than the level of significance ($p > 0.05$) for all the vessel-like structure characteristics analyzed (Table 22 – Variation of FCS). The variation of HF had a significant impact only on the vascular area (VA) with the TS > Fcrit and $p = 0.024 < 0.05$ (Table 22). All other investigated parameters were not found to be significantly influenced by HF (Table 22 – Variation of HF). In contrast, the variation of OS exhibited a TS > Fcrit and a $p < 0.05$ for all vasculogenic and angiogenic parameters (Table 22 – Variation of OS). Thus, the variation of OS significantly influenced the formation of vascular structures in MSC/HDMEC CC.

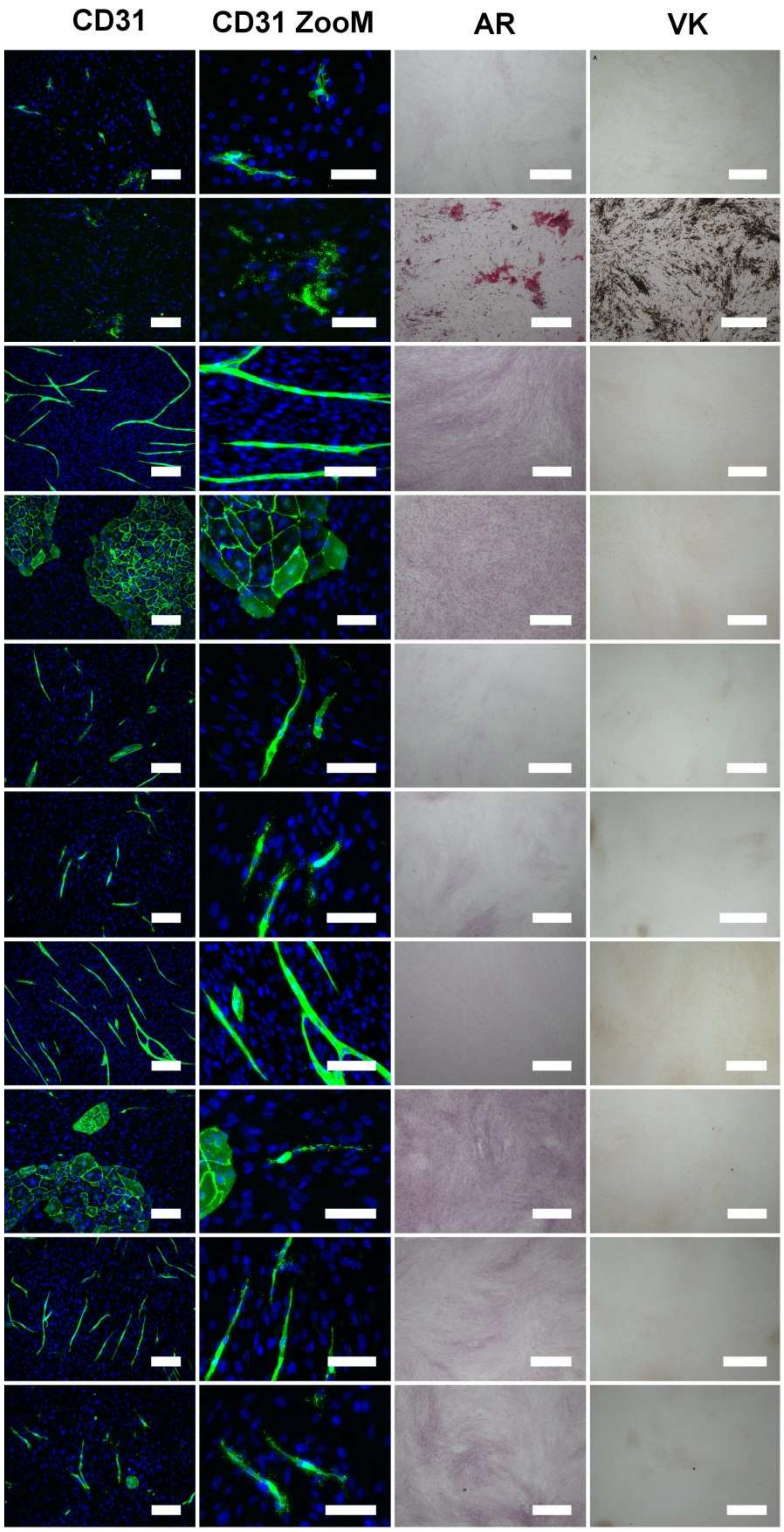

Medium	FCS [%]	HF	OS
aMEM	10	-	-
aMEM	10	-	+
ECGM	10	+	-
ECGM	10	+	+
ECGM	10	-	-
ECGM	10	-	+
ECGM	15	+	-
ECGM	15	+	+
ECGM	15	-	-
ECGM	15	-	+

Figure 18: Evaluation of VLS formation and osteogenic differentiation in MSC/HDMEC CCs performed according to the screening overview given in Table 21; CD31: IF staining for CD31, scale bars: 200 µm; CD31 Zoom: Changes in vessel morphology visualized by increased magnification, scale bars: 100 µm; AR: Alizarin Red staining, scale bars: 500 µm; VK: Von Kossa staining, scale bars: 500 µm

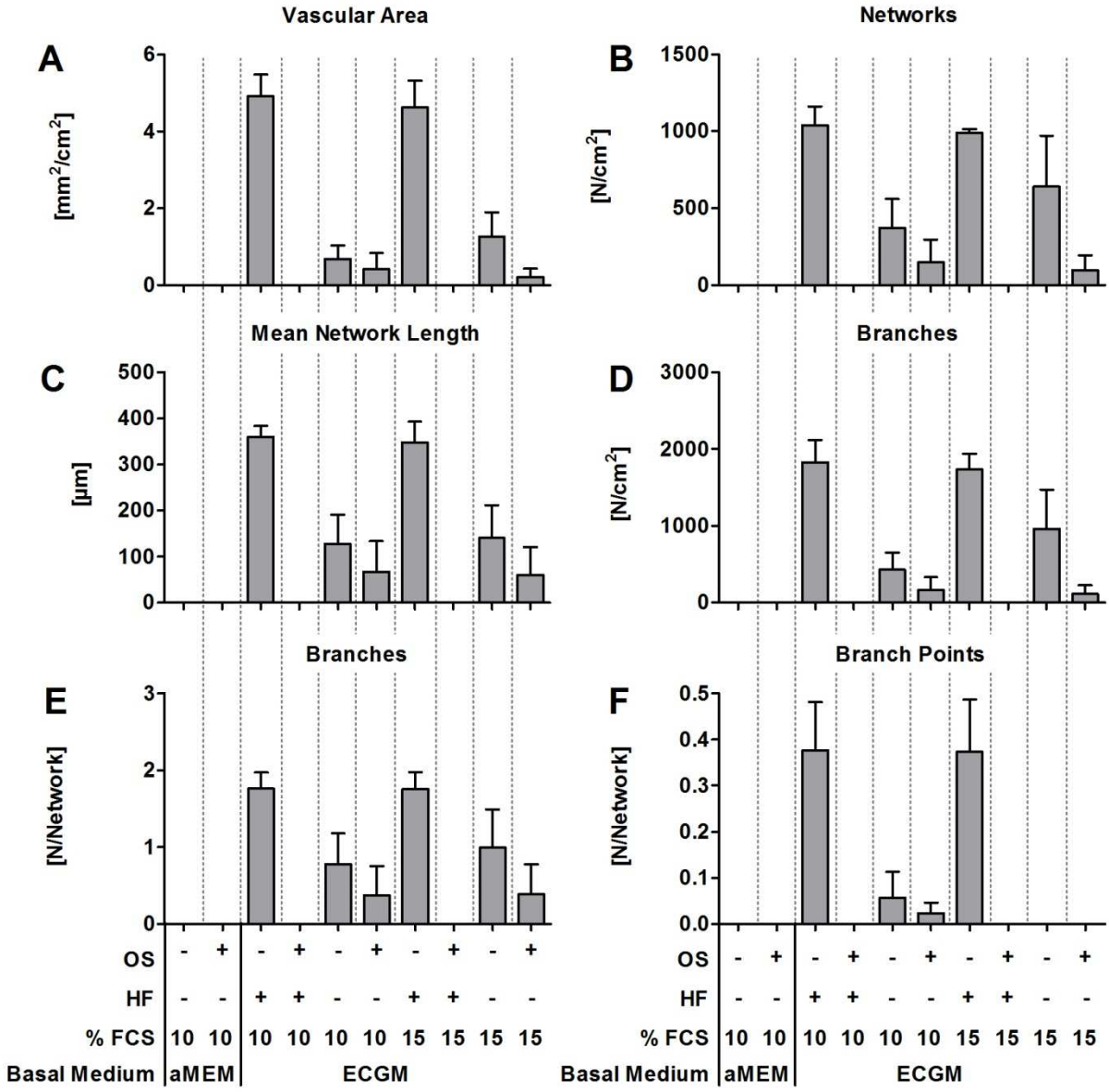

Figure 19: Image-based quantification of VLS in MSC/HDMEC CCs cultivated in various cell culture media given in Table 21; A: Vascular area; B: Number of networks; Mean network length; D: Number of branches per area; E: Number of branches per network; F: Number of branch points per network; Results are shown as means (± SEM) of three biological replicates

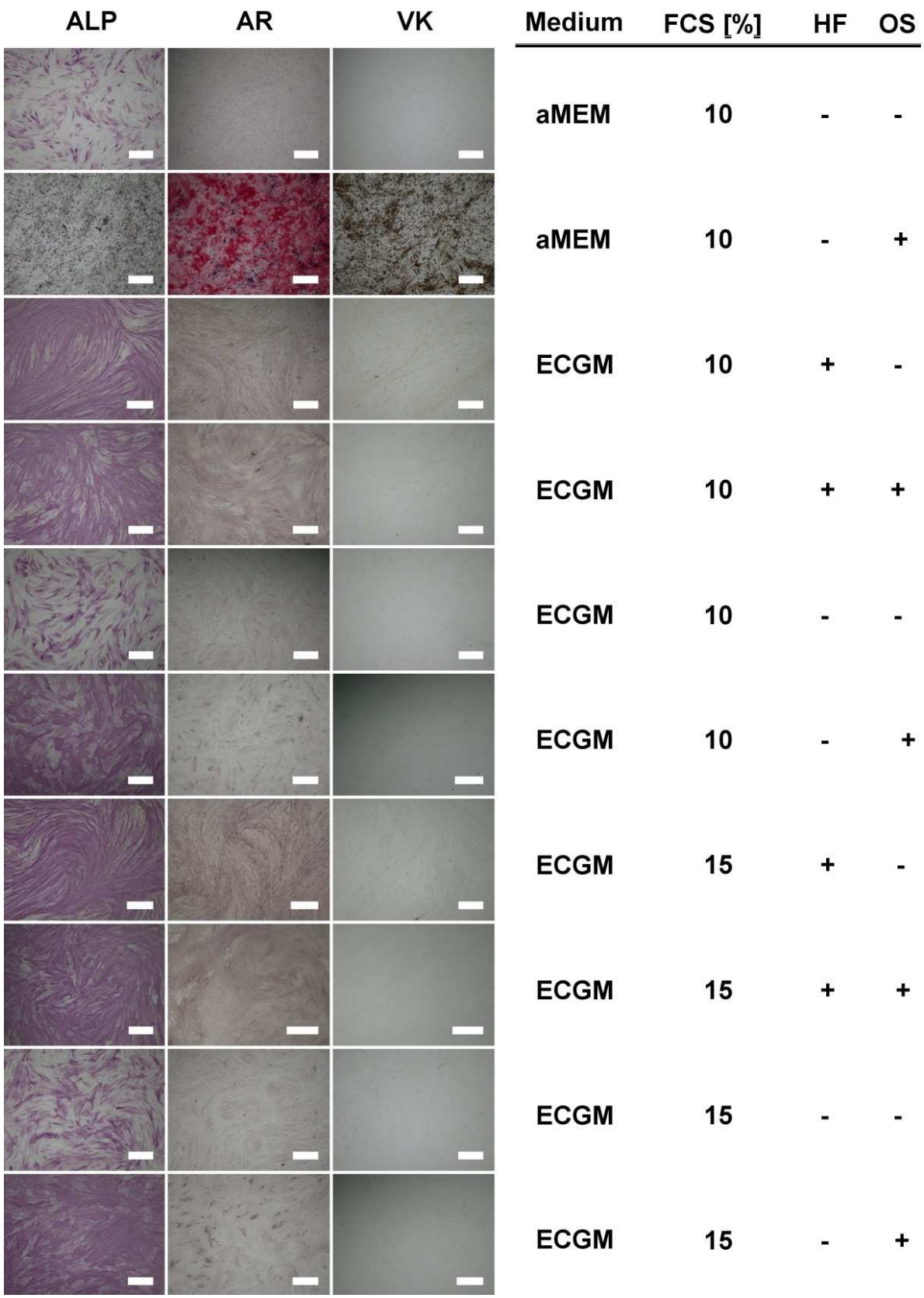

Figure 20: Evaluation of osteogenic differentiation in MSC MCs performed according to the screening overview given in Table 21; Column ALP: ALP activity staining; Column AR: Alizarin Red staining; Column VK: Von Kossa staining; Scale bars: 500 µm; HF: heparin + bFGF; OS: osteogenic supplements; "-": omitted; "+": added

Table 22: Evaluation of the significant influences of FCS, the addition of bFGF + heparin (HF) or osteogenic supplements (OS) on the formation of VLS in MSC/HDMEC CCs using single factor ANOVA; Vascular structures are evaluated for characteristic shapes: vascular area (VA, mm^2/cm^2), number of networks (N, N/cm^2), branches per network (B, 1/N) and network length (NL, µm); TS: test statistic, p: p-value

	Variation of FCS		Variation of HF		Variation of OS		All
Parameter	**TS**	**p**	**TS**	**p**	**TS**	**p**	**F_{crit}**
VA	0,01339	0,91	5,92	0,024	15,98	0,00061	4,301
N	0,01154	0,92	3,17	0,089	22,46	0,00010	4,301
B	0,02542	0,87	0,53	0,475	22,27	0,00010	4,301
NL	0,00044	0,98	1,58	0,222	21,47	0,00013	4,301

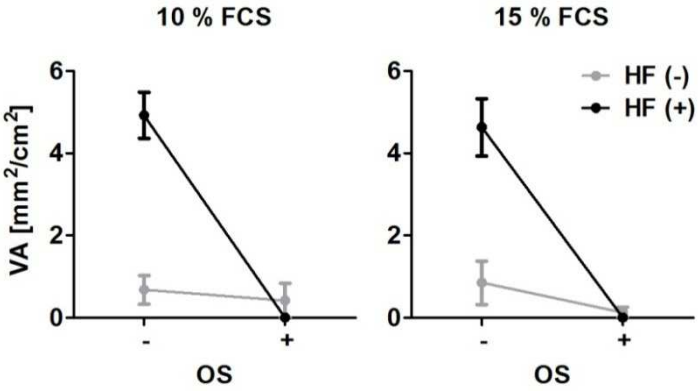

Figure 21: Interaction plot identifying a connection between the supplementation of OS and HF and its influence on the quantification of the vascular area VA; OS: osteogenic supplements; HF: bFGF + heparin

To visualize the impact of FCS, HF or OS supplementation of the CC media, the data obtained were introduced into an interaction plot (Figure 21). Using such an interaction plot can help identify interactions between different factors based on their presence or absence. This is realized by plotting data obtained from the experimental quantification via an interconnected line. Factors are considered to interact when the resulting lines are not parallel (Kleppmann, 2013). In addition, the interaction is considered especially strong when both lines intersect (Kleppmann, 2013). The data for an interaction between OS and HF can be seen in Figure 21. The interconnected data points clearly demonstrate a strong decrease in the VA when OS were added (OS (+)) independent of the presence or absence of HF (HF (+)/HF (-)) (Figure 21). This finding was also observed when the FCS concentration was raised from 10 % to 15 % (Figure 21). Taken together these data show that under the conditions evaluated the addition of OS suppresses microcapillary-like vessel formation and this was influenced by a strong statistical interaction between HF and OS. Since no osteogenic differentiation was achieved in MSC/HDMEC CCs and MSC MCs in ECGM-based media the data further indicate that supplementation with angiogenic-stimulating factors or the use of media supporting angiogenesis was not adequate for the osteogenic differentiation of MSC.

3.5 The impact of osteogenic priming of MSC on the prevascularization in co-cultures with HDMEC

Based on the findings described in the previous section an alternative strategy was developed, which aimed to investigate a chronologically separated induction of the osteogenic differentiation of MSC and the prevascularization of MSC/EC CCs. In this context, it was previously shown that pre-differentiated MSC supported bone formation to a higher extent *in vivo* compared to non-differentiated MSC (Breitbart et al., 1998, Liu et al., 2015). To determine whether an osteogenic priming of MSC would also have a positive effect on the formation of VLS in CCs *in vitro*, CCs of osteogenically primed MSC with HDMEC and non-differentiated MSC with HDMEC were performed and compared using a constant CSR of 3:2. For these studies, MSC MCs were cultivated under osteogenic-differentiating conditions in ODM for 2 wk or 4 wk, termed as oMSC-2wk or oMSC-4wk, respectively. As a control MSC MCs were cultivated under non-osteogenic inducing conditions in basal medium (referred to as Basal (Table 8) and abbreviated as BM in this section) for 2 wk or 4 wk, termed as MSC-BM2wk and MSC-BM4wk, respectively (see also Supplementary Figure 5).

3.5.1 Evaluation of osteogenic priming in MSC mono-cultures

ALP activity staining indicated an increased ALP activity in oMSC-2wk and oMSC-4wk compared to MSC-BM2wk or MSC-BM4wk (Figure 22A - ALP). The staining intensities of the AR and VK staining of oMSC-2wk showed a weak signal (Figure 22A - AR/VK) compared to oMSC-4wk, which exhibited strong staining intensities for both AR and VK staining (Figure 22A - AR/VK). No AR or VK staining was observed in MSC-BM2wk and MSC-BM4wk cultures (Figure 22A - inserts in AR/VK).

To evaluate changes in the release of GFs during the osteogenic differentiation VEGF and Ang-1 were quantified in the supernatants of oMSC and MSC-BM over a period of 4 wk (Figure 22B). VEGF increased with time in MSC-BM, whereas a constantly low concentration of approximately 0.3 ng/mL was measured in supernatants of oMSC (Figure 22B VEGF). In contrast, Ang-1 increased with time in oMSC reaching a plateau concentration of approximately 10 ng/mL after 19d (Figure 22B Ang-1 – grey bars). MSC-BM produced only low levels of Ang-1 (1 ng/mL) for the entire culture period (Figure 22B Ang-1 - white bars). Taken together these results indicated that an osteogenic priming of MSC for 4 wk using ODM reduced their vasculogenic and angiogenenic inductivity compared to MSC cultivated under non-osteogenic conditions. To evaluate this hypothesis MSC-BM and oMSC were co-cultivated with HDMEC for 2 wk (2wk CC) in ECGM using four comparative CC approaches as shown in Figure 23.

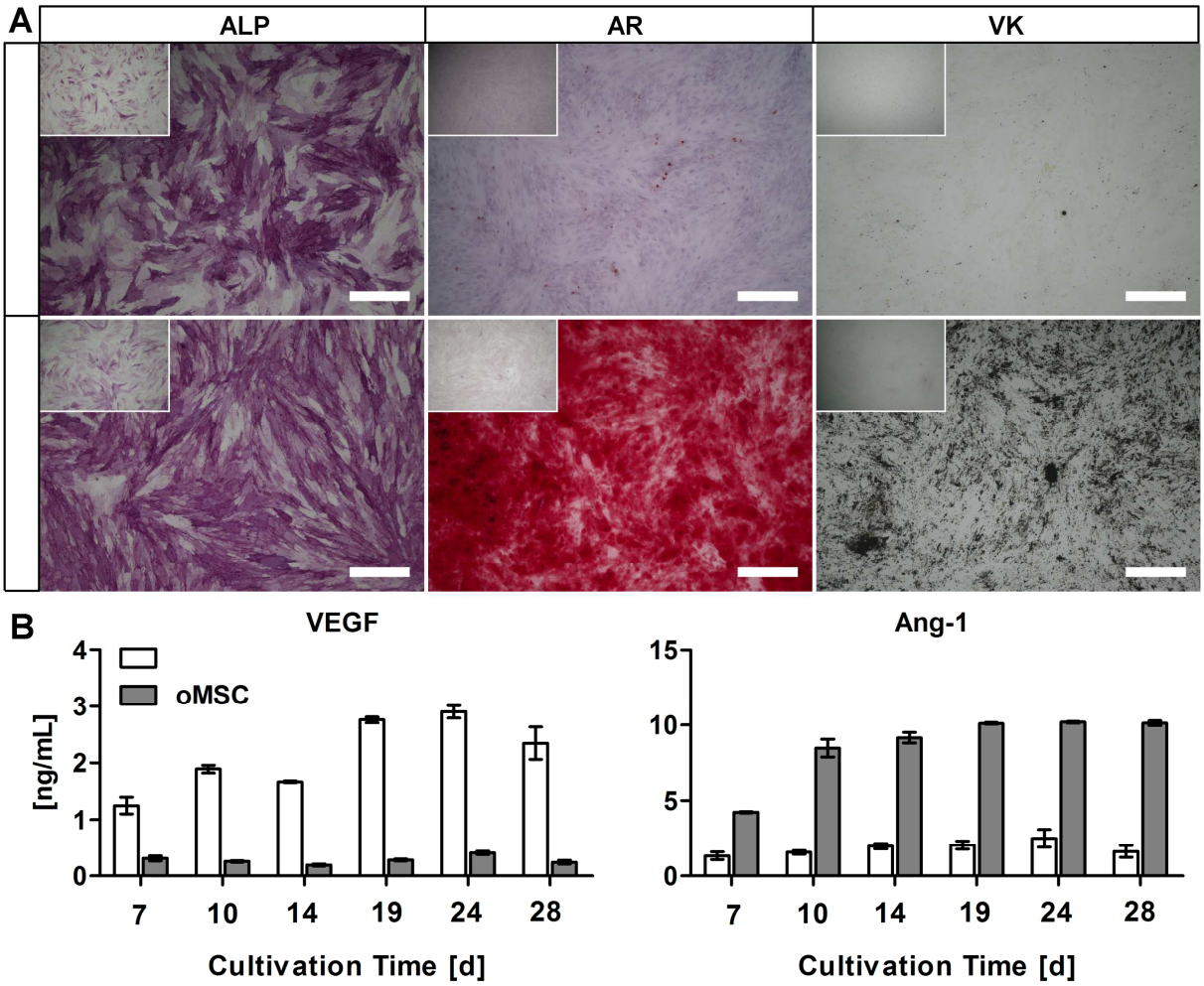

Figure 22: Osteogenic priming of MSC in ODM over 4 wk. A: Evaluation of the degree of osteogenic differentiation in MSC after 2 wk (oMSC-2wk) and 4 wk (oMSC-4wk) of cultivation in ODM compared to their corresponding controls cultivated under non-osteogenic conditions (small inserts); ALP: ALP activity staining; AR: Alizarin red staining; VK: Von Kossa staining; Scale bars: 500 µm; B: ELISA-based quantification of VEGF and Ang-1 in supernatants of oMSC and MSC-BM over 4 wk

3.5.2 Co-cultivation of osteogenically primed MSC with HDMEC

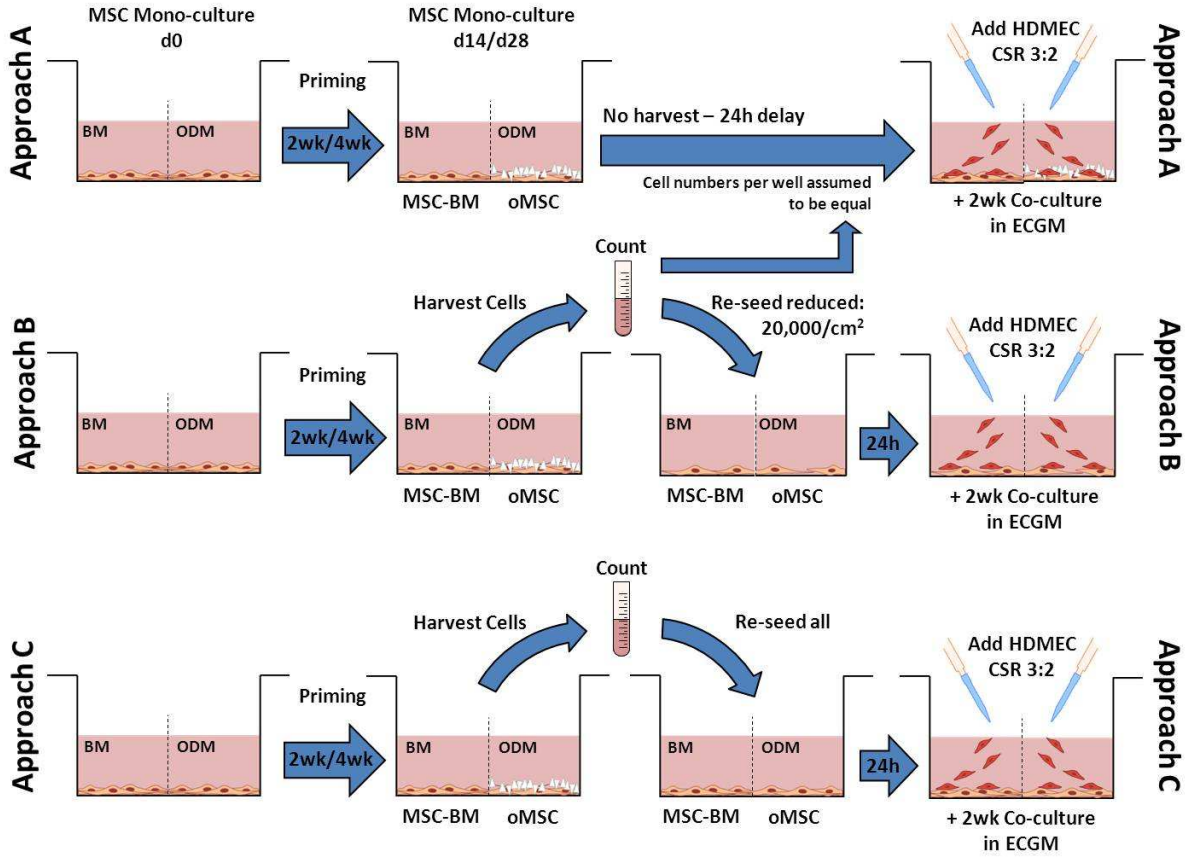

Figure 23: Schematic workflow for the generation of comparative co-culture approaches to investigate the influence of MSC primed in either BM or ODM on the prevascularization in a CC system with HDMEC. The generation of MSC-BM and oMSC is schematically represented in Supplementary Figure 5.

To study the direct effect of oMSC and MSC-BM on vessel formation in the CC system HDMEC were added directly to oMSC-2wk/4wk or MSC-BM2wk/4wk shown in approach “A” (Figure 23). In approach “B” (Figure 23) oMSC or MSC-BM were harvested and re-seeded at a reduced CSD of 20,000 cells/cm2 prior to initiating the CC by the addition of HDMEC. To investigate whether the vessel formation would be influenced by any osteogenic or non-osteogenic matrix formed during co-cultivation of HDMEC with either oMSC or MSC-BM, the respective MSC MCs were removed by trypsinization and re-seeded after the initial priming phase without any reduction of the CSD in approach “C” (Figure 23). In this context, Approach “C” served as a control to approach “A” with both approaches differing in the presence of an osteogenic matrix. In parallel, a standard 2 wk CC of non-primed MSC with HDMEC (Control/Ctrl) was performed. When oMSC or MSC-BM were transferred to fresh wells for the co-cultivation with HDMEC in approach “B” or “C” their absolute cell number per area was determined prior to reseeding. Having initially seeded 20,000 MSC/cm2 the cell densities increased upon priming in BM to a mean density of

30,000 cells/cm2 in both MSC-BM2wk and MSC-BM4wk (Supplementary Figure 6). On the contrary, in oMSC cultures the mean cell density was found to have only slightly increased after 2 wk of priming in ODM (oMSC-2wk) and to have decreased below the initial CSD of 20,000 cells/cm2 after 4 wk (oMSC-4wk) (Supplementary Figure 6). These changes in the cell densities upon osteogenic priming underline the process of osteogenic differentiation in oMSC cultures that is known to be linked to apoptosis and cell death in the final differentiation stage (Manolagas, 2000).

The microscopic evaluation of the immunofluorescence staining for CD31 clearly indicated the formation of VLS in the CCs of oMSC-2wk or MSC-BM2wk with HDMEC (Figure 24A). No enhancement of VLS formation by oMSC-2wk compared to MSC-BM2wk was detected in the CC with HDMEC (Figure 24A – MSC-BM2wk/oMSC-2wk + 2 wk CC). This outcome was found to be constant among the different CC approaches (Approach “A”, “B”, “C” - Figure 24A). The microscopic evaluation was supported by the results of the image-based quantification of the VLS formation in 2 wk CC of MSC-BM2wk or oMSC-2wk with HDMEC (Figure 24B – exemplary shown for approach “A”). In this context, the vascular area, the number of networks, the mean network length, the total number of branches, the number of branches per network and the number of branch points per network (all Figure 24B) were quantified. The quantification of the parameters mentioned above demonstrated similar values compared to those observed in the control independent of whether the 2 wk CC consisted of oMSC-2wk or MSC-BM2wk with HDMEC (Figure 24B – light grey bars). This outcome was found to be consistent among the different CC approaches (Supplementary Figure 7 and Supplementary Figure 8). ELISA measurements of the pro-angiogenic GF VEGF, Ang-1 and Ang-2 in the control revealed that all three GF were present at high concentrations (Figure 24C). In this context, VEGF and Ang-1 were solely expressed by MSC while Ang-2 was exclusively expressed by HDMEC (Figure 24C).

When MSC-BM4wk or oMSC-4wk were co-cultivated with HDMEC for 2 wk in ECGM all quantified vascular network parameters were clearly affected. The mean values for the vascular area, the number of networks, the number of total branches and the number of branch points per network were markedly reduced (Figure 24B - dark grey bars). However, the mean network length and the number of branches per network (Figure 24B – Mean Network Length and Branches per Network, respectively) were less affected when MSC-BM4wk were co-cultivated with HDMEC. The described effects were found to be independent of the CC conditions (Supplementary Figure 7 and Supplementary Figure 8). Although no statistical significance was achieved the overall trend was found to be consistent at the single donor level (Supplementary Figure 9, Supplementary Figure 10, Supplementary Figure 11).

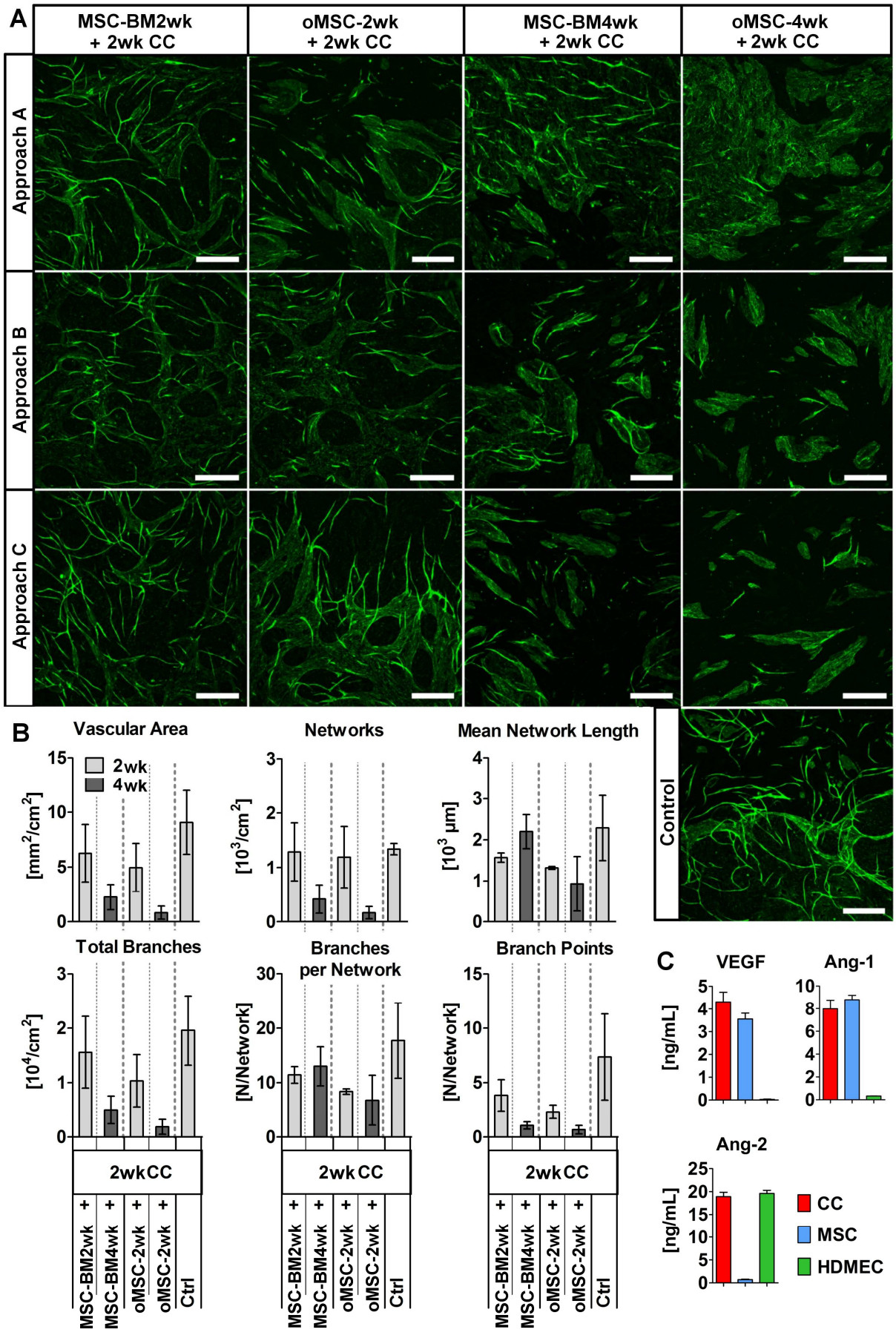
A
MSC-BM2wk + 2wk CC
oMSC-2wk + 2wk CC
MSC-BM4wk + 2wk CC
oMSC-4wk + 2wk CC
Approach A
Approach B
Approach C
Control
B
Vascular Area
[mm²/cm²]
2wk
4wk
Networks
[10³/cm²]
Mean Network Length
[10³ µm]
Total Branches
[10⁴/cm²]
Branches per Network
[N/Network]
Branch Points
[N/Network]
2wk CC
MSC-BM2wk +
MSC-BM4wk +
oMSC-2wk +
oMSC-2wk +
Ctrl
C
VEGF
Ang-1
Ang-2
[ng/mL]
CC
MSC
HDMEC

Figure 24: Influence of oMSC on the formation of VLS in a CC model with HDMEC. A: IF staining for CD31 in 2 wk CC of MSC-BM2wk/4wk or oMSC-2wk/4wk with HDMEC cultivated according to approach “A”, “B”, “C” or Ctrl (for schematic representation see Figure 23); Scale bars: 500 µm; B: Quantification of vasculogenic and angiogenic parameters in CCs cultivated according to approach A (see Figure 23) based on IF staining for CD31; C: Quantification of release of VEGF, Ang-1 and Ang-2 in supernatants of control CC of non-primed MSC with HDMEC (control) after 2 wk

Taken together these results clearly demonstrate that prevascularization in MSC/HDMEC CCs is negatively influenced by priming the MSC with osteogenic differentiation factors prior to their co-cultivation with HDMEC. Additionally, the results point out that the observed effects are independent of the incorporation of an osteogenic matrix or the change of absolute cell numbers.

3.6 Prevascularized MSC/HDMEC co-cultures cultivated under osteogenic conditions

Having shown that an initial osteogenic priming of MSC negatively affects the formation of vessel-like structures by HDMEC in subsequent CCs an opposite approach was investigated. In this approach, conditions were used to first stimulate HDMEC within the CC to form vessel-like structures what was then followed by changing the medium to osteogenic-inducing conditions using ODM (termed as osteogenic co-culture “oCC” in the following).

For this, CCs of non-primed MSC with HDMEC were cultivated for 2 wk in ECGM leading to the formation of vessel-like structures. Subsequently, the medium in this prevascularized CC was changed to ODM for osteogenic co-cultivation for 2 wk (2wk oCC) or 4W (4wk oCC) and the resulting level of calcification in the oCC was investigated. As a differentiation control (DC) MSC MCs were cultivated in ECGM for 2 wk and the medium was subsequently replaced with ODM for the same period of time as in the oCC. After 2wk oCC a high degree of calcification was detectable (Figure 25A – 2wk oCC). Positive AR and VK staining revealed the deposition of calcium and calcium phosphates, respectively (Figure 25A – 2wk oCC – AR/VK). Furthermore, the IF staining for CD31 confirmed the incorporation of an endothelial cell fraction (Figure 25A – 2wk oCC – CD31). The same result was achieved after 4wk oCC (Figure 25A – 4wk oCC – CD31). Although the same high degree of calcification was histochemically detectable (Figure 25A – 4wk oCC – AR/VK) no additional increase in the AR staining intensity compared to 2wk oCC was observed (Figure 25B). IF staining for CD31 demonstrated the presence of endothelial cells organized in a homogeneous cell layer within the calcified CC (Figure 25A – 4wk oCC – CD31). In the DC a less intense staining for AR and VK after 2 wk and 4 wk was observed (Figure 25A – 2wk/4wk DC AR/VK) and lower amounts of calcium deposits were confirmed by a quantitative analysis of the AR staining (Figure 25B).

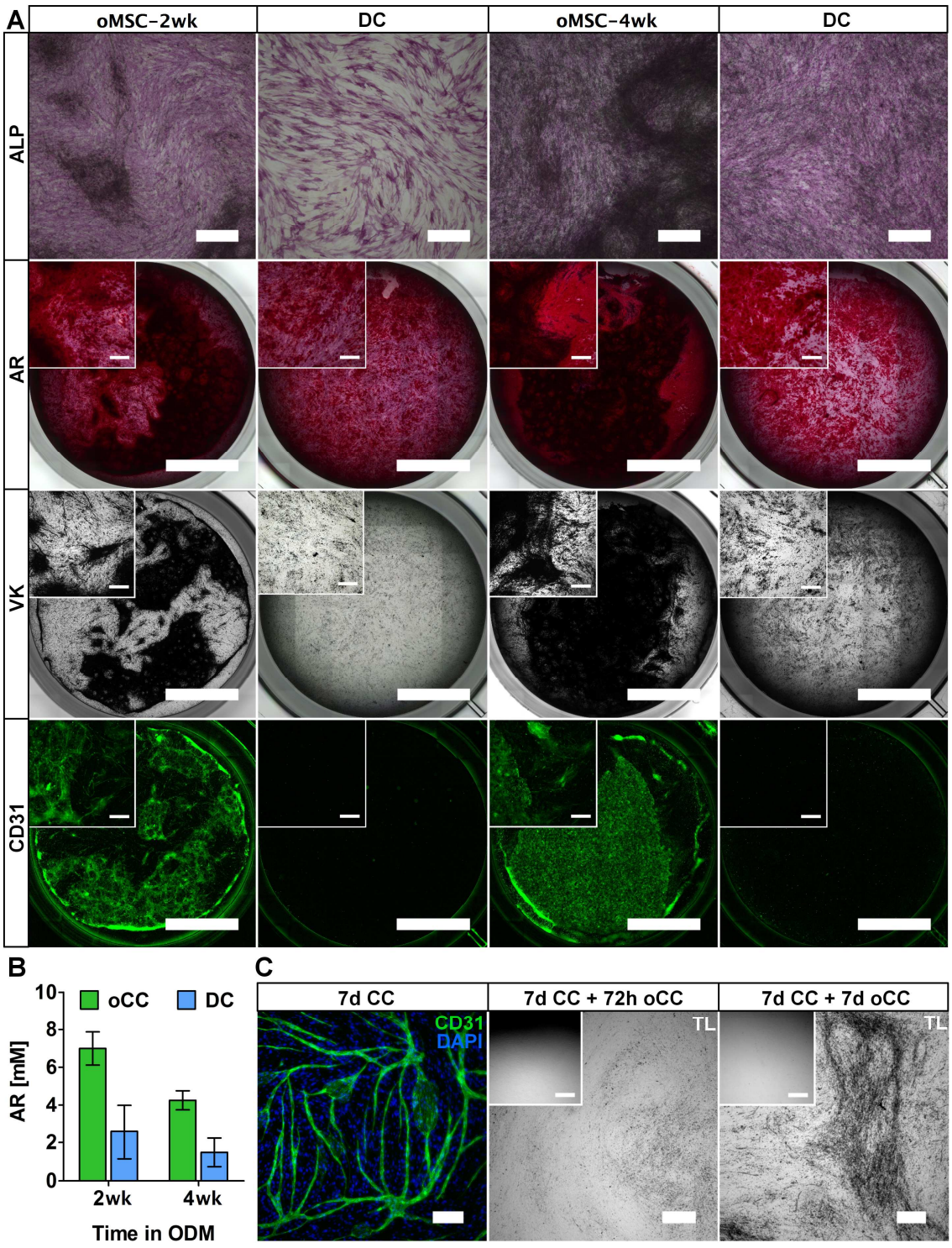

Figure 25: Microscopic evaluation of MSC differentiation and VLS formation after cultivation of prevascularized 2wk CC under osteogenic conditions for 2wk (2wk oCC) or 4wk (4wk oCC); A: ALP activity staining (ALP), Alizarin Red staining (AR), Von Kossa staining (VK) and IF staining for CD31 (CD31) in 2wk-oCC and 4wk-oCC cultures compared to their corresponding differentiation control (DC); Scale bars: ALP = 500 µm; AR, VK, CD31 = 5 mm, inserts = 500 µm; B: Quantitative analysis of AR staining intensity in 2wk oCC and 4wk oCC cultures compared to their corresponding DC; C: Detection of VLS in 7d CC using IF staining for CD31 (CD31/DAPI) and microscopic evaluation of matrix calcification after additional 72h oCC and 7d oCC using transmitted light microscopy (TL); Scale bars: 200 µm

The ALP activity staining revealed a lower expression and activity of ALP in the 2wk-DC compared to the 2wk oCC (Figure 25A – 2wk oCC/2wk DC - ALP) whereby equal staining intensities were obtained in 4wk-DC and 4wk-oCC (Figure 25A – 4wk oCC/4wk DC - ALP). Both the 2wk DC and the 4wk DC were found to be negative for the IF staining for CD31 (Figure 25A – 2wk DC/4wk DC – CD31). These results indicate that the cultivation of prevascularized MSC/HDMEC CCs under osteogenic conditions allows for the generation of calcified samples containing an endothelial fraction organized in homogeneous cell layers.

Reduction of the time to implantation of an *in vitro* prevascularized biomaterial to be used in regenerative medicine is a major goal in tissue engineering (Rouwkema et al., 2008) Therefore, a shortened phase of prevascularization was investigated in the context of a subsequent phase of oCC to obtain prevascularized calcified cultures within a reduced time frame. CCs of non-primed MSC with HDMEC were cultivated under angiogenic conditions in ECGM for 3d (3d CC), 7d (7d CC) or 2wk (2wk CC) to generate the formation of VLS. Subsequently, the medium in these prevascularized CCs was changed to ODM for osteogenic co-cultivation for 72h (72h oCC) or 7d (7d oCC) and the resulting levels of calcification in the oCC were monitored using transmitted light microscopy. IF staining for CD31 demonstrated the formation of VLS in 7d CC (Figure 25C – CD31/DAPI), while no VLS were obtained after 3 d of co-cultivation (Supplementary Figure 12). Slight amounts of matrix calcification were observed after 72h oCC and 7d oCC in 7d CC (Figure 25C - TL). This outcome was comparable to 2wk CC cultivated under osteogenic conditions (Supplementary Figure 12). No evidence of matrix calcification was found after 72h oCC but 7d oCC in 3d CC (Supplementary Figure 12). Comparative DC exhibited no matrix calcification at any of the investigated time points (Figure 25C – TL/small inserts; Supplementary Figure 12 – small inserts).

3.6.1 Evaluation of the osteogenic co-cultivation in a time-dependent manner

Since the degree of matrix calcification was found to attain a maximum after 2 wk of oCC (Figure 25B) the cultivation of prevascularized MSC/HDMEC CCs was studied in a time-dependent manner over a 14d period (Figure 26). The formation of a calcified matrix in 7d CC followed by oCC for 12h, 24h, 48h, 72h, 5d, 7d and 14d was investigated by AR, VK and ALP activity staining.

The evaluation of osteoblastic differentiation markers revealed an initial calcification after 72h oCC as demonstrated by a positive AR and VK staining (Figure 26 – 72h oCC – AR/VK). The intensities of both staining methods (VK and AR) were found to increase in a time-dependent manner up to 14d oCC by all of the individual donors (Figure 26 – 72h to 14d oCC – AR/VK; Supplementary Figure 13A1-D1). The analysis of the microscopic images was supported by the quantitative measurements of the AR staining (Figure 27A – 7d CC + oCC). The result was not found to be consistent at the single donor level (Supplementary Figure 13) as the donors 1 and 2

exhibited an initial calcification after 5d oCC (Supplementary Figure 13 A1 and B1), whereas the donors 3 and 4 showed an initial calcification after 72h oCC and 7d oCC, respectively (Supplementary Figure 13 C1 and D1). The ALP activity staining showed a constant intensity during oCC (Figure 26 – oCC – ALP). In the corresponding DC, a positive staining for ALP was first observed after 14d oCC (Figure 26 – 14d DC – AR/VK). The quantitative analysis of the AR staining could not confirm the microscopic observations (Figure 27A – (7d+7d) DC; for single donor analysis see Supplementary Figure 13A1-D1).

To determine what effects a prolonged prevascularization phase had on the cultures, ECGM was replaced after 2 wk and the CC were cultivated under osteogenic conditions for an additional 12h, 24h, 48h, 72h, 5d, 7d and 14d in ODM. The quantitative analysis of the AR staining exhibited a time-dependent increase with a positive signal initially detected after 48h oCC (Figure 27A – 2W CC + oCC). At the single donor level 2 of 3 donors represented the course of the mean value (Supplementary Figure 13 B2 and C2) while one donor exhibited an initial calcification after 5d oCC (Supplementary Figure 13 A2). A similar pattern was observed in the DC. An initial increase of the mean AR staining intensity was detected after 5d in ODM followed by a slight increase up to 14d (Figure 27A – (2W+7d) DC). At the single donor level 2 of 3 donors represented the course of the mean value while one donor remained negative for the quantitative analysis of the AR staining (Supplementary Figure 13 A2, B2 and C2). In comparison, when prevascularized CC (7d CC and 14d CC) were maintained under prolonged angiogenic conditions (angCC) for 12h, 24h, 48h, 72h, 5d, 7d and 14d as a control no calcification was detected (Figure 27A – 7d CC/14d CC + ang CC).

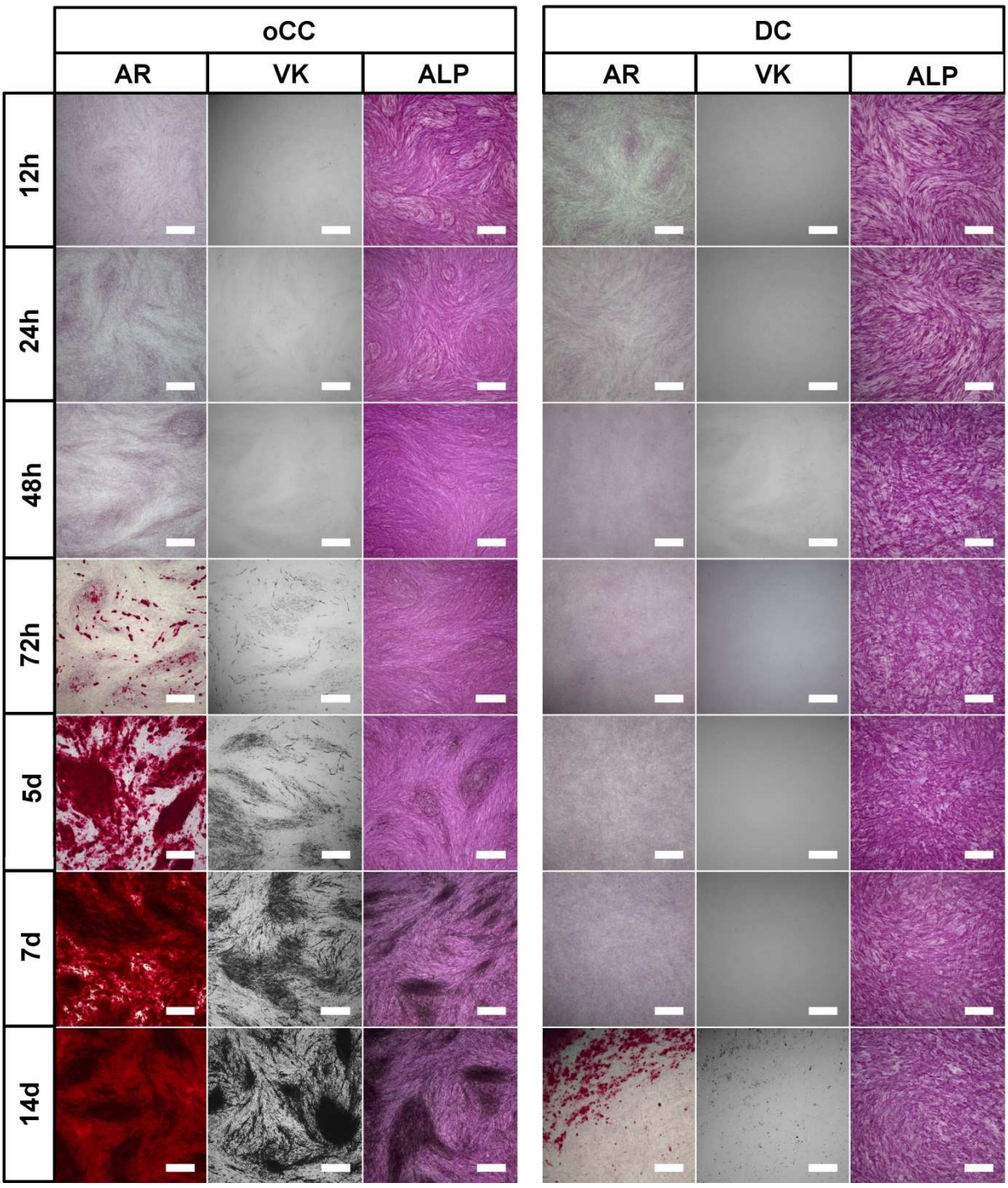

Figure 26: Microscopic evaluation of the matrix mineralization and ALP activity during the osteogenic co-cultivation (oCC) of prevascularized 7d CC compared to a differentiation control (DC) by AR, VK and ALP activity staining, Scale bars: 500 µm. All images shown in A correspond to donor 2 in Supplementary Figure 13.

3.6.2 Evaluation of the osteogenic co-cultivation at the protein level

To evaluate the osteogenic differentiation during oCC at the protein level, the ALP activity during oCC, angCC and DC was determined in protein lysates of the cell cultures. The ALP is widely accepted as an early stage marker for the analysis of osteogenic differentiation in MSC (Beck et al., 2000, Tsai et al., 2009, Honda et al.,

2013). The activity of ALP was measured after 24h and 5d of oCC, angCC and DC (Figure 27B), thus investigating a time point prior to the first detectable calcification during oCC and a time point were calcification was initiated by all donors (Figure 27A; Supplementary Figure 13 A1, B1, C1 and D1). The activity of ALP was upregulated during oCC and angCC compared to the DC (Figure 27B). Furthermore, a time-dependent increase of the ALP activity was detected during co-cultivation in oCC (Figure 27B). A similar time-dependent trend was measured in the DC (Figure 27B – blue bars), although the ALP activity level remained below the level measured during oCC (Figure 27B – blue versus red bars). MCs of HDMEC exhibited no ALP activity (Figure 27B). Altogether, these results indicate that the cultivation of prevascularized CCs under osteogenic conditions in ODM allows for the rapid induction of osteogenesis and the mineralization of the extracellular matrix. At the same time, the results suggest that under comparable culture conditions osteogenic differentiation is induced at a statistically much lower level in the DC.

Based on these findings further studies were carried out to determine if endochondral ossification (ECO) was induced in prevascularized MSC/HDMEC CCs during oCC. In this context, it was shown that endothelial cells exhibit regulatory functions in the physiological process of ECO *in vivo* (Babarina et al., 2001, Bittner et al., 1998). To address a possible connection between the cultivation of prevascularized CC under osteogenic conditions and the induction of ECO 2D samples obtained after 7d oCC were stained for the expression of glycosaminoglycans (GAG) using Alcian Blue (AB) and the expression and activity of ALP using ALP activity staining. In this context, it has been shown by others that an increased ALP expression and activity is also connected to ECO (Scotti et al., 2010, Mackie et al., 2008b). It can be seen from Figure 27C (ALP/AB) that a positive signal was obtained from the AB staining in the CC after 7d oCC (yellow arrows). The remaining areas are linked to an increased intensity of ALP activity staining (Figure 27C – ALP/AB/white arrows). Furthermore, IF staining for CD31 revealed the AB-positive location to be covered by remaining endothelial cell layers (Figure 27C – ALP/AB/CD31/white arrows). To evaluate time-dependent changes in the AB staining intensity prevascularized 7d CC cultivated under osteogenic conditions for 12h, 24h, 48h, 72h, 5d, 7d and 14d were stained using ALP activity staining and AB staining. A time-dependent increase of the AB staining intensity was found in the CC during oCC with an optical maximum intensity obtained after 14d oCC (Figure 27D - oCC). A similar result was found when the prevascularized 7D CC were cultivated under prolonged angiogenic conditions (Figure 27D - angCC). No AB signal was detected in the DC at any investigated time point (Figure 27D - DC). The microscopic observations were supported by quantitative data from image analysis of the AB staining intensity, demonstrating the time-dependent trend during oCC and angCC and unchanged intensities in the DC comparable to the control (Figure 27E). To assess an influence of the incorporated endothelial cell fraction on the final degree of osteogenic differentiation during oCC the proportion of endothelial cells in the co-culture was increased.

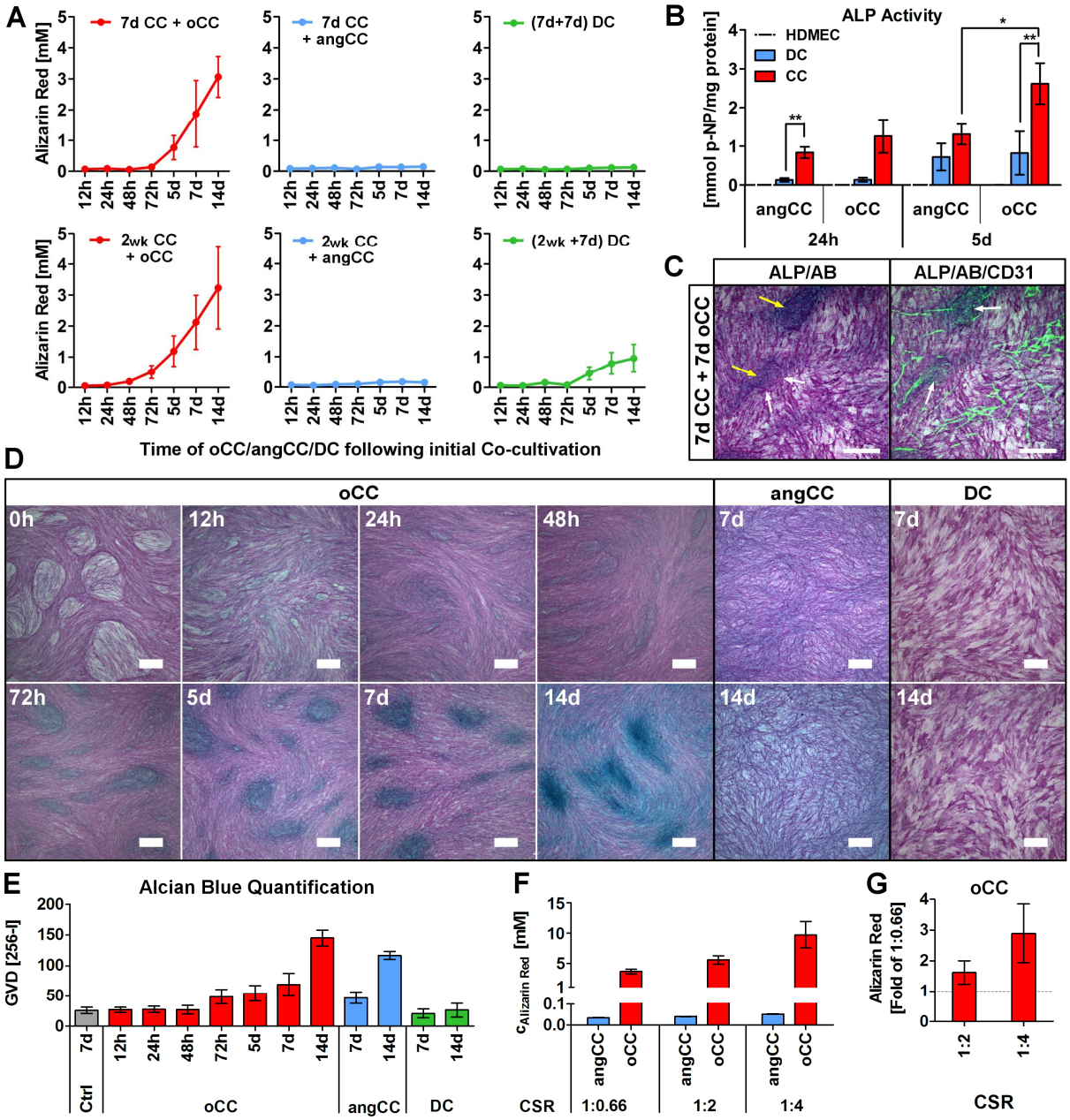

Figure 27: Evaluation of the osteogenic differentiation in MSC/HDMEC CCs during oCC, angCC and in DC. A: Quantitative analysis of AR staining during oCC and angCC of MSC/HDMEC CCs prevascularized for 7d (7d CC, n = 4) or 2 wk (2wk CC, n = 3) and in DC; B: Determination of the ALP activity in CCs during oCC and angCC and in DC, asterisks indicate statistical significance: *: $p < 0.05$, **: $p < 0.01$, n = 3; C: Correlation of ALP activity staining (ALP) with Alcian Blue (AB) staining and IF staining for CD31 after 7d oCC, Scale bars: 200 µm; D: Time-dependent evaluation of GAG deposition during oCC and angCC as well as in DC using AB staining, Scale bars: 200 µm; E: Image-based quantification of AB staining intensities from time-dependent AB staining during oCC, angCC and in DC as exemplarily shown in D, n = 3; F: Quantitative analysis of AR staining in CCs with varying CSR after 7d oCC and 7d angCC, n = 3; G: Values for CSR of 1:2 and 1:4 shown in F normalized to 1:0.66, n = 3

By varying the MSC:HDMEC CSR from 1:0.66 to 1:2 or 1:4 the degree of matrix calcification was increased after 7d oCC, resulting in a maximum value when a CSR

of 1:4 was used (Figure 27F – red bars). Compared to a CSR of 1:0.66 the changes represent a 1.5-fold and 3-fold increase in the AR staining intensity for a CSR of 1:2 and 1:4, respectively (Figure 27G). No matrix calcification was observed after 7d angCC (Figure 27F – blue bars). These data indicate that the degree of osteogenic differentiation during oCC can be adjusted by controlling the proportion of endothelial cells present in the CC.

3.6.3 Osteogenic co-cultivation and vessel regression

The regression of VLS detected by IF staining was observed in CCs undergoing osteogenic differentiation during oCC. After 7d oCC a strong degree of regression of VLS linked to an intense calcification along the former VLS was observed by TL microscopy, IF staining for CD31 as well as AR and VK staining (Figure 28A – F, respectively). While matrix calcification was initially detected after 72h oCC (Figure 29A - oCC) VLS stained positively by AR and VK staining appeared at the same time (Figure 29A – 72h oCC). This effect was not observed at any earlier time point or during angCC (Figure 29A – oCC/angCC).

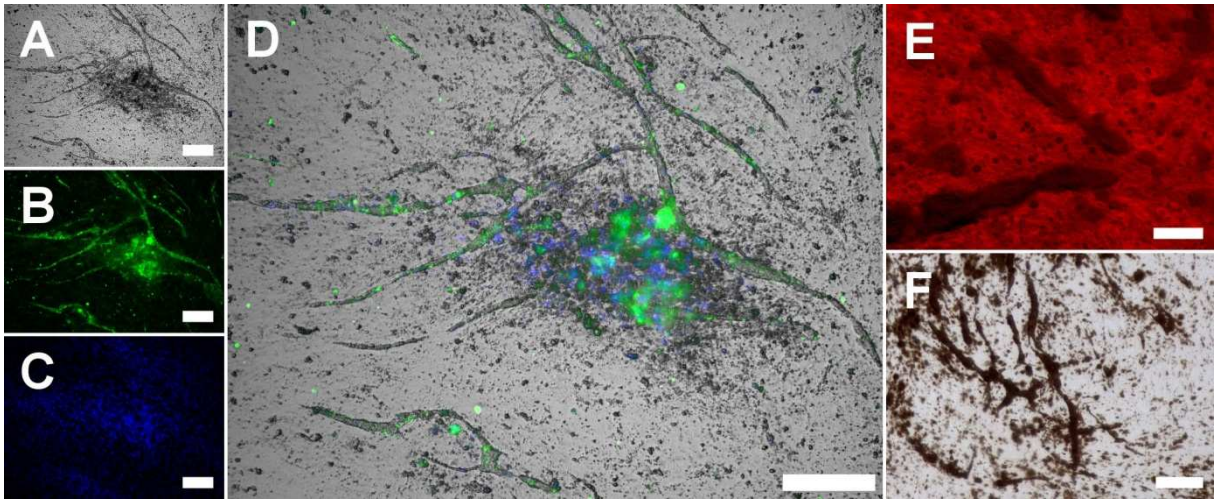

Figure 28: Visualization of calcification along VLS after 7d oCC. A: Transmitted light microscopic image of calcified vessel structure; B: IF staining for CD31; C: IF staining for DAPI; D: Merge of A, B and C; Scale bars in A – D: 200 µm; E: AR staining of calcified VLS; F: VK staining of calcified VLS; Scale bars in E and F: 100 µm

3.6.3.1 Evaluation of vessel regression during osteogenic co-cultivation

The evaluation of vessel regression (VR) using IF staining for CD31 revealed a time-dependent trend (Figure 29A – CD31/DAPI - oCC). The appearance of an inhomogeneous vessel morphology correlated with the course of calcification initially detected after 72h oCC (Figure 29A – CD31/DAPI/AR/VK – 72h oCC). Following the 7d CC to allow for prevascularization, homogeneous VLS were detectable by IF staining up to 48h oCC (Figure 29A – CD31/DAPI – 0h oCC), whereas a massive regression of VLS was observed after 7d oCC (Figure 29A – CD31/DAPI - 7d oCC).

A similar effect could not be observed during angCC (Figure 29A – CD31/DAPI - angCC).

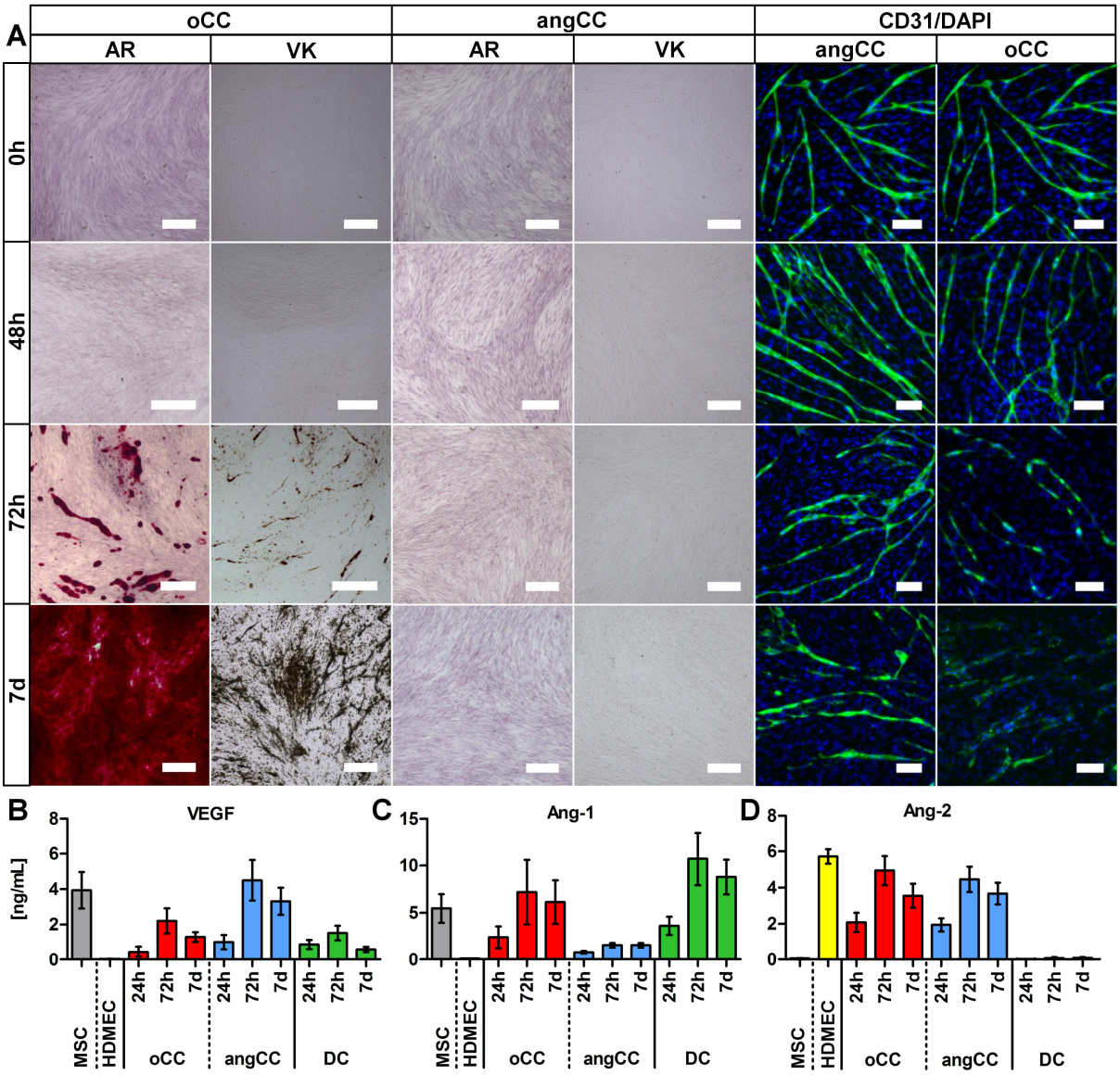

Figure 29: Evaluation of time-dependent angiogenic changes during the cultivation of prevascularized MSC/HDMEC CCs under angiogenic (angCC) or osteogenic conditions (oCC) by IF staining for CD31 (A) after 48h, 72h and 7d of angCC or oCC; Scale bars: 100 µm. Variations in the secretion of the angiogenesis-related GF VEGF, Ang-1 and Ang-2 were quantified after 24h, 72h and 7d of angCC or oCC using ELISA

To investigate a possible correlation of VR with the release of angiogenesis-related GF the absolute concentrations of VEGF, Ang-1 and Ang-2 were quantified using ELISA in CC supernatants after 24h, 72h and 7d oCC/angCC and in DC. VEGF was found to be expressed at lower levels during oCC compared to angCC (Figure 29B - VEGF) while Ang-1 was expressed at increased concentrations during oCC and in DC and at decreased concentrations during angCC (Figure 29B – Ang-1). The expression of Ang-2 during oCC and angCC was present at comparable levels and

no Ang-2 was detected in the DC (Figure 29B – Ang-2). MSC MCs and HDMEC MCs demonstrated that VEGF and Ang-1 were expressed by MSC and Ang-2 was produced by HDMEC (Figure 29B).

Taken together these results indicate i) that the rapid calcification during oCC is linked to parallel VR and ii) that the regression of VLS is linked to a shift in the secretion of VEGF, Ang-1 and Ang-2 towards an excess of Ang-2 during oCC.

3.6.3.2 The response of endothelial cells to components of osteogenic medium

Since VR was detected during oCC studies were performed to determine if individual supplements in ODM were responsible for the changes in the proliferation and phenotype of HDMEC, leading to apoptosis or cell death. For example, it is known that the addition of glucocortocoids to EC MCs enhances the endothelial barrier function (Keil et al., 2013, Romero et al., 2003) and inhibits angiogenic changes in EC (Logie et al., 2010). A similar inhibitory effect on tube formation was demonstrated for increased levels of inorganic phosphorous (P_i) in human cardiac EC cultures (Di Marco et al., 2013). To test if the phenotype of HDMEC is affected by Dex or βGP cells were first cultivated as MCs for 7d in ECGM, ODM, ODM without Dex (ODMw/oDex) and ODM without βGP (ODMw/oβGP) and subsequently analyzed for the expression of CD90, CD105, CD73, CD44, CD31, CD34 and CD146 using flow cytometry. These markers were shown to be involved in the inflammatory activation of EC (CD90 (Saalbach et al., 1999)), in metabolism and GF signaling of EC (CD73, CD105 (Narravula et al., 2000, Li et al., 2003)), in cell-cell and cell-matrix adhesion of EC (CD31, CD146, CD44 (Albelda et al., 1991, Cao et al., 2006, Bardin et al., 2001)) and in the identification of tip-cells in EC cultures and adhesive function of EC (CD34 (Siemerink et al., 2012, Delia et al., 1993)).

The flow cytometric analyses revealed a medium-independent expression of all markers on HDMEC except CD34 (Supplementary Figure 22). The expression of CD90 and CD44 was absent and remained unchanged in the different media (Supplementary Figure 22). The expression of CD34 was the only factor found to be changed and this was slightly decreased by 14.5 %, 25 % and 15.2 % when medium was changed from ECGM to ODM, ODMw/oDex or ODMw/oβGP, respectively (Supplementary Figure 23). These results suggest that the phenotype of HDMEC is not affected upon cultivation of HDMEC MCs in ECGM, ODM, ODMw/oDex or ODMw/oβGP. Since CD34 was demonstrated to be linked to angiogenic tip cell identification or the overall adhesive function of EC (Delia et al., 1993, Siemerink et al., 2012), the changes of CD34 expression found here probably indicate that the adhesive functions of HDMEC or the number of tip cells in HDMEC MCs might be affected upon cultivation of HDMEC in osteogenic medium most prominently when only high levels of βGP (10 mM) are present.

Similarly, morphological changes were detectable by TL microscopy (Figure 30A). HDMEC cultivated in ECGM exhibited a typical cobblestone-like morphology (Figure 30A – ECGM), which, however, was changed to a more flattened appearance when HDMEC were grown in ODM or ODMw/oβGP (Figure 30A – ODM/ODMw/oβGP). The avoidance of Dex from ODM (ODMw/oDex) resulted in an optical reduction of the cell density and the break-up of the confluent EC layer (Figure 30A – ODMw/oDex). IF staining for CD31 and F-actin further confirmed a medium-dependent impact on cell-cell contacts and the arrangement of the cytoskeleton. In HDMEC cultivated in ECGM CD31 and F-actin formed a delicate linear expression pattern that closely overlapped (Figure 30B – ECGM, Figure 30C – asterisks indicate location of CD31 positive cell - cell contacts, black arrows indicate F-actin signal). By contrast, HDMEC MCs cultivated in ODM or ODMw/oβGP exhibited a thickened expression pattern of CD31 and the formation of peripheral stress fibers in the cytoskeleton (Figure 30B – ODM/ODMw/oβGP). The increased staining intensities and structural changes were confirmed by the plot profile analysis showing wide peaks of F-actin (black arrows) around CD31 signal structures (black asterisks) (Figure 30C - ODM/ODMw/oβGP). In HDMEC MCs cultivated in ODMw/oDex the IF signal for F-actin revealed an irregular distribution of F-actin while the CD31 signal was clearly reduced compared to the other media (Figure 30B – DAPI/CD31/F-actin - ODMw/oDex). This observation was underlined by the plot profile analysis (Figure 30C - ODMw/oDex). Intensity measurements of phalloidin staining reactions using image analysis and flow cytometry clearly indicated that both the staining intensity in adherent cells (Figure 31A) and the intensity in detached cells (Figure 31B) was increased in ODM and ODMw/oβGP compared to ECGM or ODMw/oDex. This outcome suggests that during cultivation of HDMEC MCs in ODM or ODMw/oβGP F-actin is not only morphologically rearranged but also increasingly expressed. Based on the morphological changes described above, effects of the medium composition on the proliferation of HDMEC were evaluated by image analysis. The results demonstrated that the proliferation of HDMEC in general was not inhibited by ODM, Dex or βGP, as indicated by increasing cell densities over time (Figure 31C). Since HDMEC were exposed for 7d to the differentiation medium during oCC a total duration of 7d was investigated in HDMEC MCs. Although no inhibition of proliferation was observed, the quantitative analysis of cell densities after 1d, 2d, 5d and 7d revealed differences in the absolute densities and growth rates (Figure 31D) with ECGM demonstrating the strongest increase of density over time (green line) and ODMw/oDex exhibiting the lowest (blue line). Independently, the cell density constantly increased up to 7d when HDMEC MCs were grown in ODMw/oDex while a plateau was reached after 5d to 7d when HDMEC MCs were cultivated in ODM or ODMw/oβGP. In ECGM an overall maximum density of 0.86×10^5 cells/cm^2 ($\pm 0.03 \times 10^5$ cells/cm^2) was reached after 5d, whereby a decrease was detected leading to a final cell density of 0.65×10^5 cells/cm^2 ($\pm 0.015 \times 10^5$ cells/cm^2) after 7d that was similar to the final densities obtained in ODM or ODMw/oβGP (Figure 31D – green, red and purple line).

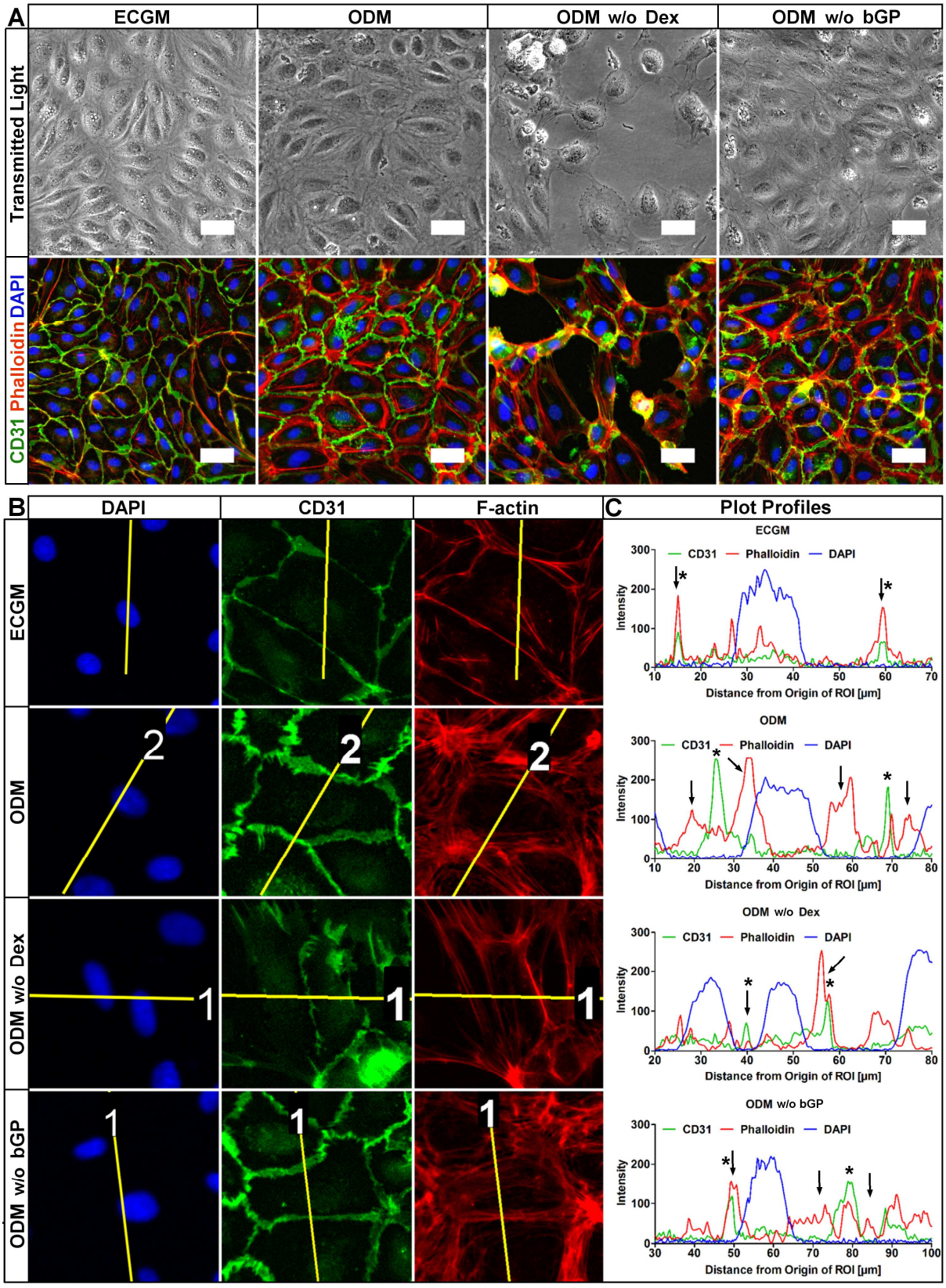

Figure 30: Microscopic evaluation of morphological changes in HDMEC MCs grown under comparative conditions in ECGM, ODM, ODMw/oDex and ODMw/oβGP; A: Overview - Phase contrast imaging and IF staining for cell-cell contacts (CD31/green), cytoskeleton (phalloidin/red) and cell nuclei (DAPI /blue), Scale bars = 20 µm; B: Exemplary region of interest (ROI) for plot profile analyses indicated by straight line; C: Plot profiles based on ROI indicated in B

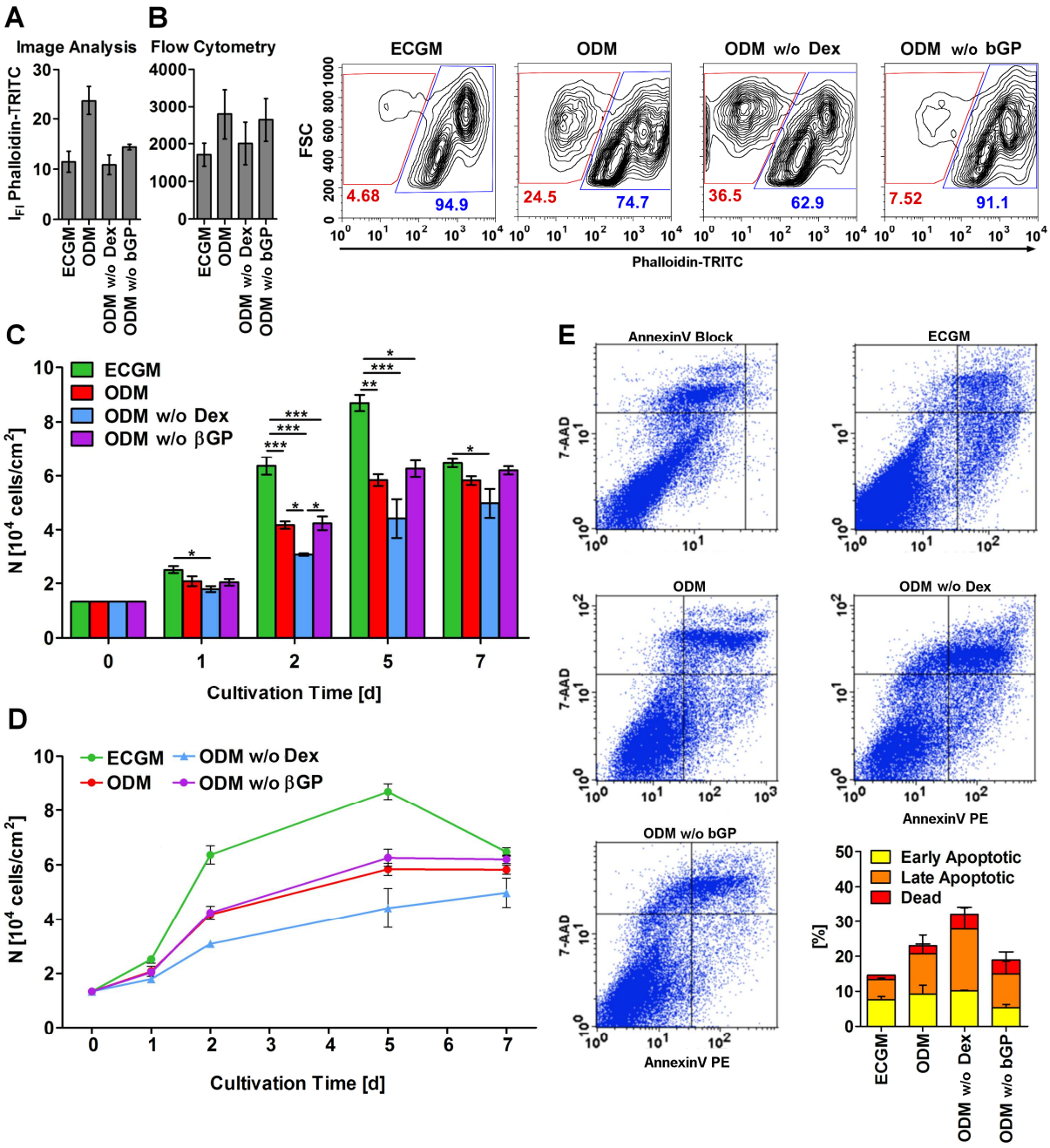

Figure 31: Quantification of structural changes in the cytoskeleton, the proportion of apoptotic cells and cell proliferation in HDMEC MCs grown under comparative conditions in ECGM, ODM, ODMw/oDex and ODMw/oβGP; A: Quantification of phalloidin-TRITC staining intensities (adherent HDMEC) from images shown in Figure 30A using image analysis; B: flow cytometric analysis and quantification of phalloidin-TRITC staining intensities in detached HDMEC, region plots and numbers indicate percentages of phalloidin-positive (blue) and phalloidin-negative (red) cells; C: Determination of cell densities after 1d,2d,5d and 7d, indicated significance: *: $p < 0.05$, **: $p < 0.01$, ***: $p < 0.001$; D: Determination of cell densities after 1d,2d,5d and 7d to indicate different growth rates; E: Flow cytometric analysis and quantification of live, early apoptotic, late apoptotic and dead cell fractions in HDMEC MCs after 7d in ECGM, ODM, ODMw/oDex or ODMw/oβGP

In ODMw/oDex a slightly lowered final cell density of 0.49 x 10^5 (± 0.054) was measured (Figure 31D – blue line). To assess whether morphological changes and differences in the cell growth rate were linked to the induction of apoptosis during the cultivation of HDMEC in ECGM, ODM, ODMw/oDex or ODMw/oβGP HDMEC MCs were double-stained with 7-AAD and an anti-AnnexinV antibody (AnV) after 7d of cultivation. With this method it is possible to distinguish healthy cells (7-AAD$^-$ AnV$^-$) from early apoptotic cells (7-AAD$^-$ AnV$^+$), late apoptotic cells (7-AAD$^+$ AnV$^+$) or dead cells (7-AAD$^+$ AnV$^-$) (Vermes et al., 1995). The analysis shown in Figure 31E confirmed the presence of all of the mentioned cell fractions, independent of the medium type. The percentage of early apoptotic cells was slightly higher in ODM (9.15 %) and ODMw/oDex (10.2 %) compared to ECGM (7.5 %) or ODMw/oβGP (5.35 %) (Figure 31F – yellow bars). The percentage of late-apoptotic cells was clearly increased in ODM (11.64 %), ODMw/oDex (17.6 %) and ODMw/oβGP (9.56 %) compared to ECGM (5.75 %; Figure 31F – orange bars). A similar trend was detected when the fraction of dead cells was quantified in ECGM (1.28 %), ODM (2.25 %), ODMw/oDex (4.34 %) and ODMw/oβGP (3.98 %; Figure 31F – red bars). To evaluate whether βGP alone (ODMw/oDex) exhibited a pro-apoptotic effect and Dex alone (ODMw/oβGP) exhibited an anti-apoptotic effect on HDMEC cultivated in ODM the corresponding percentages were set in proportion to the values obtained for all fractions in ODM. The results demonstrated that increased fractions of early apoptotic cells (+ 1.05 %), late apoptotic cells (+ 5.96 %) and dead cells (+ 2.09 %) were detected in ODMw/oDex compared to ODM (Supplementary Table 4). In contrast, decreased fractions of early apoptotic cells (- 3.8 %) and late apoptotic cells (- 2.08 %) and a slightly increased fraction of dead cells were detected in ODMw/oβGP compared to ODM (Supplementary Table 4).

Altogether, these results indicate that the addition of Dex to ODM buffers the negative effect of βGP supplementation on cell proliferation and apoptosis.

3.6.4 Re-establishing a pro-angiogenic environment to maintain vascular structures or re-induce vascularization

With regard to the maintenance of a vascular network during oCC an investigation was carried out to determine if vascularization and angiogenesis could be re-initiated once VR had begun. To determine this, prevascularized 7d CC were transferred to ODM for 48h oCC or 7d oCC to obtain VR (Figure 32A – green frame) and subsequently returned to ECGM (Recovery) for 24h, 72h or 7d or cultivated under prolonged oCC conditions (prl-oCC) in ODM for 24h, 72h or 7d as a negative control (Figure 32A – red frame). The re-inducibility of vascularization and angiogenesis was assessed by IF staining for CD31 and comparison of VLS obtained after Recovery or prl-oCC to VLS present after 7d CC+48h oCC and 7d CC+7d oCC. Additionally, matrix calcification as occurring during oCC (see section 3.6.1) was determined by AR staining and quantitative analysis of AR intensities and compared in the same manner. Since it was found earlier in this study that the oCC of prevascularized CCs

is linked to the deposition of GAGs (see section 3.6.2) AB staining was used to detect GAGs at the baseline level after 7d CC+48h oCC and 7d CC+7d oCC. The deposition and maintenance of GAGs after Recovery in ECGM or prl-oCC in ODM was evaluated by comparison of corresponding AB stains to the baseline level thereafter. To evaluate any changes in the release of GF as detected during oCC in previous sections (see section 3.6.3.1) levels of VEGF, Ang-1 and Ang-2 were determined by ELISA. GF measurements were also performed to estimate the status of angiogenic re-induction (VEGF, Ang-2) and vessel stabilization (Ang-1) during Recovery and prl-oCC. Furthermore, ELISA measurements were performed for BMP-4 released into the supernatants during oCC, Recovery and prl-oCC. BMP-4 has been described as an “osteogenic BMP” released by EC (Dudakov et al., 2015, Sorescu et al., 2004) and acting in a pro-osteogenic manner on the osteogenic differentiation of MSC (Luu et al., 2007, Wang et al., 2014). By using these methods, it should be possible to determine whether a pro-osteogenic stimulus released by the HDMEC would be constantly present in the CC system or whether the stimulus is changed during oCC, Recovery or prl-oCC.

Following the initial co-cultivation for 7d to achieve prevascularization VLS-forming angiogenic networks were detectable (Figure 32B – 7d CC/CD31/DAPI and CD31/DAPI-z). No matrix calcification was observed by AR staining at this time point (Figure 32B – 7d CC/AR). A similar result was obtained after 48h oCC (Figure 32B - +48h oCC). After 7d oCC advanced VR was observed by IF staining for CD31 (Figure 32B - +7d oCC/CD31/DAPI) and a large amount of calcification of the extracellular matrix was confirmed by AR staining (Figure 32B - +7d oCC/AR). The upward trend of the intensity found in AR stains was also represented by AB stains performed in 7d CC, 48h oCC and 7d oCC samples (Figure 32B – rows AR and AB), thus indicating the deposition of GAGs in the course of oCC but not after initial 7d CC. The microscopic observations were supported by a quantitative analysis of AR intensity and image-based quantification of AB intensities (Figure 32C). ELISA measurements performed to determine changes in the expression of VEGF, Ang-1 and Ang-2 as described in the context of VR in previous sections (see section 3.6.3.1, see also Figure 29B and Figure 22B) demonstrated a decreasing trend in the expression of VEGF, an increasing expression of Ang-1 and a constant expression of Ang-2 in supernatants of 7d CC, 48h oCC and 7d oCC samples, respectively (Figure 32D). BMP-4 was detected by ELISA at comparable concentrations in supernatants of 7d CC and 7d oCC samples but slighty decreased concentrations in supernatants of 48h oCC samples (Figure 32D). Taken together, the baseline level (Figure 32A – green frame) for the evaluation of the maintenenance or re-induction of VLS during Recovery or prl-oCC is characterized by VR and matrix calcification obtained after 7d oCC but not 48h oCC. Further characteristics are the deposition of GAGs in the course of oCC and the disregulation of angiogenic factors and BMP-4.

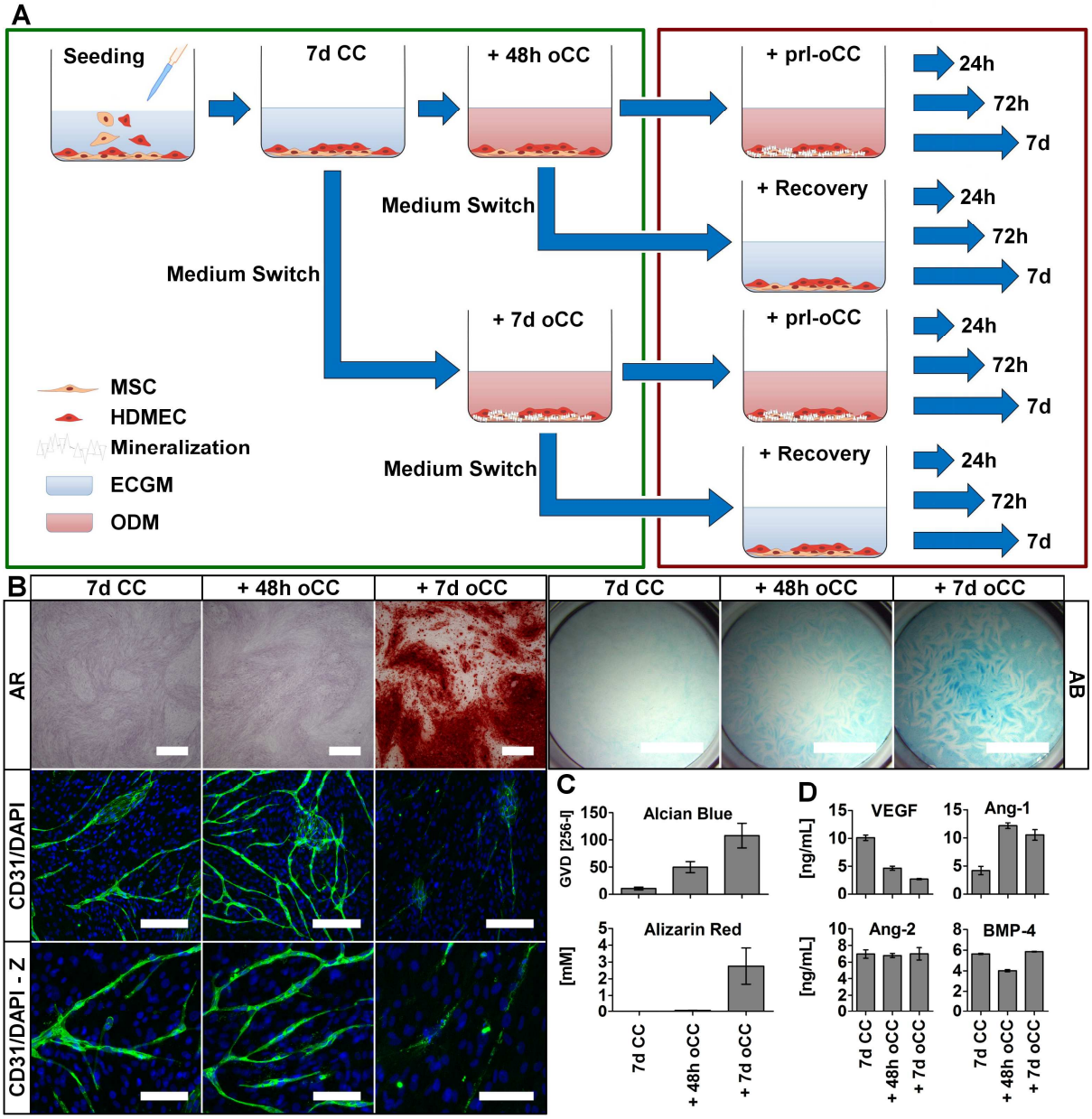

Figure 32: A: Schematic representation of a sequential medium strategy for the maintenance or re-induction of VLS in prevascularized CC of MSC with HDMEC after oCC; Green frame: schematic representation of the generation of control cultures (baseline level); Red frame: Schematic experimental procedure for the investigation of angiogenic re-induction; B: Microscopic evaluation of vessel formation, vessel morphology, matrix calcification and GAG deposition in CC after 7d of prevascularization (7d CC) and additional 48h oCC (+48h oCC) or 7d oCC (+7d oCC); Scale bars: AR/CD31 = 200 µm, CD31-z = 50 µm, AB = 5 mm; C: Quantitative analysis of alcian blue (AB) and alizarin red (AR) staining intensities using image analysis and acidic dissolution, respectively; D: Quantification of VEGF, Ang-1, Ang-2 and BMP-4 in CC supernatants using ELISA.

In this context, VEGF was found to be decreased by ≈70%, Ang-1 was found to be increased by ≈120%, Ang-2 was found to be present at constant excess concentrations and BMP-4 was found to be slightly disregulated after 48h oCC. As indicated by the experimental procedure to re-establish a pro-angiogenic

environment (Figure 32A – red frame) the maintenance of VLS was achieved upon recovery of 48h oCC cultures in ECGM (Figure 33A – 48h oCC/CD31-DAPI/Recovery). In 7d oCC samples the formation of newly formed VLS was observed by IF staining for CD31 (Figure 33B – 7d oCC/CD31-DAPI/Recovery). In contrast, a constant VR was detected during prl-oCC of 48h oCC samples (Figure 33A - 48h oCC/ CD31-DAPI/prl-oCC), whereas the total extinction of VLS resulted from prl-oCC of 7d oCC samples (Figure 33A – 7d oCC/CD31-DAPI/prl-oCC). When AR staining was applied, it could be observed that VR during prl-oCC of 48h oCC samples correlated with an increased matrix calcification (Figure 33A - 48h oCC/AR/prl-oCC). Likewise, this time-dependent matrix calcification was detected during recovery in ECGM, although to a lower extent. Moreover, VLS were maintained (Figure 33A – 48h oCC/AR/Recovery). In 7d oCC samples a constant degree of calcification was detected during recovery or prl-oCC (Figure 33A – 7d oCC/AR/Recovery/prl-oCC). These microscopic observations were confirmed by quantitative analysis of the AR staining (Supplementary Figure 20).

Following the evaluation of vessel maintenance and matrix calcification during recovery and prl-oCC of 48h oCC and 7d oCC samples it was evaluated whether the deposition of GAGs would be affected by the sequential medium strategy. For this, the corresponding CCs were stained with AB after 7d of recovery or prl-oCC. It was found that the deposition of GAGs was maintained and was also independent of the medium strategy (Figure 33B). The observed trend was confirmed by quantitative image analysis. The final intensity was found to be increased in 7d oCC samples compared to 48h oCC samples after 7d of recovery or prl-oCC (Supplementary Figure 21).When ELISA measurements were performed to determine the expression of angiogenic GFs and BMP-4 during recovery or prl-oCC of 48h oCC samples and 7d oCC samples the expression of VEGF was found to be re-increased during the recovery of the corresponding CCs in ECGM in a time-dependent manner (Figure 33C – VEGF/blue bars). This effect was observed when both 48h oCC and 7d oCC samples were placed into ECGM (Figure 33C – VEGF/blue bars). The expression of VEGF was found to be constantly decreased when the corresponding 48h oCC and 7d oCC samples were cultivated under prl-oCC conditions (Figure 33C – VEGF/red bars). The opposite behavior was detected for the expression of Ang-1 (Figure 33C – Ang-1) while the expression of Ang-2 and BMP-4 by the cells remained unaffected after placing the CCs into ECGM during recovery or into ODM for prl-oCC (Figure **33**C – Ang-2/BMP-4).

Taken together, these results demonstrate that sequential medium conditions can re-establish a pro-angiogenic GF environment to re-induce vessel formation following a period in which VR occurs. Increasing matrix calcification and maintained GAG deposition further reveal that the osteogenic differentiation induced during oCC is not reduced or inhibited by changing medium type.

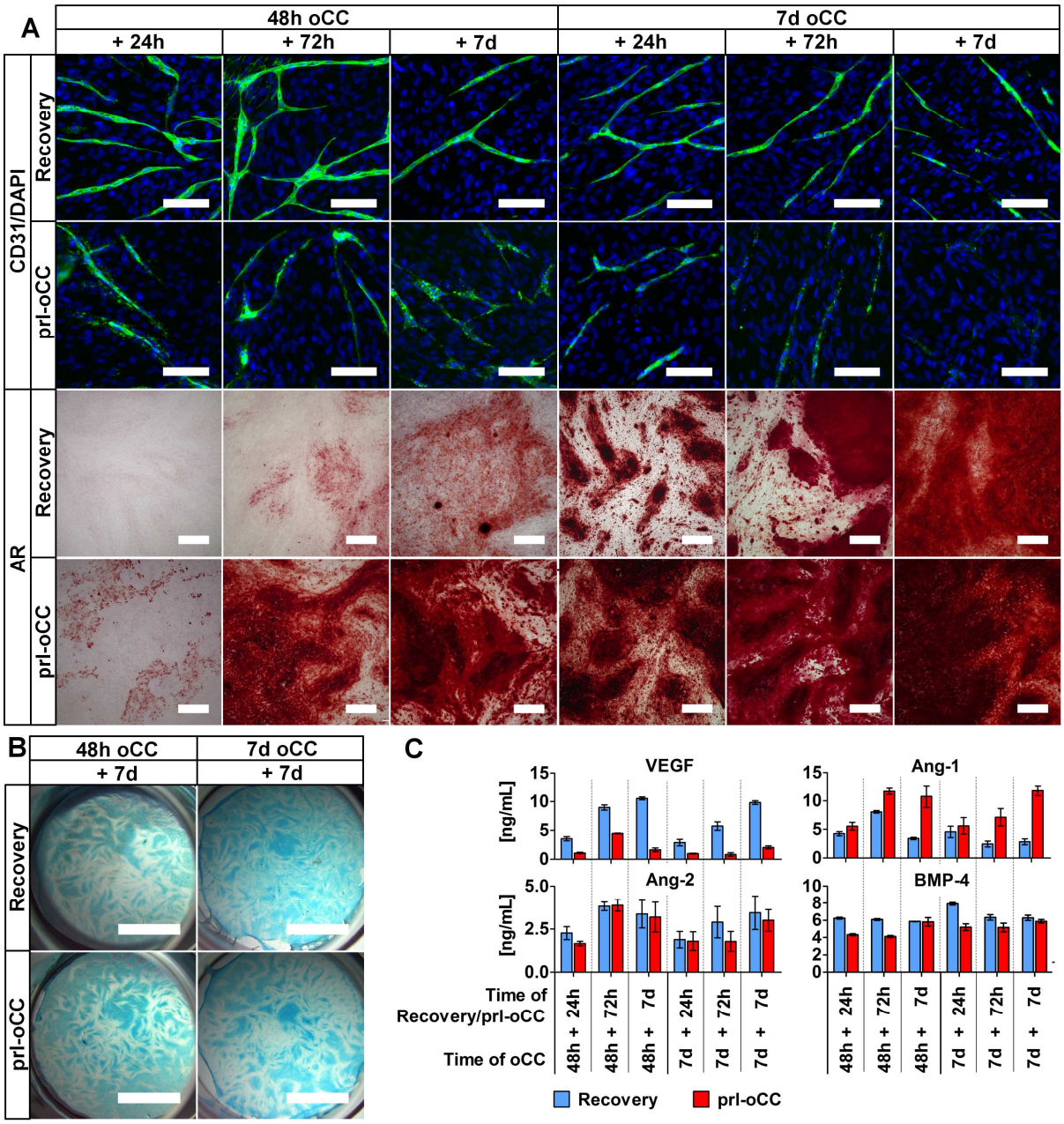

Figure 33: Evaluation of a sequential medium strategy to re-establish a pro-angiogenic environment; A: Microscopic evaluation of VLS formation, VR and matrix calcification in 48h oCC and 7d oCC samples during 24h to 7d of recovery in ECGM or prl-oCC in ODM using IF staining for CD31 and AR staining, Scale bars: 500 µm; B: AB staining after 7d of recovery or prl-oCC reveals GAG deposition, Scale bars: 5 mm; C: Quantification of VEGF, Ang-1, Ang-2 and BMP-4 during recovery and prl-oCC using ELISA

3.6.5 Investigation of the osteogenesis pattern of MSC in an indirect co-culture of MSC with endothelial cells.

Based on the effect generated in prevascularized CC during oCC a study was performed to determine if indirect CC could be used to induce the osteogenic differentiation via secreted signaling molecules in MSC MCs in a cell CC model where cells did not have direct contact. It has been shown that GFs like BMP-2 or

BMP-4 secreted by EC (Helbing et al., 2011, Mohan et al., 1998) can influence the osteogenic differentiation of bone marrow-derived MSC (Kaigler et al., 2005, Beederman Maureen, 2013). To assess the involvement of a GF-based signaling an indirect CC model was generated in a transwell system (Figure 34A).

To establish this system, a 7d CC was performed with EC in the bottom chamber (BC) of a transwell chamber allowing for prevascularization. An MSC MC of the same donor was cultivated in the top chamber (TC) on the upper side of the transwell membrane (MSC/CC). This system was cultivated for 7d in ECGM followed by 7d oCC and subsequently analyzed by AR staining to estimate whether the rapid matrix calcification obtained in the CC during oCC could be induced in the MSC MC as well. To evaluate whether secreted GF or cytokines, and thus a paracrine effect, were responsible for the osteogenic differentiation induced during oCC, similar systems were cultivated which combined an MSC MC in the TC with a bare BC (MSC/Blank), a MSC MC in the TC with an MSC MC in the BC (MSC/MSC) and a CC in the BC with a MSC MC in the TC that was added at the time the oCC was initiated (MSC-7d/CC). Finally, the calcification was assessed by quantitative analysis of the AR staining intensity.

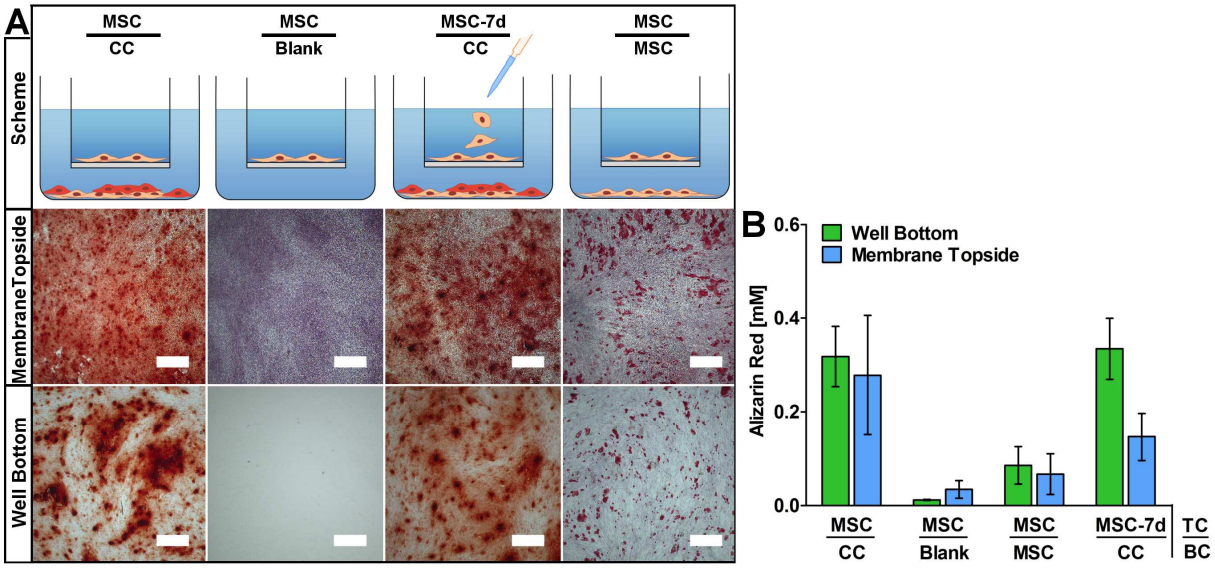

Figure 34: Evaluation of direct cell-cell contact and CC composition on osteogenic differentiation during oCC; A: Investigation of paracrine interactions during oCC in a transwell system, Scale bars: 200 µm; B: Quantification of AR intensities shown in A obtained from AR staining applied to transwell systems

The microscopic evaluation of the AR staining showed comparable AR intensities in MSC MC (Membrane Topside) and CC (Well Bottom) in MSC/CC samples and MSC-7d/CC samples after 7d oCC (Figure 34A – MSC/CC and MSC-7d/CC). In MSC/MSC samples a less intense AR signal was obtained (Figure 34A – MSC/MSC) while a negative staining resulted from MSC/Blank samples after 7d oCC (Figure 34A – MSC/Blank). The microscopic observations were confirmed by the quantitative

analysis of the AR staining, showing the highest values in MSC/CC and MSC-7d/CC samples compared to about 3 to 6-fold reduced values in MSC/MSC samples (Figure 34B).

In summary, the above-mentioned results indicate that the osteogenic differentiation of MSC is rapidly induced in a non-contact triple-culture with prevascularized MSC/HDMEC CC. This suggests i) that the induction of osteogenic differentiation by prevascularized MSC/HDMEC CCs during oCC does not require direct cell-cell contact and ii) that prevascularized MSC/HDMEC CCs could be used to enhance the osteogenesis in MSC MCs via non-direct contact approaches. This also indicates that extracellular compounds are being released in a paracrine signaling context that could diffuse to other cells and influence protein expression.

3.6.6 The influence of the type of endothelial cells on the osteogenic co-cultivation with MSC

Following the evaluation of osteogenesis in prevascularized MSC/HDMEC CCs studies were initiated to determine whether the osteogenic effect obtained during oCC can be induced in CCs of MSC with other types of EC or if it is exclusively linked to microvascular EC, such as HDMEC. For this purpose, CCs of MSC with macrovascular HUVEC or peripheral blood OEC were performed for 7d to permit prevascularization, and subsequently cultivated under oCC conditions in ODM for 7d. It can be seen from Figure 35C that intense AR and VK stains resulted after 7d oCC independent of the type of EC. Negative stains for AR or VK resulted after 7d angCC, in which CCs were cultivated in ECGM as a control, independent of the type of EC (Figure 35A – AR/VK - inserts). Quantitative measurements of the AR staining supported these findings (Figure 35C). In addition, ALP activity staining exhibited a lower intensity after 7d angCC compared to 7d oCC (Figure 35A - ALP – insert versus general image). When 7d CC of MSC with HUVEC or MSC with OEC were analyzed for the formation of VLS after 7d oCC by IF staining for CD31 a very weak or no tube formation was detectable (Figure 35B – CD31/DAPI). Nevertheless, the CD31 staining demonstrated the presence of EC linked to an intense AB staining after 7d oCC (Figure 35A – ALP/AB – MSC+HUVEC and MSC+OEC). After 7d angCC a negative AB staining was obtained independent on the type of EC (Figure 35A – ALP/AB – inserts).

The strong osteogenic effect obtained in CCs of MSC with either HDMEC, HUVEC or OEC during oCC indicates that the osteogenic differentiation of the MSC within the CCs can be induced by EC independent of their microvascular or macrovascular origins. Since HUVEC are linked to embryonic development the osteogenic effect induced in MSC/HUVEC CCs during oCC suggests a connection to a mechanistic background that is conserved among EC. To further confirm this hypothesis CCs of MSC with the human hemangiosarcoma cell line ISO-HAS-1 (Masuzawa et al., 1999) were performed for 7d in ECGM followed by 7d oCC. Similar to the results obtained

with MSC/HUVEC and MSC/OEC CCs a large amount of calcification and the incorporation of endothelial cells organized in homogeneous layers were detected after 7d oCC of MSC/ISO-HAS-1 CCs using AR staining and IF staining for CD31 (Supplementary Figure 16).

Altogether, the results suggest a mechanism highly conserved among EC that can be utilized to stimulate osteogenesis in MSC/EC CCs.

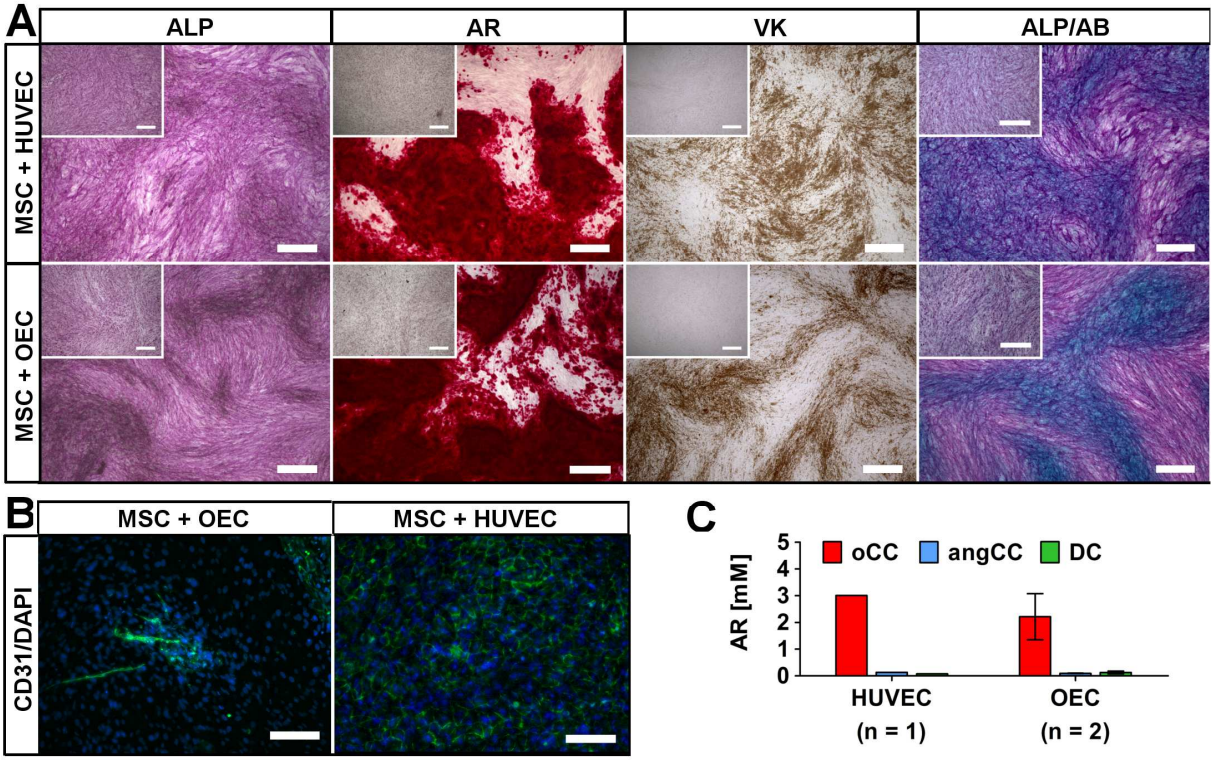

Figure 35: Evaluation of the osteogenic differentiation and presence of an endothelial fraction in CCs of MSC with HUVEC and MSC with OEC after 7d oCC; A: Evaluation of osteogenic differentiation, matrix deposition and GAG deposition by ALP activity staining, AR + VK staining and AB staining, Scale bars: 500 µm; B: IF stainng for CD31 and DAPI to detect EC fractions after 7d oCC, Scale bars: 500 µm; C: Quantification of AR intensities in CC of MSC with HUVEC (HUVEC) and MSC with OEC (OEC) after 7d oCC

3.6.7 The influence of the type of MSC on the osteogenic co-cultivation with HDMEC

Since the effect described during oCC was found to be independent of the type of EC used in the CC, studies were carried out to determine whether osteogenic differentiation can be stimulated when the type of MSC was varied. It has previously been shown that MSC derived from adipose tissue (atMSC) can be differentiated into osteoblastic cells using ODM (Kroeze et al., 2011, Schubert et al., 2011). As a negative control CCs of human dermal fibroblasts (HDF) with HDMEC were performed under the same conditions. The induction of osteogenic differentiation and matrix calcification in all CCs was assessed by ALP activity staining and AR staining.

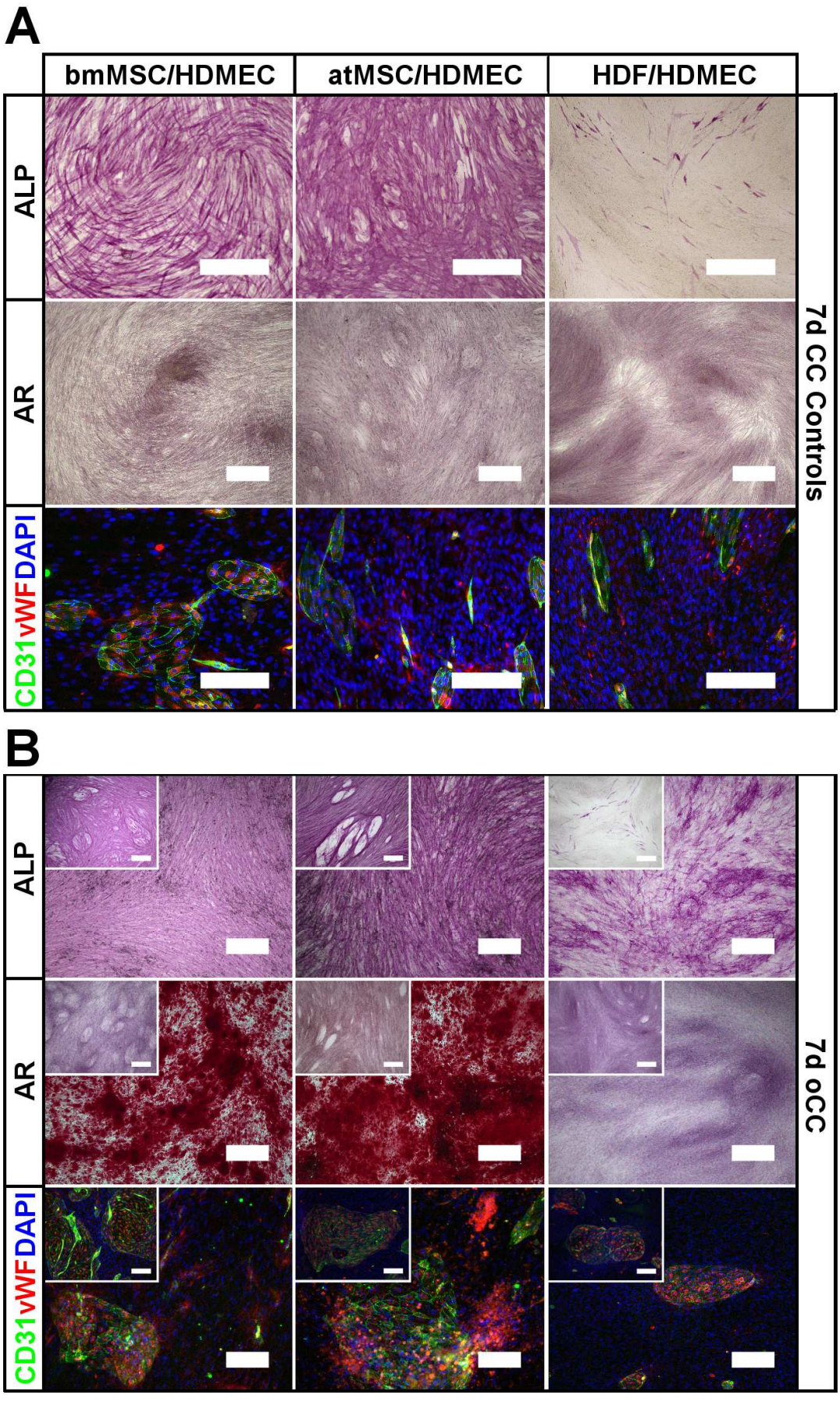
A
bmMSC/HDMEC
atMSC/HDMEC
HDF/HDMEC
ALP
AR
CD31 vWF DAPI
7d CC Controls
B
ALP
AR
CD31 vWF DAPI
7d oCC

Figure 36: A: Characterization bmMSC/HDMEC, adMSC/HDMEC and NHDF/HDMEC CCs after 7d in ECGM for the activity of ALP, the deposition of calcium and the localization of EC using ALP activity staining, AR staining and IF staining for DAPI (cell nuclei, blue), CD31 (green) and vWF (red), respectively; Scale bars: 500 µm; B: Comparative evaluation of CCs of bmMSC/HDMEC (positive control), atMSC/HDMEC and NHDF/HDMEC (negative control) after 7d oCC using ALP activity staining (ALP), AR staining for the deposition of calcium and IF staining for CD31, vWF and DAPI (green, red, blue, respectively) for the localization of EC; Small inserts represent the corresponding control after 7d angCC; Scale bars: Rows "ALP" and "AR" = 500 µm; Row "DAPI/CD31/vWF" = 200 µm

Initially, bmMSC, atMSC and HDF were evaluated for their potential to differentiate into cells of the osteoblastic, adipogenic or chondrogenic lineage using standard differentiation assays (Supplementary Figure 17). After 4 wk of cultivation in ODM, adipogenic differentiation medium (ADM) or chondrogenic differentiation medium (CDM) the cells were stained for calcium deposition, phosphate deposition, oil droplet formation and GAG deposition using AR, VK, OR-O, AB and SO staining, respectively. Bone marrow-derived MSC and atMSC exhibited a tri-lineage differentiation potential as indicated by positive staining for AR, VK, OR-O, B and SO (Supplementary Figure 17 – bmMSC and atMSC). It is noteworthy that atMSC showed a strong formation of oil droplets (Supplementary Figure 17 – atMSC/OR-O) but only a minor deposition of calcium and phosphate (Supplementary Figure 17 – atMSC/AR/VK). A limited differentiation potential was detected for HDF, exhibiting no signs of matrix calcification (Supplementary Figure 17 – HDF/AR/VK).

Following this pre-experimental characterization, the bmMSC, atMSC and HDF were co-cultivated with HDMEC for 7d in ECGM and transferred into ODM for 7d oCC or kept in ECGM for 7d angCC as a control. The ALP activity staining revealed an increased staining intensity in all CCs after 7d oCC compared to each corresponding 7d CC control (Figure 36B - ALP). The same was true when the CCs were transferred to 7d angCC, except for CCs of HDF with HDMEC, which remained negative for the ALP activity staining (Figure 36B – ALP/inserts). The AR staining revealed a strong matrix calcification in CCs of bmMSC and atMSC with HDMEC but no calcification in CCs of HDF with HDMEC after 7d oCC (Figure 36B - AR). Similarly, negative AR stains were obtained from all CCs after 7d angCC (Figure 36B - AR/inserts). IF staining for CD31 and vWF demonstrated the presence of HDMEC after 7d oCC and 7d angCC in CCs of bmMSC, atMSC and HDF with HDMEC. However, VLS were only present in CCs of bmMSC with HDMEC (Figure 36B - DAPI/CD31/vWF and inserts).

Taken together these findings indicate that the rapid osteogenic induction in MSC/EC CCs during oCC is not exclusively limited to the use of bmMSC. The results further underline the fact that each CC comprises system-specific parameter optima which have to be addressed to achieve formation of VLS.

3.6.8 The evaluation of medium-based artifacts during osteogenic co-cultivation

Based on the analysis of parameters influencing the osteogenic differentiation of MSC in MSC/EC CCs during oCC studies were performed to determine whether other differentiation media could also induce osteogenic differentiation or whether this was exclusively limited to ODM. For these studies, CCs of MSC with HDMEC were cultivated in ECGM for 7d (7d CC Ctrl) to obtain VLS and subsequently transferred into various customized and commercial media for another 7d period referred to as “7d + name of the corresponding medium” (as indicated in Table 23). The purpose of these studies was to clarify whether matrix calcification, as described earlier for MSC/HDMEC CCs during oCC in ODM, could be a medium artifact.
In the previous sections osteogenic differentiation was achieved by cultivation of cells in ODM supplemented with 10 mM βGP (for detailed supplementation see Table 23). To induce osteogenesis in MSC Dex is also added as a supplement (Grigoriadis et al., 1988, Langenbach and Handschel, 2013). Supplemented P_i has recently been discussed as a possible cause of non-physiological formation of amorphous calcium phosphate at elevated P_i levels, that is, above 2 mM (Langenbach and Handschel, 2013). Therefore, one customized medium was supplemented with physiological concentrations (Nishizawa et al., 2005, Lau et al., 2010)) of 1.4 mM βGP (ODM (1.4 mM βGP) while a phosphate source was completely omitted from a control medium (ODM (w/oβGP)). ECGM served as a positive control for the evaluation of vessel formation while ECGM (+OS) served as a negative control since it was identified in a previous section as a medium in which a reduction of vessel formation and osteogenic differentiation occurred in MSC/HDMEC CCs (Figure 18; Figure 19). In addition, commercially available adipogenic, chondrogenic and osteogenic differentiation media (Comm.ADM, Comm.CDM and Comm.ODM, respectively, see Table 23) were included. The incorporation of Comm.ADM and Comm.CDM should address the tri-lineage differentiation potential of MSC in the MSC/HDMEC CCs, thus investigating whether VLS could be maintained while adipogenic or chondrogenic differentiation was induced. Following 7d of cultivation in the customized or commercial media listed in Table 23 osteogenic differentiation in the MSC/HDMEC CCs was evaluated by ALP activity staining and AR staining. The ALP activity staining indicated a homogeneous expression and constant ALP activity in all CCs independent of the medium applied (Figure 37A - ALP). The AR staining showed a specific signal for matrix calcification in CCs after 7d ODM (10 mM βGP), 7d ODM (1.4 mM βGP) and 7d Comm.ODM (Figure 37A - AR). No specific AR staining was obtained from CCs after 7d in the other media (Figure 37A - AR). MSC MCs performed as DC exhibited an ALP activity staining that appeared to be less homogenous but nevertheless independent of the differentiation medium used (Supplementary Figure 18 - ALP). No matrix calcification was detected in DC after 7d of cultivation in any of the media described in Table 23 (Supplementary Figure 18 - AR).

Table 23: Customized and commercial differentiation media analyzed for their impact on the osteogenic differentiation of MSC/HDMEC CCs and MSC MCs

Medium	Detailed Description	Customized/ Commercial
ODM (10 mM βGP)	aMEM + 10% FCS, 1% P/S, 50 µM Asc2P, 100 nM Dex and 10 mM βGP	Customized
ODM (1.4 mM βGP)	β-GP level reduced to 1.4 mM	Customized
ODMw/oβGP	No βGP added to ODM	Customized
ECGM	ECBM + 15% FCS, heparin, bFGF	Customized
ECGM + OS	Addition of 50 µM Asc2P, 100 nM Dex and 10 mM β-GP	Customized
Comm.ADM	Gibco StemPro® adipogenic differentiation medium	Commercial
Comm.CDM	Gibco StemPro® chondrogenic differentiation medium	Commercial
Comm.ODM	Gibco StemPro® osteogenic differentiation medium	Commercial

The microscopic evaluation was confirmed by the quantitative analysis of the AR staining. Mean AR concentrations of approximately 3 mM, 0.25 mM and 1.5 mM were detected after 7d ODM (10 mM βGP), 7d ODM (1.4 mM βGP) and 7d Comm.ODM, respectively (Figure 37B – red bars). These mean values represent a 33-fold, 2.5-fold and 23-fold increase compared to their corresponding DC (Figure 37B). In the DC constant, absolute AR concentrations of approximately 0.08 mM were measured (Figure 37B – blue bars). To evaluate the maintenance of vascular structures IF staining for CD31 was performed (Figure 37C). CD31-positive VLS were present after 7d in all media except after 7d Comm.ADM or 7d Comm.CDM (Supplementary Figure 19). The assessment of vessel morphology in the different media indicated VR after 7d ODM (10 mM βGP), 7d (ECGM (+OS) and 7d Comm.ODM (Figure 37C). In contrast, when βGP in ODM was reduced to 1.4 mM or completely omitted a homogeneous vessel morphology was maintained (Figure 37C – ODM (1.4 mM βGP) and ODM (w/oβGP)). Independently, CCs exhibited a stable vessel morphology after 7d ECGM (Figure 37C - ECGM) that was negatively affected when OS were added to ECGM (Figure 37C – ECGM (+OS)). Furthermore,

the overall vessel density was found to be reduced after 7d in all media compared to 7d ECGM (Supplementary Figure 19).

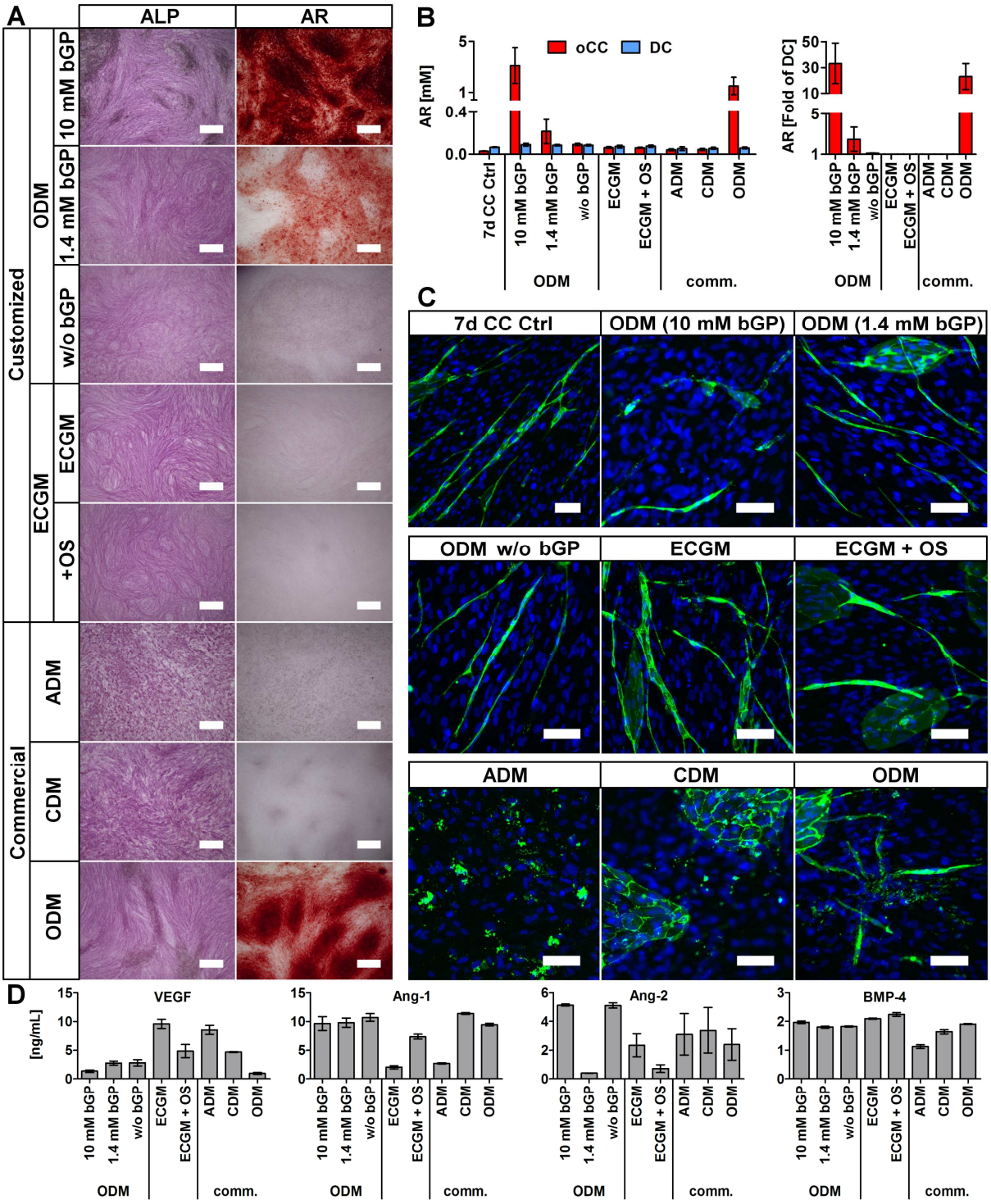

Figure 37: A: Microscopic evaluation of osteogenic differentiation in MSC/HDMEC CCs after 7d oCC in customized and commercial differentiation media described in Table 23 using ALP activity staining and AR staining, Scale bars: 100 µm; B: Quantification of AR staining after oCC compared to DCs; C: Evaluation of vessel desnity and norphology in MSC/HDMEC CCs after 7d oCC in customized and commercial differentiation media described in Table 23 using IF staining for CD31, Scale bars: 100 µm; D: Quantification of VEGF, Ang-1, Ang-2 and BMP-4 in MSC/HDMEC CCs after 7d oCC in customized and commercial differentiation media described in Table 23 using ELISA

Following the evaluation of vessel morphology, CC supernatants were analyzed after 7d in all media listed in Table 23 for the concentrations of GFs involved in induction and stabilization of angiogenesis. It can be seen from Figure 37D that VEGF was secreted at varying levels among the cell culture media, with a tendency towards lower levels secreted in media containing Dex (Figure 37D – VEGF - ODM (10 mM βGP), ODM (1.4 mM βGP), ODM (w/oβGP), ECGM (+OS) and Comm.ODM). By contrast, in these media Ang-1 was increasingly expressed after 7d (Figure 37D – Ang-1). Lowered concentrations of Ang-1 were detected after 7d ECGM or 7d Comm.ADM (Figure 37D - Ang-1). Ang-2, which acts synergistically with VEGF was found secreted at high concentrations of around 5 ng/mL after 7d ODM (10 mM βGP) and 7d ODM (w/oβGP) (Figure 37D – Ang-2). Interestingly, Ang-2 concentrations were markedly reduced to 0.38 ng/mL (± 0.02 ng/mL) when βGP was lowered from 10 mM to 1.4 mM (Figure 37D – Ang-2). Similarly, low Ang-2 concentrations of 0.72 ng/mL (± 0.266 ng/mL) were detected after 7d ECGM+OS, whereas Ang-2 level were found to increase to 2.33 ng/mL (± 0.8 ng/mL) when OS were omitted from ECGM (Figure 37D – Ang-2 – ECGM+OS and ECGM). After 7d Comm.ADM, 7d Comm.CDM or 7d Comm.ODM intermediate Ang-2 concentrations of 3.09 ng/mL (± 1.44 ng/mL), 3.37 ng/mL (± 1.59 ng/mL) and 2.4 ng/mL (± 1.09 ng/mL) respectively were measured. (Figure 37D – Ang-2). The quantification of BMP-4 demonstrated the expression of constitutive levels in supernatants, independent of the medium (Figure 37D – BMP4). Slightly lowered BMP-4 concentrations were only detected after 7d Comm.ADM (Figure 37D – BMP4 – Comm.ADM).

Taken together, the results described above indicate that i) the induction of osteogenic differentiation and matrix calcification is not exclusively limited to the use of customized ODM (10 mM βGP) (referred to as “ODM” in all previous sections) and that ii) the induction of osteogenesis and matrix calcification during oCC can very likely be achieved at physiological P concentrations.

3.6.9 Undifferentiated MSC in co-cultures of MSC with HDMEC under osteogenic culture conditions

To investigate whether the cultures obtained after 7d oCC contain a fraction of undifferentiated and expandable stromal cells, which might serve as a constant stem cell source, corresponding CCs were enzymatically digested after 7d oCC or 7d angCC and subsequently transferred into T75 flasks for cell expansion over 2 passages. After reaching approximately 80 - 90% confluence the expanded cells were harvested and analyzed for a tri-lineage differentiation potential using differentiation assays. The cells exhibited the potential to differentiate into cells of the osteogenic, the adipogenic and the chondrogenic lineage as shown by positive AR and VK staining (deposition of calcium and phosphate, respectively), positive OR-O staining (oil-droplet formation) as well as positive AB and SO staining (deposition of GAG) (Figure 38). The tri-lineage differentiation potential was also found to be

independent of both oCC and angCC. Additionally, the expanded cells were analyzed for the expression of surface markers recommended for the characterization of MSC using flow cytometry (Dominici et al., 2006). Cells isolated and expanded following 7d angCC were found negative for the expression of CD11b, HLA-DR, CD19, CD34, CD45, CD31 and CD146 and highly positive for the expression of CD73, CD90, CD105, CD29 and CD44 (Supplementary Figure 24). When cells were isolated and expanded following 7d oCC they were found negative for the expression of CD11b, CD19, CD45, CD31 and CD146, slightly positive for the expression of HLA-DR and CD34 and highly positive for the expression of CD73, CD90, CD105, CD29 and CD44 (Supplementary Figure 25). Taken together, these results demonstrate that an undifferentiated and expandable pool of MSC is present in prevascularized CCs after 7d oCC.

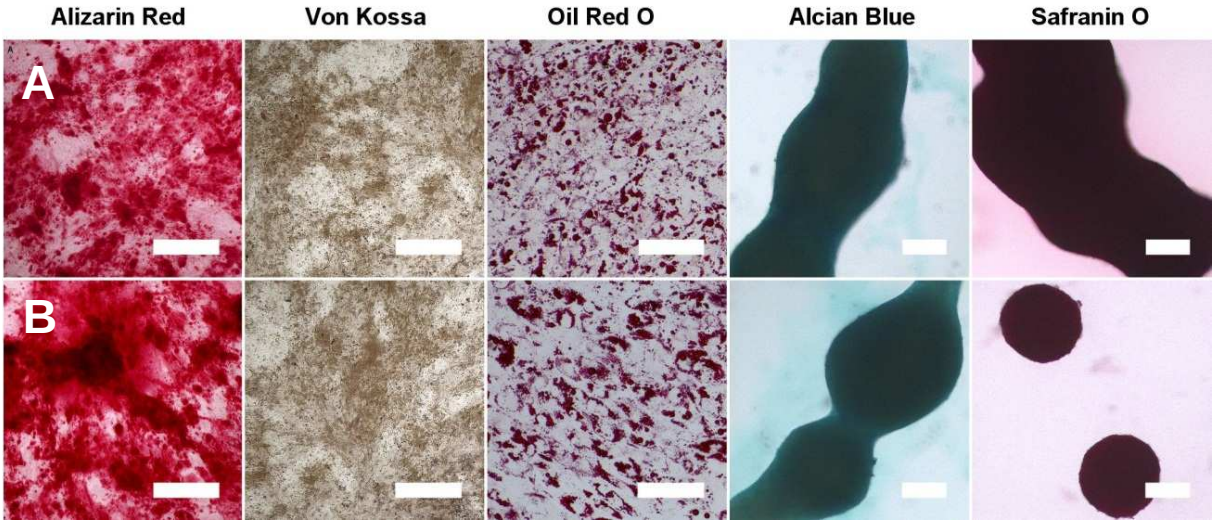

Figure 38: Evaluation of a tri-lineage differentiaion potential of MSC isolated from CCs after 7d oCC (row A) or 7d angCC (row B); Scale bars: AR/VK = 500 µm, OR-O = 200 µm, AB/Saf-O = 500 µm

4 Discussion

In the present study the basis for a strategy to generate prevascularized and osteogenic tissue samples using a MSC/EC CC model was developed. A comparable strategy focusing on minimal GF supplementation to highlight paracrine cellular crosstalk has not been described to-date. By establishing a step-by-step approach first the osteogenic differentiation of MSC was optimized in 2D and 3D serving as a basis for sequential medium strategies to induce the formation of VLS in a competitive manner.

The present study successfully evaluated a newly introduced bone substitute material, namely tNiTi, as a promising candidate material for advanced BTE strategies using a perfusion bioreactor (see section 3.2). While MSC have been shown to be differentiated into osteoblastic cells on 3D tNiTi scaffolds using ODM (Gotman et al., 2013), the present study demonstrated for the first time that human primary MSC osteogenesis is not induced solely by medium perfusion in the absence of OS (see section 3.2). The optimized CSD for the osteogenic differentiation of MSC (see section 3.2) was then transferred into a CC system analogous to a scale-down from 3D to a 2D environment to exclude multidimensional gradients and mechanical stimuli observed in a dynamic 3D microenvironment. Based on this, the present study demonstrates for the first time that varying cell proportions of MSC and HDMEC affects the secreted level of GFs in the applied CC model and that this might generate a therapeutic window clearly affecting VLS formation *in vitro*. The present study further identified a specific range of cell proportions that were optimal for the formation of VLS *in vitro* (see section 3.3.2). Further studies improved the CSD and CSR of a CC model of MSC with OEC to enhance VLS formation (see section 3.3.3) compared to already published protocols (Dohle et al., 2010, Fuchs et al., 2007, Kolbe et al., 2011). By transferring the findings into a CC system that would also target the osteogenic differentiation of the incorporated MSC fraction the present study performed CCs of MSC with HDMEC in various media aiming to stimulate simultaneously osteogenesis and VLS formation in the CC (see section 3.4). The present study found that the supplementation of OS suppresses VLS formation while the supplementation of HF suppresses osteogenesis of MSC (see section 3.4). This is reported here for the first time in the context of a medium with minimal GF supplementation highlighting paracellular crosstalk. To circumvent the described competitive effects studies were performed to sequentially stimulate osteogenesis in MSC and VLS formation by HDMEC in the same CC. The present study found that osteogenic priming of MSC dramatically reduces their expression of pro-angiogenic VEGF (see section 3.5.1), and that the subsequent co-cultivation with HDMEC negatively influences VLS formation (see section 3.5.2). By contrast, when CC of MSC with HDMEC were initially prevascularized and subsequently transferred into osteogenic medium the formation of a calcified matrix containing VLS could be achieved (see section 3.6). The present study further characterized the involved

dynamics during oCC of prevascularized CCs (see section 3.6.1). The rapid osteogenic differentiation in the CC model was found to be linked to VR based on a disregulated GF environment (see section 3.6.3.1) caused by OS and their effects on HDMEC (see section 3.6.3.2). However, the present study described for the first time that VLS and angiogenesis can be maintained and re-initiated (see section 3.6.4). Subsequent studies investigated the involvement of direct or non-direct GF signaling in the rapid osteogenic differentiation of MSC in prevascularized CCs during oCC. The presented data indicate that prevascularized CCs of MSC with HDMEC cultivated under osteogenic conditions during oCC can stimulate the osteogenic phenotype in MSC MCs that are locally separated by a filter membrane in a Transwell system (see section 3.6.5). Further studies found that the described CC model can be varied in its composition by exchanging the type of EC or MSC (see section 3.6.6 and 3.6.7). By using commercial ODM or customized ODM with reduced βGP concentrations it was also possible to exclude the rapid osteogenic differentiation of MSC and the related matrix calcification as an artifact from customized ODM supplemented with high level of βGP (see section 3.6.8). Finally, the present study was able to demonstrate that within the investigated time frame the prevascularized and osteogenically differentiated CC model still contains an expandable and non-differentiated subfraction of MSC (see section 3.6.9). To further highlight the described findings all results are discussed in the context of known facts and the state-of-the-art research in the following sections.

4.1 The osteogenic differentiation of MSC is influenced by basic cell culture parameters

For the development of tissue engineering strategies various studies have shown that basic cell culture parameters can significantly influence the structure, function and overall outcome of the approach (Govindasamy et al., 2010, Hoemann et al., 2009, McBeath et al., 2004). In terms of the osteogenic differentiation of MSC the concentration of osteogenic supplements, the choice of BM and the initial CSD all modulate the final degree of osteogenesis (Hoemann et al., 2009). It is noteworthy that no universally valid protocol for the osteogenic differentiation of hMSC exists and therefore controversial data exist with regard to single culture parameters. In this context, McBeath and colleagues showed an initial CSD of 3000 MSC/cm^2 to be optimal for the osteogenic differentiation of hMSC (McBeath et al., 2004). In contrast, Hagmann et al. seeded approximately 18,000 MSC/cm^2 in osteogenic differentiation experiments (Hagmann et al., 2013). A study comparing different BM for ODM found αMEM BM to be superior to DMEM-F12 BM for the relative expression of the osteogenic genes *osterix* and *osteocalcin* in hMSC (Govindasamy et al., 2010). Independently, both DMEM and αMEM are widely used as BM in ODM (Zhang et al., 2008, Ayatollahi et al., 2012, Le Blanc et al., 2003, Hanada et al., 1997, Donzelli et al., 2007, D'Ippolito et al., 1999). Additionally, varying experimental durations of 10 d, 18 d, 2W, 3W, 4W or 4-5W for the investigation of osteogenic differentiation can be

found in numerous studies (Rodriguez et al., 2004, Hanada et al., 1997, Ginis et al., 2012, Hagmann et al., 2013, Le Blanc et al., 2003, Donzelli et al., 2007, D'Ippolito et al., 1999).

Based on the facts found in the literature different CSDs and BM were compared for their supportive effect on the osteogenic differentiation of hMSC in this study (Supplementary Figure 1; Supplementary Figure 2). The results are in accordance with the findings of Govindasamy and colleagues, highlighting αMEM-GlutaMAX BM as superior to DMEM/F-12 BM for the induction of osteogenesis in hMSC (Supplementary Figure 2; (Govindasamy et al., 2010)). In contrast, the present study could not confirm a CSD of 3,000 MSC/cm^2 (McBeath et al., 2004) but a CSD of 20,000 MSC/cm^2 to be the most optimal for the osteogenic differentiation of hMSC (Supplementary Figure 1). Although detailed analyses by western blot or real-time PCR as described by McBeath and colleagues were not performed (McBeath et al., 2004), our results showing CSDs above 3,000 MSC/cm^2 to be more efficient for the osteogenic differentiation of MSC were in accordance with the CSDs used by others (Le Blanc et al., 2003, Schneider et al., 2010).

4.2 Trabecular Nitinol scaffolds permit enhanced osteogenic differentiation of MSC under medium perfusion

Following the initial optimization studies, the osteogenic differentiation of MSC was transferred to a dynamic environment and combined with state-of-the-art technology. Thus, a commercial perfusion bioreactor system was used to investigate the influence of medium perfusion through 3D trabecular Nitinol (tNiti) scaffolds on the osteogenic differentiation of primary hMSC. A previous study demonstrated that hMSC differentiate into cells of the osteogenic lineage on tNiTi, as shown by enhanced ALP activity and calcium deposition on the scaffolds compared to plastic controls (Gotman et al., 2013). However, since the experiments in this latter study were performed under static conditions, the resulting question was whether medium perfusion through tNiTi scaffolds could enhance the osteogenic differentiation process. The hMSC that were used for the flow-based investigations showed an expression pattern of surface markers, as well as the tri-lineage differentiation potential as recommended by the ISCT guideline (Dominici et al., 2006). In addition, based on the marker constellation, subpopulations of hematopoietic stem or progenitor cells, adult hematopoietic cells and endothelial cells could be excluded (Figure 4).

To study the effects of medium perfusion on the osteogenic differentiation of hMSC on tNiTi scaffolds cell-seeded scaffolds were cultivated under comparative static and dynamic conditions in a perfusion bioreactor. It is known that medium perfusion through three-dimensional scaffolds may increase the distribution and uniformity of the growing and differentiating cells, as well as of the formed matrix (Wendt et al., 2003, Liao et al., 2010). The results of the present study clearly support these

findings by demonstrating increased ALP activities, mineralization of deposited collagen matrix (Figure 5) and the distribution throughout the tNiTi scaffolds when medium perfusion is applied (Figure 9). In the static samples, cell growth as well as matrix deposition were predominantly limited to the scaffold surface and peripheral region. A similar outcome was shown by other groups for statically cultivated and differentiated 3D scaffolds (Glowacki et al., 1998). It is important to note that all scaffolds used in the present study were dynamically seeded to generate cell-loaded scaffolds with a comparable cell distribution pattern at the baseline level. Therefore, it is likely that cell death in the central areas of the scaffolds and migration to the scaffold periphery occur in all static samples as previously described (Goldstein et al., 2001). In contrast, enhanced cell growth, intracellular collagen expression, matrix deposition and calcification as well as the more homogeneous distribution of cells in dynamic cultures showed that medium perfusion clearly had a beneficial effect on the osteogenic differentiation of hMSC on tNiTi scaffolds (Figure 9). However, the question remained whether this effect of medium perfusion was a result of better cell distribution or whether medium flow could serve as a mechanical stimulus to induce osteogenesis in hMSC. The latter has been shown to occur with rat MSC (Holtorf et al., 2005b). Holtorf et al. investigated the osteogenic differentiation of rat MSC in the absence of dexamethasone (Dex) while adding ascorbic acid (AA) and β-glycerol phosphate (β-GP) to the cell culture medium (Holtorf et al., 2005b). Matrix calcification, as well as enhanced ALP activity was found in the absence of Dex when medium perfusion was applied. In contrast, in the present study human MSC did not show enhanced ALP activities or calcification when cultivated in the absence of Dex (ODM-Dex cultures) on tNiTi scaffolds (Figure 10), although similar concentrations of AA and β-GP were used as in the rat MSC study. Furthermore, these parameters were not influenced by the application of medium perfusion in our experiments.

Another study on the effects of perfusion on MSC showed enhanced mRNA levels of bone sialoprotein (BSP), bone morphogenic protein-2 (BMP-2) and osteopontin (OP) in response to medium flow (Yourek et al., 2010). The response to medium flow was observed even in basal medium without the addition of AA or β-GP (Yourek et al., 2010). However, these authors did not show a similar result at the protein level. Thus, it is not clear if these enhanced levels were of biological relevance to the osteogenic differentiation of hMSC. In the present study, medium perfusion in the absence of Dex led to an increase of the TIC as well as collagen type 1 deposition by hMSC on tNiTi (Figure 11). Therefore, mechanical stimuli provided by medium perfusion could also contribute to osteogenic differentiation of hMSC, while supporting the expression and secretion of collagen into the extracellular matrix. However, it did not lead to full differentiation of hMSC, since matrix calcification was not observed on tNiTi scaffolds cultivated dynamically in the absence of Dex. A possible explanation is that in the present system medium perfusion acted as a co-stimulus to Dex, where both the effects of medium flow on the distribution of cells and nutrients and the mechanical effect on the osteogenic differentiation would be of

importance. This mechanical effect could be concluded from the SEM analysis and stereomicroscopic observations of statically and dynamically differentiated hMSC on tNiTi scaffolds, which showed a morphologically differential, more evenly distributed and increased mineralization on the surface, as well as in the center of dynamically differentiated tNiTi scaffolds (Figure 9). Additionally, the atomic levels of calcium and phosphorus as detected by EDX were enhanced in dynamic cultures compared to the static situation (Figure 6; Figure 7; Figure 8; Table 19). Although a detailed atomic analysis of the mineralization by EDX was performed primarily on one donor the general trend from the EDX quantification is in accordance with the trend found for the quantification of calcium and TIC (See Table 19; Figure 10 and Figure 11). Moreover, ALP activity was found to be increased in all dynamic differentiation samples compared to the static ones (Figure 5; Figure 10).

Although further studies were not carried out on possible mechanisms or other ranges of flow velocities, it appears that medium perfusion acted synergistically with the inductive effect of Dex in the system used in the present study. The flow velocity employed in the present studies was lower (100 µm/s in 8 mm perfused diameter, resulting in a theoretical flow rate of 0.3 ml/min) than the value used by Holtdorf and colleagues (1ml/min) (Holtorf et al., 2005b). Hence, the comparability of the conclusion reached in the present study with the conclusion obtained by Holtdorf et al. is difficult. Accordingly, it is not clear whether medium perfusion through tNiTi scaffolds could enhance the osteogenic differentiation of hMSC even in the absence of Dex to ODM when a flow rate of 1 ml/min was used. Additional studies are needed to investigate this issue. In this study, medium perfusion had a positive effect on the osteogenic differentiation of hMSC and mineralization on tNiTi. The outcome of a previous study by Gotman and colleagues, proving tNiTi to be a suitable candidate as a biomaterial in bone tissue engineering (Gotman et al., 2013), is further highlighted by the behavior of tNiTi under dynamic conditions as described in the present study. Such pre-cultivation of cell-seeded tNiTi scaffolds in a perfusion bioreactor could be envisaged as a promising strategy in the application of tNiTi as a bone substitute material. Similar observations were made for scaffolds manufactured from other materials, such as hydroxyapatite (Bjerre et al., 2011) or poly(L-lactic acid) (Alvarez-Barreto et al., 2011). Nevertheless, enhanced mineralization on tNiTi obtained by cultivation of hMSC under perfusion is an important step forward towards the application of this material in BTE.

4.3 Strong interactions between angiogenic and osteogenic factors disable a synergizing medium strategy

Based on the development of a dynamic 3D cell culture model the osteogenic differentiation of MSC was investigated in a more biologically relevant context. The co-cultivation of MSC with endothelial cells (EC) or osteoprogenitor cells with EC was shown to facilitate vascularization and the formation of VLS in vitro (Unger et al., 2005, Kolbe et al., 2011, Dohle et al., 2010, Dohle et al., 2011). To generate a stable

baseline, the CSD defined as optimal for the osteogenic differentiation of MSC (0.2 x 10^5 MSC/cm^2) was applied to study the formation of VLS in MSC/EC CCs in dependence on a varying CSR. Since primary cell material is highly valuable due to its limited availability the optimization and investigation of combined prevascularization and osteogenesis in the co-culture model was performed in 2D. Furthermore, multidimensional gradients and mechanical stimuli from a dynamic 3D microenvironment could be excluded.

The findings described for an initial characterization of HDMEC, HUVEC and OEC grown in ECGM (Figure 12; Figure 13; Figure 14) are in accordance with data given in the literature (Bardin et al., 2001, Nakazato et al., 1997, Kolbe et al., 2010, Unger et al., 2002, Gougos et al., 1992, Bahramsoltani et al., 2014, Moritani et al., 1991, Languino et al., 1989, Li et al., 2006) with the exception that to-date the expression of Col-IV and LMN at the protein level in MCs of OEC in vitro was not described. Since it was shown that CD90 expression on EC is linked to inflammatory reactions (Wetzel et al., 2006, Saalbach et al., 1999) the negative expression of CD90 by flow cytometry demonstrated that neither HDMEC nor HUVEC or OEC were in an activated state due to an inflammatory stimulus during the cultivation in ECGM. The detection of CD34 on HDMEC and OEC was found to be in accordance with other studies (Unger et al., 2002, Kolbe et al., 2010, Ferreras et al., 2015). This molecule was shown to be expressed on small or newly formed vessels while EC from larger veins remain predominantly negative in vitro (Muller et al., 2002). Moreover, in HUVEC CD34 was shown to mark a minor subpopulation of tip cells (Siemerink et al., 2012) for which reason it is likely that $CD34^+$ HUVEC detected in the present study represented a minor tip cell fraction. Flow cytometric analyses for the hyaluronan receptor CD44 showed a lack of expression on HDMEC, HUVEC and OEC. It was demonstrated by others that CD44 is absent from freshly isolated HUVEC and HUVEC grown to confluence (Griffioen et al., 1997). In contrast, HDMEC and OEC are generally regarded as being able to express CD44 (Nandi et al., 2000, van Beem et al., 2009), although no data are available on CD44 dynamics in relation to cell growth in vitro. In the present study flow cytometry for the expression of CD44 was performed on confluent EC. Therefore, the data obtained for the expression of CD44 on HUVEC in this study are in accordance with the data given from Griffioen and colleagues (Griffioen et al., 1997). Most importantly, a study conducted by Nandi and colleagues identified CD44 as a trypsin-sensitive molecule (Nandi et al., 2000). Since in vitro expanded EC were harvested following trypsin treatment, the lack of CD44 expression could be generated as an artifact from the harvesting protocol. Future experiments need to address this issue in terms of an alternative harvesting protocol since CD44 was shown to be critically involved in angiogenesis in vitro and in vivo (Cao et al., 2006). Despite the missing CD44 expression, HDMEC and OEC were able to form vessel-like structures when co-cultivated with MSC, as discussed in the following section.

The CC system of MSC with HDMEC served as a standard model in this study, since the isolation of HDMEC requires less single steps and is less time consuming compared to the isolation of OEC. The initial investigation on varying CSR in CC of MSC with HDMEC in 2D clearly demonstrated that tube formation is strictly dependent on the cellular proportions. Other studies successfully demonstrated the prevascularization reaction in 2D or 3D using CC of pOB with HDMEC at CSR of 1:4 and 1:6 (Santos et al., 2009, Unger et al., 2010, Unger et al., 2007). It is noteworthy that following an initial optimization it was described that an excess of pOB lead to the disappearance of HDMEC after 1W of co-cultivation (Unger et al., 2007). Independently, the described protocols differ markedly in the absolute cell numbers used to study prevascularization *in vitro*. In this context, Santos et al. co-cultivated 0.375×10^5 pOB with 1.125×10^5 HDMEC on starch poly-caprolactone fiber-mesh scaffolds, while Unger et al. used 0.2×10^5 pOB and 1.3×10^5 HDMEC on silk fibroin scaffolds or 0.0415×10^5 pOB with 0.27×10^5 HDMEC per cm^2 of a 3.5 cm petri dish, thereby representing CSR of 1:4, 1:5 or 1:6, respectively (Santos et al., 2009, Unger et al., 2010, Unger et al., 2007).

The findings of the present study underlined the results obtained in the mentioned studies inasmuch as the formation of VLS was detectable at CSRs characterized by an excess of HDMEC in the CC with MSC (CSR 1:4; Figure 15). Nevertheless, decreasing the endothelial fraction towards an excess of MSC (CSR of 1:0.66 or 1:0.25) resulted in an increased VLS formation in CCs of MSC with HDMEC (Figure 15). This was also confirmed by the quantification of VLS, demonstrating that both prevascularization and angiogenesis *in vitro* occurred to an increased extent at CSR of 1:0.66 and 1:0.25 compared to CSR of 1:4 or 1:2, predominantly exhibiting single tubes. The effect was found to be connected to varying release profiles of VEGF, Ang-1 and Ang-2, as indicated by ELISA measurements after 7d and 14d (Figure 15). These factors are crucially involved in the induction and stabilization of angiogenesis and angiogenic networks *in vitro* and *in vivo* where high levels of Ang-2 combined with low levels of VEGF were shown to highly reduce angiogenesis and support VR (Lobov et al., 2002). In this context, it was demonstrated by Ozawa et al., that the microenvironmental concentration of VEGF released into the surrounding tissue markedly influenced the formation of normal or abberant angiogenesis *in vivo* (Ozawa et al., 2004b). Thus, by adjusting the CSR in CCs of MSC with HDMEC it is likely that the absolute concentrations of VEGF, Ang-1 and Ang-2 measured in the closed *in vitro* system were shifted towards a more pro-angiogenic environment using a CSR of 1:0.66 or 1:0.25. This was also evident from the IF staining for Col-IV, a major component of the basement membrane of maturating vessels *in vitro* and *in vivo* (Kubota et al., 1988, Carmeliet, 2003), showing homogenous basement membranes along vessels at CSR of 1:0.66 and 1:0.25 (Figure 15). In contrast, using CSR of 1:4 or 1:2 the basement membranes were less positive for the expression of Col-IV and exhibited a less homogenous morphology (Figure 15), thus indicating that VLS were in a less matured state in these CCs.

Altogether, these results demonstrate that simple variations of cellular proportions during co-cultivation can be used for the fine-tuning of the complex cellular interplay involved in angiogenesis to optimally achieve the formation of maturing vascular structures in vitro. This was also confirmed by the optimization of a CC model of MSC with OEC (Figure 16; Figure 17), which represent a therapeutically relevant autologous cell source highlighted in different reports (Martin-Ramirez et al., 2012, Lin et al., 2002, Griese et al., 2003, Medina et al., 2010). The use of OEC for the development of prevascularization strategies was investigated by others (Dohle et al., 2010, Dohle et al., 2011, Fuchs et al., 2007, Fuchs et al., 2009b, Kolbe et al., 2011). Dohle et al. and Fuchs et al. described the co-cultivation of 3 x 10^5 pOB with 2 x 10^5 OEC per well of a 24-well plate to achieve the formation of VLS in vitro, thus using a CSR of 1:0.66 (Dohle et al., 2010, Dohle et al., 2011, Fuchs et al., 2007). Similar cell numbers and a similar CSR were applied by Kolbe et al. in a CC model of MSC with OEC (Kolbe et al., 2011). Notably, no investigation of other ranges of absolute cell numbers was performed in any of the mentioned studies. Therefore, the present study found that an approximately 8-fold reduction in the CSDs for MSC and OEC at a constant CSR of 1:0.66 enhanced the formation of VLS (e.g. 12-fold increased number of networks), as indicated by the quantification of VLS formation (Figure 17). This finding is in accordance with the results obtained for the CC model of MSC with HDMEC, thus highlighting the common size of the MSC compartment with respect to the osteogenesis of MSC and the prevascularization in MSC/EC CCs.

It requires to be stressed that further studies are needed to investigate vessel homeostasis in the described CC models. Although the formation of a basement membrane was confirmed in CCs of MSC with HDMEC this information is missing from CCs of MSC with OEC. Furthermore, long-term studies (4 W. and longer) might allow a more detailed evaluation of vessel stabilization in vitro. Perivascular cells are known to be a key component of mature vessels and capillaries (Carmeliet, 2003, Bergers and Song, 2005). Therefore, to finally determine the maturational state of the VLS formed in vitro it is necessary to demonstrate the attachment of perivascular cells (e.g. NG2+ cells, αSMA+ cells) in addition to the expression of basement membrane proteins (e.g. Col-IV, laminin) (according to (Bergers and Song, 2005, Hirschi and D'Amore, 1996)). In contrast, vascular structures generated within 7d in vitro on 3D silk fibroin scaffolds using CC of pOB with HDMEC were successfully implanted subcutaneously into immune-deficient CD-1 mice and shown to connect to the host vasculature after 14d of implantation (Unger et al., 2010). Similar results were obtained by Chen and colleagues using CC of HUVEC with fibroblasts for the in vitro prevascularization of fibrin scaffolds for 7d followed by anastomosis after 5d during implantation into immuno-deficient Rag-2 mice (Chen et al., 2009). Therefore, the question remains whether a high maturational state of vascular structures formed in vitro is generally necessary to achieve anastomosis and vascular perfusion in vivo.

The CC model of MSC with HDMEC was also evaluated for the simultaneous induction of vascularization and osteogenesis in vitro. Medium screening

demonstrated that the combined addition of OS and HF to ECGM led to the complete inhibition of vascular network formation, while the supplementation of HF alone was mandatory to achieve stable vascular networks (Figure 18; Figure 19). In ODM VLS formation was not observed whereas osteogenic differentiation and matrix calcification were obtained. CCs performed in ECGM-based media exhibited no osteogenic differentiation (Figure 18). The same was true for MSC MCs cultivated under the same conditions (Figure 20). These results are similar to findings observed by others, demonstrating that EC (HUVEC or OEC) did not survive or form VLS in ODM (Correia et al., 2011, Kolbe et al., 2011). Furthermore, by using CCs of MSC with OEC, Kolbe and colleagues showed that co-cultivation in EGM-2 medium supplemented with OS resulted in a decreased calcium deposition and ALP activity after 2wk (Kolbe et al., 2011). Although this study used a different angiogenic medium (EGM-2, Lonza) and osteogenic BM (DMEM/F-12-GlutaMAX, Gibco) similar concentrations of OS as described in the present study were added to the CCs and resulted in the reduction of osteogenesis or the prevention of vessel formation in the corresponding experimental groups (Kolbe et al., 2011). In this context, Pi was shown to induce apoptosis in EC when applied at high concentrations (> 1.4 mM) (Di Marco et al., 2008) and appears to be attributed to non-specific cellular calcification following induction of apoptosis in MSC during osteogenic differentiation (Langenbach and Handschel, 2013). Pi can be generated upon hydrolyzation of βGP by ALP (Khouja et al., 1990). Thus, the supplementation of 10 mM βGP to the ECGM in the present study might have generated high levels of Pi. Although no calcification was detectable in CCs grown in ECGM supplemented with OS the induction of apoptosis due to an increased level of Pi must be considered.

Similar to βGP, Dex was shown to exhibit a negative effect on angiogenesis by binding to the GR and thus leading to the reduction of VEGF-induced angiogenesis in MCs of HUVEC (Logie et al., 2010). The same effect of Dex was described for the inhibition of tumor angiogenesis in vivo (Yano et al., 2006). Since in the present study no calcification was detected in CCs performed in ECGM supplemented with OS it is likely that the absence of vascular structures was not necessarily caused by βGP-induced apoptosis but more likely by the binding of Dex to the GR in MSC, thus decreasing the expression of pro-angiogenic factors like VEGF. This hypothesis is supported by the decreased VEGF level measured in MSC MCs during osteogenic differentiation experiments as described later in this study (see section 4.4.1). On the other hand, the absence of matrix calcification was most probably not suppressed by the addition of HF, since several studies have shown a supportive function of bFGF (Hanada et al., 1997, Ng et al., 2008, Montesano et al., 1986) and the non-inhibitory effect of heparin on the osteogenic differentiation of MSC (Papathanasopoulos et al., 2011, Battula et al., 2007). It is possible that ECGM was insufficient to permit induction of osteogenesis in MSC within 2wk, and that osteogenic differentiation might be achieved at later time points (e.g. 4wk or 6wk). Future studies are needed to address this question. Interestingly, when CCs of MSC with HDMEC were

cultivated in ODM matrix calcification was obtained. Although VLS and even EC were absent from these CCs the question remains whether βGP-induced apoptosis of EC contributed to the degree of calcification, since matrix calcification was also obtained in MSC MCs after 2wk in ODM (Figure 17). It is important to note that apoptosis of either EC or MSC in the corresponding media was not determined in the present study. Nevertheless, the induction of vascularization in ECGM is most probably supressed when Dex is supplemented to induce the osteogenic differentiation of MSC.

Contrary to the findings described in this study, Pedersen and colleagues showed the formation of vascular networks in CC of MSC with HUVEC cultivated in pure ODM in addition to other media containing 3.5 mM βGP and 10 nM Dex (Pedersen et al., 2012). However, this study used a commercial differentiation medium (MesenCult™ Osteogenic Stimulatory Kit (Human); StemCell Technologies) which contained 15% "osteogenic stimulatory supplements" of unknown composition (Data not provided by manufacturer). In the present study vessel formation was absent in CCs of MSC with HDMEC when 100 nM Dex and 10 mM βGP were added to ECGM. Moreover, a previous study demonstrated a comparable significant Dex-mediated reduction of VEGF expression and angiogenesis in a prostate cancer xenograft model when concentrations of 10 nM and 100 nM Dex were used (Yano et al., 2006). Nevertheless, it is not clear whether the commercial medium used by Pedersen et al. contained other GFs or chemical substances that were able to buffer the effects of βGP and Dex on EC and *in vitro* vascularization, thus supporting both angiogenesis and osteogenesis.

4.4 Development of a sequential medium-change strategy for the generation of prevascularized osteogenic tissue samples

To circumvent the described disadvantages observed when using a single medium that did not simultaneously support both osteogenesis and angiogenesis in CCs of MSC with HDMEC a different strategy was examined. The processes of vascularization and angiogenesis i*n vivo* are stimulated in a sequential manner during bone growth or bone repair (Gerstenfeld et al., 2003b, Maes and Carmeliet, 2008, Marsell and Einhorn, 2011). Based on this, a sequential medium strategy was examined to determine whether osteoblastic cells derived from the osteogenic differentiation of MSC can actively contribute to the formation of VLS and angiogenesis by endothelial cells.

4.4.1 The wrong way: Co-cultures of HDMEC with osteogenically primed MSC

Initially, MSC MCs were primed in ODM to achieve an osteoblastic phenotype and subsequently co-cultivated with HDMEC to investigate the formation of VLS in various experimental settings. Furthermore, this strategy served to evaluate the Dex-mediated changes in the expression of pro-angiogenic GFs like VEGF as described

in the previous section. The strategy also addressed the question as to whether fresh MSC or MSC pre-cultivated in non-osteogenic medium (MSC-BM) were superior to osteoblasts generated upon osteogenic differentiation of MSC (oMSC) to obtain VLS formation *in vitro*. A number of previous studies have successfully described the formation of VLS in CC of EC with pOB (Dohle et al., 2014, Dohle et al., 2010, Dohle et al., 2011, Fuchs et al., 2009a, Fuchs et al., 2007, Fuchs et al., 2010, Fuchs et al., 2009b, Kolbe et al., 2011, Unger et al., 2010, Unger et al., 2007, Ma et al., 2011, Herzog et al., 2014).

In the present study, an osteogenic phenotype was induced in MSC following cultivation in ODM (Figure 22). This is in keeping with results observed by others (Govindasamy et al., 2010, Ma et al., 2011, Pittenger et al., 1999). More importantly, the present study demonstrates for the first time that the expression of VEGF was continuously reduced during both short-term and long-term cultivation of MSC in ODM compared to non-osteogenic medium (Figure 22). In preivous studies, data on VEGF expression were generally only available for single time points, e.g. 7d (Hoch et al., 2012). Since Dex is added as a supplement to ODM to induce osteogenesis in MSC, these results indicate that VEGF expression is negatively influenced by the addition of Dex. This is supported by the finding that VEGF expression remains unaffected when βGP is omitted from ODM (see section 4.5.4) and that VEGF expression can be re-established by switching to a Dex-free medium (see section 4.4.3.2) as described later in this study.

In contrast to the expression of VEGF, an ELISA assay demonstrated that Ang-1 expression increased in a time-dependent manner during the cultivation of MSC in ODM (Figure 22). An increased Ang-1 secretion from decellularized osteogenic matrices compared to non-osteogenic matrices was reported by Prewitz et al. but not investigated for a time-dependent course of expression (Prewitz et al., 2013). Taken together, these results may explain the findings observed during the co-cultivation of MSC with HDMEC in ODM that led to the suppression of VLS formation as described in a previous section (see section 3.6.2). These studies indicated that altered release profiles of VEGF and Ang-1 in oMSC and the osteoblasts generated upon MSC differentiation resulted in a reduced pro-angiogenic potential compared to noMSC. To confirm this hypothesis oMSC and noMSC were co-cultivated with fresh HDMEC under various experimental conditions (Figure 23).In general, it was found that the co-cultivation of oMSC with HDMEC exhibited no differences in VLS formation compared to control samples when oMSC were generated under short-term differentiation in ODM condtions (2wk) (Figure 24). In contrast, the formation of vascular structures was dramatically reduced in CC of oMSC with HDMEC when oMSC were generated upon long-term differentiation in ODM (4wk) (Figure 24). Most interestingly, a similar effect, although to a lesser extent, was achieved when oMSC-4wk were co-cultivated with HDMEC (Figure 24).
By varying the experimental conditions, it was shown that the effects on vascularization were independent of the extracellular matrix (ECM) formed during

osteogenic priming or pre- cultivation of MSC (Figure 23 – Approach A versus C). Previous studies have shown that the ECM can bind GFs like bFGF or VEGF and actively influence cellular processes such as proliferation or angiogenesis (Flaumenhaft and Rifkin, 1991, Schultz and Wysocki, 2009). The active release of GFs such as Ang-1 from ECM was demonstrated by Prewitz and colleagues in a study investigating the use of decellularized osteogenic ECM to support the function of human hematopoietic stem cells *in vitro* (Prewitz et al., 2013). Although in the present study GFs were not quantified during the co-cultivation of oMSC and MSC-BM with HDMEC, it can be assumed that the ECM produced during priming of MSC in osteogenic (oMSC) or non-osteogenic medium (MSC-BM) as well as pro-angiogenic GFs bound to and released from the formed ECM were generally of less importance for the formation of VLS during the following co-cultivation with HDMEC. It appears that both oMSC and MSC-BM exhibited a different capacity to re-establish a proangiogenic environment when co-cultivated with HDMEC that was dependent on the total period of priming time in osteogenic or non-osteogenic media (2wk or 4wk). Based on the VLS quantification and IF staining for CD31 a comparable extent of VLS was detected in the CC independent of whether MSC-BM2wk or oMSC-2wk were co-cultivated with HDMEC (Figure 24). This indicates that, in addition to the low levels of VEGF initially expressed by oMSC-2wk, the expression could be rapidly increased upon co-cultivation in Dex-free ECGM thus leading to VLS formation after 2wk in CC. In contrast, the highly reduced VLS formation in CCs of HDMEC with MSC-BM4wk or oMSC-4wk suggests a different regulation pattern in the cells.

In MSC-BM, a high level of VEGF and a constitutive level of Ang-1 was expressed as detected by ELISA (Figure 22), thus indicating that MSC-BM initially exhibited the potential to induce angiogenic changes in HDMEC. When MSC-BM were harvested after 2wk or 4wk no differences in cell numbers were found (Supplementary Figure 6) suggesting that a maximum cell density was reached after 2wk. As proliferation and apoptosis were not investigated, it was difficult to clearly identify which cellular changes were taking place. In general, both the growth and expansion of MSC *in vitro* are connected to substrate limitation and quiescence (Peiffer et al., 2007, Jones et al., 2005, Lin et al., 2014). Even though substrate concentrations were not determined during the cultivation of MSC-BM it is conceivable that the constant cell numbers harvested after 2wk and 4wk represent an equilibrium state of the cells that was due to the available amount of substrate in the well plates. Changes in the substrate availability were demonstrated to affect senescence in human dermal fibroblasts (Zwerschke et al., 2003) and the cell cycle in human cells (Lin et al., 2014, Jones et al., 2005). However, cell cycle analysis was not performed in MSC-BM, although it has been shown by others that 75% of expanded MSC reside in the G0/G1 phase of the cell cycle (Achille et al., 2011) thus representing cells that were metabolically active but not yet replicative and, most importantly, cells that were quiescent and non-proliferative (Cooper, 2000). The fraction of MSC residing in G0/G1 phase could be increased to 90% by cell cycle synchronization following GF

deprivation (Achille et al., 2011). Since bmMSC were cultivated in GF-free medium following expansion in the presence of bFGF it is likely that quiescent cells accumulated to different percentages after 2wk or 4wk, with the latter containing the highest fraction of quiescent cells due to the longer incubation period. Quiescent G0 cells are able to re-enter the cell cycle and to actively proliferate (Cooper, 2000). Based on this, it is possible that potentially varying G0 fractions contained in MSC-BM exhibited a differential proliferative behavior in the CC with HDMEC, thus leading to delayed induction of and finally reduced vascularization in CCs of HDMEC with MSC-BM4wk.

When oMSC were co-cultivated with HDMEC at the beginning of CC it is possible that a low level of VEGF and high level of Ang-1 both released from oMSC and a high level of Ang-2 released from HDMEC were present. This was observed by decreased levels of VEGF detected during the generation of oMSC and the high Ang-2 concentrations measured in HDMEC MCs and CC controls (Figure 24). This is in keeping with the fact that the same size of the HDMEC fraction was applied to all CC approaches. In a pupillary membrane *in vivo* model Lobov and colleagues demonstrated that a high level of Ang-2 in combination with low level of VEGF induced EC death (Lobov et al., 2002). The same study also suggested that Ang-2 administration combined with VEGF inhibition “would be the best way to achieve vessel regression in other settings” (Lobov et al., 2002). It is possible that in the CCs of oMSC with HDMEC the initial GF environment was shifted towards an anti-angiogenic setting. The observation that in CCs of oMSC-2wk with HDMEC VLS formation was induced may have been due to the lower stage of differentiation of the oMSC-2wk compared to oMSC-4wk and that the 2wk cells had a higher remaining proliferative potential. It is possible that oMSC-2wk responsed to the absence of OS and the presence of bFGF in ECGM by exhibiting extensive proliferation. This may have resulted in re-establishing VEGF expression and the angio-inductive environment, whereas the absence of such a response of oMSC-4wk might be limited due to their advanced stage of differentiation.

Others have shown that MSC undergoing osteogenic differentiation exhibit a decreasing proliferative potential (Aubin, 2001). Additionally, it can be speculated that MSC, once harvested and re-seeded in medium containing bFGF, change the phenotype expressed during osteogenic differentiation and return to an MSC phenotype. A similar observation was described for cells isolated from trabecular bone fragments following collagenase treatment (Sakaguchi et al., 2004). Likewise, Hofmann and colleagues generated osteoblastic cells by outgrowth from trabecular bone fragments in the presence of Dex and βGP, and demonstrated vascularization during the subsequent co-cultivation with HUVEC in Dex-free medium (Ma et al., 2011). Osteogenic differentiation of MSC is a multi-stage process (Huang et al., 2007) characterized by matrix calcification that is absent in an early differentiation stage (up to 14d), but present in the late stage of differentiation (14d to 28d) (Hoemann et al., 2009, Huang et al., 2007). According to this, oMSC-2wk and oMSC-

4wk correspond to the early and late stage of differentiation, respectively. This is also supported by AR and VK staining, both indicating the absence of a calcified osteogenic matrix in oMSC-2wk (Figure 22). However, changes to the specific regulation of the various GFs cannot be identified or described in detail, since GFs from cell culture supernatants were not quantified. Future studies using cell cycle analysis are needed to examine the regulation of GFs after re-initiation of proliferation in ECGM. In this context, it is known that differentiated cells exhibit a prolonged G0/G1 phase, whereas proliferating cells exhibit an increased S and G2/M phase, indicating DNA replication and protein synthesis, respectively (Cooper, 2000, White and Dalton, 2005, Roccio et al., 2013). However, the results clearly point out that osteoblastic cells generated following osteogenic differentiation of MSC in ODM exhibit a decreased potential to induce vascularization and angiogenesis *in vitro* when co-cultured with HDMEC.

4.4.2 The right way: Prevascularized co-cultures cultivated in osteogenic medium

A third sequential medium strategy was investigated and focussed on the induction of VLS formation in CCs of MSC with HDMEC prior to the induction of osteogenesis in the incorporated MSC fraction. This strategy was examined, since from the process of bone formation and bone healing *in vivo* it is known that the formation of new blood vessels along VEGF gradients is necessary to supply adequate remodeling (Gerber et al., 1999, Ortega et al., 2004) and GF signaling (Gerber et al., 1999, Maes and Carmeliet, 2008) as the basis for matrix mineralization and osteoblastic differentiation during IMO (Marsell and Einhorn, 2011, Gilbert, 2000) or ECO (Mackie et al., 2008a). To examine this, *in vitro* CCs of fresh MSC with HDMEC were prevascularized for 2wk in ECGM and subsequently transferred to ODM for 2wk or 4wk, designated as osteogenic co-cultivation (oCC) in the following sections. For the prevascularization and osteogenic stimulation the same durations as used in the previous section were initially applied (see section 4.4.1).

The oCC of prevascularized CCs resulted in a high amount of calcification of the extracellular matrix after 2wk and 4wk (Figure 25). A similar degree of osteogenesis could not be achieved in mono-cultures of MSC serving as a DC (differentiation control) (Figure 25). Furthermore, it was found that an endothelial compartment was present after oCC independent of the CC duration (Figure 25). These results demonstrate that the presence of EC actively modulates the osteogenic differentiation of MSC. The outcome is similar to results described by others (Bulnheim et al., 2014, Correia et al., 2011, Kaigler et al., 2005, Pedersen et al., 2012). Furthermore, the sequential medium strategy utilized potentially mimics the physiological situation of EC activity, which appears to be necessary to induce osteoblastic differentiation (Gerber et al., 1999, Maes and Carmeliet, 2008). This is further supported by the fact that a reduction of the initial prevascularization period from 14d to 3d continuosly resulted in matrix calcification (Figure 25; Supplementary

Figure 12). Most importantly, stable VLS formation was still achieved when the period available for prevascularization was reduced to 7d (Figure 25). Since the duration of time to implant is an important factor for *in vitro* tissue engineering strategies applied in regenerative medicine (Rouwkema et al., 2008) the period for prevascularization was reduced to 7d for the evaluation of the model system in the present study.

When the oCC was investigated in a time-dependent manner it was observed that osteogenesis in the MSC was rapidly induced, with matrix calcification detectable after 72h oCC (Figure 26). Comparable data on the dynamics of matrix calcification in CC of MSC with EC have not been previously reported, although an inductive function of EC on the osteogenic differentiation of MSC has been described (Bulnheim et al., 2014, Kaigler et al., 2005). The time-dependent evaluation of oCC clearly demonstrated that osteogenesis took place and was shown to occur at the level of extra- and intracellular protein expression. Alizarin Red and VK staining are standard methods applied to examine the deposition of calcium and calcium phosphates in matrix mineralization (Jaiswal et al., 1997, Pittenger et al., 1999, Bonewald et al., 2003), while ALP is a marker of the early stage of osteogenesis in MSC *in vitro* (Prins et al., 2014). Furthermore, this enzyme is known to be involved in the generation of P_i from βGP in the process of matrix mineralization (Khouja et al., 1990). The quantification of ALP activity in the present study showed that osteogenesis was induced during both oCC and angCC compared to DC, thus demonstrating that EC modulate osteogenesis when co-cultivated with MSC. Similar observations were described by other groups (Bulnheim et al., 2014, Kaigler et al., 2005). In addition, it appears that osteogenesis was delayed in DC since ALP activity was found to be increased initially after 5d (Figure 27). This shows the influence of EC on MSC differentiation. Further studies demonstrated that the time of co-cutivation initially applied for prevascularization influenced the osteogenic differentiation of MSC during oCC. Matrix calcification was achieved after 24h to 48h oCC when 14d of initial prevascularization were first carried out, whereas calcification was detected after 72h oCC following a 7d prevascularization period. Similar kinetics have not been described previously.

The differences in initial calcification may be due to changes in the ECM and the degree of osteogenesis that was induced by the presence of EC during co-cultivation. It is known that ECM can bind GFs like VEGF or bFGF, and that this actively influences cellular processes such as angiogenesis (Flaumenhaft and Rifkin, 1991, Schultz and Wysocki, 2009). A prolonged prevascularization incubation period could allow for enhanced binding of GFs that were either supplied exogenously in the prevascularization period (bFGF) or released from EC. For example, bone morphogenic proteins-2, 4 and 6 have been shown to be secreted by EC (Bouletreau et al., 2002, Csiszar et al., 2006, Kersten et al., 2005, Schluesener and Meyermann, 1995, Shin et al., 2004, Sorescu et al., 2004, Sorescu et al., 2003, Willette et al., 1999) and to exert an influence on the osteogenic differentiation of MSC (Friedman et al., 2006, Shin et al., 2004). The same is true for bFGF (Hagmann et al., 2013,

Hanada et al., 1997), which was also shown to support osteogenesis when co-administered with BMP-2 (Hanada et al., 1997). It is thus possible that MSC exhibited different stages of osteogenic differentiation via osteogenic priming by EC, either indirectly by GFs bound to the ECM, or directly through cell-cell contact. Nevertheless, the dynamics highlight the inductive potential of EC on the osteogenic differentiation in CCs with MSC.

Independently, oCC induced the rapid calcification of prevascularized CCs *in vitro* that contained VLS following oCC (Figure 27). These findings have not been described previously in culture conditions under 14d. Most interestingly, AB staining revealed the deposition of GAGs (Figure 27) which are known to be key matrix proteins in adult cartilage (Mankin and Lippiello, 1971) or cartilaginous intermediates during ECO (Poole et al., 1982, Suzuki et al., 1981). Moreover, the GAG-positive regions correlated with remaining endothelial islands (Figure 27), thus suggesting that the deposition of GAGs might be related to direct contact of MSC with EC. It is worthy of note that GAGs are a central component of proteoglycans and are also present in the basement membranes of tissues *in vivo* (Young et al., 1992, Kanwar and Carone, 1984). They may be locations of basal lamina of VLS and EC islands. Since a more detailed analysis of the protein composition was not performed it is still not clear if the GAG-positive regions represent basement membranes of VLS formed *in vitro* or whether they indicate regions of induced endochondral tissue formation. To clarify this, the deposition of collagen type X and the release of indian hedgehog (Ihh) would identify further key proteins involved in ECO (Wu et al., 2010, Sugita et al., 2013).

In separate studies, Saleh and colleagues demonstrated enhanced active β-catenin signaling in a spheroid 3D CC model of MSC with HUVEC (Saleh et al., 2011). Active β-catenin signaling as well as the translocation of β-catenin to the cell nucleus are key elements of the canonical WNT/β-catenin signaling pathway involved in ECO (Hartmann, 2007), indicating both the development of mature osteoblasts from mesenchymal precursors (Day et al., 2005) and their suppressed commitment to chondrogenesis (Hill et al., 2005). However, increased active β-catenin signaling was also shown to be essential in hypertrophic chondrocytes of the growth plate for the control of osteoclast activity and trabecular bone formation during ECO (Makrydima et al., 2014). Therefore, it might be speculated that the study conducted by Saleh et al. provided indirect evidence of ECO being induced in CC of MSC with HUVEC. In this study active β-catenin was detected by WB, while osteogenic differentiation of MSC induced in the CC with HUVEC was concluded from enhanced ALP fluorescence intensities and VK staining (Saleh et al., 2011). Due to the cultivation of the MSC/HUVEC spheroids in the presence of 10 nM Dex, 5 mM βGP and 50 µg/mL AA (Saleh et al., 2011) it is likely that osteogenic differentiation was stimulated in the MSC.

Nevertheless, it must be noted that enhanced ALP activity as well as mineralization detected by VK staining were also demonstrated in hypertrophic chondrocytes during ECO (Newton et al., 2005, Erl, 2005, Hill et al., 2005). The same is true for BMP signaling (Natarajan et al., 2005) also detected in spheroid CCs of MSC with HUVEC (Saleh et al., 2011). Although Col-X or Ihh were not investigated in the present study it can be speculated that ECO was induced in CCs of MSC with HDMEC during oCC. This hypothesis is supported by the BMP signaling detected during oCC, as discussed below (see section 4.4.3.2; Figure 32). Therefore, it is possible that ECO was induced during oCC, which would correlate with the AB-positive regions found to co-localize with endothelial islands (Figure 27). Similarly, AR and VK staining gave rise to comparable island-like locations of mineralization (Figure 26). Since mineralization was shown to occur in endochondral tissue formation by hypertrophic chondrocytes as they undergo apoptosis (Hill et al., 2005) this supports the hypothesis that ECO was locally induced in the course of oCC. Of major interest is the image-based quantification of AB-stains, which revealed an increasing trend during both oCC and angCC but not in the DC (Figure 27), thus indicating that changes in the matrix composition were induced upon basic co-cultivation of MSC with HDMEC in ECGM. However, the results indicated that the changes were enhanced during oCC compared to angCC, suggesting that Dex supplementation provided an additional stimulus. In relation to ECO, Cheng et al. demonstrated accelerated ECO upon Dex administration in chick embryos (Danhaive and Rousseau, 1988).

In a final experiment, an evalution was carried out to determine whether the degree of matrix calcification (or as hypothesized ECO) could be driven by an increased size of the EC fraction. The results showed that the degree of matrix calcification can be influenced by the CSD of HDMEC and by this the CSR (Figure 27), thus underlining the fact that EC-derived signaling regulates osteogenic differentiation (or as hypothesized ECO) *in vitro*. These results are unique and have not been described previously. However, since a detailed analysis of cell signaling during oCC was not performed, it is not clear whether the oCC of prevascularized CCs of MSC with HDMEC might contain endochondral tissue formation, an intermediate stage (e.g. hypertrophic stage) or represent an IMO. Nevertheless, the results presented in this section describe for the first time the rapid generation of prevascularized osteogenic CC samples within less than 14d, possibly representing endochondral tissue formation. Moreover, this model mimics *in vitro* what is observed *in vivo*, namely that EC signaling and vascularization are required in order to obtain osteogenic differentiation either via ECO or via IMO.

4.4.3 The plus: Re-establishing a pro-angiogenic environment following vessel regression

4.4.3.1 Obtaining vessel regression

The described sequential medium strategy including prevascularization of MSC/HDMEC CCs followed by oCC in ODM is based on the administration of Dex during oCC. As described previously in this study and shown by others, Dex administration reduces angiogenic differentiation in EC (Logie et al., 2010) and a reduction of VEGF expression by the MSC (see section 3.5.1; Figure 22). Therefore, it was not surprising that as Dex administration accelerated osteogenesis (or as hypothesized ECO) during oCC it also induced VR (Figure 28; Figure 29). Furthermore, in combination with βGP supplementation (10 mM) the regressing VLS accumulated calcium phosphates as indicated by TL microscopy, AR and VK staining (Figure 28). Such findings have not been previously described. In time-dependent experiments it was found that VR appeared during oCC but not angCC (Figure 29). Additionally, several staining methods revealed that VR appeared together with vessel calcification, both initially detected after 72h oCC (Figure 29). By contrast, no calcification was present during angCC.

GF quantifications of VEGF, Ang-1 and Ang-2 indicated that their expression pattern was shifted towards an anti-angiogenic setting thus supporting VR (Figure 29). As mentioned earlier in this study, low levels of VEGF linked to high levels of Ang-2, induced EC death (Lobov et al., 2002). The interplay of both GFs was also described to “be able to induce VR in other settings” (Lobov et al., 2002). Quantification by ELISA demonstrated that when lowered concentrations of VEGF were expressed higher concentrations of Ang-2 were released from MSC and HDMEC, respectively, during oCC (Figure 29). Therefore, the shifted GF environment may be responsible for the induction of VR. The involvement of Dex in this shift can be concluded from VEGF and Ang-1 levels of the DC (Figure 29), which were found to be lowered or increased, respectively, up to 7d oCC similar to the release profiles of VEGF and Ang-1 during monitoring of long-term osteogenic differentiation of MSC (Figure 22). Nevertheless, it is likely that high concentrations of Pi generated upon conversion of βGP by ALP supported VR by inducing apoptosis in EC, which was demonstrated elsewhere for Pi concentrations above 2.5 mM (Di Marco et al., 2008).

To investigate possible toxic effects of medium supplementation during oCC on EC, mono-cultures of HDMEC were cultivated in various medium settings and analyzed for morphological changes and apoptosis (Figure 30; Figure 31). The analysis of cell morphology by IF revealed that a tightening of cell-cell contacts as well as the formation of peripheral stress fibres were observed when EC were cultivated in medium containing Dex (Figure 30). Similar results were attributed to an increased barrier function in EC monolayers (Danhaive and Rousseau, 1986, Rousseau and Baxter, 1979). Addition of Dex was shown previously to increase the endothelial

barrier function by enhancing the expression of cell-cell contact proteins (Salvador et al., 2014). It is important to note that *in vivo* this effect was found specifically for EC in the blood-brain barrier (BBB), but not for myocardial EC (Higgins et al., 1979). In contrast, the effect of Dex on enhancing endothelial barrier function was shown in several *in vitro* models of the BBB containing HUVEC (Rousseau and Baxter, 1979, Rousseau et al., 1975). Therefore, the Dex-mediated increase of endothelial barrier function might not be limited, as described by Förster and colleagues. Although barrier integrity was not determined by transendothelial electrical resistance (TEER) measurements, the changes in F-actin cytoskeleton and expression pattern of CD31-positive cell-cell contacts point to an increased barrier function and monolayer integrity. This was further supported by the increased fluorescence intensities obtained after Dex supplementation of media, thus indicating enhanced protein expression (Figure 30). IF staining for F-actin demonstrated peripheral ring formation and an enhanced F-actin signal in HDMEC cultivated in the presence of Dex. The overall increased F-actin expression was confirmed by intensity measurements using flow cytometry (Figure 31). Since the results obtained by flow cytometric analysis of detached cells correlate with the intensity trend obtained by image analysis performed on attached HDMEC it can be concluded that F-actin expression was enhanced by Dex. It can also be concluded that F-actin expression is not enhanced when only βGP is given as supplement (Figure 30; Figure 31). Furthermore, the HDMEC monolayer was disrupted upon Dex deprivation from ODM (Figure 30), supporting the conclusion that Dex positively influences endothelial integrity in mono-layers of HDMEC. Under these conditions, peripheral F-actin fibers were not detectable, demonstrating that cell-cell contacts were decreasing and of irregular shape (Figure 30).

Moreover, when Dex was added the negative effects of the high level of phosphate present in the medium were clearly demonstrated. Di Marco and colleagues demonstrated that Pi could induce apoptosis in EC at concentrations above 2.5 mM (Di Marco et al., 2008). Nevertheless, similar results were not observed for organic phosphate in mono-cultures of EC, most probably because ALP able to generate Pi from βGP is not present in EC, except for those involved in the BBB (Nakazato et al., 1997) or EC from myocardial capillaries (Baxter et al., 1972). In the present study, ALP activity was neither detected by activity measurements in protein lysates nor by ALP staining on HDMEC, HUVEC or OEC (Figure 27; Figure 12; Figure 13; Figure 14). Therefore, it is likely that organic phosphate creates a similar effect as described by Di Marco et al. for P_i (Di Marco et al., 2008). This assumption is supported by the AnnexinV staining for apoptotic cells, showing that following Dex deprivation (only βGP supplemented) both the early and late apoptotic cell fraction increased leading to enhanced cell death (Figure 31). Thus, the results obtained for high levels of organic phosphate (10 mM) are in agreement with the findings of high levels of Pi (above 2.5 mM) shown to induce apoptosis in EC (Di Marco et al., 2008). In addition, it can be concluded that Dex provides an anti-apoptotic effect on HDMEC as has

been shown for EC and other cell types by other groups (Makrydima et al., 2014, Newton et al., 2002, Messmer et al., 2001). It can be speculated that supplementation of Dex not only provides a general anti-apoptotic effect but also buffers the pro-apoptotic effect from high βGP levels. This is further supported by cell number determinations in HDMEC MCs, clearly demonstrating the rate of proliferation in ODM to be comparable to and very similar to the rate obtained from supplementation of Dex alone (Figure 31). The results indicate that VR during oCC is linked to a GF environment shifted towards an anti-angiogenic milieu. Additionally, it appears that aopotosis may be mildly induced in ODM, where the main pro-apoptotic effect of βGP is buffered by the anti-apoptotic function of Dex. Nevertheless, HDMEC exhibited an increased barrier function in ODM that has been shown to result in EC quiescence (Yuan and Rigor, 2011, Natarajan et al., 2005). At the same time proliferation of HDMEC was slightly reduced but not inhibited by ODM during oCC.

4.4.3.2 Re-establishing a pro-angiogenic environment

To evaluate whether a pro-angiogenic GF signaling environment could be re-established following oCC a recovery phase consisting of a pro-angiogenic ECGM was added to the model. Various durations of oCC were applied following initial co-cultivation and examined to determine if a re-induction or maintenance of VLS and angiogenesis (Figure 32) occurs. Such dynamic studies have not been previously reported. The microscopic evaluation and the quantification of GFs involved as key regulators demonstrated that a pro-angiogenic environment is re-established when prevascularized osteogenic CCs are transferred to pro-angiogenic ECGM following oCC (Figure 32). It was found that VLS were maintained when 48h oCC samples were recovered in ECGM (Figure 33). It appears that during the recovery incubation period of 7d oCC in ECGM a re-induction of vessel formation occurs. A quantification was not possible since image-based quantification of vascular structures or the fractions of apoptotic cells were not performed. Nevertheless, the decreasing release of VEGF during oCC (Figure 32) was shown to be reversed during recovery in ECGM (Figure 33), this being independent of the duration of oCC. The re-induced VEGF secretion from MSC following Dex-mediated suppression has not been previously reported. The observations of the maintenance of VLS in 48h oCC or the re-induced vessel formation in 7d oCC samples recovered in ECGM are similar to the findings of Yano and colleagues, who showed that binding of Dex to the GR was reversible in HUVEC, thus making them responsive to VEGF-induced angiogenic changes (Yano et al., 2006). The binding of Dex to the GR was described as being generally reversible (Rousseau and Baxter, 1979, Krieger et al., 1976). Since the re-initiated VEGF secretion correlated with constitutive concentrations of Ang-2 (Figure 33) these reversible steps may be responsible for the re-induction of angiogenesis. These results are in keeping with previous studies demonstrating EC death at low VEGF concentrations together with high Ang-2 levels (Lobov et al., 2002).

This hypothesis is further supported by the observation that VLS and VEGF secretion were constantly suppressed under prl-oCC conditions (Figure 33). Most importantly, matrix calcification and potential GAG deposition (and as hypothesized ECO) were maintained during recovery of 7d oCC samples in ECGM and even induced in 48h oCC samples during the recovery incubation period (Figure 33). These data suggest that, once initiated, the osteogenic differentiation (and as hypothesized ECO) is not suppressed or inhibited by medium change and the absence of Dex. Furthermore, ECGM was supplemented with bFGF, which is known to support osteogenic differentiation in MSC (Ng et al., 2008, Montesano et al., 1986, Hanada et al., 1997). At the same time, it is known that not only Dex but also BMP-4 exhibits an osteo-inductive potential (Friedman et al., 2006). During oCC and the recovery period in ECGM BMP-4 was present at high constitutive concentrations and although not detected in the present study BMP-2 is known to be secreted by EC (Bouletreau et al., 2002, Sammons et al., 2004). This indicates a potential supportive function of bFGF by inducing a pro-osteogenic stimulus provided by BMP-4 and possibly BMP-2. Therefore, it can be speculated that the supplementation of bFGF during recovery in ECGM maintained the described differentiation-associated effects elicited by oCC.

4.5 Firm as a rock: The evaluation of prevascularized osteogenic co-cultures under varying culture conditions

To evaluate the stability of the CC model system that allows the generation of prevascularized osteogenic CC as well as the maintenance or re-induction of VLS or VLS formation, different parameters of the model including the type of co-cultivation, the incorporated cell types, and the applied cell culture media were varied.

4.5.1 Osteogenesis via direct and non-direct contact

Direct cell-cell signaling was shown to be crucially involved in capillary formation within 2D or 3D CCs of EC with pOB *in vitro* (Unger et al., 2007, Stahl et al., 2004, Wenger et al., 2004) while paracrine signaling is generally involved in cell communication *in vitro* (Kolbe et al., 2011, Paschos et al., 2015). By using a transwell system to focus on non-direct cell-cell contact it was found that osteogenic differentiation can be rapidly induced in MSC MCs that were cultivated (top chamber) in the presence of a prevascularizing CC of MSC with HDMEC (bottom chamber) (Figure 34). This effect also occurred when MSC MCs were added to the culture system at the point when oCC was initiated (Figure 34). While the same effect did not develop in other experimental groups (MSC/MSC or MSC/Blank; see Figure 34) this clearly demonstrates that paracrine signaling actively contributes to the induction of osteogenesis in MSC. The induction of osteogenesis in MSC induced by EC was observed by others using CCs of MSC with HDMEC cultivated on various 3D scaffolds (Bulnheim et al., 2014). By performing the CCs in ECGM this latter study found enhanced osteogenic markers at the level of gene expression after 48h and 7d in direct but not in indirect CCs. Apparently direct cell-cell contact is needed for EC

to induce osteogenic differentiation in MSC even in the absence of OS (Bulnheim et al., 2014). This outcome is in contrast to the findings described in the present study. Osteogenic differentiation was not obtained during angCC (see section XXX; Figure 27) but during oCC in a non-direct CC model (Figure 34), thus indicating paracrine signaling from either HDMEC or MSC most likely activated by EC.

Although, Bulnheim and colleagues did not demonstrate the relevance of gene regulation at the protein level or the calcification of an osteogenic matrix they reported an enhanced gene expression of BMP-2 (Bulnheim et al., 2014) which has been shown by others to exhibit an osteo-inductive potential (Cheng et al., 2001, Cheng et al., 2003, Kang et al., 2004) and to be released by EC (Bouletreau et al., 2002, Kersten et al., 2005, Willette et al., 1999, Schluesener and Meyermann, 1995, Shin et al., 2004, Sorescu et al., 2004, Sorescu et al., 2003,). Therefore, it is likely that BMP-2 secreted by HDMEC exhibited an osteo-inductive function on MSC even via non-direct cell-cell contact and thus contributed to the induction of matrix calcification as described in the present study (Figure 34). This conclusion is supported by the expression of BMP-4 detected during oCC and the fact that final matrix calcification was clearly lowered or absent in MSC/MSC and MSC/Blank groups, respectively (Figure 32). It is of special interest that enhanced matrix calcification in MSC was also found when the latter cells were added to the culture system up to the point at which oCC was initiated (Figure 34). Although the final degree of matrix calcification in those MSC was slightly lower compared to MSC that were added when co-cultivation with HDMEC was started, this strongly supports the hypothesis that EC-derived paracrine signaling supports osteogenic differentiation of MSC. At the same time, it can be hypothesized that this strategy could be used to accelerate the osteogenic differentiation of MSC in other bone tissue engineering strategies using CCs of MSC with HDMEC as osteo-inductive units. Nevertheless, a certain effect of non-direct induction of osteogenesis in MSC by prevascularized CCs of MSC with HDMEC has not been previously described.

4.5.2 Changing the type of endothelial cell

To determine whether other parameters could affect the generation of prevascularized osteogenic CC, changing cell types was initially examined. First, HUVEC or OEC were substituted for HDMEC and co-cultured with MSC to determine whether the effect obtained during oCC was primarily linked to microvascular HDMEC. Several reports described that EC exhibit differences in cell signaling as well as pattern of protein expression, dependent on their microvascular or macrovascular origin (Brouillet et al., 2010, Jackson and Nguyen, 1997, Lang et al., 2003). Both macrovascular HUVEC (Murthi et al., 2007) connected to embryonic development (Pansky, 1982) and non-macrovascular OEC (Jiang et al., 2007) isolated from peripheral blood precursors (Martin-Ramirez et al., 2012) are widely used to study prevascularization and angiogenesis *in vitro* (Correia et al., 2011, Logie et al., 2010, Pedersen et al., 2012, Chen et al., 2009, Verseijden et al., 2012, Thein-

Han and Xu, 2013, Dohle et al., 2014, Dohle et al., 2010, Dohle et al., 2011, Fuchs et al., 2009a, Fuchs et al., 2007, Fuchs et al., 2010, Fuchs et al., 2009b, Holnthoner et al., 2015, Li et al., 2014, Groeneveld et al., 2015). It was found that 7d CC of MSC with HUVEC or OEC resulted in the same rapid induction of osteogenic differentiation following oCC as described in CCs of MSC with HDMEC in the previous sections (Figure 34). The results did not identify any differential effect of the type of EC on the osteogenic differentiation of MSC during oCC. However, VLS formation was found to differ in the CC models (Figure 34), suggesting that the conditions identified for VLS formation in CCs of MSC with HDMEC might not be optimal for CCs of MSC with HUVEC or OEC. This points towards possible differences in cell signaling and protein expression in the different phenotypes of EC, as mentioned above. However, the results obtained from oCC upon varying the type of EC clearly demonstrate that the inductive effect of EC on the osteogenic differentiation of MSC is conserved among the ECs. This was further illustrated by the induction of osteogenesis during oCC of MSC with a transformed EC line derived from a human hemangioblast (ISO-HAS-1; (Masuzawa et al., 1999, Unger et al., 2002)).

4.5.3 Changing the type of MSC

Experiments investigating the variation of the MSC type underlined the reproducibility of EC-driven enhancement of the osteogenic differentiation of MSC. Initial differentiation assays underlined the findings for bmMSC and atMSC described by several reports (Dominici et al., 2006), but were in contrast to the tri-lineage differentiation potential of HDF described by others (Aloise et al., 2014, Junker et al., 2010). Upon co-cultivation with HDEMC for 7d followed by 7d oCC it was found that the rapid induction of osteogenesis in the MSC fraction was not limited to bmMSC (Figure 36). Both bmMSC and atMSC exhibited a comparable pattern, whereas CCs of HDF with HDMEC did not show osteogenic differentiation or matrix calcification after 7d oCC (Figure 36). It can be concluded that the cellular crosstalk in the described model leading to rapid osteogenesis during oCC is not dependent on the bone marrow origin of MSC. Since the degree of osteogenic differentiation was initially lower in atMSC compared to bmMSC (Figure 36) it can be further concluded that the induction of rapid osteogenesis during oCC with HDMEC is independent of the initial differentiation potential of MSC. Furthermore, since no VLS were detectable following 7d oCC in any of the CCs VR might be occuring as was described earlier in this study. However, a low amount of vessel formation was generally found after 7d of co-cultivation in ECGM prior to oCC (Figure 36). Therefore, it is possible that the CSDs and CSRs applied in the coculture studies were sub-optimal for CCs of atMSC or HDF with HDMEC. Altogether, these observations support the results obtained when varying EC cell type and highlight the fact that the cellular crosstalk leading to enhanced induction of osteogenesis in MSC during oCC is not limited to a certain tissue of origin but specific to MSC in general.

4.5.4 Excluding media-derived artifacts

Having found that the EC-enhanced osteogenic differentiation during oCC was not limited to a certain type of EC or MSC, cell culture medium was evaluated to determine whether this enhancement was due to components present in the medium applied during oCC. As mentioned above the supplementation of Dex decreases the responsiveness of EC to VEGF by binding to the GR in EC (Logie et al., 2010). In addition it suppresses VEGF expression in cultures of smooth muscle cells, head and neck cancer cells and hinders keloid fibroblasts *in vitro* (Nauck et al., 1998, Shim et al., 2010, Wu et al., 2006), the latter being similar to the MSC MCs during osteogenic differentiation in the present study (Figure 22). Although expressed during initial co-cultivation in ECGM (Figure 29) VEGF was suppressed during oCC (Figure 29), thus creating an anti-angiogenic microenvironment. In contrast, Dex was found to buffer the pro-apoptotic function of βGP (10 mM) by reducing the fractions of early and late stage apoptotic and dead cells (Figure 31). Since it was shown by others that P_i induces apoptosis when administered at concentrations above 2.5 mM (Di Marco et al., 2008) studies were performed to determine if matrix calcification was observed when βGP was supplemented at physiological concentrations of 1.4 mM (Staum et al., 1972, Nishizawa et al., 2005).

By conducting the oCC in various media (Table 23) it was found that matrix calcification occured at physiological phosphate concentrations (assuming 100% conversion of βGP by ALP; Figure 37), under standard oCC conditions (10 mM βGP, 100 nM Dex, 50 µM AA2P) and in a commercial osteogenic differentiation medium (Comm.ODM; Figure 37). Furthermore, the results agree with findings described above which show that ECGM supplemented with OS is insufficient to induce osteogenic differentiation or matrix calcification in CCs of MSC with HDMEC (see section XXX; Figure 18; Figure 19; Figure 20; Figure 21). Of special interest are the data obtained with various media, showing a clear effect of βGP on the maintenance of VLS. Since VR occurred with standard oCC conditions and when ECGM was supplemented with OS (Figure 37) the existing VLS were maintained at physiological P_i concentrations or βGP deprivation (Figure 37). This supports the pro-apoptotic effect of βGP on HDMEC in the CC system, as concluded from apoptotic cell fractions in HDMEC MCs exposed to high levels of βGP (Figure 31). These results are similar to findings of Langenbach and colleagues, who described that βGP exhibits a pro-apoptotic function at high doses (e.g. 10 mM; (Langenbach and Handschel, 2013). It must be noted that VR might be still ongoing due to Dex administration, but was possibly delayed upon βGP deprivation, thus leading to maintained VLS after 7d oCC in the corresponding experimental groups (Figure 37). This is supported by ELISA measurements which demonstrate a low VEGF level linked to high Ang-2 levels when Dex is present in the medium (Figure 37). Moreover, the VEGF levels were approximately doubled when βGP was lowered from 10 mM to 1.4 mM or absent in ODM thus possibly causing a delay of VR in the corresponding groups. Nevertheless, the data obtained by the various media

correlate with findings demonstrated in the previous sections which underline the reproducibility of the described medium strategy, including oCC to permit the generation of prevascularized osteogenic CC within 14d.

5 Conclusions

The goal of the present study was to develop and optimize culture conditions using a perfusion-based strategy to rapidly generate a prevascularized osteogenic tissue-like sample to be used for implantation in bone-tissue regeneration applications. For this, cell culture parameters such as the MSC CSD or the cell culture medium were optimized to achieve the optimal environment for osteogenic differentiation of MSC initially. The experiments clearly identified αMEM-GM and a CSD of 20,000 MSC/cm^2 to give the best results. Both parameters were applied to the evaluation of osteogenesis in MSC on 3D scaffolds.

As a 3D scaffold material to study the osteogenic differentiation of hMSC under comparative static and dynamic conditions in a perfusion bioreactor tNiTi as produced according to Gotman and colleagues was used (Gotman, 2010). The results described in the present study demonstrated that osteogenic differentiation of hMSC takes place on tNiTi scaffolds, thus providing a possibility to generate cell-loaded tNiTi constructs for bone tissue engineering (BTE) applications. Furthermore, the use of medium perfusion represents a powerful tool to optimize the cellular environment of the hMSC needed for an adequate osteogenic differentiation process, as medium perfusion through tNiTi scaffolds enhanced the distribution of extracellular matrix and differentiating cells and also increased the degree of mineralization. In addition, it appeared that medium perfusion could act as a mechanical stimulus in a synergistic manner with biological inducers of osteogenesis, such as dexamethasone (Dex). In contrast, the results described in the present study revealed that medium perfusion as a sole mechanical stimulus was not sufficient to induce osteogenesis in human MSC in the absence of Dex. *Summa summarum*, the cultivation of cell-loaded tNiTi scaffolds in a perfusion bioreactor positively influenced the differentiation of hMSC and therefore favors tNiTi as a promising biomaterial for BTE applications.

Based on these conclusions and optimized parameters a co-culture system of MSC with HDMEC was developed. In order to optimaly use the limited primary cell material as well as the influence of multi-dimensional flow fields or gradients on the cellular crosstalk the co-culture system was initially established in 2D. Having optimized the CSD of MSC MCs targeting osteogenesis it was investigated first if the MSC CSD could be transferred into co-cultures of MSC with HDMEC to allow for vascularization and angiogenesis parallel to osteogenesis. The initially performed experiments targeting a strategy to simultaneously stimulate both cellular processes found that osteogenesis and angiogenesis are individually but not simultaneously inducible in the initial co-culture model system evaluated. This outcome was confirmed by statistical analyses of single factor ANOVA as well as analyses of factor interactions clearly pointing towards strong interactions between osteogenic supplements (OS) and heparin+bFGF (pro-angiogenic supplements, HF), either targeting osteogenesis in MSC (OS) or vascularization and angiogenesis from EC (HF) seemingly counteracting each other in a repressive manner. A similar effect in a comparable

context has not been described before in the literature. Thus, the results highlight the need for a careful optimization process for the development of an adequate cell culture model. Independently, further studies are needed to investigate prolonged experimental periods addressing for instance the question of whether osteogenesis is induced at later culture stages or is generally suppressed in a pro-angiogenic environment as described. Similarly, the experiments should be repeated using other pro-angiogenic media either customized or commercially available, such as EGM2. However, the results presented here underline the necessity for the development of sequential medium strategies that aim to stimulate osteogenesis and angiogenesis separately.

In this context, a sequential medium strategy was developed in the present study. By doing so, the stimulation of osteogenesis in MSC after priming in ODM and their subsequent co-cultivation with HDMEC in a pro-angiogenic stimulating medium was investigated first. The results demonstrated in the present study clearly indicate that osteoblastic cells generated by osteogenic differentiation of MSC exhibit a decreased potential to induce vascularization *in vitro* when co-cultured with HDMEC. To a lesser extent, prevascularization is slightly reduced when MSC were pre-cultivated for long-term periods (e.g. 4wk) in regular basal medium (BM) prior to their co-cultivation with HDMEC, thus indicating that MSC should generally not exceed a certain time period of growth prior to their co-cultivation with HDMEC. As data on growth factor (GF) secretion or cell cycle analysis are missing from the phase of co-cultivation the regulatory mechanisms cannot be described in detail. By varying the co-culture set-up, it was found that the observed effect was independent of any extracellular matrix generated during osteogenic priming or regular pre-cultivation. Moreover, the observed effect was independent of the cell seeding density of the respective osteogenically primed MSC or pre-cultivated MSC at the point of initiation of the co-cultures. Nevertheless, the effect was highly reproducible, thus providing further evidence that fresh MSC, long-term cultivated MSC or osteoblasts derived from long-term differentiation of MSC are all active enhancers of the prevascularization process *in vitro*. Although these findings are in contrast to other *in vitro* reports (Ma et al., 2011) they are in agreement with data obtained during *in vivo* studies, demonstrating that final osteoblast differentiation is chronologically subsequent to vascularization and angiogenesis during fracture healing (Gerstenfeld et al., 2003b, Maes and Carmeliet, 2008, Marsell and Einhorn, 2011). Nevertheless, control experiments addressing senescence in the mono-cultures of during osteogenic priming or pre-cultivation should be realized to obtain further insight into possible regulatory mechanisms that might explain the differential behavior of MSC in the following co-cultures with HDMEC. Furthermore, recombinant VEGF administration should be applied in repeated co-culture experiments to evaluate the hypothesis that Dex-mediated decreased VEGF secretion next to cellular senescence is a main factor in determining the differences in vessel-like structure formation as described.

Since vessel-like structure formation was found to be decreased when osteogenically primed MSC were co-cultivated with HDMEC an alternative approach was investigated with the aim of first stimulating prevascularization in co-cultures, followed by the induction of osteogenic differentiation in the MSC fraction. The data generated in the present study describe for the first time the rapid formation of prevascularized osteogenic co-cultures within less than 14d and possibly containing endochondral tissue. Moreover, the model mimics *in vitro* what is observed *in vivo*, namely endothelial cell signaling and vascularization are pre-requisites to obtain osteogenic differentiation of MSC either via endochrondral or intramembraneous ossification. Furthermore, the results indicate that a sequential medium strategy is optimal when applied in a bone tissue engineering context to address the generation of VLS and osteogenesis in MSC within a common sample. However, future studies should address the transcriptome and proteome of the CC system. Although osteogenic differentiation was demonstrated by increased ALP activity and the formation of a mineralized matrix the activation of key transcription factors, such as RUNX2 or osterix as specific for the induction of osteogenesis, was not investigated. In addition, proteins involved in the progress of ECO, including Col-X or secreted Ihh, should be evaluated to underline the presence of ECO via AB staining.

The present study found that oCC of prevascularized MSC/HDMEC CCs is characterized by a time-dependent osteogenic differentiation possibly linked to ECO on the one hand, but exhibited a reverse correlation with the appearance of VR on the other hand. The time-dependent investigation of prevascularization and osteogenesis as described identified a time-window of 7d CC + 48h oCC to obtain and maintain VLS in the CCs. At the same time this time-window theoretically allows for the evaluation of the described sequential medium strategy *in vivo*. It can be assumed that the application of 48h oCC following 7d prevascularization on 3D scaffolds would allow for the transplantation of prevascularized osteogenic tissue constructs containing intact VLS. In addition, the results show that the *in vitro* model is limited in its functionality, as VR occurs following paracrine signaling, with the generation of an anti-angiogenic system in the course of oCC.

Thus, the development of an alternative to circumvent the manifestation of VR during the presented sequential medium strategy was another aim of the present study. The results presented here described for the first time that a repetitive sequential stimulation of vascularization and osteogenesis allows for the fine-tuning of the vascular system while maintaining an osteogenic cell fraction and osteogenic matrix even derived from short-term stimulation (48h oCC). Altough mechanistically undefined, the studies demonstrate that VR obtained during oCC can be reversed by a following phase of recovery in pro-angiogenic medium to target pro-angiogenic GF release while maintaining an osteogenic cell fraction. Serially applied in several cycles, this approach could enable the generation of more mature BTE samples which contain a complex vascular bed. However, it is necessary to identify the regulatory mechanisms leading to the induction of VR to possibly suppress this

phenomenon, for example, by blocking agents supplemented to the medium either during oCC or during recovery. Independently, the approach highlights the time-effective character of the developed sequential medium strategy for the generation of prevascularized osteogenic CC samples and the maintenance of their vascular system within a time frame of 2 to 3wk. Additionally, the robustness of this strategy was underlined by the variation of the system's individual components. By varying the type of MSC and the type of EC it can be concluded that neither the initial prevascularization nor the osteogenic differentiation or matrix mineralization during oCC is linked to a specific type of MSC or EC. Moreover, the inducibilty of osteogenesis in MSC during oCC by either HDMEC, HUVEC, OEC or ISO-HAS-1 points towards a mechanism that is conserved among EC in general and not linked to a microvascular, macrovascular or oncogenic cell character. Following variation of βGP concentrations during oCC it can also be concluded that the mineralization of the extracellular matrix does not represent an artifact induced by high levels of βGP, as discussed. Since matrix mineralization was present at physiological P_i , the sequential medium strategy as reported here might serve as a powerful basis for the evaluation of prevascularized osteogenic CC samples *in vivo*. For this, future studies need to transfer the 2D CC system onto 3D scaffolds.

As identified by the present study 3D tNiTi represents a promising candidate material for BTE applications and is thus an attractive material for the evaluation of the sequential medium strategy in 3D. By applying the optimized parameters like CSDs and CSRs the CC system should be evaluated for its initial scale-up under static conditions and investigated in an *in vivo* set-up according to Unger et al. (Unger et al., 2010). The static evaluation should be followed by its evaluation under dynamic conditions in a perfusion bioreactor. At this point future studies need to investigate the influence of shear stress and medium perfusion on the formation and maintenance of VLS. Although osteogenesis in MSC is supported by medium perfusion, the question remains whether prevascularization is also maintained. Since NiTi is a metal alloy µCT represents the tool of choice to determine the overall surface of 3D tNiTi scaffolds. Furthermore, computational fluid dynamics can be applied based on the µCT data to simulate the composition and distribution of flow fields, thus providing detailed information about the expected shear stress, flow velocities and local pressures throughout the scaffold body.

6 Summary

The development of a successful strategy for the generation of bone tissue engineering constructs *in vitro* is highly dependent on the integration of a complex vascular system. For this purpose, co-cultures (CC) of stromal cells with endothelial cells (EC) have been developed and evaluated in order to stimulate the formation of vessel-like structures (VLS) *ex vivo*. In this context, the time for *in vitro* processing aiming at tissue formation has to be optimized according to the overall time span and maximum therapeutic outcome of the chosen strategy. Furthermore, the application of state-of-the-art technologies such as perfusion bioreactors can additionally support the cells within a generated construct. Therefore, the present study aimed at developing a cultivation strategy that permits the generation of prevascularized osteogenic CC samples *in vitro*.

An initial evaluation of osteogenesis in mesenchymal stem cell mono-cultures (MSC MC) found a cell seeding density (CSD) of 20,000 MSC/cm^2 to result in the highest degree of osteogenic differentiation. When evaluating osteogenesis in MSC MCs on 3D trabecular nickel-titanium alloy (tNiTi) scaffolds in a perfusion bioreactor it was found that medium perfusion supports the osteogenic differentiation of MSC. In contrast, medium perfusion as sole stimulus was not sufficient to induce osteogenesis in human MSC. These results represent a starting point for the evaluation of a CC system of MSC with EC under comparable dynamic conditions. However, primary EC are limited in their angiogenic activity and total available numbers upon expansion *in vitro*. Therefore, strategies focusing on the stimulation of osteogenesis and VLS formation in a common CC system were initially performed in 2D. This should allow for an initial screening, the adequate optimization and evaluation of individual factors of the culture system, as well as the determination of their respective impact. The initial evaluation of the cell seeding ration (CSR) in CC of MSC with human dermal microvascular EC (HDMEC) demonstrated a remarkable effect on the formation of VLS. VLS formation was found to reach a maximum when a CSR of 3:2 (MSC:HDMEC) was combined with a MSC CSD of 20,000 MSC/cm^2. Interestingly, this CSD also resulted in maximum osteogenesis in MSC MCs.

The following screening studies aimed at examining the combination of pro-osteogenic and pro-angiogenic factors in order to simultaneously stimulate osteogenesis and VLS formation in the CC system. The results clearly indicated that osteogenic supplements (OS) suppress VLS formation while pro-angiogenic supplements (HF, heparin+bFGF) suppress osteogenic differentiation by the incorporated MSC fraction. The interaction between OS and HF indicated that a sequential strategy involving separate stimulation of osteogenesis in MSC and the formation of VLS might be superior to a simultaneous stimulation strategy. For this purpose, two sequential strategies were evaluated. In a first strategy MSC MCs were primed in osteogenic differentiation medium (ODM) to induce osteogenic differentiation and subsequently evaluated for their capacity to induce VLS formation

in a CC with EC. The results clearly demonstrated that osteogenic priming of MSC in ODM reduced their potential to induce the formation of VLS in CC with EC, most likely due to the dexamethasone (Dex)-mediated reduction of VEGF expression by the MSC. The observed effects were found to be independent of the initial number of MSC present in the CC or of osteogenic matrix that was formed during the osteogenic priming process. However, since VEGF expression is required for the induction of VLS formation *in vitro* a second sequential cultivation strategy focused on the induction of VLS formation before osteogenesis by the incorporated MSC fraction was stimulated. This approach reliably resulted in the generation of CC samples that contained pre-formed vascular networks embedded within an osteogenic matrix. Analysis of other factors produced in the model indicated that inhibition effects on the VLS formation were found upon exogeneous phosphorus supplementation and that this could be reversed by re-switching the CC to a pro-angiogenic medium. At the same time, the formation of osteogenic matrix could be maintained. Furthermore, the results showed that the observed rapid osteogenic differentiation of MSC within prevascularized CC is dependent on the presence of but independent of the type of EC. Similarly, the rapid osteogenic induction could be obtained when exchanging bone marrow-derived MSC (bmMSC) with adipose tissue-derived MSC (atMSC). Nevertheless, by varying the type of ODM it could be demonstrated that the outcome of the second sequential cultivation strategy does not represent an artifact induced as a response to a specific differentiation medium.

Altogether, the present study established a reproducible strategy for the generation of a prevascularized CC containing an osteogenic matrix within a well-defined time frame of less than 14d. At the same time, the evaluation of the opposite sequential strategy or the simulateous stimulation strategy revealed reducing or inhibitory effects of medium components on either vascularization and angiogenesis or osteogenesis. Together with the findings of enhanced osteogenesis in MSC MCs on 3D scaffolds by medium perfusion the present study defined conditions applicable for the transfer of the promising sequential cultivation strategy into a 3D dynamic environment.

7 Zusammenfassung

Die Entwicklung einer erfolgreichen Strategie zur Erzeugung von Konstrukten für das Tissue Engineering von Knochengewebe *in vitro* ist stark abhängig von der Integration eines komplexen Gefäßsystems. Zu diesem Zweck wurden Co-Kulturen von Stromazellen mit Endothelzellen etabliert und evaluiert, mit dem Ziel, die Bildung von VLS *ex vivo* zu stimulieren. In diesem Zusammenhang ist die Zeit für die *in vitro*-Bearbeitung, mit dem Ziel der Gewebebildung, hinsichtlich der Gesamtzeitspanne und maximalem therapeutischen Ergebnis der jeweiligen Strategie zu optimieren. Zusätzlich kann die Anwendung von state-of-the-art-Technologien wie Perfusionsbioreaktoren die Zellen innerhalb eines erzeugten Konstrukts unterstützen. Ziel der vorliegenden Studie war die Entwicklung einer Kultivierungsstrategie, welche die Erzeugung von prevaskularisierten und osteogen differenzierten Co-Kulturproben *in vitro* ermöglicht.

Eine erste Untersuchung der Osteogenese in MSC Mono-Kulturen identifizierte den höchsten Grad der osteogenen Differenzierung bei Verwendung einer CSD von 20.000 MSC/cm^2 Eine Evaluierung der Osteogenese in MSC Mono-Kulturen auf 3D tNiTi Scaffolds in einem Perfusionsbioreaktor bewies, daß Mediumperfusion die osteogene Differenzierung von MSC unterstützt. Im Gegensatz dazu war die Mediumperfusion als alleiniger Stimulus nicht ausreichend, um die Osteogenese in menschlichen MSC zu induzieren. Diese Ergebnisse repräsentieren einen Ausgangspunkt für die Bewertung eines Co-Kultursystems von MSC mit Endothelzellen unter vergleichbaren dynamischen Bedingungen. Jedoch sind primäre Endothelzellen in ihrer angiogenen Aktivität und verfügbaren totalen Zellzahl durch die Expansion *in vitro* begrenzt. Um einzelne Einflussfaktoren adäquat bewerten und optimieren sowie Ihre jeweiligen Auswirkungen bestimmen zu können, wurden aus diesem Grund die Strategien, die sich auf die Stimulation der Osteogenese und Gefäßbildung in einem gemeinsamen Co-Kultursystem konzentierten, anfänglich in 2D durchgeführt. So ergab ein erste Untersuchung zum Einfluss des MSC:HDMEC CSR einen deutlichen Einfluss auf die Bildung von VLS. Eine maximale VLS Bildung resultierte aus der Anwendung eines CSR von 3: 2 (MSC:HDMEC) verbunden mit einer anfänglichen MSC CSD von 20.000 MSC/cm^2. Die gleiche MSC CSD ergab auch eine maximale Induktion der Osteogenesis in MSC Mono-Kulturen.

Eine aufbauende Screening-Studie hatte im Folgenden das Ziel, die Kombination von pro-osteogenen (OS) und pro-angiogenen Faktoren (HF) in einem Zellkulturmedium zu untersuchen. Das Ziel bestand in der gleichzeitigen Stimulation der Osteogenese in MSC und der Bildung von VLS im Co-Kultursystem. Die Ergebnisse zeigten deutlich, dass die Zugabe von OS die VLS Bildung unterdrückte, während die Supplementierung von HF die osteogene Differenzierung der MSC-Fraktion verhinderte. Die Wechselwirkung zwischen OS und HF deutete zudem darauf hin, dass eine sequenzielle Mediumstrategie zur separaten Stimulation der Osteogenese

in MSC und der Bildung von VLS möglicherweise vorteilhafter ist. Hierzu wurden zwei aufeinanderfolgende Strategien untersucht. In einer ersten Strategie wurden MSC Mono-Kulturen zur Stimulation der osteogenen Differenzierung in ODM vorkultiviert und anschließend hinsichtlich ihrer Fähigkeit zur Stimulation der VLS-Bildung in einer Co-Kultur mit Endothelzellen evaluiert. Die Ergebnisse zeigten deutlich, dass die osteogene Vorstimulation von MSC in ODM deren Potential zur Stimulation der VLS Bildung in einer Co-Kultur mit Endothelzellen reduziert. Dieser Effekt kann möglicherweise auf eine Dex-vermittelte Reduktion der VEGF-Expression seitens der MSC zurückgeführt werden. Die Resultate waren in diesem Zusammenhang unabhängig sowohl von der initialen Anzahl der MSC in der Co-Kultur als auch von osteogener Matrix, die während der osteogenen Vorstimulation der MSC in ODM gebildet wurde. Da die Expression von VEGF jedoch für die Induktion der VLS-Bildung *in vitro* essentiell ist, zielte eine alternative zweite sequentielle Kultivierungsstrategie darauf ab, zuerst die Bildung von VLS in der Co-Kultur zu stimulieren und anschließend die osteogene Differenzierung der beinhalteten MSC-Fraktion zu induzieren. Dieser Ansatz ermöglichte die reproduzierbare Generierung von Co-Kulturen, die vorgeformte Gefäßnetzwerke eingebettet in einer osteogenen Matrix enthalten. Eine Analyse weiterer Einflussfaktoren im Modell ergab, dass eine hemmende Wirkung durch exogen supplementiertes Phosphat auf die VLS-Bildung durch eine wiederholte Umstellung der Co-Kultur auf ein pro-angiogenes Medium umgekehrt werden konnte. Gleichzeitig konnte die Ausbildung einer osteogenen Matrix aufrechterhalten werden. Darüber hinaus zeigten die Ergebnisse, dass die beobachtete rasche osteogene Differenzierung der MSC innerhalb der prevaskularisierten Co-Kultur abhängig von der Anwesenheit, jedoch unabhängig von der Art der verwendeten Endothelzellen ist. Des Weiteren konnte die schnelle Induktion der Osteogenese neben bmMSC auch in atMSC erzielt werden.Zusätzlich konnte durch Variation der Zusammensetzung des ODM gezeigt werden, dass das reproduzierbare Ergebnis der zweiten sequentiellen Kultivierungsstrategie kein Artefakt als Antwort auf ein spezifisches Differenzierungsmedium repräsentiert.

Zusammengefasst hat die vorliegende Studie eine reproduzierbare Kultivierungsstrategie etabliert, mit der in weniger als 14d Co-Kulturproben generiert werden können, welche vorgeformte Gefäßstrukturen eingebettet in eine osteogene Matrix enthalten. Zugleich wies die Auswertung der gegenübergestellten ersten sequentiellen Kultivierungsstrategie oder der simultanen Stimulationsstrategie eine reduzierende oder hemmende Wirkung einzelner Mediumkomponenten sowohl auf die Vaskularisierung und Angiogenese als auch auf die Osteogenese in MSC nach. Zusammen mit den Ergebnissen der verstärkten Osteogenese in MSC Mono-Kulturen auf 3D-Scaffolds durch Mediumperfusion hat die vorliegende Studie klare Rahmenbedingungen für die Maßstabsübertragung einer vielversprechenden sequentiellen Kultivierungsstrategie in eine dynamische 3D-Umgebung definiert.

8 List of figures

9 List of tables

10 Publications and scientific presentation

1. Zhang Y, **Böse T**, Unger RE, Jansen JA, Kirkpatrick CJ, van den Beucken JJJP. Macrophage type modulates osteogenic differentiation of adipose tissue MSCs. *Cell Tissue Res*. 2017. doi:10.1007/s00441-017-2598-8.

2. **Böse T**, Unger RE, Götz H, Gotman I, Gutmanas EY, Tsaryk R, Kirkpatrick CJ. Enhanced mesenchymal stem cell differentiation on load-bearing trabecular nitinol scaffolds by medium perfusion. *Advanced Biomaterials and Devices in Medicine*. 2015;(2):95-109. http://abiodem.com/article.php?id=105.

3. Grützner V, Unger RE, Baier G, Choritz L, Freese C, **Böse T**, Landfester K, Kirkpatrick CJ. Enzyme-responsive nanocomposites for wound infection prophylaxis in burn management: in vitro evaluation of their compatibility with healing processes. *Int J Nanomedicine*. 2015;10:4111-4124. doi:10.2147/IJN.S81263.

4. Dohle E, Bischoff I, **Böse T**, Marsano A, Banfi A, Unger RE, Kirkpatrick CJ. Macrophage-mediated angiogenic activation of outgrowth endothelial cells in co-culture with primary osteoblasts. *eCM*. 2014;27:149-165. doi:10.22203/eCM.v027a12.

5. Li M, Fuchs S, **Böse T**, Schmidt H, Hofmann A, Tonak M, Unger RE, Kirkpatrick CJ. Mild Heat Stress Enhances Angiogenesis in a Co-culture System Consisting of Primary Human Osteoblasts and Outgrowth Endothelial Cells. *Tissue Eng Part C Methods*. 2014;20(4):328-339. doi:10.1089/ten.tec.2013.0087.

Böse T, Unger RE, Götz H, Gotman I, Gutmanas EY, Tsaryk R, Kirkpatrick CJ. Evaluation of the osteogenic differentiation of human mesenchymal stem cells in response to trabecular NiTiNOL scaffolds - progress report.
Poster presentation. 25th European Conference on Biomaterials ESB.
2013 September 8-12. Madrid, Spain

Böse T, Unger RE, Götz H, Gotman I, Gutmanas EY, Tsaryk R, Kirkpatrick CJ. Evaluation of the osteogenic differentiation of human mesenchymal stem cells in response to trabecular NiTiNOL scaffolds.
Oral presentation. 9th World Biomaterials Congress WBC.
2012 June 1 – 5, Chengdu, China

11 References

ACHILLE, V., MANTELLI, M., ARRIGO, G., NOVARA, F., AVANZINI, M. A., BERNARDO, M. E., ZUFFARDI, O., BAROSI, G., ZECCA, M. & MACCARIO, R. 2011. Cell-cycle phases and genetic profile of bone marrow-derived mesenchymal stromal cells expanded in vitro from healthy donors. *Journal of Cellular Biochemistry,* 112**,** 1817-21.

AHLERS, J. 1975. The mechanism of hydrolysis of beta-glycerophosphate by kidney alkaline phosphatase. *Biochem J,* 149**,** 535-46.

ALBELDA, S. M., MULLER, W. A., BUCK, C. A. & NEWMAN, P. J. 1991. Molecular and cellular properties of PECAM-1 (endoCAM/CD31): a novel vascular cell-cell adhesion molecule. *Journal of Cell Biology,* 114**,** 1059-68.

ALOISE, A. C., PEREIRA, M. D., DUAILIBI, S. E., GRAGNANI, A. & FERREIRA, L. M. 2014. TGF-beta1 on induced osteogenic differentiation of human dermal fibroblast. *Acta Cir Bras,* 29 Suppl 1**,** 1-6.

ALVAREZ-BARRETO, J. F., LANDY, B., VANGORDON, S., PLACE, L., DEANGELIS, P. L. & SIKAVITSAS, V. I. 2011. Enhanced osteoblastic differentiation of mesenchymal stem cells seeded in RGD-functionalized PLLA scaffolds and cultured in a flow perfusion bioreactor. *J Tissue Eng Regen Med,* 5**,** 464-75.

ARAKI, S., SHIMADA, Y., KAJI, K. & HAYASHI, H. 1990. Apoptosis of vascular endothelial cells by fibroblast growth factor deprivation. *Biochem Biophys Res Commun,* 168**,** 1194-200.

ASAHARA, T., CHEN, D., TAKAHASHI, T., FUJIKAWA, K., KEARNEY, M., MAGNER, M., YANCOPOULOS, G. D. & ISNER, J. M. 1998. Tie2 receptor ligands, angiopoietin-1 and angiopoietin-2, modulate VEGF-induced postnatal neovascularization. *Circ Res,* 83**,** 233-40.

AUBIN, J. E. 2001. Regulation of osteoblast formation and function. *Rev Endocr Metab Disord,* 2**,** 81-94.

AYATOLLAHI, M., SALMANI, M. K., GERAMIZADEH, B., TABEI, S. Z., SOLEIMANI, M. & SANATI, M. H. 2012. Conditions to improve expansion of human mesenchymal stem cells based on rat samples. *World J Stem Cells,* 4**,** 1-8.

BABA, K., YAMAZAKI, Y., TAKEDA, A. & UCHINUMA, E. 2014. Bone Regeneration Using Wharton's Jelly Mesenchymal Stem Cells. *In:* ATALA, A. & MURPHY, V. S. (eds.) *Perinatal Stem Cells.* New York, NY: Springer New York.

BABARINA, A. V., MOLLERS, U., BITTNER, K., VISCHER, P. & BRUCKNER, P. 2001. Role of the subchondral vascular system in endochondral ossification: endothelial cell-derived proteinases derepress late cartilage differentiation in vitro. *Matrix Biology,* 20**,** 205-13.

BAHRAMSOLTANI, M., SLOSAREK, I., DE SPIEGELAERE, W. & PLENDL, J. 2014. Angiogenesis and Collagen Type IV Expression in Different Endothelial Cell Culture Systems. *Anatomia Histologia Embryologia,* 43**,** 103-115.

BAILLY-MAITRE, B., DE SOUSA, G., BOULUKOS, K., GUGENHEIM, J. & RAHMANI, R. 2001. Dexamethasone inhibits spontaneous apoptosis in primary cultures of human and rat hepatocytes via Bcl-2 and Bcl-xL induction. *Cell Death Differ,* 8**,** 279-88.

BANCROFT, G. N., SIKAVITSAS, V. I. & MIKOS, A. G. 2003. Design of a flow perfusion bioreactor system for bone tissue-engineering applications. *Tissue Engineering,* 9**,** 549-554.

BANFI, A., MURAGLIA, A., DOZIN, B., MASTROGIACOMO, M., CANCEDDA, R. & QUARTO, R. 2000. Proliferation kinetics and differentiation potential of ex vivo expanded human bone marrow stromal cells: Implications for their use in cell therapy. *Exp Hematol,* 28**,** 707-15.

BARDIN, N., ANFOSSO, F., MASSE, J. M., CRAMER, E., SABATIER, F., LE BIVIC, A., SAMPOL, J. & DIGNAT-GEORGE, F. 2001. Identification of CD146 as a component of the endothelial junction involved in the control of cell-cell cohesion. *Blood,* 98**,** 3677-3684.

BASTIAN, O., PILLAY, J., ALBLAS, J., LEENEN, L., KOENDERMAN, L. & BLOKHUIS, T. 2011. Systemic inflammation and fracture healing. *J Leukoc Biol,* 89**,** 669-73.

BATSALI, A. K., KASTRINAKI, M. C., PAPADAKI, H. A. & PONTIKOGLOU, C. 2013. Mesenchymal stem cells derived from Wharton's Jelly of the umbilical cord: biological properties and emerging clinical applications. *Curr Stem Cell Res Ther,* 8**,** 144-55.

BATTULA, V. L., BAREISS, P. M., TREML, S., CONRAD, S., ALBERT, I., HOJAK, S., ABELE, H., SCHEWE, B., JUST, L., SKUTELLA, T. & BUHRING, H. J. 2007. Human placenta and bone marrow derived MSC cultured in serum-free, b-FGF-containing medium express cell surface frizzled-9 and SSEA-4 and give rise to multilinelage differentiation. *Differentiation,* 75**,** 279-291.

BAXTER, J. D., ROUSSEAU, G. G., BENSON, M. C., GARCEA, R. L., ITO, J. & TOMKINS, G. M. 1972. Role of DNA and specific cytoplasmic receptors in glucocorticoid action. *Proc Natl Acad Sci U S A,* 69**,** 1892-6.

BECK, G. R., ZERLER, B. & MORAN, E. 2000. Phosphate is a specific signal for induction of osteopontin gene expression. *Proceedings of the National Academy of Sciences of the United States of America,* 97**,** 8352-8357.

BEEDERMAN MAUREEN, J. D. L., GUOXIN NAN, JINHUA WANG, XING LIU, LIANGJUN YIN, RUIDONG LI, WEI SHUI, HONGYU ZHANG, STEPHANIE H. KIM, WENWEN ZHANG, JIYE ZHANG, YUHAN KONG, SAHITYA DENDULURI, MARY ROSE ROGERS, ABDULLAH PRATT, REX C. HAYDON, HUE H. LUU, JOVITO ANGELES, LEWIS L. SHI, TONG-CHUAN HE 2013. BMP signaling in mesenchymal stem cell differentiation and bone formation. *Journal of biomedical science and engineering,* 6**,** 32-52.

BELLOWS, C. G., AUBIN, J. E. & HEERSCHE, J. N. 1991. Initiation and progression of mineralization of bone nodules formed in vitro: the role of alkaline phosphatase and organic phosphate. *Bone Miner,* 14**,** 27-40.

BELLOWS, C. G., HEERSCHE, J. N. & AUBIN, J. E. 1992. Inorganic phosphate added exogenously or released from beta-glycerophosphate initiates mineralization of osteoid nodules in vitro. *Bone Miner,* 17**,** 15-29.

BERGERS, G. & BENJAMIN, L. E. 2003. Tumorigenesis and the angiogenic switch. *Nat Rev Cancer,* 3**,** 401-10.

BERGERS, G. & SONG, S. 2005. The role of pericytes in blood-vessel formation and maintenance. *Neuro Oncol,* 7**,** 452-64.

BIANCO, P., CAO, X., FRENETTE, P. S., MAO, J. J., ROBEY, P. G., SIMMONS, P. J. & WANG, C.-Y. 2013. The meaning, the sense and the significance: translating the science of mesenchymal stem cells into medicine. *Nat Med,* 19**,** 35-42.

BIANCO, P., KUZNETSOV, S. A., RIMINUCCI, M. & GEHRON ROBEY, P. 2006. Postnatal skeletal stem cells. *Methods Enzymol,* 419**,** 117-48.

BIANCO, P., ROBEY, P. G. & SIMMONS, P. J. 2008. Mesenchymal stem cells: revisiting history, concepts, and assays. *Cell Stem Cell,* 2**,** 313-9.

BITTNER, K., VISCHER, P., BARTHOLMES, P. & BRUCKNER, P. 1998. Role of the subchondral vascular system in endochondral ossification: endothelial cells specifically derepress late differentiation in resting chondrocytes in vitro. *Exp Cell Res,* 238**,** 491-7.

BJERRE, L., BUNGER, C., BAATRUP, A., KASSEM, M. & MYGIND, T. 2011. Flow perfusion culture of human mesenchymal stem cells on coralline hydroxyapatite scaffolds with various pore sizes. *Journal of Biomedical Materials Research Part A,* 97A**,** 251-263.

BOGDANOVIC, E., NGUYEN, V. P. & DUMONT, D. J. 2006. Activation of Tie2 by angiopoietin-1 and angiopoietin-2 results in their release and receptor internalization. *J Cell Sci,* 119**,** 3551-60.

BOMMER, J., ALEXIOU, C., MULLER-BUHL, U., EIFERT, J. & RITZ, E. 1987. Recombinant human erythropoietin therapy in haemodialysis patients--dose determination and clinical experience. *Nephrol Dial Transplant,* 2**,** 238-42.

BONEWALD, L. F., HARRIS, S. E., ROSSER, J., DALLAS, M. R., DALLAS, S. L., CAMACHO, N. P., BOYAN, B. & BOSKEY, A. 2003. von Kossa staining alone is not sufficient to confirm that mineralization in vitro represents bone formation. *Calcif Tissue Int,* 72**,** 537-47.

BOSE, S., ROY, M. & BANDYOPADHYAY, A. 2012. Recent advances in bone tissue engineering scaffolds. *Trends Biotechnol,* 30**,** 546-54.

BOULETREAU, P. J., WARREN, S. M., SPECTOR, J. A., PELED, Z. M., GERRETS, R. P., GREENWALD, J. A. & LONGAKER, M. T. 2002. Hypoxia and VEGF up-regulate BMP-2 mRNA and protein expression in microvascular endothelial cells: implications for fracture healing. *Plast Reconstr Surg,* 109**,** 2384-97.

BREITBART, A. S., GRANDE, D. A., KESSLER, R., RYABY, J. T., FITZSIMMONS, R. J. & GRANT, R. T. 1998. Tissue engineered bone repair of calvarial defects using cultured periosteal cells. *Plast Reconstr Surg,* 101**,** 567-74; discussion 575-6.

BRINDLEY, D., MOORTHY, K., LEE, J. H., MASON, C., KIM, H. W. & WALL, I. 2011. Bioprocess forces and their impact on cell behavior: implications for bone regeneration therapy. *J Tissue Eng,* 2011**,** 620247.

BROUILLET, S., HOFFMANN, P., BENHAROUGA, M., SALOMON, A., SCHAAL, J. P., FEIGE, J. J. & ALFAIDY, N. 2010. Molecular characterization of EG-VEGF-mediated angiogenesis: differential effects on microvascular and macrovascular endothelial cells. *Molecular Biology of the Cell,* 21**,** 2832-43.

BULNHEIM, U., MULLER, P., NEUMANN, H. G., PETERS, K., UNGER, R. E., KIRKPATRICK, C. J. & RYCHLY, J. 2014. Endothelial cells stimulate osteogenic differentiation of mesenchymal stem cells on calcium phosphate scaffolds. *J Tissue Eng Regen Med,* 8**,** 831-40.

CALLE, E. A., GHAEDI, M., SUNDARAM, S., SIVARAPATNA, A., TSENG, M. K. & NIKLASON, L. E. 2014. Strategies for whole lung tissue engineering. *IEEE Trans Biomed Eng,* 61**,** 1482-96.

CAMPISI, J. & D'ADDA DI FAGAGNA, F. 2007. Cellular senescence: when bad things happen to good cells. *Nat Rev Mol Cell Biol,* 8**,** 729-40.

CAO, G., SAVANI, R. C., FEHRENBACH, M., LYONS, C., ZHANG, L., COUKOS, G. & DELISSER, H. M. 2006. Involvement of endothelial CD44 during in vivo angiogenesis. *American Journal of Pathology,* 169**,** 325-36.

CARMELIET, P. 2000. Mechanisms of angiogenesis and arteriogenesis. *Nat Med,* 6**,** 389-95.

CARMELIET, P. 2003. Angiogenesis in health and disease. *Nat Med,* 9**,** 653-60.

CARMELIET, P. 2005. Angiogenesis in life, disease and medicine. *Nature,* 438**,** 932-6.

CASE, N., SEN, B., THOMAS, J. A., STYNER, M., XIE, Z., JACOBS, C. R. & RUBIN, J. 2011. Steady and oscillatory fluid flows produce a similar osteogenic phenotype. *Calcif Tissue Int,* 88**,** 189-97.

CASIRAGHI, F., PERICO, N., CORTINOVIS, M. & REMUZZI, G. 2016. Mesenchymal stromal cells in renal transplantation: opportunities and challenges. *Nat Rev Nephrol*.

CHEN, C. Y., WANG, Y. F., HUANG, W. R. & HUANG, Y. T. 2003. Nickel induces oxidative stress and genotoxicity in human lymphocytes. *Toxicol Appl Pharmacol,* 189**,** 153-9.

CHEN, D., LIU, S., MA, H., LIANG, X., MA, H., YAN, X., YANG, B., WEI, J. & LIU, X. 2015. Paracrine factors from adipose-mesenchymal stem cells enhance metastatic capacity through Wnt signaling pathway in a colon cancer cell co-culture model. *Cancer Cell Int,* 15**,** 42.

CHEN, X., ALEDIA, A. S., GHAJAR, C. M., GRIFFITH, C. K., PUTNAM, A. J., HUGHES, C. C. & GEORGE, S. C. 2009. Prevascularization of a fibrin-based tissue construct accelerates the formation of functional anastomosis with host vasculature. *Tissue Eng Part A,* 15**,** 1363-71.

CHENG, H., JIANG, W., PHILLIPS, F. M., HAYDON, R. C., PENG, Y., ZHOU, L., LUU, H. H., AN, N., BREYER, B., VANICHAKARN, P., SZATKOWSKI, J. P., PARK, J. Y. & HE, T. C. 2003. Osteogenic activity of the fourteen types of human bone morphogenetic proteins (BMPs). *J Bone Joint Surg Am,* 85-A**,** 1544-52.

CHENG, S. L., LOU, J., WRIGHT, N. M., LAI, C. F., AVIOLI, L. V. & RIEW, K. D. 2001. In vitro and in vivo induction of bone formation using a recombinant adenoviral vector carrying the human BMP-2 gene. *Calcified Tissue International,* 68**,** 87-94.

CHOUDHERY, M. S., BADOWSKI, M., MUISE, A., PIERCE, J. & HARRIS, D. T. 2014. Donor age negatively impacts adipose tissue-derived mesenchymal stem cell expansion and differentiation. *J Transl Med,* 12**,** 8.

CHUNG, A. S. & FERRARA, N. 2011. Developmental and pathological angiogenesis. *Annu Rev Cell Dev Biol,* 27**,** 563-84.

CLAES, L., ECKERT-HUBNER, K. & AUGAT, P. 2002. The effect of mechanical stability on local vascularization and tissue differentiation in callus healing. *J Orthop Res,* 20**,** 1099-105.

COLLANTES, R. S. & YOUNOSSI, Z. M. 2005. The Use of Growth Factors to Manage the Hematologic Side Effects of PEG-Interferon Alfa and Ribavirin. *Journal of Clinical Gastroenterology,* 39**,** S9-S13.

CONSENTIUS, C., REINKE, P. & VOLK, H. D. 2015. Immunogenicity of allogeneic mesenchymal stromal cells: what has been seen in vitro and in vivo? *Regen Med,* 10**,** 305-15.

COOPER, G. M. 2000. The Eukaryotic Cell Cycle. *In:* COOPER, G. M. (ed.) *The Cell: A Molecular Approach.* Sunderland: Sinauer Associates.

CORREIA, C., GRAYSON, W. L., PARK, M., HUTTON, D., ZHOU, B., GUO, X. E., NIKLASON, L., SOUSA, R. A., REIS, R. L. & VUNJAK-NOVAKOVIC, G. 2011. In vitro model of vascularized bone: synergizing vascular development and osteogenesis. *PLoS One,* 6**,** e28352.

CRISAN, M., YAP, S., CASTEILLA, L., CHEN, C. W., CORSELLI, M., PARK, T. S., ANDRIOLO, G., SUN, B., ZHENG, B., ZHANG, L., NOROTTE, C., TENG, P. N., TRAAS, J., SCHUGAR, R., DEASY, B. M., BADYLAK, S., BUHRING, H. J., GIACOBINO, J. P., LAZZARI, L., HUARD, J. & PEAULT, B. 2008. A perivascular origin for mesenchymal stem cells in multiple human organs. *Cell Stem Cell,* 3**,** 301-13.

CSISZAR, A., AHMAD, M., SMITH, K. E., LABINSKYY, N., GAO, Q., KALEY, G., EDWARDS, J. G., WOLIN, M. S. & UNGVARI, Z. 2006. Bone morphogenetic protein-2 induces proinflammatory endothelial phenotype. *American Journal of Pathology,* 168**,** 629-38.

D'IPPOLITO, G., SCHILLER, P. C., RICORDI, C., ROOS, B. A. & HOWARD, G. A. 1999. Age-related osteogenic potential of mesenchymal stromal stem cells from human vertebral bone marrow. *Journal of Bone and Mineral Research,* 14**,** 1115-1122.

DA SILVA MEIRELLES, L., CHAGASTELLES, P. C. & NARDI, N. B. 2006. Mesenchymal stem cells reside in virtually all post-natal organs and tissues. *J Cell Sci,* 119**,** 2204-13.

DANHAIVE, P. A. & ROUSSEAU, G. G. 1986. Binding of glucocorticoid antagonists to androgen and glucocorticoid hormone receptors in rat skeletal muscle. *J Steroid Biochem,* 24**,** 481-7.

DANHAIVE, P. A. & ROUSSEAU, G. G. 1988. Evidence for sex-dependent anabolic response to androgenic steroids mediated by muscle glucocorticoid receptors in the rat. *J Steroid Biochem,* 29**,** 575-81.

DAY, T. F., GUO, X., GARRETT-BEAL, L. & YANG, Y. 2005. Wnt/beta-catenin signaling in mesenchymal progenitors controls osteoblast and chondrocyte differentiation during vertebrate skeletogenesis. *Dev Cell,* 8**,** 739-50.

DELIA, D., LAMPUGNANI, M. G., RESNATI, M., DEJANA, E., AIELLO, A., FONTANELLA, E., SOLIGO, D., PIEROTTI, M. A. & GREAVES, M. F. 1993. Cd34 Expression Is Regulated Reciprocally with Adhesion Molecules in Vascular Endothelial-Cells Invitro. *Blood,* 81**,** 1001-1008.

DI MARCO, G. S., HAUSBERG, M., HILLEBRAND, U., RUSTEMEYER, P., WITTKOWSKI, W., LANG, D. & PAVENSTADT, H. 2008. Increased inorganic phosphate induces human endothelial cell apoptosis in vitro. *Am J Physiol Renal Physiol,* 294**,** F1381-7.

DI MARCO, G. S., KONIG, M., STOCK, C., WIESINGER, A., HILLEBRAND, U., REIERMANN, S., REUTER, S., AMLER, S., KOHLER, G., BUCK, F., FOBKER, M., KUMPERS, P., OBERLEITHNER, H., HAUSBERG, M., LANG, D., PAVENSTADT, H. & BRAND, M. 2013. High phosphate directly affects endothelial function by downregulating annexin II. *Kidney Int,* 83**,** 213-22.

DOHLE, E., BISCHOFF, I., BOSE, T., MARSANO, A., BANFI, A., UNGER, R. E. & KIRKPATRICK, C. J. 2014. Macrophage-mediated angiogenic activation of outgrowth endothelial cells in co-culture with primary osteoblasts. *Eur Cell Mater,* 27**,** 149-64; discussion 164-5.

DOHLE, E., FUCHS, S., KOLBE, M., HOFMANN, A., SCHMIDT, H. & KIRKPATRICK, C. J. 2010. Sonic hedgehog promotes angiogenesis and osteogenesis in a coculture system consisting of primary osteoblasts and outgrowth endothelial cells. *Tissue Eng Part A,* 16**,** 1235-7.

DOHLE, E., FUCHS, S., KOLBE, M., HOFMANN, A., SCHMIDT, H. & KIRKPATRICK, C. J. 2011. Comparative Study Assessing Effects of Sonic Hedgehog and Vegf in a Human Co-Culture Model for Bone Vascularisation Strategies. *European Cells & Materials,* 21**,** 144-156.

DOMINICI, M., LE BLANC, K., MUELLER, I., SLAPER-CORTENBACH, I., MARINI, F. C., KRAUSE, D. S., DEANS, R. J., KEATING, A., PROCKOP, D. J. & HORWITZ, E. M. 2006. Minimal criteria for defining multipotent mesenchymal stromal cells. The International Society for Cellular Therapy position statement. *Cytotherapy,* 8**,** 315-317.

DONZELLI, E., SALVADE, A., MIMO, P., VIGANO, M., MORRONE, M., PAPAGNA, R., CARINI, F., ZAOPO, A., MILOSO, M., BALDONI, M. & TREDICI, G. 2007. Mesenchymal stem cells cultured on a collagen scaffold: In vitro osteogenic differentiation. *Archives of Oral Biology,* 52**,** 64-73.

DUDAKOV, J., WERTHEIMER, T., VELARDI, E., BREDE, C., YOUNG, L., GINSBERG, M., NOLAN, D., BEILHACK, A., RAFII, S., BUTLER, J. & VAN DEN BRINK, M. 2015. Endothelial cells promote endogenous thymic regeneration via BMP4 signaling and activation of Foxn1 (HEM7P.224). *The Journal of Immunology,* 194**,** 188.4.

EGGER, D. E. A. 2015. Dynamic cultivation of human stem cells under physiological conditions. *BMC Proceedings,* 9(Suppl9)**,** 68.

EINHORN, T. A. & GERSTENFELD, L. C. 2015. Fracture healing: mechanisms and interventions. *Nat Rev Rheumatol,* 11**,** 45-54.

ENGSIG, M. T., CHEN, Q. T., VU, T. H., PEDERSEN, A. C., THERKIDSEN, B., LUND, L. R., HENRIKSEN, K., LENHARD, T., FOGED, N. T., WERB, Z. & DELAISSE, J. M. 2001. Matrix metalloproteinase 9 and vascular endothelial growth factor are essential for osteoclast recruitment into developing long bones (vol 151, pg 879, 2000). *Journal of Cell Biology,* 152**,** 419-419.

ERL, W. 2005. Statin-induced vascular smooth muscle cell apoptosis: a possible role in the prevention of restenosis? *Curr Drug Targets Cardiovasc Haematol Disord,* 5**,** 135-44.

FAN, L., LIU, R., LI, J., SHI, Z., DANG, X. & WANG, K. 2015. Low oxygen tension enhances osteogenic potential of bone marrow-derived mesenchymal stem cells with osteonecrosis-related functional impairment. *Stem Cells Int,* 2015**,** 950312.

FEKETE, N., ROJEWSKI, M. T., FURST, D., KREJA, L., IGNATIUS, A., DAUSEND, J. & SCHREZENMEIER, H. 2012. GMP-compliant isolation and large-scale expansion of bone marrow-derived MSC. *PLoS One,* 7**,** e43255.

FERNANDEZ-MOURE, J. S., CORRADETTI, B., CHAN, P., VAN EPS, J. L., JANECEK, T., RAMESHWAR, P., WEINER, B. K. & TASCIOTTI, E. 2015. Enhanced osteogenic potential of mesenchymal stem cells from cortical bone: a comparative analysis. *Stem Cell Res Ther,* 6**,** 203.

FERRERAS, C., COLE, C. L., URBAN, K., JAYSON, G. C. & AVIZIENYTE, E. 2015. Segregation of late outgrowth endothelial cells into functional endothelial CD34-and progenitor-like CD34+cell populations. *Angiogenesis,* 18**,** 47-68.

FLAUMENHAFT, R. & RIFKIN, D. B. 1991. Extracellular matrix regulation of growth factor and protease activity. *Curr Opin Cell Biol,* 3**,** 817-23.

FORBES, S. J. & ROSENTHAL, N. 2014. Preparing the ground for tissue regeneration: from mechanism to therapy. *Nat Med,* 20**,** 857-69.

FRANCIS, M. P., SACHS, P. C., ELMORE, L. W. & HOLT, S. E. 2010. Isolating adipose-derived mesenchymal stem cells from lipoaspirate blood and saline fraction. *Organogenesis,* 6**,** 11-4.

FREESE, C., REINHARDT, S., HEFNER, G., UNGER, R. E., KIRKPATRICK, C. J. & ENDRES, K. 2014. A novel blood-brain barrier co-culture system for drug targeting of Alzheimer's disease: establishment by using acitretin as a model drug. *PLoS One,* 9**,** e91003.

FREIMAN, A., SHANDALOV, Y., ROZENFELD, D., SHOR, E., SEGAL, S., BEN-DAVID, D., MERETZKI, S., EGOZI, D. & LEVENBERG, S. 2016. Adipose-derived endothelial and mesenchymal stem cells enhance vascular network formation on three-dimensional constructs in vitro. *Stem Cell Res Ther,* 7**,** 5.

FRIEDMAN, M. S., LONG, M. W. & HANKENSON, K. D. 2006. Osteogenic differentiation of human mesenchymal stem cells is regulated by bone morphogenetic protein-6. *Journal of Cellular Biochemistry,* 98**,** 538-554.

FUCHS, S., GHANAATI, S., ORTH, C., BARBECK, M., KOLBE, M., HOFMANN, A., EBLENKAMP, M., GOMES, M., REIS, R. L. & KIRKPATRICK, C. J. 2009a. Contribution of outgrowth endothelial cells from human peripheral blood on in vivo vascularization of bone tissue engineered constructs based on starch polycaprolactone scaffolds. *Biomaterials,* 30**,** 526-34.

FUCHS, S., HERMANNS, M. I. & KIRKPATRICK, C. J. 2006. Retention of a differentiated endothelial phenotype by outgrowth endothelial cells isolated from human peripheral blood and expanded in long-term cultures. *Cell and Tissue Research,* 326**,** 79-92.

FUCHS, S., HOFMANN, A. & KIRKPATRICK, C. J. 2007. Microvessel-like structures from outgrowth endothelial cells from human peripheral blood in 2-dimensional and 3-dimensional co-cultures with osteoblastic lineage cells. *Tissue Eng,* 13**,** 2577-88.

FUCHS, S., JIANG, X., GOTMAN, I., MAKAROV, C., SCHMIDT, H., GUTMANAS, E. Y. & KIRKPATRICK, C. J. 2010. Influence of polymer content in Ca-deficient hydroxyapatite-polycaprolactone nanocomposites on the formation of microvessel-like structures. *Acta Biomater,* 6**,** 3169-77.

FUCHS, S., JIANG, X., SCHMIDT, H., DOHLE, E., GHANAATI, S., ORTH, C., HOFMANN, A., MOTTA, A., MIGLIARESI, C. & KIRKPATRICK, C. J. 2009b. Dynamic processes involved in the pre-vascularization of silk fibroin constructs for bone regeneration using outgrowth endothelial cells. *Biomaterials,* 30**,** 1329-38.

GERBER, H. P., VU, T. H., RYAN, A. M., KOWALSKI, J., WERB, Z. & FERRARA, N. 1999. VEGF couples hypertrophic cartilage remodeling, ossification and angiogenesis during endochondral bone formation. *Nat Med,* 5**,** 623-8.

GERHARDT, H., GOLDING, M., FRUTTIGER, M., RUHRBERG, C., LUNDKVIST, A., ABRAMSSON, A., JELTSCH, M., MITCHELL, C., ALITALO, K., SHIMA, D. & BETSHOLTZ, C. 2003. VEGF guides angiogenic sprouting utilizing endothelial tip cell filopodia. *J Cell Biol,* 161**,** 1163-77.

GERSTENFELD, L. C., CHO, T. J., KON, T., AIZAWA, T., TSAY, A., FITCH, J., BARNES, G. L., GRAVES, D. T. & EINHORN, T. A. 2003a. Impaired fracture healing in the absence of TNF-alpha signaling: the role of TNF-alpha in endochondral cartilage resorption. *J Bone Miner Res,* 18**,** 1584-92.

GERSTENFELD, L. C., CULLINANE, D. M., BARNES, G. L., GRAVES, D. T. & EINHORN, T. A. 2003b. Fracture healing as a post-natal developmental process: molecular, spatial, and temporal aspects of its regulation. *Journal of Cellular Biochemistry,* 88**,** 873-84.

GILBERT, S. F. 2000. Osteogenesis: The Development of Bones. *In:* GILBERT, S. F. (ed.) *Developmental Biology.* 6 ed. Sunderland: Sinauer Associates.

GINIS, I., WEINREB, M., ABRAMOV, N., SHINAR, D., MERCHAV, S., SCHWARTZ, A. & SHIRVAN, M. 2012. Bone progenitors produced by direct osteogenic differentiation of the unprocessed bone marrow demonstrate high osteogenic potential in vitro and in vivo. *Biores Open Access,* 1**,** 69-78.

GLOWACKI, J., MIZUNO, S. & GREENBERGER, J. S. 1998. Perfusion enhances functions of bone marrow stromal cells in three-dimensional culture. *Cell Transplant,* 7**,** 319-26.

GOBAA, S., HOEHNEL, S., ROCCIO, M., NEGRO, A., KOBEL, S. & LUTOLF, M. P. 2011. Artificial niche microarrays for probing single stem cell fate in high throughput. *Nat Methods,* 8**,** 949-55.

GOLDSTEIN, A. S., JUAREZ, T. M., HELMKE, C. D., GUSTIN, M. C. & MIKOS, A. G. 2001. Effect of convection on osteoblastic cell growth and function in biodegradable polymer foam scaffolds. *Biomaterials,* 22**,** 1279-1288.

GOMES, M. E., BOSSANO, C. M., JOHNSTON, C. M., REIS, R. L. & MIKOS, A. G. 2006. In vitro localization of bone growth factors in constructs of biodegradable scaffolds seeded with marrow stromal cells and cultured in a flow perfusion bioreactor. *Tissue Eng,* 12**,** 177-88.

GOMIDE, V. S., ZONARI, A., OCARINO, N. M., GOES, A. M., SERAKIDES, R. & PEREIRA, M. M. 2012. In vitro and in vivo osteogenic potential of bioactive glass-PVA hybrid scaffolds colonized by mesenchymal stem cells. *Biomed Mater,* 7**,** 015004.

GOTMAN, I. 2010. Fabrication of Load-Bearing NiTi Scaffolds for Bone Ingrowth by Ni Foam Conversion. *Advanced Engineering Materials,* 12**,** B320-B325.

GOTMAN, I., BEN-DAVID, D., UNGER, R. E., BOSE, T., GUTMANAS, E. Y. & KIRKPATRICK, C. J. 2013. Mesenchymal stem cell proliferation and differentiation on load-bearing trabecular Nitinol scaffolds. *Acta Biomater,* 9**,** 8440-8.

GOTMAN, I. & REINER, T. 2010. Biomimetic calcium phosphate coating on Ti wires versus flat substrates: structure and mechanism of formation. *Journal of Materials Science-Materials in Medicine,* 21**,** 515-523.

GOUGOS, A., ST JACQUES, S., GREAVES, A., O'CONNELL, P. J., D'APICE, A. J., BUHRING, H. J., BERNABEU, C., VAN MOURIK, J. A. & LETARTE, M. 1992. Identification of distinct epitopes of endoglin, an RGD-containing glycoprotein of endothelial cells, leukemic cells, and syncytiotrophoblasts. *Int Immunol,* 4**,** 83-92.

GOVINDASAMY, V., RONALD, V. S., TOTEY, S., DIN, S. B., MUSTAFA, W. M. B., TOTEY, S., ZAKARIA, Z. & BHONDE, R. R. 2010. Micromanipulation of culture niche permits long-term expansion of dental pulp stem cells-an economic and commercial angle. *In Vitro Cellular & Developmental Biology-Animal,* 46**,** 764-773.

GRIESE, D. P., EHSAN, A., MELO, L. G., KONG, D. L., ZHANG, L. N., MANN, M. J., PRATT, R. E., MULLIGAN, R. C. & DZAU, V. J. 2003. Isolation and transplantation of autologous circulating endothelial cells into denuded vessels and prosthetic grafts - Implications for cell-based vascular therapy. *Circulation,* 108**,** 2710-2715.

GRIFFIOEN, A. W., COENEN, M. J. H., DAMEN, C. A., HELLWIG, S. M. M., VANWEERING, D. H. J., VOOYS, W., BLIJHAM, G. H. & GROENEWEGEN, G. 1997. CD44 is involved in tumor angiogenesis; an activation antigen on human endothelial cells. *Blood,* 90**,** 1150-1159.

GRIGORIADIS, A. E., HEERSCHE, J. N. & AUBIN, J. E. 1988. Differentiation of muscle, fat, cartilage, and bone from progenitor cells present in a bone-derived clonal cell population: effect of dexamethasone. *Journal of Cell Biology,* 106**,** 2139-51.

GROENEVELD, D. J., VAN BEKKUM, T., DIRVEN, R. J., WANG, J. W., VOORBERG, J., REITSMA, P. H. & EIKENBOOM, J. 2015. Angiogenic characteristics of blood outgrowth endothelial cells from patients with von Willebrand disease. *Journal of Thrombosis and Haemostasis,* 13**,** 1854-66.

GURTNER, G. C., WERNER, S., BARRANDON, Y. & LONGAKER, M. T. 2008. Wound repair and regeneration. *Nature,* 453**,** 314-21.

GUZMAN-MORALES, J., EL-GABALAWY, H., PHAM, M. H., TRAN-KHANH, N., MCKEE, M. D., WU, W., CENTOLA, M. & HOEMANN, C. D. 2009. Effect of chitosan particles and dexamethasone on human bone marrow stromal cell osteogenesis and angiogenic factor secretion. *Bone,* 45**,** 617-26.

HAGMANN, S., MORADI, B., FRANK, S., DREHER, T., KAMMERER, P. W., RICHTER, W. & GOTTERBARM, T. 2013. Different culture media affect growth characteristics, surface marker distribution and chondrogenic differentiation of human bone marrow-derived mesenchymal stromal cells. *BMC Musculoskelet Disord,* 14**,** 223.

HANADA, K., DENNIS, J. E. & CAPLAN, A. I. 1997. Stimulatory effects of basic fibroblast growth factor and bone morphogenetic protein-2 on osteogenic differentiation of rat bone marrow-derived mesenchymal stem cells. *Journal of Bone and Mineral Research,* 12**,** 1606-14.

HARTMANN, C. 2007. Skeletal development--Wnts are in control. *Mol Cells,* 24**,** 177-84.

HARTMANN, C. 2009. Transcriptional networks controlling skeletal development. *Curr Opin Genet Dev,* 19**,** 437-43.

HASS, R., KASPER, C., BOHM, S. & JACOBS, R. 2011. Different populations and sources of human mesenchymal stem cells (MSC): A comparison of adult and neonatal tissue-derived MSC. *Cell Commun Signal,* 9**,** 12.

HEINEMANN, C., HEINEMANN, S., WORCH, H. & HANKE, T. 2011. Development of an osteoblast/osteoclast co-culture derived by human bone marrow stromal cells and human monocytes for biomaterials testing. *Eur Cell Mater,* 21**,** 80-93.

HELBING, T., ROTHWEILER, R., KETTERER, E., GOETZ, L., HEINKE, J., GRUNDMANN, S., DUERSCHMIED, D., PATTERSON, C., BODE, C. & MOSER, M. 2011. BMP activity controlled by BMPER regulates the proinflammatory phenotype of endothelium. *Blood,* 118**,** 5040-9.

HELLSTROM, M., PHNG, L. K., HOFMANN, J. J., WALLGARD, E., COULTAS, L., LINDBLOM, P., ALVA, J., NILSSON, A. K., KARLSSON, L., GAIANO, N., YOON, K., ROSSANT, J., IRUELA-ARISPE, M. L., KALEN, M., GERHARDT, H. & BETSHOLTZ, C. 2007. Dll4 signalling through Notch1 regulates formation of tip cells during angiogenesis. *Nature,* 445**,** 776-780.

HEO, S. J., THORPE, S. D., DRISCOLL, T. P., DUNCAN, R. L., LEE, D. A. & MAUCK, R. L. 2015. Biophysical Regulation of Chromatin Architecture Instills a Mechanical Memory in Mesenchymal Stem Cells. *Sci Rep,* 5**,** 16895.

HERZOG, D. P., DOHLE, E., BISCHOFF, I. & KIRKPATRICK, C. J. 2014. Cell communication in a coculture system consisting of outgrowth endothelial cells and primary osteoblasts. *Biomed Res Int,* 2014**,** 320123.

HIGGINS, S. J., BAXTER, J. D. & ROUSSEAU, G. G. 1979. Nuclear binding of glucocorticoid receptors. *Monogr Endocrinol,* 12**,** 135-60.

HILL, T. P., SPATER, D., TAKETO, M. M., BIRCHMEIER, W. & HARTMANN, C. 2005. Canonical Wnt/beta-catenin signaling prevents osteoblasts from differentiating into chondrocytes. *Dev Cell,* 8**,** 727-38.

HIRSCHI, K. K. & D'AMORE, P. A. 1996. Pericytes in the microvasculature. *Cardiovasc Res,* 32**,** 687-98.

HOCH, A. I., BINDER, B. Y., GENETOS, D. C. & LEACH, J. K. 2012. Differentiation-dependent secretion of proangiogenic factors by mesenchymal stem cells. *PLoS One,* 7**,** e35579.

HOEBEN, A., LANDUYT, B., HIGHLEY, M. S., WILDIERS, H., VAN OOSTEROM, A. T. & DE BRUIJN, E. A. 2004. Vascular endothelial growth factor and angiogenesis. *Pharmacol Rev,* 56**,** 549-80.

HOEMANN, C. D., EL-GABALAWY, H. & MCKEE, M. D. 2009. In vitro osteogenesis assays: influence of the primary cell source on alkaline phosphatase activity and mineralization. *Pathol Biol (Paris),* 57**,** 318-23.

HOLNTHONER, W., HOHENEGGER, K., HUSA, A. M., MUEHLEDER, S., MEINL, A., PETERBAUER-SCHERB, A. & REDL, H. 2015. Adipose-derived stem cells induce vascular tube formation of outgrowth endothelial cells in a fibrin matrix. *Journal of Tissue Engineering and Regenerative Medicine,* 9**,** 127-136.

HOLSTEIN, J. H., KARABIN-KEHL, B., SCHEUER, C., GARCIA, P., HISTING, T., MEIER, C., BENNINGER, E., MENGER, M. D. & POHLEMANN, T. 2013. Endostatin inhibits Callus remodeling during fracture healing in mice. *J Orthop Res,* 31**,** 1579-84.

HOLTORF, H. L., DATTA, N., JANSEN, J. A. & MIKOS, A. G. 2005a. Scaffold mesh size affects the osteoblastic differentiation of seeded marrow stromal cells cultured in a flow perfusion bioreactor. *Journal of Biomedical Materials Research Part A,* 74A**,** 171-180.

HOLTORF, H. L., JANSEN, J. A. & MIKOS, A. G. 2005b. Flow perfusion culture induces the osteoblastic differentiation of marrow stromal cell-scaffold constructs in the absence of dexamethasone. *Journal of Biomedical Materials Research Part A,* 72A**,** 326-334.

HOLTORF, H. L., SHEFFIELD, T. L., AMBROSE, C. G., JANSEN, J. A. & MIKOS, A. G. 2005c. Flow perfusion culture of marrow stromal cells seeded on porous biphasic calcium phosphate ceramics. *Annals of Biomedical Engineering,* 33**,** 1238-1248.

HOLZWARTH, C., VAEGLER, M., GIESEKE, F., PFISTER, S. M., HANDGRETINGER, R., KERST, G. & MULLER, I. 2010. Low physiologic oxygen tensions reduce proliferation and differentiation of human multipotent mesenchymal stromal cells. *BMC Cell Biol,* 11**,** 11.

HONDA, Y., DING, X., MUSSANO, F., WIBERG, A., HO, C. M. & NISHIMURA, I. 2013. Guiding the osteogenic fate of mouse and human mesenchymal stem cells through feedback system control. *Sci Rep,* 3**,** 3420.

HUANG, Z., NELSON, E. R., SMITH, R. L. & GOODMAN, S. B. 2007. The sequential expression profiles of growth factors from osteoprogenitors [correction of osteroprogenitors] to osteoblasts in vitro. *Tissue Eng,* 13**,** 2311-20.

HUGHEY, C. C., ALFARO, M. P., BELKE, D. D., ROTTMAN, J. N., YOUNG, P. P., WASSERMAN, D. H. & SHEARER, J. 2012. Increased oxygen consumption and OXPHOS potential in superhealer mesenchymal stem cells. *Cell Regen (Lond),* 1**,** 3.

JACKSON, C. J. & NGUYEN, M. 1997. Human microvascular endothelial cells differ from macrovascular endothelial cells in their expression of matrix metalloproteinases. *International Journal of Biochemistry & Cell Biology,* 29**,** 1167-1177.

JACOBS, C. R., YELLOWLEY, C. E., DAVIS, B. R., ZHOU, Z., CIMBALA, J. M. & DONAHUE, H. J. 1998. Differential effect of steady versus oscillating flow on bone cells. *J Biomech,* 31**,** 969-76.

JAFFE, E. A., NACHMAN, R. L., BECKER, C. G. & MINICK, C. R. 1973. Culture of human endothelial cells derived from umbilical veins. Identification by morphologic and immunologic criteria. *J Clin Invest,* 52**,** 2745-56.

JAISWAL, N., HAYNESWORTH, S. E., CAPLAN, A. I. & BRUDER, S. P. 1997. Osteogenic differentiation of purified, culture-expanded human mesenchymal stem cells in vitro. *Journal of Cellular Biochemistry,* 64**,** 295-312.

JIANG, A., PAN, W., MILBAUER, L. C., SHYR, Y. & HEBBEL, R. P. 2007. A practical question based on cross-platform microarray data normalization: are BOEC more like large vessel or microvascular endothelial cells or neither of them? *J Bioinform Comput Biol,* 5**,** 875-93.

JIN, K., LI, B., LOU, L., XU, Y., YE, X., YAO, K., YE, J. & GAO, C. 2016. In vivo vascularization of MSC-loaded porous hydroxyapatite constructs coated with VEGF-functionalized collagen/heparin multilayers. *Sci Rep,* 6**,** 19871.

JONES, R. G., PLAS, D. R., KUBEK, S., BUZZAI, M., MU, J., XU, Y., BIRNBAUM, M. J. & THOMPSON, C. B. 2005. AMP-activated protein kinase induces a p53-dependent metabolic checkpoint. *Mol Cell,* 18**,** 283-93.

JUNKER, J. P., SOMMAR, P., SKOG, M., JOHNSON, H. & KRATZ, G. 2010. Adipogenic, chondrogenic and osteogenic differentiation of clonally derived human dermal fibroblasts. *Cells Tissues Organs,* 191**,** 105-18.

KAIGLER, D., KREBSBACH, P. H., WEST, E. R., HORGER, K., HUANG, Y. C. & MOONEY, D. J. 2005. Endothelial cell modulation of bone marrow stromal cell osteogenic potential. *Faseb Journal,* 19**,** 665-7.

KALFAS, I. H. 2001. Principles of bone healing. *Neurosurg Focus,* 10**,** E1.

KANAJI, A., ORHUE, V., CAICEDO, M. S., VIRDI, A. S., SUMNER, D. R., HALLAB, N. J., YOSHIAKI, T. & SENA, K. 2014. Cytotoxic effects of cobalt and nickel ions on osteocytes in vitro. *J Orthop Surg Res,* 9**,** 91.

KANG, Q., SUN, M. H., CHENG, H., PENG, Y., MONTAG, A. G., DEYRUP, A. T., JIANG, W., LUU, H. H., LUO, J., SZATKOWSKI, J. P., VANICHAKARN, P., PARK, J. Y., LI, Y., HAYDON, R. C. & HE, T. C. 2004. Characterization of the distinct orthotopic bone-forming activity of 14 BMPs using recombinant adenovirus-mediated gene delivery. *Gene Therapy,* 11**,** 1312-1320.

KANWAR, Y. S. & CARONE, F. A. 1984. Reversible changes of tubular cell and basement membrane in drug-induced renal cystic disease. *Kidney Int,* 26**,** 35-43.

KARAGEORGIOU, V. & KAPLAN, D. 2005. Porosity of 3D biomaterial scaffolds and osteogenesis. *Biomaterials,* 26**,** 5474-91.

KARSENTY, G. 2001. Minireview: transcriptional control of osteoblast differentiation. *Endocrinology,* 142**,** 2731-3.

KEAVENY, T. M., MORGAN, E. F., NIEBUR, G. L. & YEH, O. C. 2001. Biomechanics of trabecular bone. *Annu Rev Biomed Eng,* 3**,** 307-33.

KEIL, J. M., LIU, X. & ANTONETTI, D. A. 2013. Glucocorticoid induction of occludin expression and endothelial barrier requires transcription factor p54 NONO. *Invest Ophthalmol Vis Sci,* 54**,** 4007-15.

KENNEDY, M., FIRPO, M., CHOI, K., WALL, C., ROBERTSON, S., KABRUN, N. & KELLER, G. 1997. A common precursor for primitive erythropoiesis and definitive haematopoiesis. *Nature,* 386**,** 488-93.

KERSTEN, C., SIVERTSEN, E. A., HYSTAD, M. E., FORFANG, L., SMELAND, E. B. & MYKLEBUST, J. H. 2005. BMP-6 inhibits growth of mature human B cells; induction of Smad phosphorylation and upregulation of Id1. *BMC Immunol,* 6**,** 9.

KHOUJA, H. I., BEVINGTON, A., KEMP, G. J. & RUSSELL, R. G. 1990. Calcium and orthophosphate deposits in vitro do not imply osteoblast-mediated mineralization: mineralization by betaglycerophosphate in the absence of osteoblasts. *Bone,* 11**,** 385-91.

KIM, E. J., CHO, S. W., SHIN, J. O., LEE, M. J., KIM, K. S. & JUNG, H. S. 2013. Ihh and Runx2/Runx3 signaling interact to coordinate early chondrogenesis: a mouse model. *PLoS One,* 8**,** e55296.

KIRKPATRICK, C. J., FUCHS, S. & UNGER, R. E. 2011. Co-culture systems for vascularization--learning from nature. *Adv Drug Deliv Rev,* 63**,** 291-9.

KLEPPMANN, W. 2013. *Versuchsplanung - Produkte und Prozesse optimieren*, Carl Hanser Verlag GmbH&Co.KG.

KNIGHT, M. N. & HANKENSON, K. D. 2013. Mesenchymal Stem Cells in Bone Regeneration. *Adv Wound Care (New Rochelle),* 2**,** 306-316.

KOBOLAK, J., DINNYES, A., MEMIC, A., KHADEMHOSSEINI, A. & MOBASHERI, A. 2015. Mesenchymal stem cells: Identification, phenotypic characterization, biological properties and potential for regenerative medicine through biomaterial micro-engineering of their niche. *Methods*.

KOLBE, M., DOHLE, E., KATERLA, D., KIRKPATRICK, C. J. & FUCHS, S. 2010. Enrichment of outgrowth endothelial cells in high and low colony-forming cultures from peripheral blood progenitors. *Tissue Eng Part C Methods,* 16**,** 877-86.

KOLBE, M., XIANG, Z., DOHLE, E., TONAK, M., KIRKPATRICK, C. J. & FUCHS, S. 2011. Paracrine Effects Influenced by Cell Culture Medium and Consequences on Microvessel-Like Structures in Cocultures of Mesenchymal Stem Cells and Outgrowth Endothelial Cells. *Tissue Eng Part A*.

KRIEGER, N. S., MIDDLEBROOK, J. L. & ARONOW, L. 1976. Effect of salt on reversibility of glucocorticoid receptor binding. *J Steroid Biochem,* 7**,** 395-9.

KROEZE, R. J., KNIPPENBERG, M. & HELDER, M. N. 2011. Osteogenic differentiation strategies for adipose-derived mesenchymal stem cells. *Methods Mol Biol,* 702**,** 233-48.

KUBOTA, Y., KLEINMAN, H. K., MARTIN, G. R. & LAWLEY, T. J. 1988. Role of Laminin and Basement-Membrane in the Morphological-Differentiation of Human-Endothelial Cells into Capillary-Like Structures. *Journal of Cell Biology,* 107**,** 1589-1598.

LANG, I., PABST, M. A., HIDEN, U., BLASCHITZ, A., DOHR, G., HAHN, T. & DESOYE, G. 2003. Heterogeneity of microvascular endothelial cells isolated from human term placenta and macrovascular umbilical vein endothelial cells. *Eur J Cell Biol,* 82**,** 163-73.

LANGE, J., SAPOZHNIKOVA, A., LU, C., HU, D., LI, X., MICLAU, T., 3RD & MARCUCIO, R. S. 2010. Action of IL-1beta during fracture healing. *J Orthop Res,* 28**,** 778-84.

LANGENBACH, F. & HANDSCHEL, J. 2013. Effects of dexamethasone, ascorbic acid and beta-glycerophosphate on the osteogenic differentiation of stem cells in vitro. *Stem Cell Research & Therapy,* 4**,** 117.

LANGUINO, L. R., GEHLSEN, K. R., WAYNER, E., CARTER, W. G., ENGVALL, E. & RUOSLAHTI, E. 1989. Endothelial-Cells Use Alpha-2-Beta-1 Integrin as a Laminin Receptor. *Journal of Cell Biology,* 109**,** 2455-2462.

LANZER, P., BOEHM, M., SORRIBAS, V., THIRIET, M., JANZEN, J., ZELLER, T., ST HILAIRE, C. & SHANAHAN, C. 2014. Medial vascular calcification revisited: review and perspectives. *Eur Heart J,* 35**,** 1515-25.

LAU, W. L., FESTING, M. H. & GIACHELLI, C. M. 2010. Phosphate and vascular calcification: Emerging role of the sodium-dependent phosphate co-transporter PiT-1. *Thromb Haemost,* 104**,** 464-70.

LE BLANC, K., TAMMIK, C., ROSENDAHL, K., ZETTERBERG, E. & RINGDEN, O. 2003. HLA expression and immunologic properties of differentiated and undifferentiated mesenchymal stem cells. *Exp Hematol,* 31**,** 890-6.

LEE, F. Y., CHOI, Y. W., BEHRENS, F. F., DEFOUW, D. O. & EINHORN, T. A. 1998. Programmed removal of chondrocytes during endochondral fracture healing. *J Orthop Res,* 16**,** 144-50.

LESZCZYNSKA, J., ZYZYNSKA-GRANICA, B., KOZIAK, K., RUMINSKI, S. & LEWANDOWSKA-SZUMIEL, M. 2013. Contribution of endothelial cells to human bone-derived cells expansion in coculture. *Tissue Eng Part A,* 19**,** 393-402.

LI, C., ISSA, R., KUMAR, P., HAMPSON, I. N., LOPEZ-NOVOA, J. M., BERNABEU, C. & KUMAR, S. 2003. CD105 prevents apoptosis in hypoxic endothelial cells. *Journal of Cell Science,* 116**,** 2677-85.

LI, J., ZHOU, L., TRAN, H. T., CHEN, Y., NGUYEN, N. E., KARASEK, M. A. & MARINKOVICH, M. P. 2006. Overexpression of laminin-8 in human dermal microvascular endothelial cells promotes angiogenesis-related functions. *J Invest Dermatol,* 126**,** 432-40.

LI, M., FUCHS, S., BOSE, T., SCHMIDT, H., HOFMANN, A., TONAK, M., UNGER, R. & KIRKPATRICK, C. J. 2014. Mild Heat Stress Enhances Angiogenesis in a Co-culture System Consisting of Primary Human Osteoblasts and Outgrowth Endothelial Cells. *Tissue Engineering Part C-Methods,* 20**,** 328-339.

LIAO, J. H., GUO, X. A., NELSON, D., KASPER, F. K. & MIKOS, A. G. 2010. Modulation of osteogenic properties of biodegradable polymer/extracellular matrix scaffolds generated with a flow perfusion bioreactor. *Acta Biomaterialia,* 6**,** 2386-2393.

LIN, D. W., CHUNG, B. P. & KAISER, P. 2014. S-adenosylmethionine limitation induces p38 mitogen-activated protein kinase and triggers cell cycle arrest in G1. *Journal of Cell Science,* 127**,** 50-9.

LIN, Y., CHANG, L. M., SOLOVEY, A., HEALEY, J. F., LOLLAR, P. & HEBBEL, R. P. 2002. Use of blood outgrowth endothelial cells for gene therapy for hemophilia A. *Blood,* 99**,** 457-462.

LIU, Y., CHAN, J. K. & TEOH, S. H. 2015. Review of vascularised bone tissue-engineering strategies with a focus on co-culture systems. *J Tissue Eng Regen Med,* 9**,** 85-105.

LOBOV, I. B., BROOKS, P. C. & LANG, R. A. 2002. Angiopoietin-2 displays VEGF-dependent modulation of capillary structure and endothelial cell survival in vivo. *Proceedings of the National Academy of Sciences of the United States of America,* 99**,** 11205-11210.

LOGIE, J. J., ALI, S., MARSHALL, K. M., HECK, M. M., WALKER, B. R. & HADOKE, P. W. 2010. Glucocorticoid-mediated inhibition of angiogenic changes in human endothelial cells is not caused by reductions in cell proliferation or migration. *PLoS One,* 5**,** e14476.

LONG, F. 2012. Building strong bones: molecular regulation of the osteoblast lineage. *Nat Rev Mol Cell Biol,* 13**,** 27-38.

LUU, H. H., SONG, W. X., LUO, X., MANNING, D., LUO, J., DENG, Z. L., SHARFF, K. A., MONTAG, A. G., HAYDON, R. C. & HE, T. C. 2007. Distinct roles of bone morphogenetic proteins in osteogenic differentiation of mesenchymal stem cells. *J Orthop Res,* 25**,** 665-77.

MA, J., VAN DEN BEUCKEN, J. J., YANG, F., BOTH, S. K., CUI, F. Z., PAN, J. & JANSEN, J. A. 2011. Coculture of osteoblasts and endothelial cells: optimization of culture medium and cell ratio. *Tissue Eng Part C Methods,* 17**,** 349-57.

MACKIE, E. J., AHMED, Y. A., TATARCZUCH, L., CHEN, K. S. & MIRAMS, M. 2008a. Endochondral ossification: how cartilage is converted into bone in the developing skeleton. *Int J Biochem Cell Biol,* 40**,** 46-62.

MACKIE, E. J., AHMED, Y. A., TATARCZUCH, L., CHEN, K. S. & MIRAMS, M. 2008b. Endochondral ossification: How cartilage is converted into bone in the developing skeleton. *International Journal of Biochemistry & Cell Biology,* 40**,** 46-62.

MAES, C. & CARMELIET, G. 2008. Vascular and Nonvascular Roles of VEGF in Bone Development. *In:* RUHRBERG, C. (ed.) *VEGF in Development.* Landes Bioscience; Springer Science + Business Media.

MAKRYDIMA, S. F., PISTIKI, A. C., CHRELIAS, C. G., SIOULAS, V. D., SIRISTATIDIS, C. S., GIAMARELLOS-BOURBOULIS, E. J. & KASSANOS, D. P. 2014. The immunomodulatory and anti-apoptotic effect of dexamethasone in imminent preterm labor: an experimental study. *Eur J Pharmacol,* 730**,** 31-5.

MANKIN, H. J. & LIPPIELLO, L. 1971. The glycosaminoglycans of normal and arthritic cartilage. *J Clin Invest,* 50**,** 1712-9.

MANOLAGAS, S. C. 2000. Birth and death of bone cells: basic regulatory mechanisms and implications for the pathogenesis and treatment of osteoporosis. *Endocr Rev,* 21**,** 115-37.

MARINO, S., LOGAN, J. G., MELLIS, D. & CAPULLI, M. 2014. Generation and culture of osteoclasts. *Bonekey Rep,* 3**,** 570.

MARSELL, R. & EINHORN, T. A. 2011. The biology of fracture healing. *Injury-International Journal of the Care of the Injured,* 42**,** 551-555.

MARTIN-RAMIREZ, J., HOFMAN, M., VAN DEN BIGGELAAR, M., HEBBEL, R. P. & VOORBERG, J. 2012. Establishment of outgrowth endothelial cells from peripheral blood. *Nat Protoc,* 7**,** 1709-15.

MARTINO, M. M., BRKIC, S., BOVO, E., BURGER, M., SCHAEFER, D. J., WOLFF, T., GURKE, L., BRIQUEZ, P. S., LARSSON, H. M., GIANNI-BARRERA, R., HUBBELL, J. A. & BANFI, A. 2015. Extracellular matrix and growth factor engineering for controlled angiogenesis in regenerative medicine. *Front Bioeng Biotechnol,* 3**,** 45.

MASUZAWA, M., FUJIMURA, T., HAMADA, Y., FUJITA, Y., HARA, H., NISHIYAMA, S., KATSUOKA, K., TAMAUCHI, H. & SAKURAI, Y. 1999. Establishment of a human hemangiosarcoma cell line (ISO-HAS). *Int J Cancer,* 81**,** 305-8.

MATESANZ, M. C., FEITO, M. J., ONADERRA, M., RAMIREZ-SANTILLAN, C., DA CASA, C., ARCOS, D., VALLET-REGI, M., ROJO, J. M. & PORTOLES, M. T. 2014. Early in vitro response of macrophages and T lymphocytes to nanocrystalline hydroxyapatites. *J Colloid Interface Sci,* 416**,** 59-66.

MBALAVIELE, G., JAISWAL, N., MENG, A., CHENG, L., VAN DEN BOS, C. & THIEDE, M. 1999. Human mesenchymal stem cells promote human osteoclast differentiation from CD34+ bone marrow hematopoietic progenitors. *Endocrinology,* 140**,** 3736-43.

MCBEATH, R., PIRONE, D. M., NELSON, C. M., BHADRIRAJU, K. & CHEN, C. S. 2004. Cell shape, cytoskeletal tension, and RhoA regulate stem cell lineage commitment. *Dev Cell,* 6**,** 483-95.

MCCOY, R. J. & O'BRIEN, F. J. 2010. Influence of shear stress in perfusion bioreactor cultures for the development of three-dimensional bone tissue constructs: a review. *Tissue Eng Part B Rev,* 16**,** 587-601.

MEDINA, R. J., O'NEILL, C. L., HUMPHREYS, M. W., GARDINER, T. A. & STITT, A. W. 2010. Outgrowth Endothelial Cells: Characterization and Their Potential for Reversing Ischemic Retinopathy. *Investigative Ophthalmology & Visual Science,* 51**,** 5906-5913.

MEDYOUF, H., MOSSNER, M., JANN, J. C., NOLTE, F., RAFFEL, S., HERRMANN, C., LIER, A., EISEN, C., NOWAK, V., ZENS, B., MUDDER, K., KLEIN, C., OBLANDER, J., FEY, S., VOGLER, J., FABARIUS, A., RIEDL, E., ROEHL, H., KOHLMANN, A., STALLER, M., HAFERLACH, C., MULLER, N., JOHN, T., PLATZBECKER, U., METZGEROTH, G., HOFMANN, W. K., TRUMPP, A. & NOWAK, D. 2014. Myelodysplastic cells in patients reprogram mesenchymal stromal cells to establish a transplantable stem cell niche disease unit. *Cell Stem Cell,* 14**,** 824-37.

MELNYK, M., HENKE, T., CLAES, L. & AUGAT, P. 2008. Revascularisation during fracture healing with soft tissue injury. *Arch Orthop Trauma Surg,* 128**,** 1159-65.

MESHER, A. L. 2013. *Junqueira's Basic Histology: Text and Atlas*, McGraw-Hill Education.

MESSMER, U. K., PEREDA-FERNANDEZ, C., MANDERSCHEID, M. & PFEILSCHIFTER, J. 2001. Dexamethasone inhibits TNF-alpha-induced apoptosis and IAP protein downregulation in MCF-7 cells. *Br J Pharmacol,* 133**,** 467-76.

MESSMER, U. K., WINKEL, G., BRINER, V. A. & PFEILSCHIFTER, J. 2000. Suppression of apoptosis by glucocorticoids in glomerular endothelial cells: effects on proapoptotic pathways. *Br J Pharmacol,* 129**,** 1673-83.

MOHAN, R. R., KIM, W. J., MOHAN, R. R., CHEN, L. & WILSON, S. E. 1998. Bone morphogenic proteins 2 and 4 and their receptors in the adult human cornea. *Investigative Ophthalmology & Visual Science,* 39**,** 2626-2636.

MONTESANO, R., VASSALLI, J. D., BAIRD, A., GUILLEMIN, R. & ORCI, L. 1986. Basic Fibroblast Growth-Factor Induces Angiogenesis Invitro. *Proceedings of the National Academy of Sciences of the United States of America,* 83**,** 7297-7301.

MORGAN, E. F., SALISBURY PALOMARES, K. T., GLEASON, R. E., BELLIN, D. L., CHIEN, K. B., UNNIKRISHNAN, G. U. & LEONG, P. L. 2010. Correlations between local strains and tissue phenotypes in an experimental model of skeletal healing. *J Biomech,* 43**,** 2418-24.

MORITANI, S., NEGISHI, K., WATANABE, T., SHUNTO, S., SERIZAWA, N., SUZUKI, M., TAKAHASHI, M., KATAYAMA, S., ISHII, J. & KAWAZU, S. 1991. Glucose-induced production of type IV collagen and laminin P1 from cultured human umbilical vein endothelial cells. *J Diabet Complications,* 5**,** 201-3.

MULLER, A. M., HERMANNS, M. I., SKRZYNSKI, C., NESSLINGER, M., MULLER, K. M. & KIRKPATRICK, C. J. 2002. Expression of the endothelial markers PECAM-1, vWf, and CD34 in vivo and in vitro. *Exp Mol Pathol,* 72**,** 221-9.

MURPHY, M. B., BLASHKI, D., BUCHANAN, R. M., FAN, D., DE ROSA, E., SHAH, R. N., STUPP, S. I., WEINER, B. K., SIMMONS, P. J., FERRARI, M. & TASCIOTTI, E. 2011. Multi-composite bioactive osteogenic sponges featuring mesenchymal stem cells, platelet-rich plasma, nanoporous silicon enclosures, and Peptide amphiphiles for rapid bone regeneration. *J Funct Biomater,* 2**,** 39-66.

MURTHI, P., SO, M., GUDE, N. M., DOHERTY, V. L., BRENNECKE, S. P. & KALIONIS, B. 2007. Homeobox genes are differentially expressed in macrovascular human umbilical vein endothelial cells and microvascular placental endothelial cells. *Placenta,* 28**,** 219-23.

NAKAMURA, M., HIRATAI, R., HENTUNEN, T., SALONEN, J. & YAMASHITA, K. 2016. Hydroxyapatite with High Carbonate Substitutions Promotes Osteoclast Resorption through Osteocyte-like Cells. *ACS Biomaterials Science & Engineering,* 2**,** 259-267.

NAKASHIMA, K., ZHOU, X., KUNKEL, G., ZHANG, Z. P., DENG, J. M., BEHRINGER, R. R. & DE CROMBRUGGHE, B. 2002. The novel zinc finger-containing transcription factor Osterix is required for osteoblast differentiation and bone formation. *Cell,* 108**,** 17-29.

NAKAZATO, H., DEGUCHI, M., FUJIMOTO, M. & FUKUSHIMA, H. 1997. Alkaline phosphatase expression in cultured endothelial cells of aorta and brain microvessels: induction by interleukin-6-type cytokines and suppression by transforming growth factor betas. *Life Science Part 1 Physiology & Pharmacology,* 61**,** 2065-72.

NANDI, A., ESTESS, P. & SIEGELMAN, M. H. 2000. Hyaluronan anchoring and regulation on the surface of vascular endothelial cells is mediated through the functionally active form of CD44. *Journal of Biological Chemistry,* 275**,** 14939-14948.

NARRAVULA, S., LENNON, P. F., MUELLER, B. U. & COLGAN, S. P. 2000. Regulation of endothelial CD73 by adenosine: paracrine pathway for enhanced endothelial barrier function. *J Immunol,* 165**,** 5262-8.

NATARAJAN, V., USATYUK, P. V. & PATTERSON, C. E. 2005. Chapter 4 - Membrane Signaling of Integrity and Acute Activation. *Advances in Molecular and Cell Biology,* 35**,** 105-138.

NAUCK, M., KARAKIULAKIS, G., PERRUCHOUD, A. P., PAPAKONSTANTINOU, E. & ROTH, M. 1998. Corticosteroids inhibit the expression of the vascular endothelial growth factor gene in human vascular smooth muscle cells. *Eur J Pharmacol,* 341**,** 309-15.

NEWTON, C. J., RAN, G., XIE, Y. X., BILKO, D., BURGOYNE, C. H., ADAMS, I., ABIDIA, A., MCCOLLUM, P. T. & ATKIN, S. L. 2002. Statin-induced apoptosis of vascular endothelial cells is blocked by dexamethasone. *J Endocrinol,* 174**,** 7-16.

NEWTON, C. J., RAN, G., XIE, Y. X., BILKO, D., BURGOYNE, C. H., ADAMS, I., ABIDIA, A., MCCOLLUM, P. T. & ATKIN, S. L. 2005. Notice of inadvertent duplicate publication: statin-induced apoptosis of vascular endothelial cells is blocked by dexamethasone. *J Endocrinol,* 187**,** 167.

NG, F., BOUCHER, S., KOH, S., SASTRY, K. S. R., CHASE, L., LAKSHMIPATHY, U., CHOONG, C., YANG, Z., VEMURI, M. C., RAO, M. S. & TANAVDE, V. 2008. PDGF, TGF-beta, and FGF signaling is important for differentiation and growth of mesenchymal stem cells (MSCs): transcriptional

profiling can identify markers and signaling pathways important in differentiation of MSCs into adipogenic, chondrogenic, and osteogenic lineages. *Blood,* 112**,** 295-307.

NISHIZAWA, Y., JONO, S., ISHIMURA, E. & SHIOI, A. 2005. Hyperphosphatemia and vascular calcification in end-stage renal disease. *J Ren Nutr,* 15**,** 178-82.

OLERUD, S. & STROMBERG, L. 1986. Intramedullary reaming and nailing: its early effects on cortical bone vascularization. *Orthopedics,* 9**,** 1204-8.

ORTEGA, N., BEHONICK, D. J. & WERB, Z. 2004. Matrix remodeling during endochondral ossification. *Trends Cell Biol,* 14**,** 86-93.

OZAWA, C. R., BANFI, A., GLAZER, N. L., THURSTON, G., SPRINGER, M. L., KRAFT, P. E., MCDONALD, D. M. & BLAU, H. M. 2004a. Microenvironmental VEGF concentration, not total dose, determines a threshold between normal and aberrant angiogenesis. *J Clin Invest,* 113**,** 516-27.

OZAWA, C. R., BANFI, A., GLAZER, N. L., THURSTON, G., SPRINGER, M. L., KRAFT, P. E., MCDONALD, D. M. & BLAU, H. M. 2004b. Microenvironmental VEGF concentration, not total dose, determines a threshold between normal and aberrant angiogenesis. *Journal of Clinical Investigation,* 113**,** 516-527.

PANSKY, B. 1982. *Review of Embryonic Development*, Macmillan USA.

PAPADIMITROPOULOS, A., SCHERBERICH, A., GUVEN, S., THEILGAARD, N., CROOIJMANS, H. J., SANTINI, F., SCHEFFLER, K., ZALLONE, A. & MARTIN, I. 2011. A 3D in vitro bone organ model using human progenitor cells. *Eur Cell Mater,* 21**,** 445-58; discussion 458.

PAPATHANASOPOULOS, A., KOUROUPIS, D., HENSHAW, K., MCGONAGLE, D., JONES, E. A. & GIANNOUDIS, P. V. 2011. Effects of Antithrombotic Drugs Fondaparinux and Tinzaparin on In Vitro Proliferation and Osteogenic and Chondrogenic Differentiation of Bone-Derived Mesenchymal Stem Cells. *Journal of Orthopaedic Research,* 29**,** 1327-1335.

PARK, D., SPENCER, J. A., KOH, B. I., KOBAYASHI, T., FUJISAKI, J., CLEMENS, T. L., LIN, C. P., KRONENBERG, H. M. & SCADDEN, D. T. 2012. Endogenous bone marrow MSCs are dynamic, fate-restricted participants in bone maintenance and regeneration. *Cell Stem Cell,* 10**,** 259-72.

PASCHOS, N. K., BROWN, W. E., ESWARAMOORTHY, R., HU, J. C. & ATHANASIOU, K. A. 2015. Advances in tissue engineering through stem cell-based co-culture. *Journal of Tissue Engineering and Regenerative Medicine,* 9**,** 488-503.

PEDERSEN, T. O., BLOIS, A. L., XUE, Y., XING, Z., COTTLER-FOX, M., FRISTAD, I., LEKNES, K. N., LORENS, J. B. & MUSTAFA, K. 2012. Osteogenic stimulatory conditions enhance growth and maturation of endothelial cell microvascular networks in culture with mesenchymal stem cells. *J Tissue Eng,* 3**,** 2041731412443236.

PEIFFER, I., EID, P., BARBET, R., LI, M. L., OOSTENDORP, R. A., HAYDONT, V., MONIER, M. N., MILON, L., FORTUNEL, N., CHARBORD, P., TOVEY, M., HATZFELD, J. & HATZFELD, A. 2007. A sub-population of high proliferative potential-quiescent human mesenchymal stem cells is under the reversible control of interferon alpha/beta. *Leukemia,* 21**,** 714-24.

PERCIVAL, C. J. & RICHTSMEIER, J. T. 2013. Angiogenesis and intramembranous osteogenesis. *Dev Dyn,* 242**,** 909-22.

PETERS, K., SCHMIDT, H., UNGER, R. E., OTTO, M., KAMP, G. & KIRKPATRICK, C. J. 2002. Software-supported image quantification of angiogenesis in an in vitro culture system: application to studies of biocompatibility. *Biomaterials,* 23**,** 3413-9.

PETERS, K., UNGER, R. E., STUMPF, S., SCHARFER, J., TSARYK, R., HOFFMANN, B., EISENBARTH, E., BREME, J., ZIEGLER, G. & KIRKPATRICK, C. J. 2008. Cell type-specific aspects in biocompatibility testing: the intercellular contact in vitro as an indicator for endothelial cell compatibility. *Journal of Materials Science-Materials in Medicine,* 19**,** 1637-1644.

PHILLIPS, A. M. 2005. Overview of the fracture healing cascade. *Injury,* 36 Suppl 3**,** S5-7.

PITTENGER, M. F., MACKAY, A. M., BECK, S. C., JAISWAL, R. K., DOUGLAS, R., MOSCA, J. D., MOORMAN, M. A., SIMONETTI, D. W., CRAIG, S. & MARSHAK, D. R. 1999. Multilineage potential of adult human mesenchymal stem cells. *Science,* 284**,** 143-147.

PLOCK, J. A., SCHNIDER, J. T., SOLARI, M. G., ZHENG, X. X. & GORANTLA, V. S. 2013. Perspectives on the use of mesenchymal stem cells in vascularized composite allotransplantation. *Front Immunol,* 4**,** 175.

PLUNKETT, N. & O'BRIEN, F. J. 2011. Bioreactors in tissue engineering. *Technol Health Care,* 19**,** 55-69.

POOLE, A. R., PIDOUX, I. & ROSENBERG, L. 1982. Role of proteoglycans in endochondral ossification: immunofluorescent localization of link protein and proteoglycan monomer in bovine fetal epiphyseal growth plate. *Journal of Cell Biology,* 92**,** 249-60.

PREWITZ, M. C., SEIB, F. P., VON BONIN, M., FRIEDRICHS, J., STISSEL, A., NIEHAGE, C., MULLER, K., ANASTASSIADIS, K., WASKOW, C., HOFLACK, B., BORNHAUSER, M. & WERNER, C. 2013. Tightly anchored tissue-mimetic matrices as instructive stem cell microenvironments. *Nat Methods,* 10**,** 788-94.

PRINS, H. J., BRAAT, A. K., GAWLITTA, D., DHERT, W. J., EGAN, D. A., TIJSSEN-SLUMP, E., YUAN, H., COFFER, P. J., ROZEMULLER, H. & MARTENS, A. C. 2014. In vitro induction of alkaline phosphatase levels predicts in vivo bone forming capacity of human bone marrow stromal cells. *Stem Cell Res,* 12**,** 428-40.

RICHARDSON, S. M., KALAMEGAM, G., PUSHPARAJ, P. N., MATTA, C., MEMIC, A., KHADEMHOSSEINI, A., MOBASHERI, R., POLETTI, F. L., HOYLAND, J. A. & MOBASHERI, A. 2015. Mesenchymal stem cells in regenerative medicine: Focus on articular cartilage and intervertebral disc regeneration. *Methods*.

RISAU, W. & FLAMME, I. 1995. Vasculogenesis. *Annu Rev Cell Dev Biol,* 11**,** 73-91.

RIZZINO, A., KAZAKOFF, P., RUFF, E., KUSZYNSKI, C. & NEBELSICK, J. 1988. Regulatory effects of cell density on the binding of transforming growth factor beta, epidermal growth factor, platelet-derived growth factor, and fibroblast growth factor. *Cancer Res,* 48**,** 4266-71.

ROCCIO, M., SCHMITTER, D., KNOBLOCH, M., OKAWA, Y., SAGE, D. & LUTOLF, M. P. 2013. Predicting stem cell fate changes by differential cell cycle progression patterns. *Development,* 140**,** 459-70.

RODRIGUEZ, J. P., GONZALEZ, M., RIOS, S. & CAMBIAZO, V. 2004. Cytoskeletal organization of human mesenchymal stem cells (MSC) changes during their osteogenic differentiation. *Journal of Cellular Biochemistry,* 93**,** 721-731.

ROMERO, I. A., RADEWICZ, K., JUBIN, E., MICHEL, C. C., GREENWOOD, J., COURAUD, P. O. & ADAMSON, P. 2003. Changes in cytoskeletal and tight junctional proteins correlate with decreased permeability induced by dexamethasone in cultured rat brain endothelial cells. *Neurosci Lett,* 344**,** 112-6.

ROUSSEAU, G. G. & BAXTER, J. D. 1979. Glucocorticoid receptors. *Monogr Endocrinol,* 12**,** 49-77.

ROUSSEAU, G. G., HIGGINS, S. J., BAXTER, J. D., GELFAND, D. & TOMKINS, G. M. 1975. Binding of glucocorticoid receptors to DNA. *J Biol Chem,* 250**,** 6015-21.

ROUWKEMA, J., RIVRON, N. C. & VAN BLITTERSWIJK, C. A. 2008. Vascularization in tissue engineering. *Trends in Biotechnology,* 26**,** 434-441.

SAALBACH, A., WETZIG, T., HAUSTEIN, U. F. & ANDEREGG, U. 1999. Detection of human soluble Thy-1 in serum by ELISA. Fibroblasts and activated endothelial cells are a possible source of soluble Thy-1 in serum. *Cell Tissue Res,* 298**,** 307-15.

SADR, N., PIPPENGER, B. E., SCHERBERICH, A., WENDT, D., MANTERO, S., MARTIN, I. & PAPADIMITROPOULOS, A. 2012. Enhancing the biological performance of synthetic polymeric materials by decoration with engineered, decellularized extracellular matrix. *Biomaterials,* 33**,** 5085-93.

SAKAGUCHI, Y., SEKIYA, I., YAGISHITA, K., ICHINOSE, S., SHINOMIYA, K. & MUNETA, T. 2004. Suspended cells from trabecular bone by collagenase digestion become virtually identical to mesenchymal stem cells obtained from marrow aspirates. *Blood,* 104**,** 2728-35.

SALEH, F. A., WHYTE, M. & GENEVER, P. G. 2011. Effects of endothelial cells on human mesenchymal stem cell activity in a three-dimensional in vitro model. *Eur Cell Mater,* 22**,** 242-57; discussion 257.

SALVADOR, E., SHITYAKOV, S. & FORSTER, C. 2014. Glucocorticoids and endothelial cell barrier function. *Cell Tissue Res,* 355**,** 597-605.

SAMMONS, J., AHMED, N., EL-SHEEMY, M. & HASSAN, H. T. 2004. The role of BMP-6, IL-6, and BMP-4 in mesenchymal stem cell-dependent bone development: effects on osteoblastic differentiation induced by parathyroid hormone and vitamin D(3). *Stem Cells and Development,* 13**,** 273-80.

SANTOS, M. I., FUCHS, S., GOMES, M. E., UNGER, R. E., REIS, R. L. & KIRKPATRICK, C. J. 2007. Response of micro- and macrovascular endothelial cells to starch-based fiber meshes for bone tissue engineering. *Biomaterials,* 28**,** 240-8.

SANTOS, M. I., UNGER, R. E., SOUSA, R. A., REIS, R. L. & KIRKPATRICK, C. J. 2009. Crosstalk between osteoblasts and endothelial cells co-cultured on a polycaprolactone-starch scaffold and the in vitro development of vascularization. *Biomaterials,* 30**,** 4407-4415.

SCHACK, L. M., NOACK, S., WINKLER, R., WISSMANN, G., BEHRENS, P., WELLMANN, M., JAGODZINSKI, M., KRETTEK, C. & HOFFMANN, A. 2013. The Phosphate Source Influences Gene Expression and Quality of Mineralization during Osteogenic Differentiation of Human Mesenchymal Stem Cells. *PLoS One,* 8**,** e65943.

SCHLUESENER, H. J. & MEYERMANN, R. 1995. Immunolocalization of BMP-6, a novel TGF-beta-related cytokine, in normal and atherosclerotic smooth muscle cells. *Atherosclerosis,* 113**,** 153-6.

SCHNEIDER, R. K., PUELLEN, A., KRAMANN, R., RAUPACH, K., BORNEMANN, J., KNUECHEL, R., PEREZ-BOUZA, A. & NEUSS, S. 2010. The osteogenic differentiation of adult bone marrow and perinatal umbilical mesenchymal stem cells and matrix remodelling in three-dimensional collagen scaffolds. *Biomaterials,* 31**,** 467-80.

SCHUBERT, T., XHEMA, D., VERITER, S., SCHUBERT, M., BEHETS, C., DELLOYE, C., GIANELLO, P. & DUFRANE, D. 2011. The enhanced performance of bone allografts using osteogenic-differentiated adipose-derived mesenchymal stem cells. *Biomaterials,* 32**,** 8880-8891.

SCHULTZ, G. S. & WYSOCKI, A. 2009. Interactions between extracellular matrix and growth factors in wound healing. *Wound Repair and Regeneration,* 17**,** 153-162.

SCOTTI, C., TONNARELLI, B., PAPADIMITROPOULOS, A., SCHERBERICH, A., SCHAEREN, S., SCHAUERTE, A., LOPEZ-RIOS, J., ZELLER, R., BARBERO, A. & MARTIN, I. 2010. Recapitulation of endochondral bone formation using human adult mesenchymal stem cells as a paradigm for developmental engineering. *Proceedings of the National Academy of Sciences of the United States of America,* 107**,** 7251-7256.

SETON-ROGERS, S. 2013. Microenvironment: an accommodating host. *Nat Rev Cancer,* 13**,** 145.

SHIM, S. H., HAH, J. H., HWANG, S. Y., HEO, D. S. & SUNG, M. W. 2010. Dexamethasone treatment inhibits VEGF production via suppression of STAT3 in a head and neck cancer cell line. *Oncol Rep,* 23**,** 1139-43.

SHIN, V., ZEBBOUDJ, A. F. & BOSTROM, K. 2004. Endothelial cells modulate osteogenesis in calcifying vascular cells. *J Vasc Res,* 41**,** 193-201.

SHING, Y., FOLKMAN, J., SULLIVAN, R., BUTTERFIELD, C., MURRAY, J. & KLAGSBRUN, M. 1984. Heparin affinity: purification of a tumor-derived capillary endothelial cell growth factor. *Science,* 223**,** 1296-9.

SHUM, L. & NUCKOLLS, G. 2002. The life cycle of chondrocytes in the developing skeleton. *Arthritis Res,* 4**,** 94-106.

SIEMERINK, M. J., KLAASSEN, I., VOGELS, I. M., GRIFFIOEN, A. W., VAN NOORDEN, C. J. & SCHLINGEMANN, R. O. 2012. CD34 marks angiogenic tip cells in human vascular endothelial cell cultures. *Angiogenesis,* 15**,** 151-63.

SIKAVITSAS, V. I., BANCROFT, G. N., HOLTORF, H. L., JANSEN, J. A. & MIKOS, A. G. 2003. Mineralized matrix deposition by marrow stromal osteoblasts in 3D perfusion culture increases with increasing fluid shear forces. *Proceedings of the National Academy of Sciences of the United States of America,* 100**,** 14683-14688.

SORESCU, G. P., SONG, H., TRESSEL, S. L., HWANG, J., DIKALOV, S., SMITH, D. A., BOYD, N. L., PLATT, M. O., LASSEGUE, B., GRIENDLING, K. K. & JO, H. 2004. Bone morphogenic protein 4 produced in endothelial cells by oscillatory shear stress induces monocyte adhesion by stimulating reactive oxygen species production from a nox1-based NADPH oxidase. *Circ Res,* 95**,** 773-9.

SORESCU, G. P., SYKES, M., WEISS, D., PLATT, M. O., SAHA, A., HWANG, J., BOYD, N., BOO, Y. C., VEGA, J. D., TAYLOR, W. R. & JO, H. 2003. Bone morphogenic protein 4 produced in endothelial cells by oscillatory shear stress stimulates an inflammatory response. *J Biol Chem,* 278**,** 31128-35.

STAHL, A., WENGER, A., WEBER, H., STARK, G. B., AUGUSTIN, H. G. & FINKENZELLER, G. 2004. Bi-directional cell contact-dependent regulation of gene expression between endothelial cells and osteoblasts in a three-dimensional spheroidal coculture model. *Biochemical and Biophysical Research Communications,* 322**,** 684-692.

STAUM, B. B., HAMBURGER, R. J. & GOLDBERG, M. 1972. Tracer microinjection study of renal tubular phosphate reabsorption in the rat. *J Clin Invest,* 51**,** 2271-6.

STENDERUP, K., JUSTESEN, J., CLAUSEN, C. & KASSEM, M. 2003. Aging is associated with decreased maximal life span and accelerated senescence of bone marrow stromal cells. *Bone,* 33**,** 919-926.

STERNBERG, S. R. 1983. Biomedical Image-Processing. *Computer,* 16**,** 22-34.

STERNECKERT, J. L., REINHARDT, P. & SCHOLER, H. R. 2014. Investigating human disease using stem cell models. *Nat Rev Genet,* 15**,** 625-39.

STEVENS, M. M. 2008. Biomaterials for bone tissue engineering. *Materials Today,* 11**,** 18-25.

STRAUSS, S., DUDZIAK, S., HAGEMANN, R., BARCIKOWSKI, S., FLIESS, M., ISRAELOWITZ, M., KRACHT, D., KUHBIER, J. W., RADTKE, C., REIMERS, K. & VOGT, P. M. 2012. Induction of osteogenic differentiation of adipose derived stem cells by microstructured nitinol actuator-mediated mechanical stress. *PLoS One,* 7**,** e51264.

SUGITA, D., YAYAMA, T., UCHIDA, K., KOKUBO, Y., NAKAJIMA, H., YAMAGISHI, A., TAKEURA, N. & BABA, H. 2013. Indian hedgehog signaling promotes chondrocyte differentiation in enchondral ossification in human cervical ossification of the posterior longitudinal ligament. *Spine (Phila Pa 1976),* 38**,** E1388-96.

SULLIVAN, D. H., CARTER, W. J., WARR, W. R. & WILLIAMS, L. H. 1998. Side effects resulting from the use of growth hormone and insulin-like growth factor-I as combined therapy to frail elderly patients. *J Gerontol A Biol Sci Med Sci,* 53**,** M183-7.

SUN, L., PARKER, S. T., SYOJI, D., WANG, X. L., LEWIS, J. A. & KAPLAN, D. L. 2012. Direct-Write Assembly of 3D Silk/Hydroxyapatite Scaffolds for Bone Co-Cultures. *Advanced Healthcare Materials,* 1**,** 729-735.

SUZUKI, F., TAKASE, T., TAKIGAWA, M., UCHIDA, A. & SHIMOMURA, Y. 1981. Simulation of the initial stage of endochondral ossification: in vitro sequential culture of growth cartilage cells and bone marrow cells. *Proc Natl Acad Sci U S A,* 78**,** 2368-72.

SWIFT, J., IVANOVSKA, I. L., BUXBOIM, A., HARADA, T., DINGAL, P. C., PINTER, J., PAJEROWSKI, J. D., SPINLER, K. R., SHIN, J. W., TEWARI, M., REHFELDT, F., SPEICHER, D. W. & DISCHER, D. E. 2013. Nuclear lamin-A scales with tissue stiffness and enhances matrix-directed differentiation. *Science,* 341**,** 1240104.

TAKAHASHI, Y., YAMAMOTO, M. & TABATA, Y. 2005. Osteogenic differentiation of mesenchymal stem cells in biodegradable sponges composed of gelatin and beta-tricalcium phosphate. *Biomaterials,* 26**,** 3587-96.

TENENBAUM, H. C. & HEERSCHE, J. N. 1982. Differentiation of osteoblasts and formation of mineralized bone in vitro. *Calcif Tissue Int,* 34**,** 76-9.

THEIN-HAN, W. & XU, H. H. 2013. Prevascularization of a gas-foaming macroporous calcium phosphate cement scaffold via coculture of human umbilical vein endothelial cells and osteoblasts. *Tissue Eng Part A,* 19**,** 1675-85.

THIBAULT, R. A., MIKOS, A. G. & KASPER, F. K. 2011. Protein and mineral composition of osteogenic extracellular matrix constructs generated with a flow perfusion bioreactor. *Biomacromolecules,* 12**,** 4204-12.

THOMPSON, T. J., OWENS, P. D. & WILSON, D. J. 1989. Intramembranous osteogenesis and angiogenesis in the chick embryo. *J Anat,* 166**,** 55-65.

TOMINAGA, K. 2015. The emerging role of senescent cells in tissue homeostasis and pathophysiology. *Pathobiol Aging Age Relat Dis,* 5**,** 27743.

TRIVANOVIC, D., KOCIC, J., MOJSILOVIC, S., KRSTIC, A., ILIC, V., DJORDJEVIC, I. O., SANTIBANEZ, J. F., JOVCIC, G., TERZIC, M. & BUGARSKI, D. 2013. Mesenchymal stem cells isolated from peripheral blood and umbilical cord Wharton's jelly. *Srp Arh Celok Lek,* 141**,** 178-86.

TSAI, M. T., LI, W. J., TUAN, R. S. & CHANG, W. H. 2009. Modulation of osteogenesis in human mesenchymal stem cells by specific pulsed electromagnetic field stimulation. *Journal of Orthopaedic Research,* 27**,** 1169-74.

TU, X., JOENG, K. S. & LONG, F. 2012. Indian hedgehog requires additional effectors besides Runx2 to induce osteoblast differentiation. *Dev Biol,* 362**,** 76-82.

UNGER, R. E., DOHLE, E. & KIRKPATRICK, C. J. 2015. Improving vascularization of engineered bone through the generation of pro-angiogenic effects in co-culture systems. *Adv Drug Deliv Rev,* 94**,** 116-25.

UNGER, R. E., GHANAATI, S., ORTH, C., SARTORIS, A., BARBECK, M., HALSTENBERG, S., MOTTA, A., MIGLIARESI, C. & KIRKPATRICK, C. J. 2010. The rapid anastomosis between prevascularized networks on silk fibroin scaffolds generated in vitro with cocultures of human microvascular endothelial and osteoblast cells and the host vasculature. *Biomaterials,* 31**,** 6959-67.

UNGER, R. E., KRUMP-KONVALINKOVA, V., PETERS, K. & KIRKPATRICK, C. J. 2002. In vitro expression of the endothelial phenotype: comparative study of primary isolated cells and cell lines, including the novel cell line HPMEC-ST1.6R. *Microvasc Res,* 64**,** 384-97.

UNGER, R. E., PETERS, K., HUANG, Q., FUNK, A., PAUL, D. & KIRKPATRICK, C. J. 2005. Vascularization and gene regulation of human endothelial cells growing on porous polyethersulfone (PES) hollow fiber membranes. *Biomaterials,* 26**,** 3461-9.

UNGER, R. E., PETERS, K., WOLF, M., MOTTA, A., MIGLIARESI, C. & KIRKPATRICK, C. J. 2004. Endothelialization of a non-woven silk fibroin net for use in tissue engineering: growth and gene regulation of human endothelial cells. *Biomaterials,* 25**,** 5137-46.

UNGER, R. E., SARTORIS, A., PETERS, K., MOTTA, A., MIGLIARESI, C., KUNKEL, M., BULNHEIM, U., RYCHLY, J. & KIRKPATRICK, C. J. 2007. Tissue-like self-assembly in cocultures of endothelial cells and osteoblasts and the formation of microcapillary-like structures on three-dimensional porous biomaterials. *Biomaterials,* 28**,** 3965-76.

VAN BEEM, R. T., VERLOOP, R. E., KLEIJER, M., NOORT, W. A., LOOF, N., KOOLWIJK, P., VAN DER SCHOOT, C. E., VAN HINSBERGH, V. W. & ZWAGINGA, J. J. 2009. Blood outgrowth endothelial cells from cord blood and peripheral blood: angiogenesis-related characteristics in vitro. *Journal of Thrombosis and Haemostasis,* 7**,** 217-26.

VANSTRAALEN, J. P., SANDERS, E., PRUMMEL, M. F. & SANDERS, G. T. B. 1991. Bone-Alkaline Phosphatase as Indicator of Bone-Formation. *Clinica Chimica Acta,* 201**,** 27-34.

VERMES, I., HAANEN, C., STEFFENSNAKKEN, H. & REUTELINGSPERGER, C. 1995. A Novel Assay for Apoptosis - Flow Cytometric Detection of Phosphatidylserine Expression on Early Apoptotic Cells Using Fluorescein-Labeled Annexin-V. *Journal of Immunological Methods,* 184**,** 39-51.

VERSEIJDEN, F., POSTHUMUS-VAN SLUIJS, S. J., VAN NECK, J. W., HOFER, S. O., HOVIUS, S. E. & VAN OSCH, G. J. 2012. Vascularization of prevascularized and non-prevascularized fibrin-based human adipose tissue constructs after implantation in nude mice. *J Tissue Eng Regen Med,* 6**,** 169-78.

VOLPERT, O. V., STELLMACH, V. & BOUCK, N. 1995. The modulation of thrombospondin and other naturally occurring inhibitors of angiogenesis during tumor progression. *Breast Cancer Res Treat,* 36**,** 119-26.

WALLACE, A. L., DRAPER, E. R., STRACHAN, R. K., MCCARTHY, I. D. & HUGHES, S. P. 1994. The vascular response to fracture micromovement. *Clin Orthop Relat Res***,** 281-90.

WANG, C., WANG, Y., MENG, H. Y., YUAN, X. L., XU, X. L., WANG, A. Y., GUO, Q. Y., PENG, J. & LU, S. B. 2015. Application of bone marrow mesenchymal stem cells to the treatment of osteonecrosis of the femoral head. *Int J Clin Exp Med,* 8**,** 3127-35.

WANG, R. N., GREEN, J., WANG, Z., DENG, Y., QIAO, M., PEABODY, M., ZHANG, Q., YE, J., YAN, Z., DENDULURI, S., IDOWU, O., LI, M., SHEN, C., HU, A., HAYDON, R. C., KANG, R., MOK, J., LEE, M. J., LUU, H. L. & SHI, L. L. 2014. Bone Morphogenetic Protein (BMP) signaling in development and human diseases. *Genes Dis,* 1**,** 87-105.

WATSON, L., ELLIMAN, S. J. & COLEMAN, C. M. 2014. From isolation to implantation: a concise review of mesenchymal stem cell therapy in bone fracture repair. *Stem Cell Res Ther,* 5**,** 51.

WENDT, D., MARSANO, A., JAKOB, M., HEBERER, M. & MARTIN, I. 2003. Oscillating perfusion of cell suspensions through three-dimensional scaffolds enhances cell seeding efficiency and uniformity. *Biotechnology and Bioengineering,* 84**,** 205-214.

WENGER, A., STAHL, A., WEBER, H., FINKENZELLER, G., AUGUSTIN, H. G., STARK, G. B. & KNESER, U. 2004. Modulation of in vitro angiogenesis in a three-dimensional spheroidal coculture model for bone tissue engineering. *Tissue Eng,* 10**,** 1536-47.

WETZEL, A., WETZIG, T., HAUSTEIN, U. F., STICHERLING, M., ANDEREGG, U., SIMON, J. C. & SAALBACH, A. 2006. Increased neutrophil adherence in psoriasis: role of the human endothelial cell receptor Thy-1 (CD90). *J Invest Dermatol,* 126**,** 441-52.

WHITE, J. & DALTON, S. 2005. Cell cycle control of embryonic stem cells. *Stem Cell Rev,* 1**,** 131-8.

WILLETTE, R. N., GU, J. L., LYSKO, P. G., ANDERSON, K. M., MINEHART, H. & YUE, T. L. 1999. BMP-2 gene expression and effects on human vascular smooth muscle cells. *Journal of Vascular Research,* 36**,** 120-125.

WU, A. C., RAGGATT, L. J., ALEXANDER, K. A. & PETTIT, A. R. 2013. Unraveling macrophage contributions to bone repair. *Bonekey Rep,* 2**,** 373.

WU, Q., ZHU, M., ROSIER, R. N., ZUSCIK, M. J., O'KEEFE, R. J. & CHEN, D. 2010. Beta-catenin, cartilage, and osteoarthritis. *Ann N Y Acad Sci,* 1192**,** 344-50.

WU, W. S., WANG, F. S., YANG, K. D., HUANG, C. C. & KUO, Y. R. 2006. Dexamethasone induction of keloid regression through effective suppression of VEGF expression and keloid fibroblast proliferation. *Journal of Investigative Dermatology,* 126**,** 1264-1271.

YANO, A., FUJII, Y., IWAI, A., KAGEYAMA, Y. & KIHARA, K. 2006. Glucocorticoids suppress tumor angiogenesis and in vivo growth of prostate cancer cells. *Clin Cancer Res,* 12**,** 3003-9.

YOUNG, I. D., AILLES, L., NARINDRASORASAK, S., TAN, R. & KISILEVSKY, R. 1992. Localization of the basement membrane heparan sulfate proteoglycan in islet amyloid deposits in type II diabetes mellitus. *Arch Pathol Lab Med,* 116**,** 951-4.

YOUREK, G., MCCORMICK, S. M., MAO, J. J. & REILLY, G. C. 2010. Shear stress induces osteogenic differentiation of human mesenchymal stem cells. *Regen Med,* 5**,** 713-24.

YOUSEFI, A. M., JAMES, P. F., AKBARZADEH, R., SUBRAMANIAN, A., FLAVIN, C. & OUDADESSE, H. 2016. Prospect of Stem Cells in Bone Tissue Engineering: A Review. *Stem Cells Int,* 2016**,** 6180487.

YUAN, Y. S. & RIGOR, R. R. 2011. *Regulation of Endothelial Barrier Function*, Morgan & Claypool Life Sciences.

ZHANG, L., ZHAO, Y. H., GUAN, Z., YE, J. S., DE ISLA, N. & STOLTZ, J. F. 2015. Application potential of mesenchymal stem cells derived from Wharton's jelly in liver tissue engineering. *Biomed Mater Eng,* 25**,** 137-43.

ZHANG, W., YANG, N. & SHI, X. M. 2008. Regulation of mesenchymal stem cell osteogenic differentiation by glucocorticoid-induced leucine zipper (GILZ). *J Biol Chem,* 283**,** 4723-9.

ZHOU, G., ZHENG, Q., ENGIN, F., MUNIVEZ, E., CHEN, Y., SEBALD, E., KRAKOW, D. & LEE, B. 2006. Dominance of SOX9 function over RUNX2 during skeletogenesis. *Proc Natl Acad Sci U S A,* 103**,** 19004-9.

ZWERSCHKE, W., MAZUREK, S., STOCKL, P., HUTTER, E., EIGENBRODT, E. & JANSEN-DURR, P. 2003. Metabolic analysis of senescent human fibroblasts reveals a role for AMP in cellular senescence. *Biochemical Journal,* 376**,** 403-11.

12 Appendix

Supplementary Table 1: Exemplary raw data for the impact of addition or exclusion of osteogenic supplements, angiogenic supplements (heparin+bFGF) and the concentration of FCS on the formation of vascular structures represented by the vascular area

Donor	Osteogenic Supplements	FCS [%]	Heparin + bFGF	Vascular Area
1	-	10	-	1,2
	+	10	-	0
	-	15	-	0
	+	15	-	0
	-	10	+	4,08
	+	10	+	0
	-	15	+	6
	+	15	+	0
2	-	10	-	0,83
	+	10	-	1,25
	-	15	-	1,81
	+	15	-	0,4
	-	10	+	5,99
	+	10	+	0
	-	15	+	4,19
	+	15	+	0
3	-	10	-	0
	+	10	-	0
	-	15	-	0,74
	+	15	-	0
	-	10	+	4,68
	+	10	+	0
	-	15	+	3,69
	+	15	+	0

Supplementary Table 2: Summary of raw data shown in Supplementary Table 1 sorted according to the variation of the FCS concentration

Summary Vascular Area VA [mm^2/cm^2]	
FCS (10 %)	**FCS (15 %)**
1,2	0
0	0
4,08	6
0	0
0,83	1,81
1,25	0,4
5,99	4,19
0	0
0	0,74
0	0
4,68	3,69
0	0

Supplementary Table 3: ANOVA single factor analysis of variance performed in Microsoft EXCEL on the data for vascular area shown in Supplementary Table 2

Summary

Groups	*Number*	*Sum*	*Mean*	*Variance*
Column 1	12	18,03	1,50	4,64
Column 2	12	16,83	1,40	4,32

ANOVA	*Sum of Squares (SS)*	*Degrees of freedom (df)*	*Mean SS (MS)*	*test statistic (TS)*	*p-value*	F_{crit}
Difference between groups	0,06	1	0,06	0,013	0,90	4,30
Difference within groups	98,58	22	4,48			
Total	98,64	23				

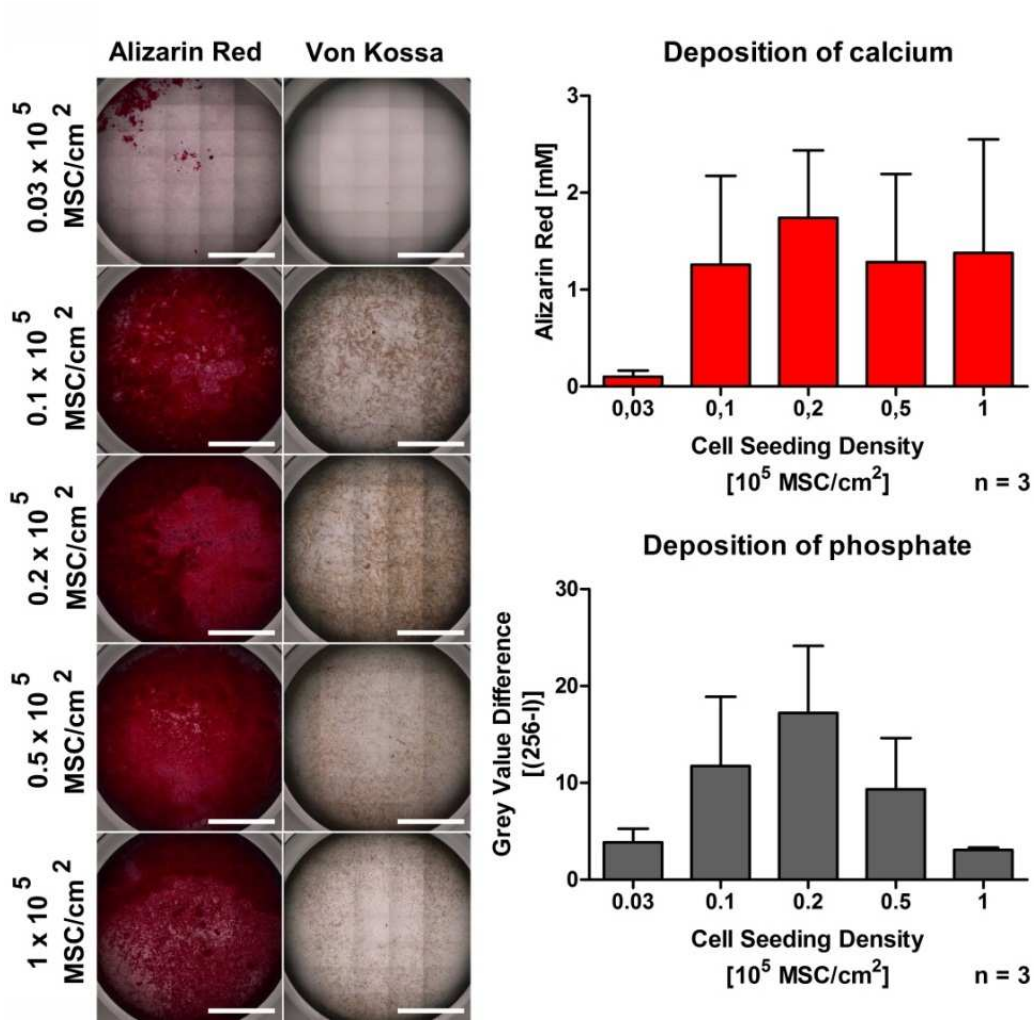

Supplementary Figure 1: Influence of the cell seeding density (CSD) on the osteogenic differentiation of MSC A: Microscopic evaluation of osteogenesis in MSC by Alizarin Red staining (calcium deposition) and von Kossa staining (phosphate deposition), Scale bars: 5 mm; B: Quantification of Alizarin Red staining in samples shown in A; C: Image-based quantification of von Kossa stainings shown in A

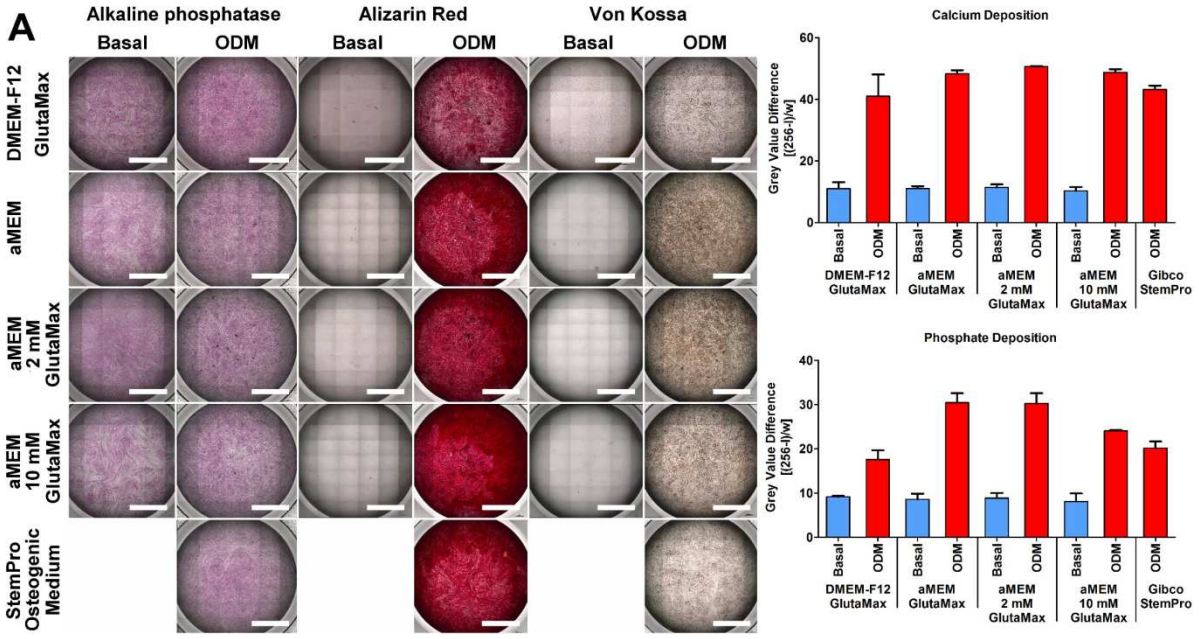

Supplementary Figure 2: Influence of the basic medium in ODM on the osteogenic differentiation of MSC after 4W. A: Osteogenesis in each medium without (Basal) or with addition of osteogenic supplements (ODM) characterized by alkaline phosphatase activity staining, Alizarin Red staining (calcium deposition) and von Kossa staining (phosphate deposition), Scale bars: 5 mm; B: Image-based quantification of calcium deposition in media screened in A; C: Image-based quantification of phosphate deposition in media screened in A

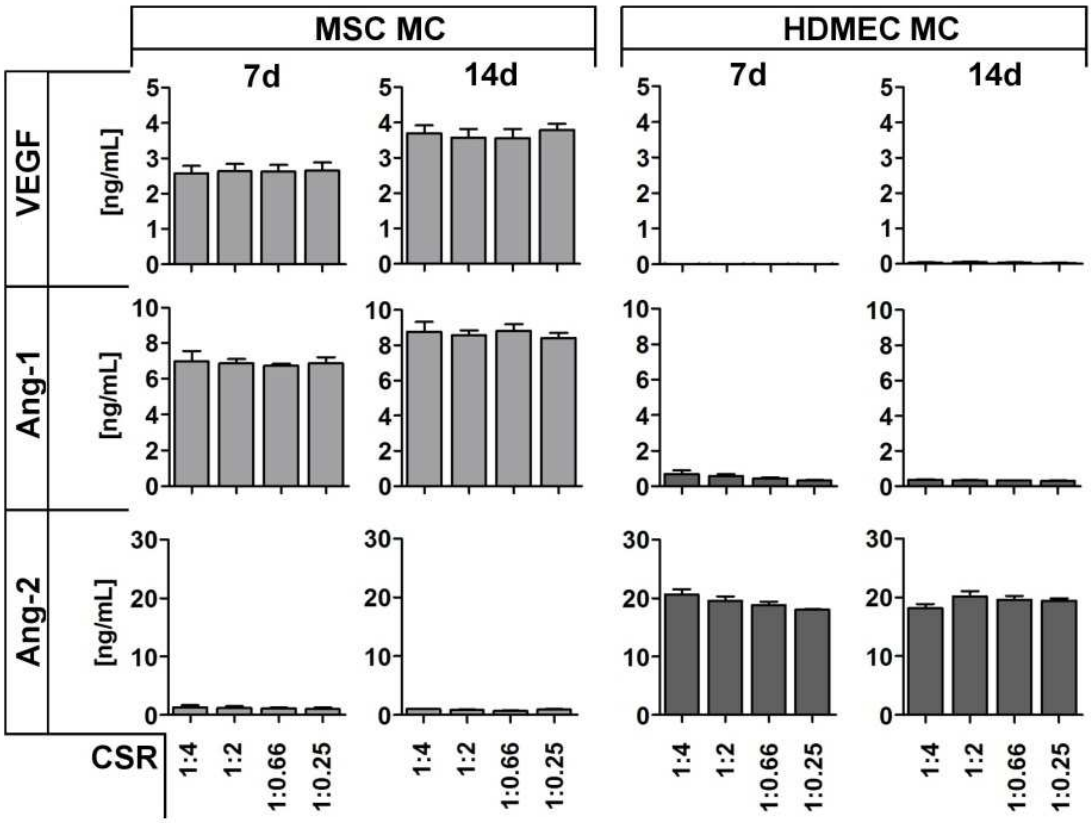

Supplementary Figure 3: CSR-dependent quantification of VEGF, Ang-1 and Ang-2 in mono-cultures of MSC (MSC MC) and HDMEC (HDMEC MC) after 7d and 14d of cultivation in ECGM

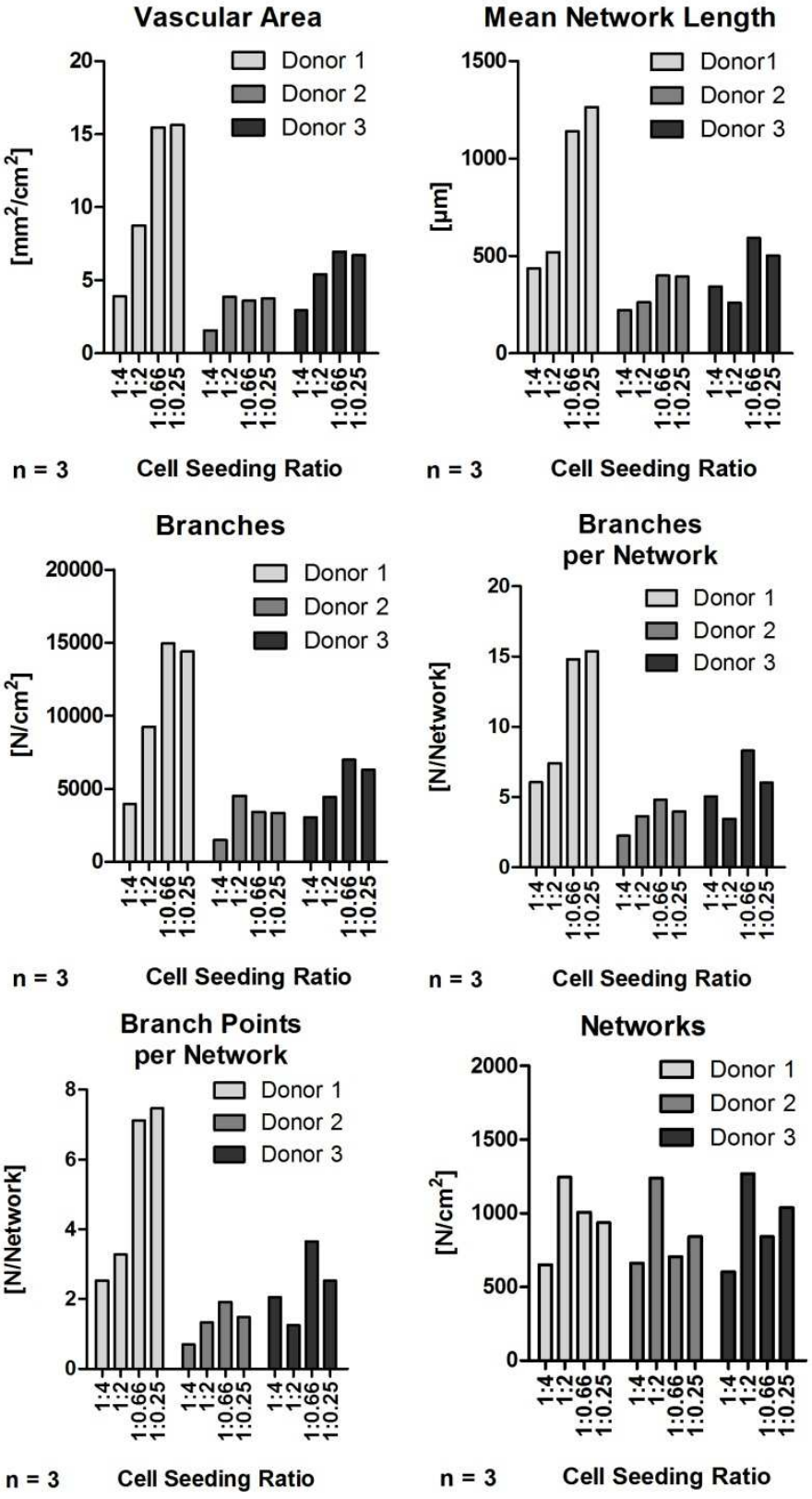

Supplementary Figure 4: Single donor quantification according to Figure 15B: Image-based quantification of CSR-dependent tube-formation and comparison of angiogenesis-related parameters in MSC/HDMEC co-cultures using varying CSR

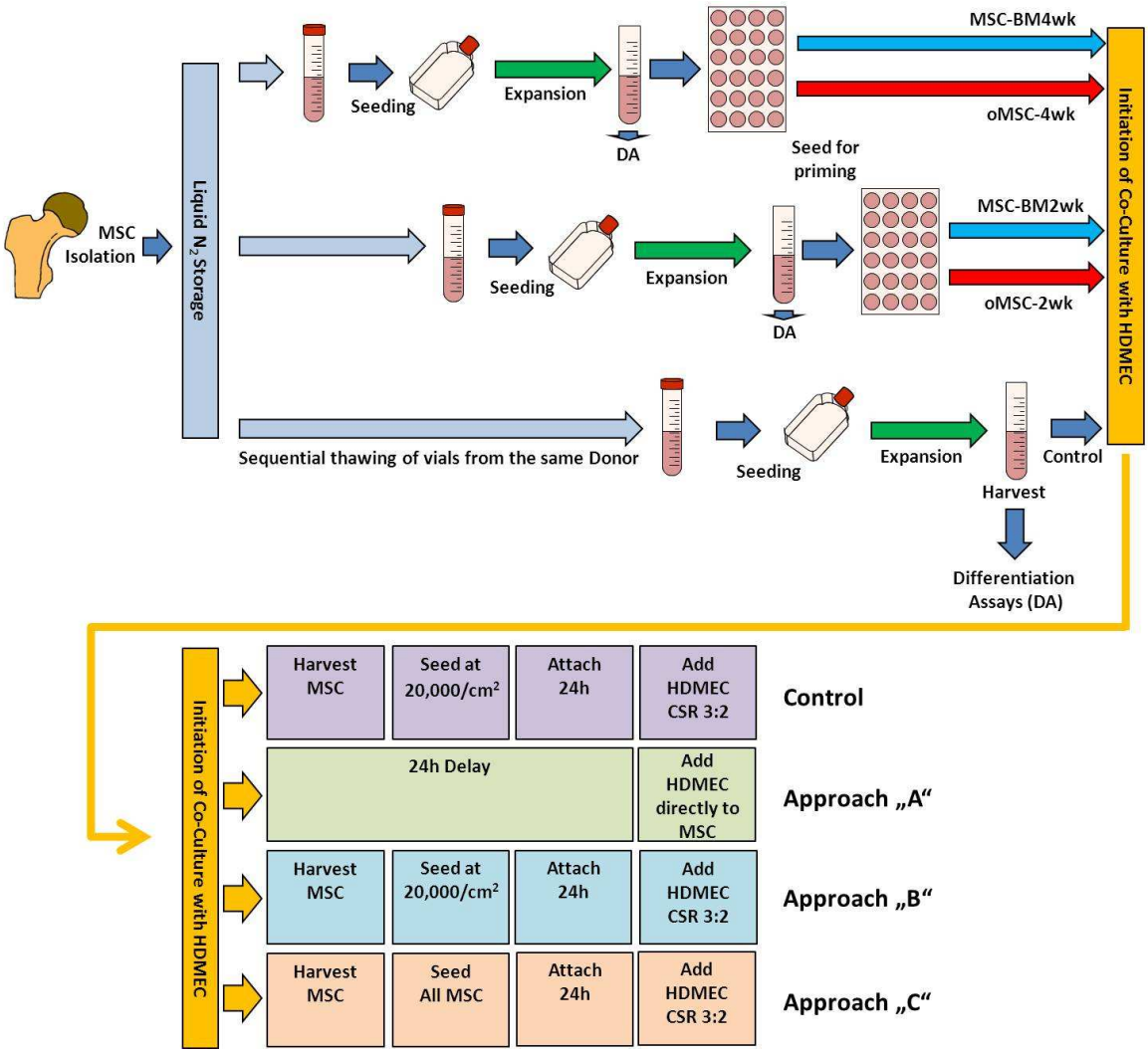

Supplementary Figure 5: Schematic representation of the workflow for the generation of MSC-BM2wk, oMSC-2wk, MSC-BM4wk and oMSC-4wk used to investigate the influence of osteogenic priming of the MSC on the prevascularization in various CC set-ups (approaches) with HDMEC described in Figure 23

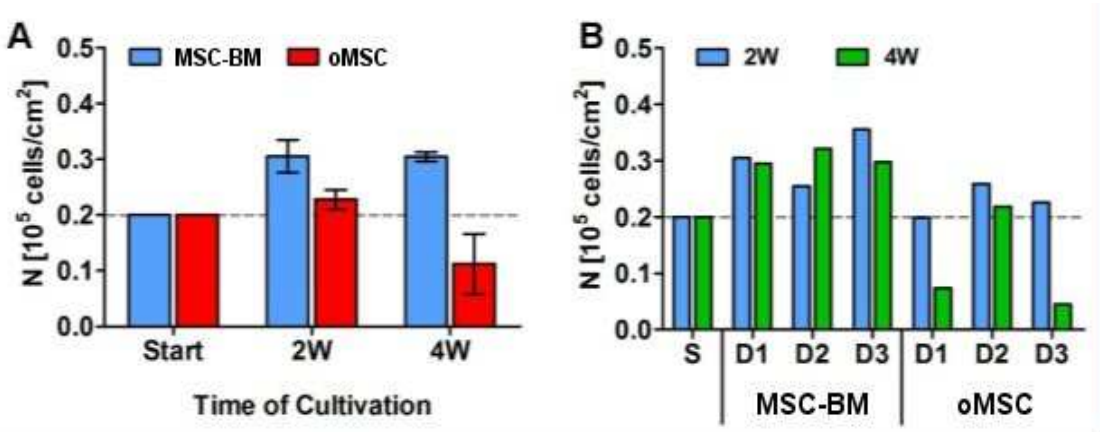

Supplementary Figure 6: Determination of cell numbers in noMSC and oMSC after 2W and 4W of cultivation in non-osteogenic medium and osteogenic medium, respectively; A: Values shown as means of three biological replicates; B: Cell numbers shown on the single donor level; Grey line indicates the initial CSD; S: Start of experiment; D1: Donor 1, D2: Donor 2; D3: Donor 3

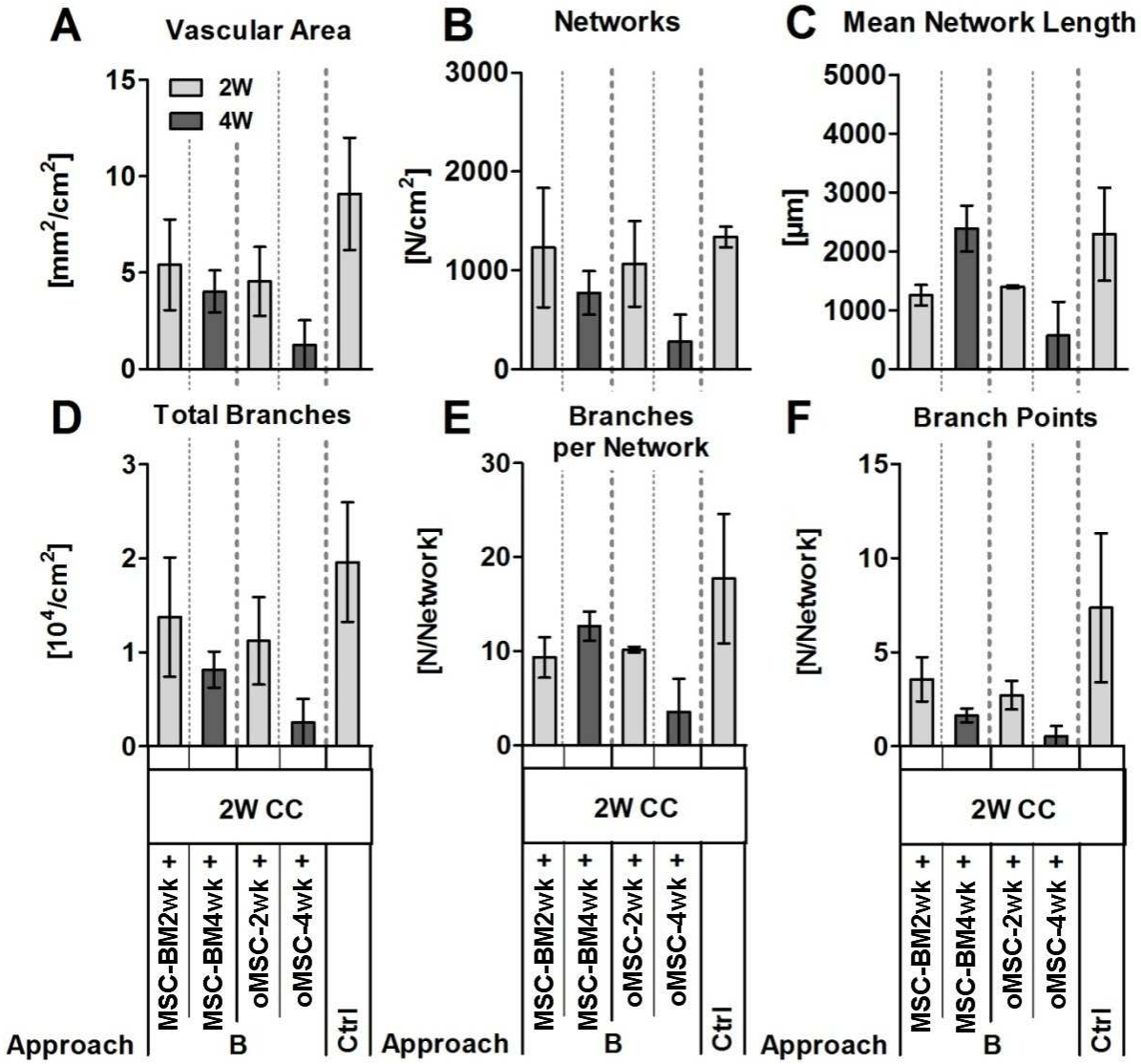

Supplementary Figure 7: Influence of MSC-BM and oMSC in 2wk CC with HDMEC (Approach B) on the formation and quantification of vessel-like structures. Vasculogenesis and angiogenesis are characterized by the image-based quantification of the "Vascular area" (A), the number of "Networks" (B), the "Mean Network Length" (C), the total number of branches ("Total Branches, (D)), the number of "Branches per Network" (E), and the number of "Branch Points" per network (F); Approach: indicates the type of CC according to scheme in Figure 23

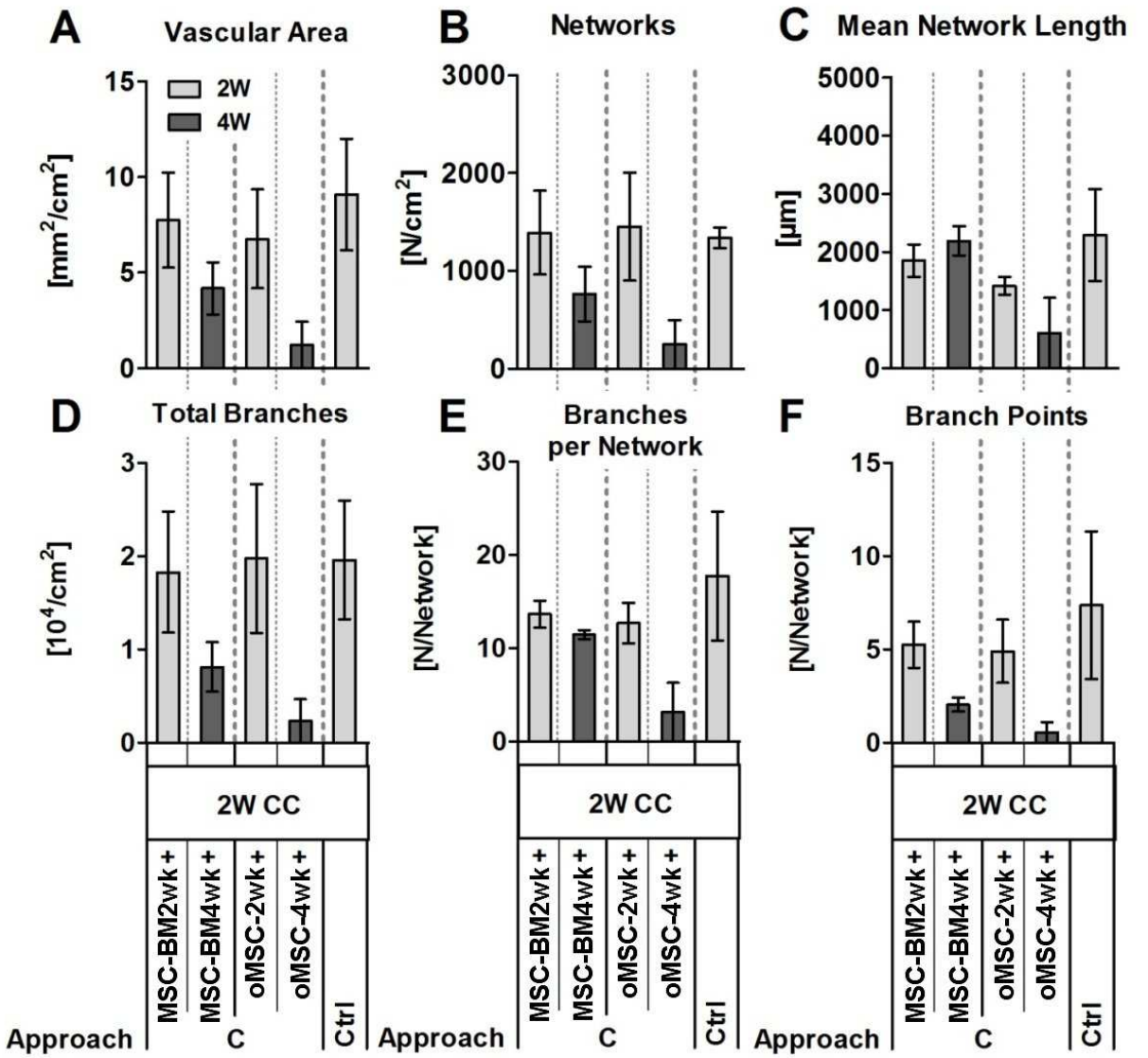

Supplementary Figure 8: Influence of MSC-BM and oMSC in 2wk CC with HDMEC (Approach C) on the formation and quantification of vessel-like structures. Vasculogenesis and angiogenesis are characterized by the image-based quantification of the "Vascular area" (A), the number of "Networks" (B), the "Mean Network Length" (C), the total number of branches ("Total Branches, (D)), the number of "Branches per Network" (E), and the number of "Branch Points" per network (F); Approach: indicates the type of CC according to scheme in Figure 23

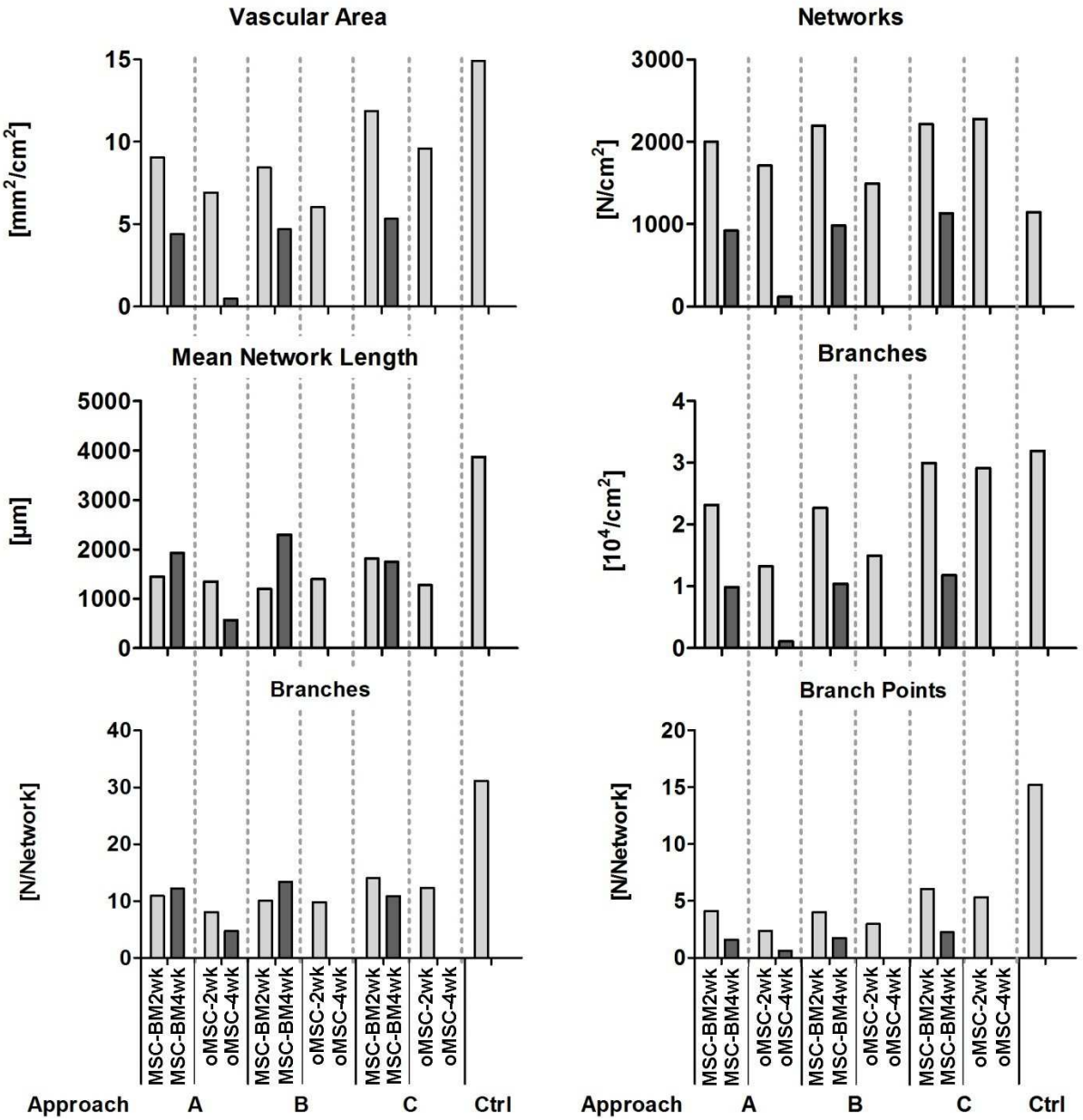

Supplementary Figure 9: Single donor level (Donor 1) according to Figure 24B, Supplementary Figure 8, Supplementary Figure 9

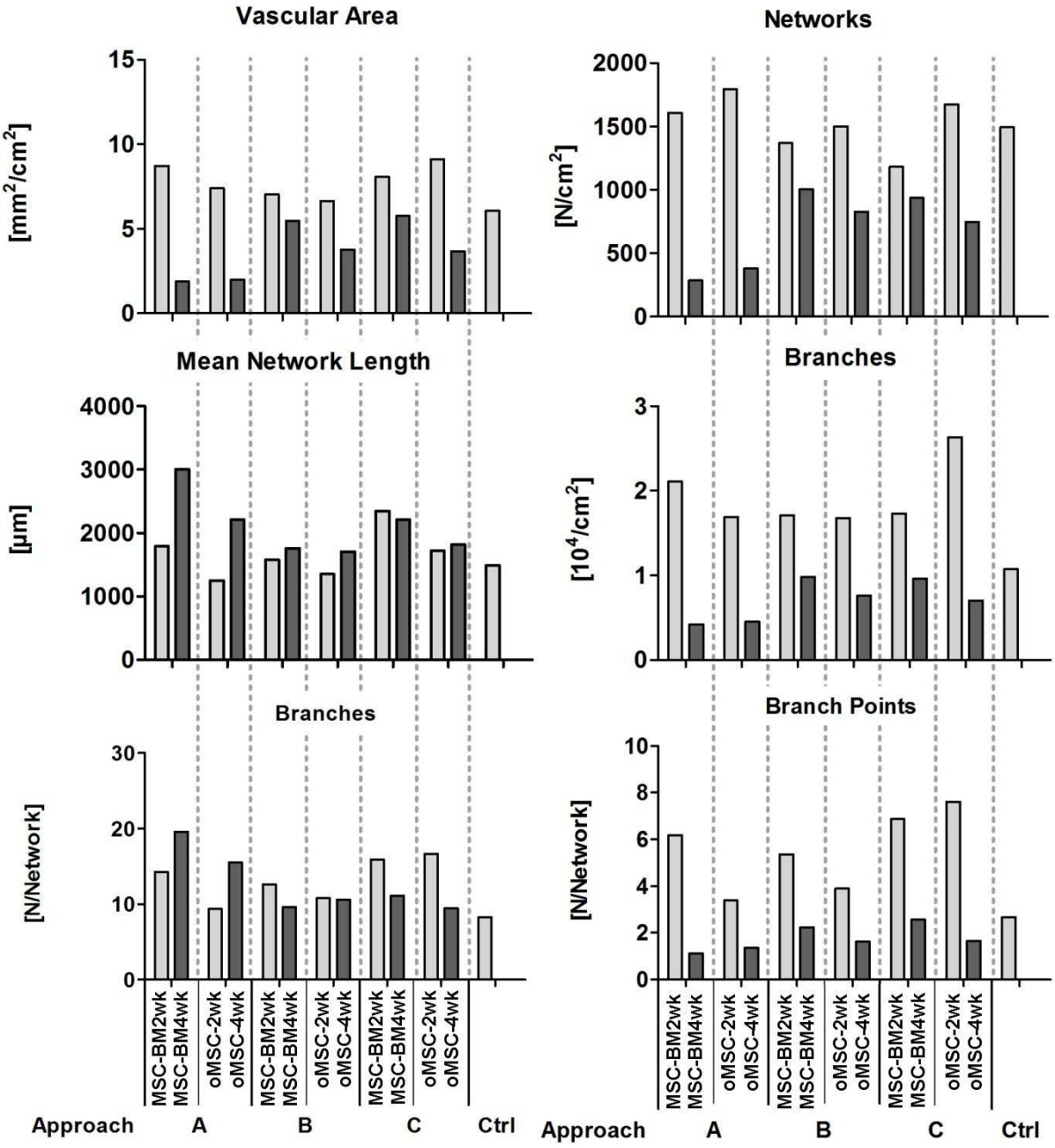

Supplementary Figure 10: Single donor level (Donor 2) according to Figure 24B, Supplementary Figure 8, Supplementary Figure 9)

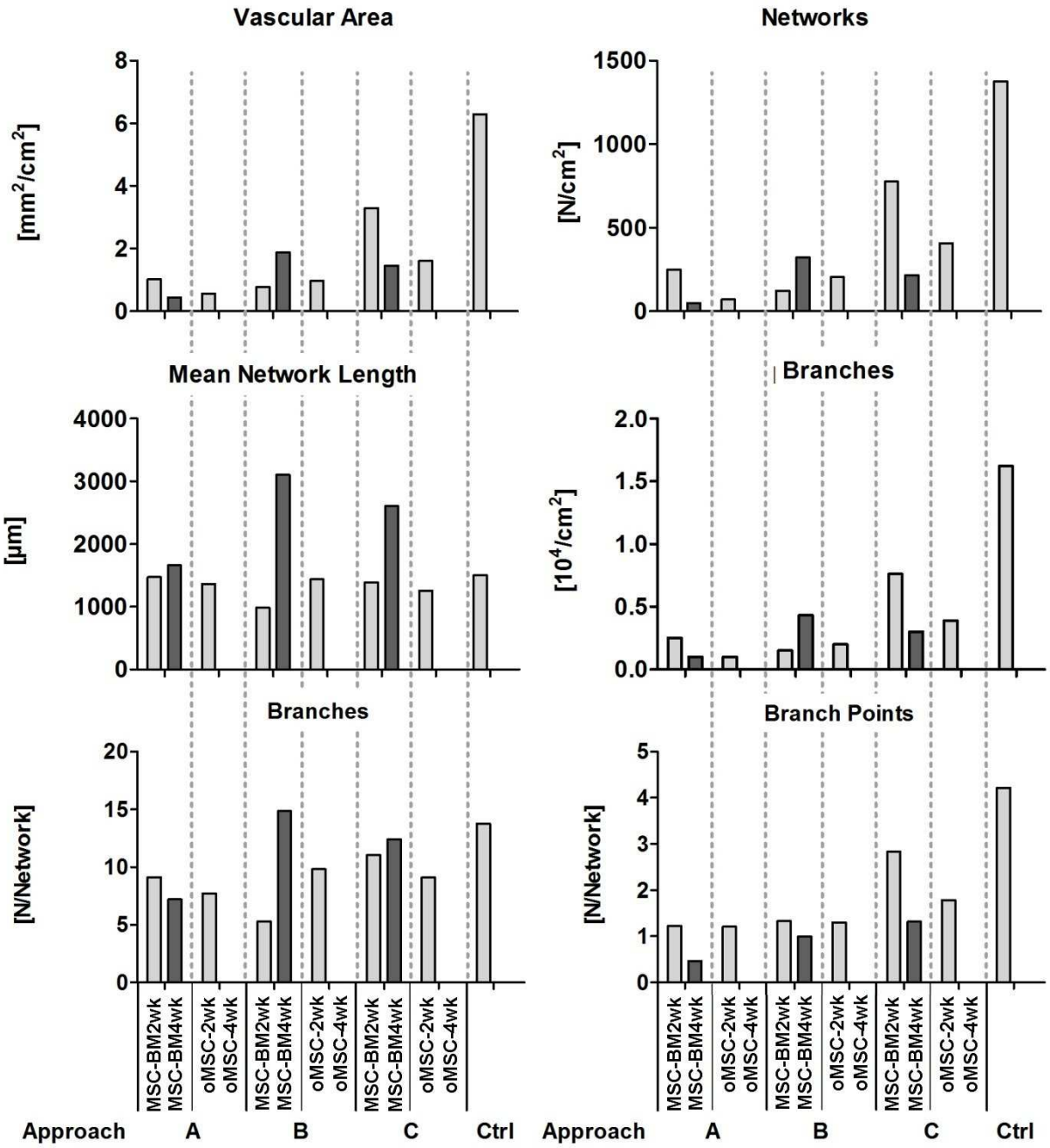

Supplementary Figure 11: Single donor level (Donor 3) according to Figure 24B, Supplementary Figure 8, Supplementary Figure 9)

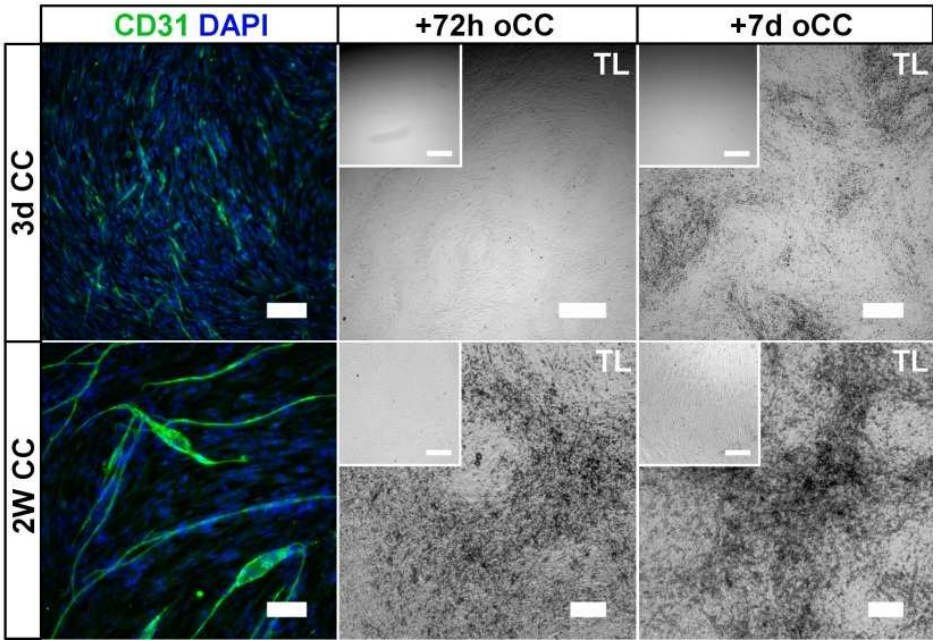

Supplementary Figure 12: Detection of vessel-like structures after 3d (3d CC) and 2W (2W CC) of co-cultivation using immunofluorescence staining for CD31 (CD31/DAPI) and microscopic evaluation of matrix calcification after additional 72h oCC and 7d oCC using transmitted light microscopy (TL); Scale bars: 200 µm

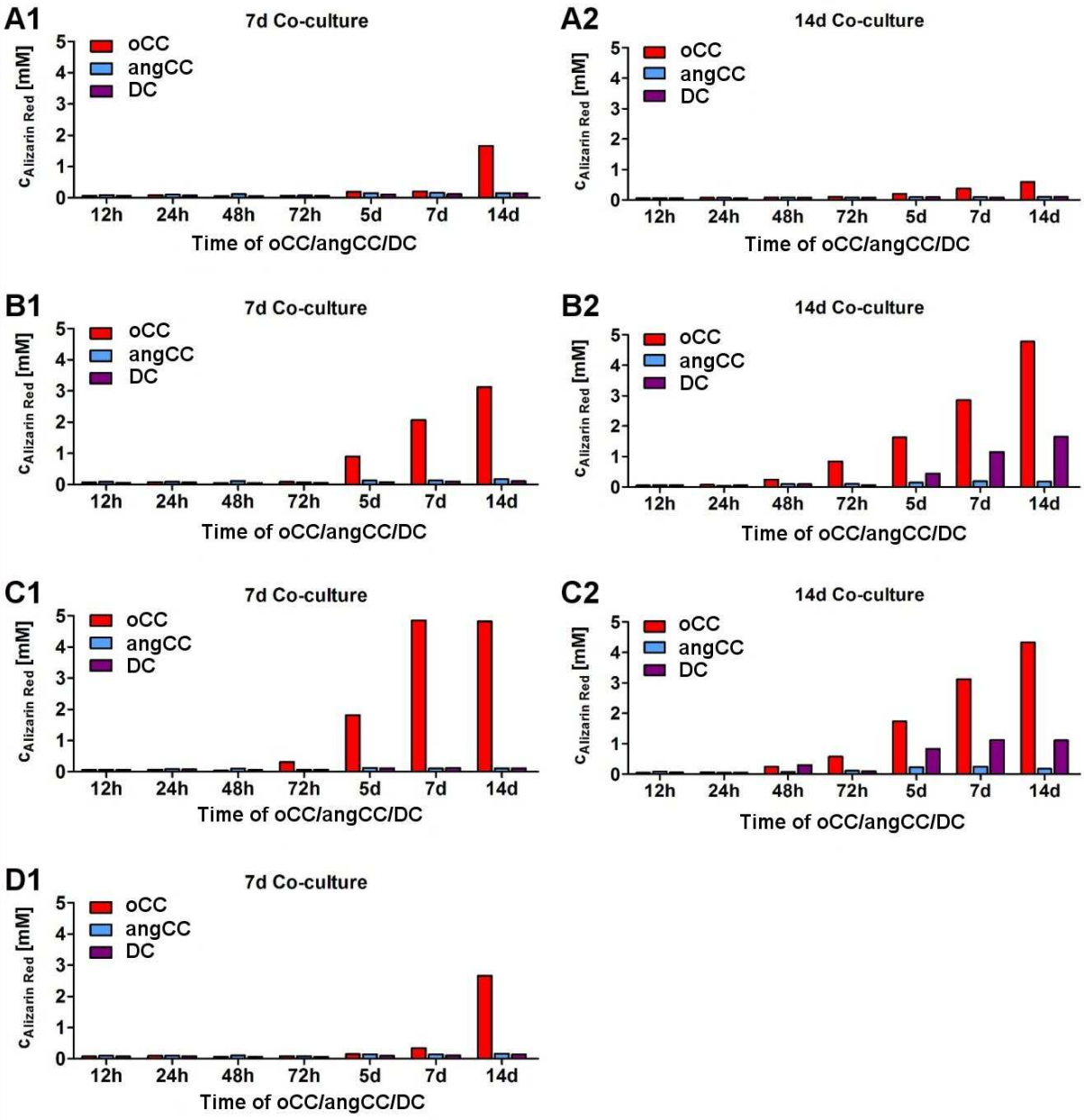

Supplementary Figure 13: Single donor investigation corresponding to Figure 27A - Quantification of Alizarin Red staining in 7d and 14d MSC/HDMEC co-cultures after oCC or angCC for 12h to 14d compared to a DC; A1/A2: Donor 1; B1/B2: Donor 2; C1/C2: Donor 3; D1: Donor 4

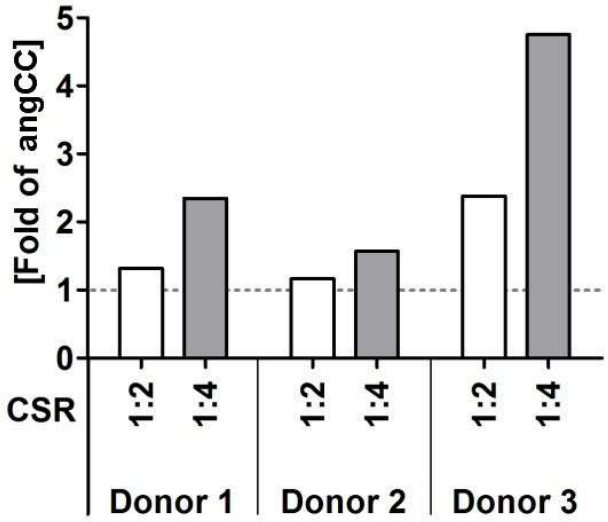

Supplementary Figure 14: Single donor evaluation corresponding to Figure 27G: Comparative quantification of Alizarin Red staining in post-differentiated MSC/HDMEC co-cultures with varying CSR of 1:2 and 1:4 normalized to the standard CSR of 1:0.66

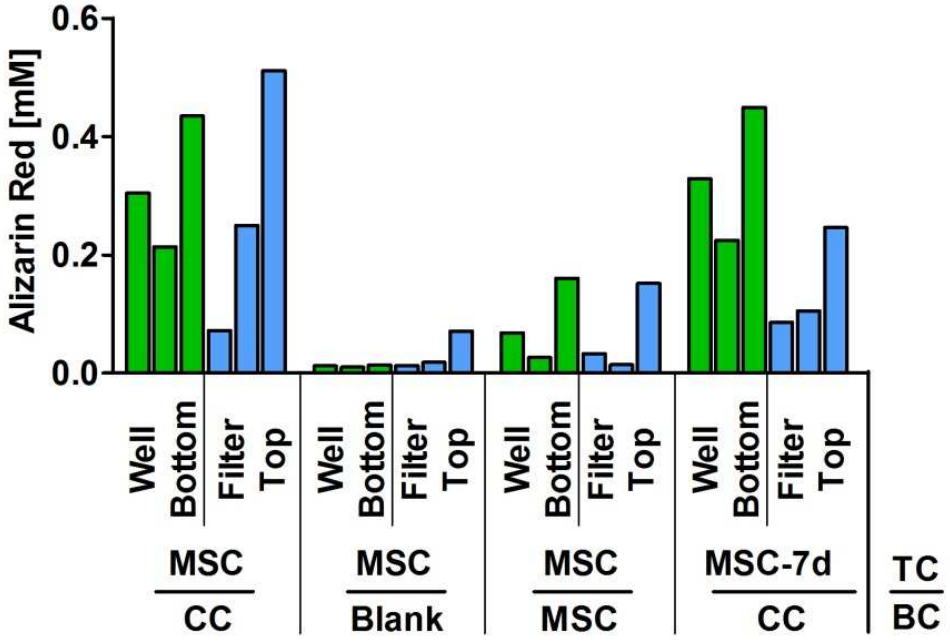

Supplementary Figure 15: Single donor level according to Figure 34B: Identification of a paracrine effect of post-differentiated co-cultures (CC) or MSC MCs (MSC) on the calcification of MSC MCs in a transwell system (description of transwell cultures according to Figure 34A) determined by quantitative analysis of AR staining intensities; TC: top chamber, BC: bottom chamber

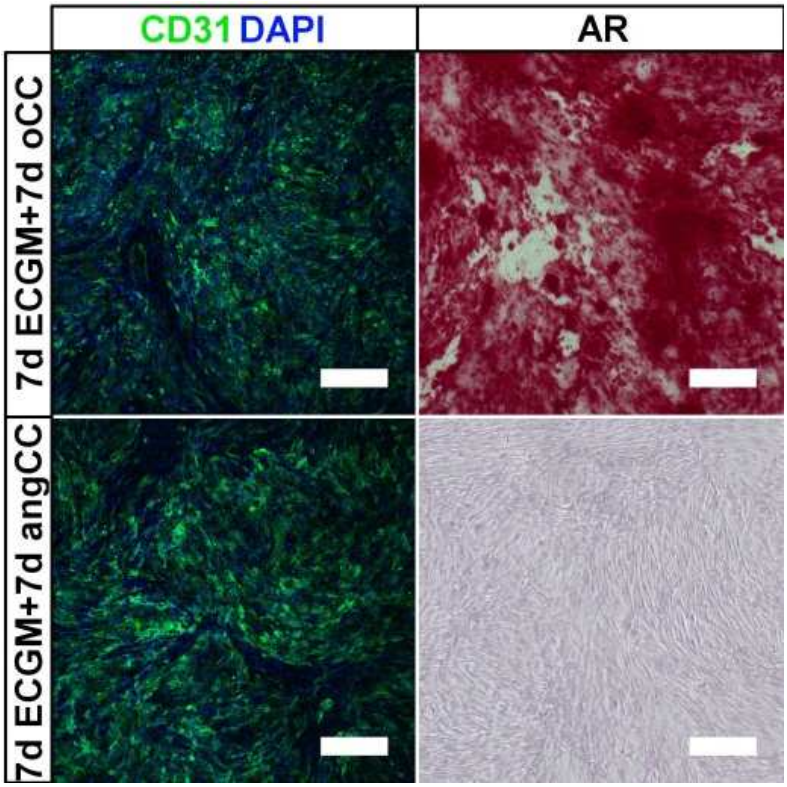

Supplementary Figure 16: Evaluation of an endothelial compartment and matrix calcification in MSC/ISO-HAS-1 Co-cultures after 7d oCC or 7dangCC using immunofluorescence staining for CD31 and AR stining; Scale bars: 200 µm

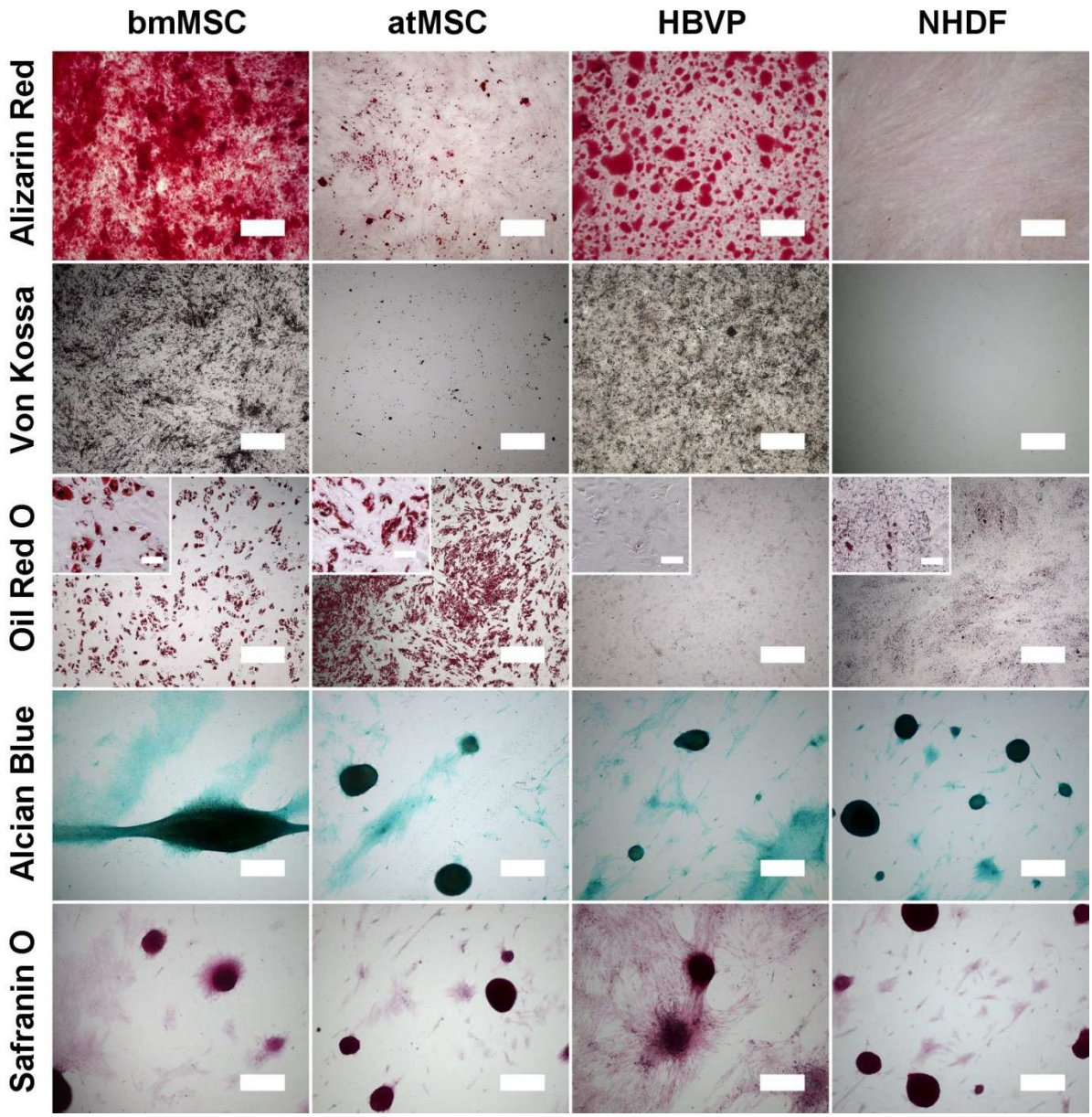

Supplementary Figure 17: Evaluation of a tri-lineage differentiation potential of bone marrow-derived MSC (bmMSC), adipose tissue-derived MSC (atMSC), human brain vascular pericytes (HBVP) and human dermal fibroblasts (HDF) cultivated in ODM, ADM or CDM and stained for osteogenic differentiation, adipogenic differentiation and chondrogenic differentiation using Alizarin Red staining + Von Kossa staining, Oil Red O staining and Alcian Blue + Safranin O staining, respectively; Scale bars: 500 µm; Scale bars in inserts: 50 µm

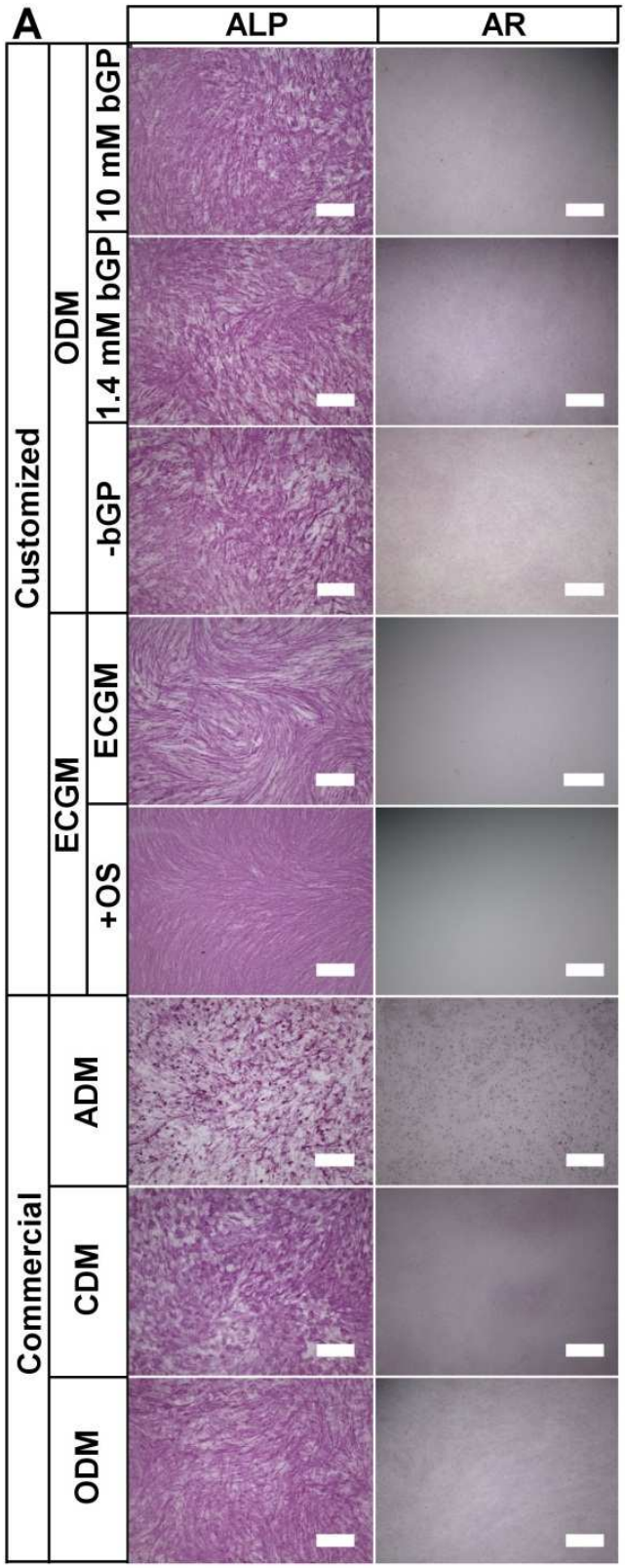

Supplementary Figure 18: Evaluation of ALP activity and matrix calcification using ALP activity staining and AR staining in MSC MC cultivated for 7d in ECGM followed by a cultivation in media as indicated in Table 23 serving as differentiation controls (DC); Scale bars: 500 µm

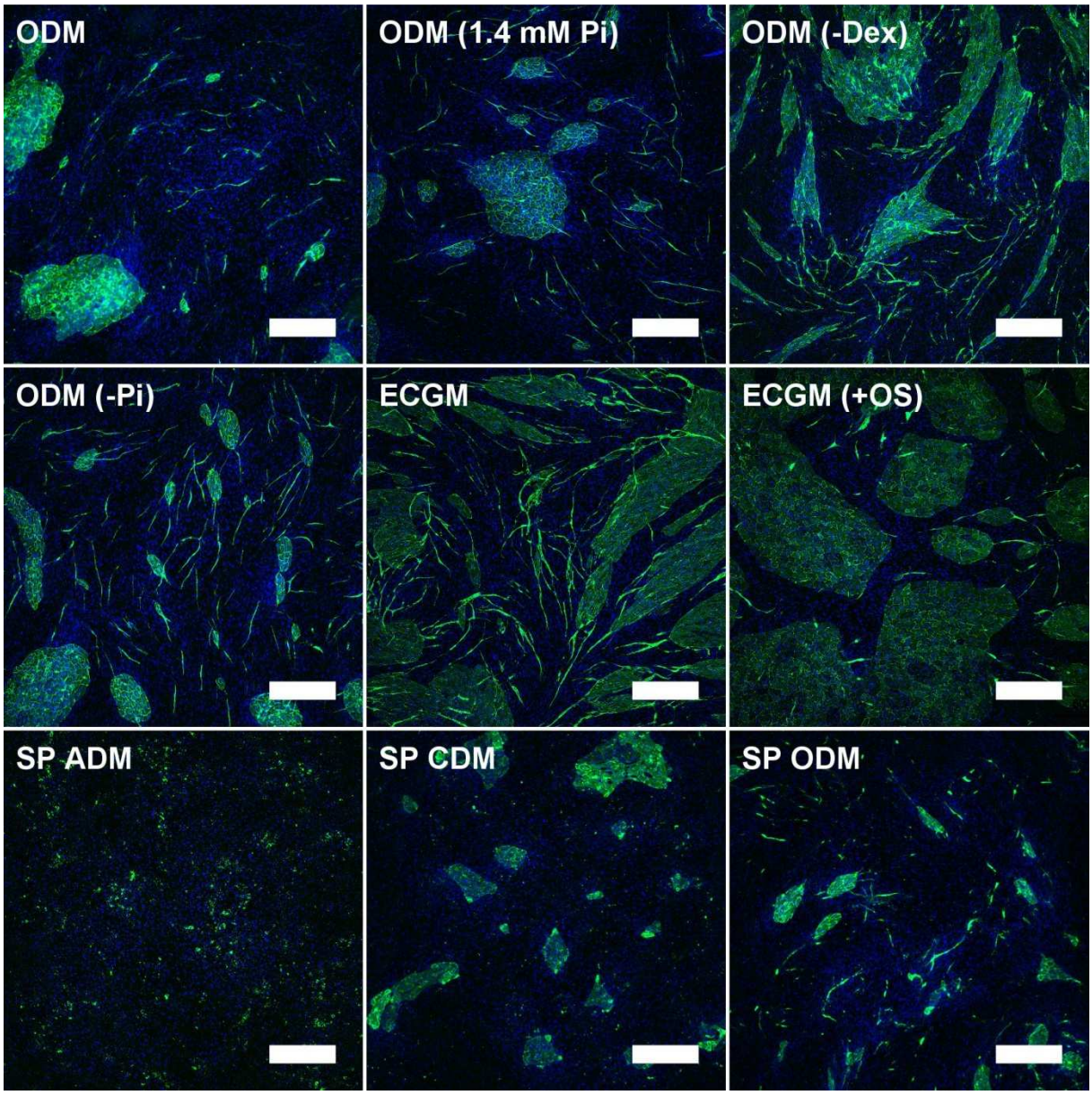

Supplementary Figure 19: Microscopic evaluation of vessel formation (overview) using IF staining for CD31 in MSC/HDMEC co-cultures after 7d oCC in customized and commercial differentiation media described in Table 23; Scale bars: 500 µm

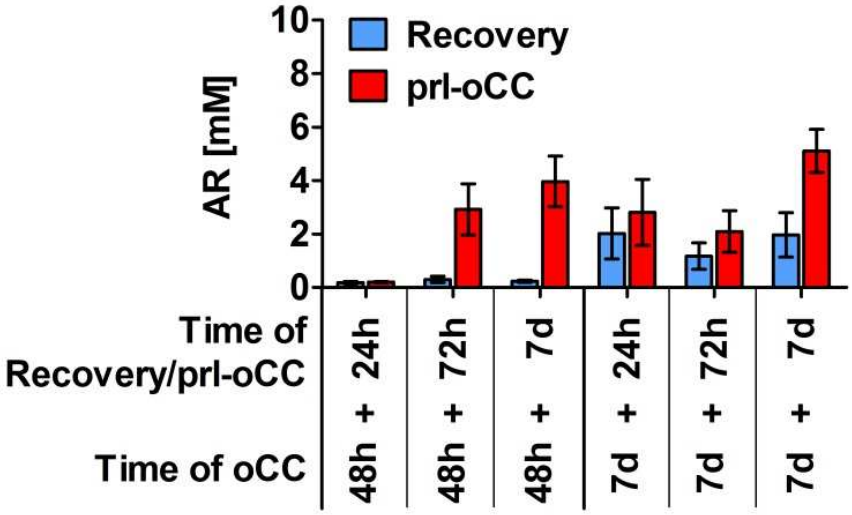

Supplementary Figure 20: Quantitative analysis of AR staining intensities in 48h oCC and 7d oCC samples after recovery in ECGM or prl-oCC in ODM

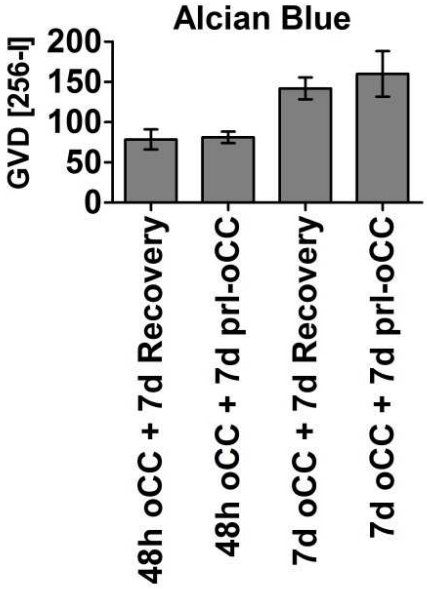

Supplementary Figure 21: Image-based quantification of AB staining intensities in 48h oCC and 7d oCC samples after 7d of recovery in ECGM or prl-oCC in ODM

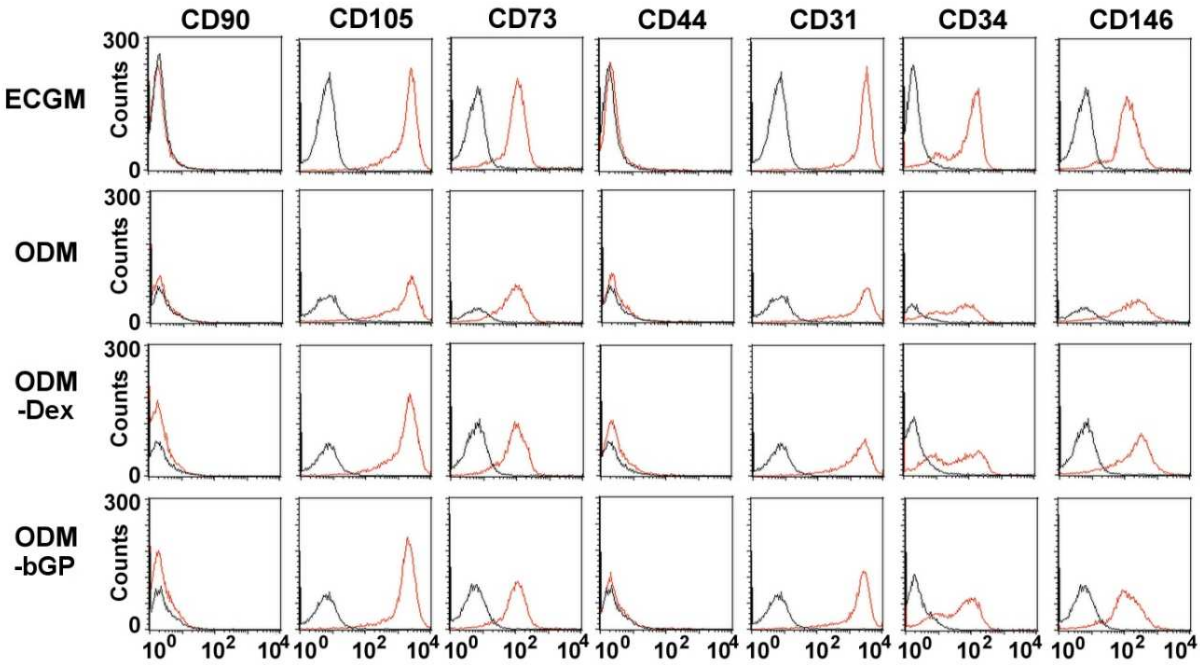

Supplementary Figure 22: Flow cytometric evaluation of the expression of CD90, CD105, CD73 and CD44 on HDMEC cultivated in ECGM, ODM, ODM-Dex or ODM-βGP; Panel shows exemplary results from 1 donor

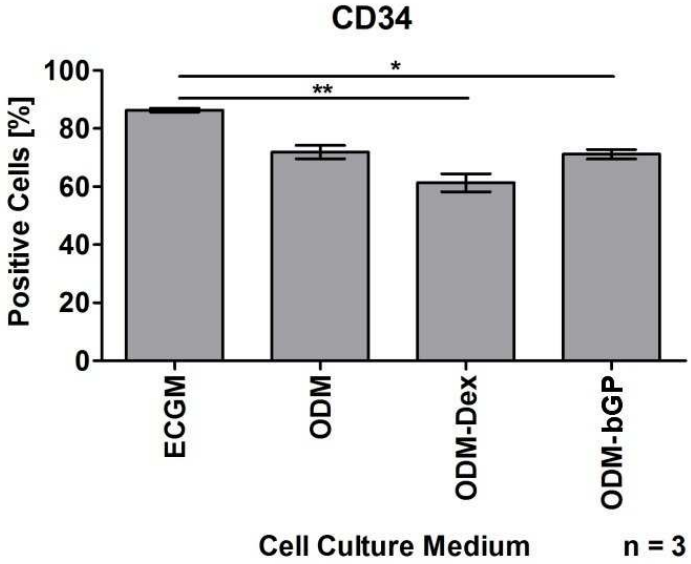

Supplementary Figure 23: Quantification of CD34 expression on HDMEC cultivated for 7d under comparative conditions in ECGM, ODM, ODM-Dex or ODM-βGP based on flow cytometric analysis shown in Supplementary Figure 22; Results are given as means (± SEM) from 3 biological replicates; Asterisks indicate statistically significant differences: *: $p < 0.05$; **: $p < 0.01$

Supplementary Table 4: Quantification of early apoptotic cells, late apoptotic cells and dead cells in HDMEC MCs cultivated in ODM, ODMw/oDex and ODMw/oβGP using flow cytometric analysis for 7-AAD/AnnexinV staining; The influence of single factors in ODM on the cell fractions is indicated as "Effect of [%]"; "-": indicates reduction of corresponding cell fraction percentage in relation to ODM; "+": indicates increase of corresponding cell fraction percentage in relation to ODM; Results represent mean values of 3 individual donors

Cell Fraction	Medium – absolute [%]			Effect of [%]	
	ODM	ODMw/oβGP	ODMw/oDex	Dex only	bGP only
Early apoptotic	9,15	5,35	10,2	-3,8	+1.05
Late apoptotic	11,64	9,56	17,6	-2,08	+5.96
Dead	2,25	3,98	4,34	+1,73	+2.09

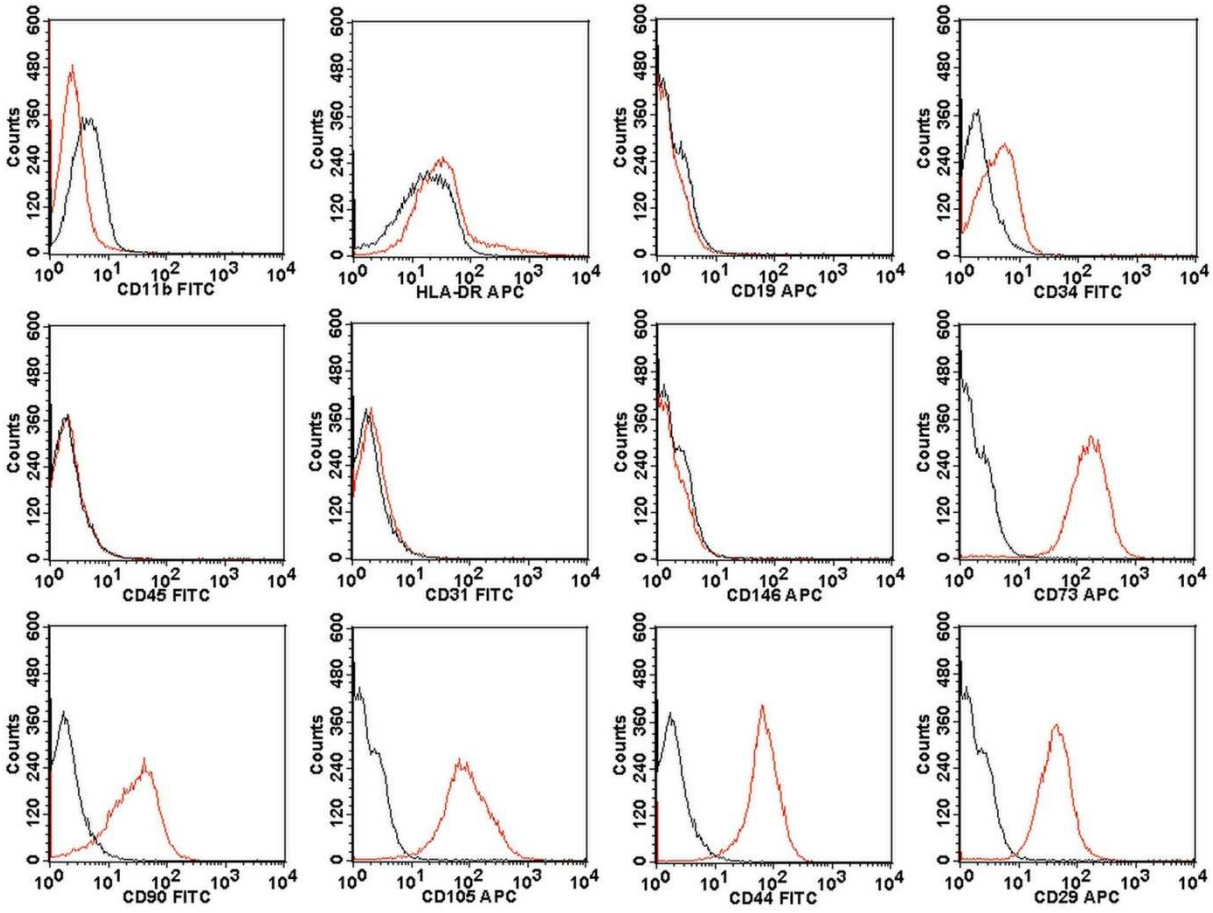

Supplementary Figure 24: Flow cytometry-based analysis of surface marker expression on MSC isolated after 7d angCC and expanded over 2 passages, Panel shows examplary results from 1 donor

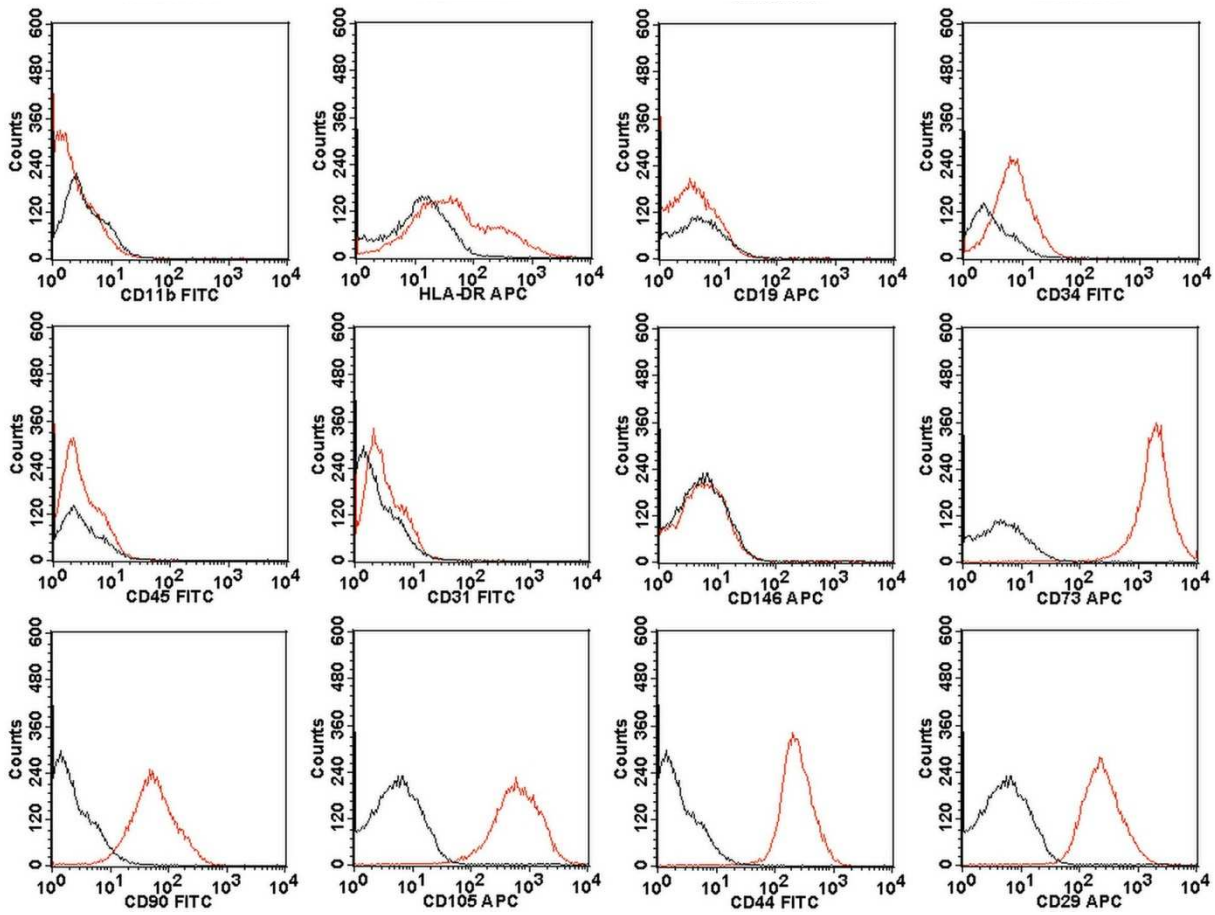

Supplementary Figure 25: Flow cytometry-based analysis of surface marker expression on MSC isolated after 7d oCC and expanded over 2 passages; Panel shows examplary results from 1 donor